Engineered Antibody and Neuropeptide Mediated Radionuclide Targeting in Prostate Cancer

A thesis submitted to the University of London
for the degree of Doctor of Philosophy

by

Roxana M. G. Kashani

Centre for Molecular Oncology and Imaging
Barts and The London School of Medicine and Dentistry
Queen Mary
University of London

DECLARATION

This report is a result of the independent work of Roxana Kashani.

I certify that this report does not incorporate without the acknowledgement, any material previously submitted for a degree or diploma in any university, and that to the best of my knowledge and belief it does not contain any material previously published or written by another person where due reference is not made clear.

Abstract

Prostate cancer (PC) is the most common cancer type in men in the western world and to date no definitive stratergy to image PC is avaliable. This thesis explores the possibility of using Prostate Specific Membrane Antigen (PSMA) and Gastrin Releasing Peptide Receptor (GRP-R) as biomarkers for the targeting and imaging of PC. The development of an imaging radiopharmaceutical to image all stages of PC growth would improve diagnosis, staging and personalised treatment, as present imaging modalities for PC rely largely on anatomical changes to allow visualisation and have limited sensitivity for imaging metastatic spread of the disease. PSMA was selected due to its up-regulation in advanced carcinoma and metastatic disease and GRP-R due to its high levels of expression in the early stages of PC. The hypothesis is that PC can be imaged by a suitably designed radioligand directed against an appropriate molecular target, such as PSMA and GRP-R. Both of these targets were believed to be appropriate as both are present preferntially in prostate tissue and they both internalise when bound by their ligand. To target PSMA, phage libraries were screened for scFv against both cell-expressed PSMA and recombinant PSMA and diabodies were also generated from high binding clones. Several promising candidates were produced which selectively bound to LNCaP cells and PSMA protein in both FACS and ELISA. Diabodies showed improved binding over corresponding scFv's. *In vivo* analysis of tumour-bearing mice failed to reveal tumour uptake of either the scFv or the diabody. *In vitro* analysis suggested that the affinity of the antibody fragments were not sufficiently high. [^{99m}Tc]-Demobesin 4 (DB 4), a radiolabelled GRP-R binding peptide was synthesised. Radioligand binding assays performed on a range of androgen-independent and androgen-dependent PC cell lines showed high GRP-R expression in the androgen dependent LNCaP line but also in the androgen-independent cell lines PC3 and DU145. GRP-R expression, measured by RT-PCR to determine the amount of GRP-R RNA, was similar to that seen using radioligand binding assays and similar patterns were observed in autoradiographic studies. *In vivo* studies on mice bearing the PC xenografts showed tumour uptake and localisation of [^{99m}Tc]-DB 4 within one hour. A limited correlation was observed between results obtained *in vivo and in vitro*. In conclusion, the results were partly consistant with the hypothesis, whereby initial aims for the PSMA project were successfully achieved with generation of scFv and diabodies that specifically bound, however they proved unsuitable as potential imaging agents, perhaps owing to low binding affinity. GRP-R was shown to be an effective candidate for radioimmaging PC which has the potential to descrininate [^{99m}Tc]-DB4 uptake between androgen-independent/dependent cells. Thus this radiopharmaceutical may prove a useful imaging agent for early prostate cancer but that further studies are required to assess its usefulness in the androgen-independent stages of the disease.

ACKNOWLEDGEMENTS

I would like to first start by thanking my supervisor Professor Stephen Mather for his guidance, support and patience throughout my PhD.

A big thank you to all at Bone and Joint Research Unit helping with my phage display project, with a special thank you to Dr. Stella Man for her work on PSMA protein production and the 3 rounds of selection as well as her guidance and invaluable help. I am indebted to Mrs. Gill Adams for her advice, support and proof reading.

Many thanks to all the members of Cancer Imaging for their help, encouragement and support. I am grateful to Miss Ciara Finucane and Dr. Julie Foster for all their help with the imaging and biodistribution work. Thank you to Mr. David Ellison, Dr. Torkjel Matzow, Mr. Iain Murray and particularly Dr. Jane Sosabowski and Miss Ana Marcelino for their invaluable help and pep-talks.

I would like to thank Dr. Neil Hartman and all at Radiopharmacy department at St. Bartholomew's Hospital who kept me in a steady supply of ^{99m}Tc. I am also grateful to Dr. David Prowse for the supply of prostate cancer cells as well as advice and in-depth knowledge on prostate cancer.

Thank you to my sponsor CRUK for giving me the opportunity to perform this project.

Finally I would like to thank all my friends, especially Mimosa, for their support and understanding when I vanished for months on end with PhD commitments, with a special thank you to Dr. Tony Smith, my great friend and mentor.

To my mother, my sister Andrea and George I am eternally grateful for your unwavering belief in me, help and support and I would like to apologise for dragging you on this rollercoaster ride with me, it is safe to get off now!

CONTENTS

LIST OF FIGURES

LIST OF TABLES

ABBREVIATIONS

^{125}I	Sodium iodide-125
^{131}I	Sodium iodide-131
^{18}F	Fluorine-18
2-D	Two-dimensional
^{32}P	Sodium phosphate-32
3-D	Three dimensional
^{89}Sr	Strontium chloride-89
^{99}Mo	Molybdenum-99
^{99m}Tc	Technetium-99m
Aa	Amino acid
ACTB	Beta-actin
ACTH	Adrenocorticotropic hormone
AIPC	Androgen independent prostate cancer
ALCA	Activated leukocyte cell adhesion
AR	Androgen receptor
BCL2	B-cell lymphoma 2
bFGF	Basic fibroblast growth factor
BHP	Benign prostatic hyperplasia
BN	Bombesin
BSA	Bovine serum albumin
CAIX	Carbonic anhydrase IX
CCK	Cholecystokinin
CDR	Complementarity-determining regions
CEA	Carcinoembryonic antigen
CPM	Counts per minute
CS	Charcoal-stripped
CT	Computed tomography
C_T	Threshold cycle
DB 4	Demobesin 4
DC	Dendritic cell
DHT	Dihydrotestosterone
DNA	Deoxyribonucleic acid
DRE	Digital rectal examination
DTPA	Diethylenetriamine-penta-acetic acid
EBRT	External beam radiation therapy
EDTA	Ethylenediaminetetraacetic acid
EGF	Epidermal growth factor
EGTA	Ethylene glycol tetraacetic acid
ELISA	Enzyme-linked immunosorbant assay
Fab	Fragment antigen binding
FACS	Fluorescence activated cell sorting
FBS	Foetal bovine serum
FDA	Food and drug administration

FDG	Fluorodeoxyglucose
FITC	Fluorescein isothiocyanate
Fmoc	9-fluorenylmethyloxycyclocarbonyl
FOLH1	Folate hydrolase 1
FP	Forward primer
FPLC	Fast protein liquid chromatography
FSC-H	Forward scatter
GF	Growth factors
Gn	Gonadotrophic hormone
GnRH	Gonadotrophin-releasing hormone
GRP	Gastrin releasing peptide
GRP-R	Gastrin releasing peptide receptor
H	Hydrogen
HCL	Hydrochloric acid
HEPES	4-(2-hydroxyethyl)-1-piperazineethanesulfonic acid
HGPIN	High grade prostatic intraepithelial neoplasia
Hi5	High Five
HK2	Human Kallikrein-2
HLA	Human leukocyte antigen
HPLC	High pressure liquid chromatography
HSP	Heat shock proteins
HYNIC	6-hydrazinopyridine-3-carboxylic acid
IgG	Immunoglobulin
IHC	Immunohistochemistry
IPTG	isopropyl-β-D-thiogalactoside
ITLC	Instant thin layer chromatography
IVS	In vivo scope
KCl	Potassium chloride
kDa	Kilodaltons
keV	Kiloelectron volt
KGF	Keratinocyte growth factor
LET	Linear energy transfer
LH	Luteinising hormone
LHRH	Luteinising hormone releasing hormone
mAb	Monoclonal antibody
MAPK	Mitogeb-activated protein kinase
MFI	Mean fluorescence intensities
MGB	Minor groove binder
$MgCl_2$	Magnesium chloride
MIBG	Metaiodobenzylguanidine
MRI	Magnetic resonance imaging
mRNA	Messenger ribonucleic acid
N	Nitrogen
NAALADase	N-acetylated acidic dipeptidase
NaCl	Sodium chloride

NaOH	Sodium hydroxide
ND	No data
NMB-R	Neuromedin B receptor
NT	Neurotensin
NTC	No template control
O	Oxygen
OCT	Optimal cutting temperature
P	Phosphate
PAP	Prostatic acid phosphatase
PBS	Phosphate buffer saline
PC	Prostate cancer
PCLA	Prostate cancer lipid antigen
PCR	Polymerase chain reaction
PEG	Polyethylene glycol
PET	Positron emission tomography
PFU	Plaque forming units
PIN	Prostatic intraepithelial neoplasia
PSA	Protein specific antigen
PSMA	Prostate specific membrane antigen
RCC	Renal cell carcinoma
RP	Reverse primer
Rpm	Rotations per minute
RTK	Receptor tyrosine kinases
scFv	Single chain variable fragment
SCID	Severe combined immunodeficiency
SCLC	Small cell lung cancer
SDS	Sodium dodecyl sulfate
SF	Survival factors
SFM	Serum free medium
SP	Substance P
SPECT	Single photon emission computed tomography
SSC-H	Side scatter
ssDNA	Single stranded deoxyribonucleic acid
TAA	Tumour-associated antigen
TcO_2	Tc-colloids
TEMED	Tetramethylethylenediamine
TFA	Trifluoroacetic acid
TMB	3,3’,5,5’-tetramethylbenzidine
Try	Tryosine
V_H	Variable heavy
VIP	Vasoative intestinal peptide
V_L	Variable light
Vol	Volume

1 INTRODUCTION

1.1 THE PROSTATE

The prostate gland is a small, walnut-shaped gland that lies in front of the rectum. It surrounds the urethra, just below the urinary bladder and can be felt during a rectal examination. Its primary function is the storage and secretion of a clear, slightly alkaline fluid that constitutes approximately one-third of the volume of semen. Although not a vital organ, it is surrounded by a complex network of nerves and blood vessels that can be damaged as a result of PC and during its treatment.

1.1.1 Prostate Cells

The normal prostate is a tubular-aveolar gland composed of a well-developed stromal compartment containing nerves, fibroblasts, infiltrating lymphocytes and macrophages, endothelial cell capillaries and smooth muscle (Figure 1.1) [1].

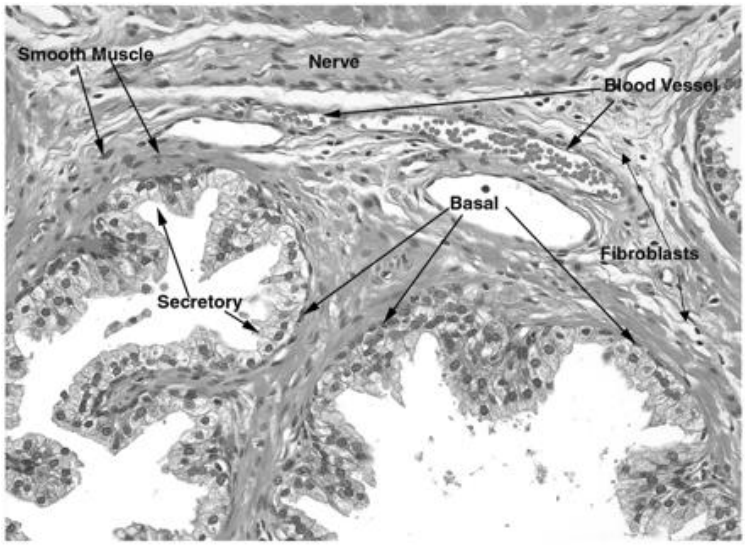

Figure 1.1: Cellular architecture of the prostate comprises of blood vessels, which provide nutrients including androgens to the fibrous stromal layer, which primarily consist of fibroblasts, smooth muscle cells, and basal and secretory cells.

Two morphologically defined components make up the prostatic epithelium, the basal and luminal layers, which contain three types of cell; basal, secretory and neuroendocrine, distinguished on the basis of their location, morphology and phenotypic characteristics. Luminal secretory or glandular cells constitute the exocrine compartment, secreting prostate specific antigen (PSA) and prostatic acid phosphatase (PAP) into the glandular lumina [2]. They are terminally differentiated and represent the major cell type in normal and hyperplastic epithelium. They express high levels of androgen receptor (AR) and are dependent on androgen for survival [3]. In contrast, basal cells are non-secretory and relatively undifferentiated. They rest on the basement membrane, express low or undetectable levels of AR, and are thus not dependent on androgen for survival. Neuroendocrine cells are distributed throughout the basal and luminal layers and are characterised by their expression of chromogranin A and serotonin, but not AR [4]. They are thought to play a role in growth and differentiation, but their function is largely unknown [3].

1.2 ANDROGENS AND THE PROSTATE

1.2.1 Androgen Production

It is important to understand how androgen affects the growth of the prostate gland and in turn PC. Testosterone, which circulates throughout the body, is primarily produced by the Leydig cells in the testes, and is mainly required for the maintenance of muscle mass, bone and cardiovascular health, spermatogenesis and sex drive [5]. Androgenic effects are also caused by adrenal androgens, such as androsterone, dehydropiandrosterone (DHEA) and its sulfate, although these are not as potent as testosterone, and make up only 10% of circulating androgens. The production of testosterone is carefully regulated through the hypothylamic-pituitary testicular axis (Figure 1.2). In a series of chain reactions, gonadotrophin-releasing hormone (GnRH)[1] is secreted by the hypothalamus; this in turn causes GnRH to bind to gonadotropes in the anterior pituitary, which

[1] Also known as luteinising hormone releasing hormone (LHRH)

stimulates the release of gonadotropic hormone (Gn)[2] and follicle-stimulating hormone (FSH). Gn reacts with the Leydig cells where it stimulates the production of androgen [6]. Circulating testosterone acts in a negative feedback loop to down-regulate the expression of GnRH. Adrenocorticotropic hormone (ACTH), also made by the pituitary, stimulates androgen synthesis in the adrenal gland (Figure 1.2) [7].

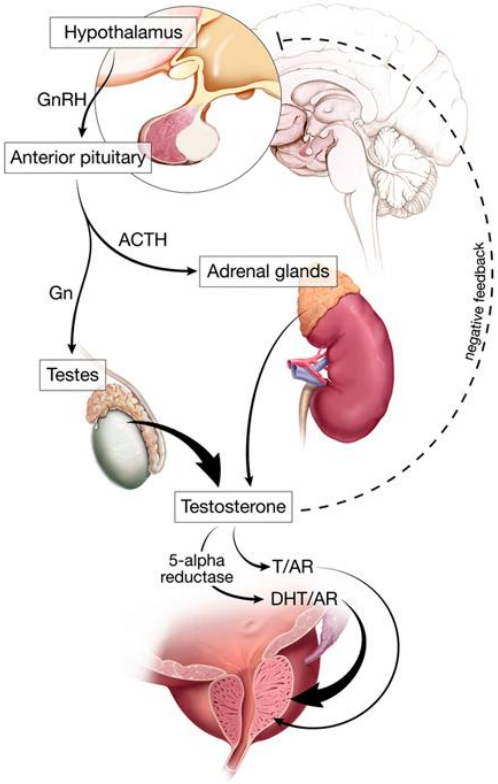

Figure 1.2: Hypothalamic-pituitary testicular axis, showing the production of testosterone regulated by the negative feedback loop. Testosterone (T) and dihydrotestosterone (DHT) bind to the androgen receptor (AR) in the prostate, causing increased expression of androgen-responsive genes [7].

Once testosterone has entered the cell in the prostate, it is usually converted to dihydrotestosterone (DHT) by 5α-reductase, which regulates intraprostatic androgen-mediated processes. Both testosterone and DHT can bind to the androgen receptor (AR), although DHT has 2- to 10-fold greater affinity for the AR, and is consequently the primary androgen bound by the AR [6].

[2] Also known as luteinising hormone (LH)

1.2.2 Androgen Receptor

The actions of both testosterone and DHT are mediated by the AR, acting as a transcription factor [8]. Although present in both sexes, AR is abundantly expressed in male sex tissues, and its functions are to promote the growth and differentiation of the male urogenital structures. It is also necessary for the initiation and maintenance of spermatogenesis [6].

During the development of the normal prostate and also prostate cancer, cell survival is dependent on the AR. In the prostate gland, AR, a member of the steroid receptor superfamily, is preferentially situated in the nuclei of stromal and secretory epithelial cells. Unbound to DHT, AR protein resides in the cytoplasm and is bound to chaperone molecules viz. heat-shock proteins (HSP). Whilst situated here, it is held inactive and precluded from DNA binding [5].

Once DHT binds to the AR, the protein dissociates from HSP, undergoes a conformational change, and is quickly translocated to the nucleus [9]. Once in the nucleus, the androgen receptor dimerises and binds to the androgen-response elements in DNA, activating the transcription of genes involved in the growth and survival of the cell [10] (Figure 1.3). The presence of androgens causes prostate epithelial and stromal cells to proliferate and differentiate, whereas depletion of androgens causes apoptosis of both the secretory epithelial and stromal compartments [1].

Androgen action in the normal prostate is a paracrine process which has different effects on different cell types [8, 11].

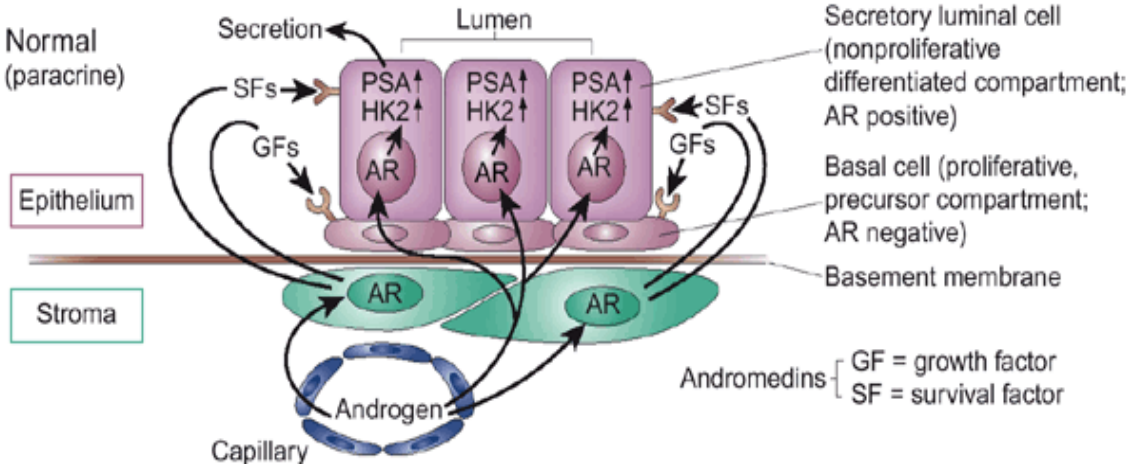

Figure 1.3: In normal prostate, growth maintenance of prostate epithelium depends on andromedins (growth (GF) and survival (SF) factors) produced by stromal cells. Production of andromedins is a result of androgen signalling through the AR. Production of secretory proteins (PSA & human kallikrein-2 (HK2)) is dependent on androgen signalling in the prostate epithelium. AR is not expressed by basal epithelial cells [12].

AR found in stromal cells activates the secretion of soluble peptide growth factors known as andromedins. Diffusion of these andromedins across the basement membrane into the epithelial compartment, which contains both basal and secretory luminal cells, allows the andromedins to bind to specific membrane receptors. Upon binding, the signalling for proliferation and epithelial cell survival is initiated [5, 11].

In the nuclei of the secretory cells, AR stimulates the transcription of a series of genes encoding prostate-specific differentiation markers, such as PSA and human glandular kallikrein-2. Although transcriptional regulation of these markers is regulated by the AR in the nuclei of the secretory luminal cells, the receptor does not stimulate proliferation or survival; it suppresses the growth of the secretory cells by inhibiting andromedin-induced proliferation [1].

1.2.3 Growth Factors

In conjunction with androgens, growth factors are important in the development of the prostate and abnormal hyperplastic growth. There is a fine balance between proliferation and apoptosis; these processes are mediated by the expression of growth factors. Interactions between the stimulatory and inhibitory growth factors regulate the stromal-epithelial interactions that are involved in the development of the prostate, and maintain homeostasis in the normal functioning gland (Figure 1.4).

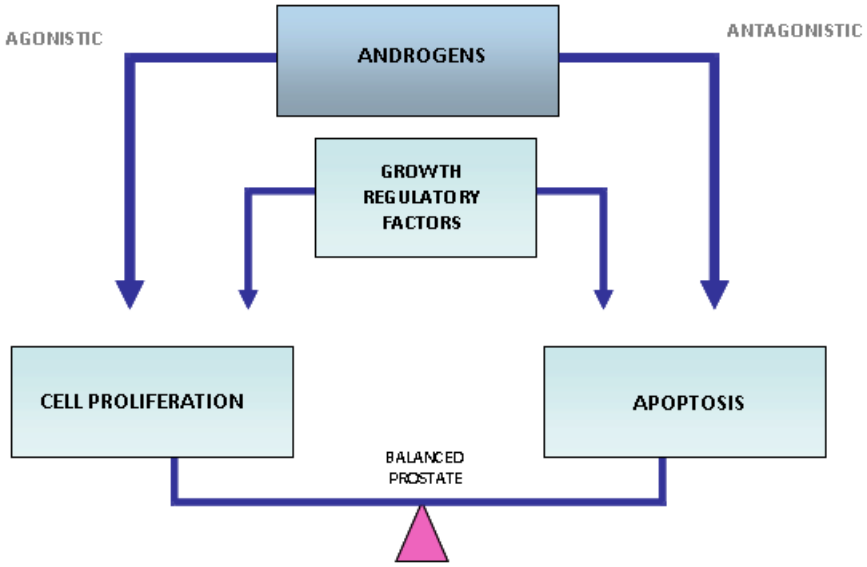

Figure 1.4: Homeostatic balance between proliferation and apoptosis is maintained by androgens and growth factors. Adapted from [13]

The DHT-AR complex in the prostatic stroma affects the expression of a number of growth factors that stimulate proliferation, including epidermal growth factor (EGR), basic fibroblast growth factor (bFGF), keratinocyte growth factor (KGF) and insulin-like growth factor (IGF). Andromedins are also up-regulated and cause signalling which represses the apoptotic pathway [1].

1.3 PROSTATE CANCER

After skin cancer, PC is one of four most common cancers in the UK, along with breast, lung and colorectal cancers [14]. A quarter of all new cases of cancer diagnosed in men are prostate cancers. Every year, over 35,000 men are diagnosed with the disease and it is the second most common cause of male cancer death, with 10,200 deaths each year in the UK alone [15]. PC primarily affects men over the age of 60, and increases by 60% in the 7th decade of life [15]. The exact trigger for development of prostatic adenocarcinoma has not yet been elucidated, although epidemiological and genetic factors are seen as possible contributors.

1.3.1 Biology of Prostate Cancer

McNeal (1981) [16] developed the concept of the zonal anatomy of the prostate. Approximately 60-70% of prostatic cancers occur in the peripheral zone (the largest zone, located near the rectum), and 10-20% in the transition zone (surrounding the proximal urethra), with only 5-10% originating from the central zone (involved in the connection of the seminal vesicles to the prostate) [17].

In excess of 99% of PCs develop from glandular epithelial cells in the prostate and are therefore described as prostatic adenocarcinomas. However the identification of the specific epithelial sub-type in which the carcinogenic process initiates remains unclear. It is thought that the precursor for most peripheral-zone prostatic carcinomas is high-grade prostatic intraepithelial neoplasia (HGPIN) [17], and that HGPIN arises from low-grade PIN, which in turn arises from normal prostate epithelium [18].

The aetiology of PC is insufficiently understood, although a number of molecular events occur during the progression of initial tumour formation in most cancers, such as abnormal methylation, proto-oncogene activation, inactivation of DNA repair mechanisms and tumour repressors, and an increase in the synthesis of growth factors and growth factor receptors [6]. Eventually, with progression, the cancer spreads out of the capsule

and metastasises to neighbouring tissues such as the lymph nodes and bone; therefore the cancer succeeds in evading apoptosis, invades tissue, and forms new blood vessels.

1.4 SCREENING AND TREATMENT

Diagnosis of the disease is made difficult by the extreme variability in the clinical course. PC can be an indolent, latent disease in elderly patients who do not present clinical symptoms. Other forms of PC take an aggressive course, spreading out from the capsule into the seminal vesicles, bladder and rectum and metastasising to lymph nodes, bone, lungs and other organs. In order to select the best first-line of treatment, it is important to know the stage and advancement of the tumour growth. Pathophysiological studies of the tumour, such as the measurement of PSA expression and histological assessment (Gleason score), are necessary.

1.4.1 Gleason Score

In the absence of more accurate and reliable tissue or blood biomarkers, the Gleason score and the stage at the time of diagnosis remain the mainstays of prognosis. Despite extensive research efforts, to date very few biomarkers of PC have been introduced into clinical practice.

The grading system is entirely based on the histological pattern of arrangement of carcinoma cells in hematoxylin and eosin-stained prostatic tissue sections. A grade is assigned to the most common tumour pattern detected in the observed area by simple visual inspection (the primary pattern) and a second grade to the next most common pattern (the secondary pattern). The sum of the two grades gives the Gleason Score. A histological score is generated for both primary and secondary patterns grading on a scale of 1 to 5; the grade of 1 is given to sections most resembling healthy prostatic tissue, and increasing grades are apportioned with decreasing normal cell morphology (grades 2-4), with grade 5 showing no healthy prostatic or organised cell growth. Diagnoses are

difficult to make from tissue samples obtained by needle biopsies, due to the small amount of tissue available for histological examination. Morphologically, PC is tricky to diagnose because the clues to malignant disease can be subtle, increasing the risk of underdiagnosis [19]. The Gleason score, was developed by Donald Gleason in 1974 [20] when very little was known about the disease, and immunohistochemistry was developed afterwards in the 1980s; therefore new screening techniques are seriously required.

1.4.2 Prostate Specific Antigen

PSA is a serine protease which is synthesised by healthy prostate tissue, in benign prostatic hyperplasia (BPH) and at all stages of PC growth. For both initial diagnosis and monitoring, PSA is widely regarded as a cancer marker, and testing for it has come into widespread use; but its reliability has been questioned, as there is no threshold with which PSA levels can be compared, because PSA expression varies between individuals [21]. Numerous non-malignant processes, including BPH and prostatitis, which occur in older men, frequently lead to PSA elevations; thus PSA screening alone is not recommended [22].

Prior to the measurement of PSA serum levels, other screening procedures were employed such as digital rectal examination (DRE); an invasive and uncomfortable procedure. A major disadvantage of this method of screening was that the tumours detected were typically already advanced and had extended beyond the organ capsule or had metastasised.

1.5 TREATMENT

For localised PC, surgery and radiation therapy can be curative. However, this is not appropriate for most of the cases that present locally advanced or widespread disease, and therefore require hormone therapy to suppress tumour growth. Despite medical and drug treatment, the majority of patients with PC will gradually transform to a metastatic

hormone-refractory state, which currently remains incurable and which will, in time (1-2 years), kill them [23].

A number of procedures are currently available for managment, all of which are dependent on the stage and aggressiveness of the cancer. Watchful waiting, although not a treatment, is a course of action taken in patients with slowly developing PC. Radiotherapy by either external beam radiation therapy (EBRT) or brachytherapy can be used to treat the cancer. EBRT uses a linear accelerator to focus powerful beams of X-rays to target the cells within the cancer. Radiation damages the DNA of these cells, preventing them from dividing [24]. Brachytherapy is a minimally invasive procedure, where small interstitial radioactive seed implants are placed within the PC [25] and can provide a 10-year disease-free survival [26]. Both treatments have given at best tumour regression without severe side-effects, but are not curative. Another option is cryotherapy, whereby a probe in which liquid nitrogen is circulated is inserted in the urethra in an attempt to destroy the cancerous tissue. Advances in recent technology including an urethral warming device and high-quality transrectal ultrasound guidance have improved the efficacy considerably, providing an encouraging 5-year disease-free survival [27].

1.5.1 Androgen Deprivation Therapy

While tumour growth is androgen dependent, PC can be effectively treated with androgen ablation. Although androgen ablation is the most effective treatment to date, it has not yet been shown to prolong survival [28]; in most cases decreased levels of androgens favour the selection and growth of tumour cells that are androgen-independent. The withdrawal of androgens by either physical or chemical castration often leads to regression of the disease, but patients tend to relapse after 12-18 months and develop Androgen Independent PC (AIPC), a lethal form of PC for which to date there is no cure.

Orchidectomy, the surgical removal of one or both testes used to be considered the standard ablation therapy for PC. Although the advantages of this procedure include cost

efficiency, low mortality and the avoidance of complications associated with drug therapy, they are heavily outweighed by the physical trauma and side-effects associated with castration.

Therapy by chemical castration involves the administration of luteinising hormone-releasing hormone (LHRH), or LHRH analogues, which bind to the receptors on the gonadotropes (pituitary gland), and can remain there for a period of up to 7-10 days. The binding causes a sudden increase in testosterone (a hormone flare) which initiates the negative feedback control in the hypothalamic–pituitary testicular axis, blocking further natural testosterone production which in time results in the decrease of circulating testosterone (Figure 1.5).

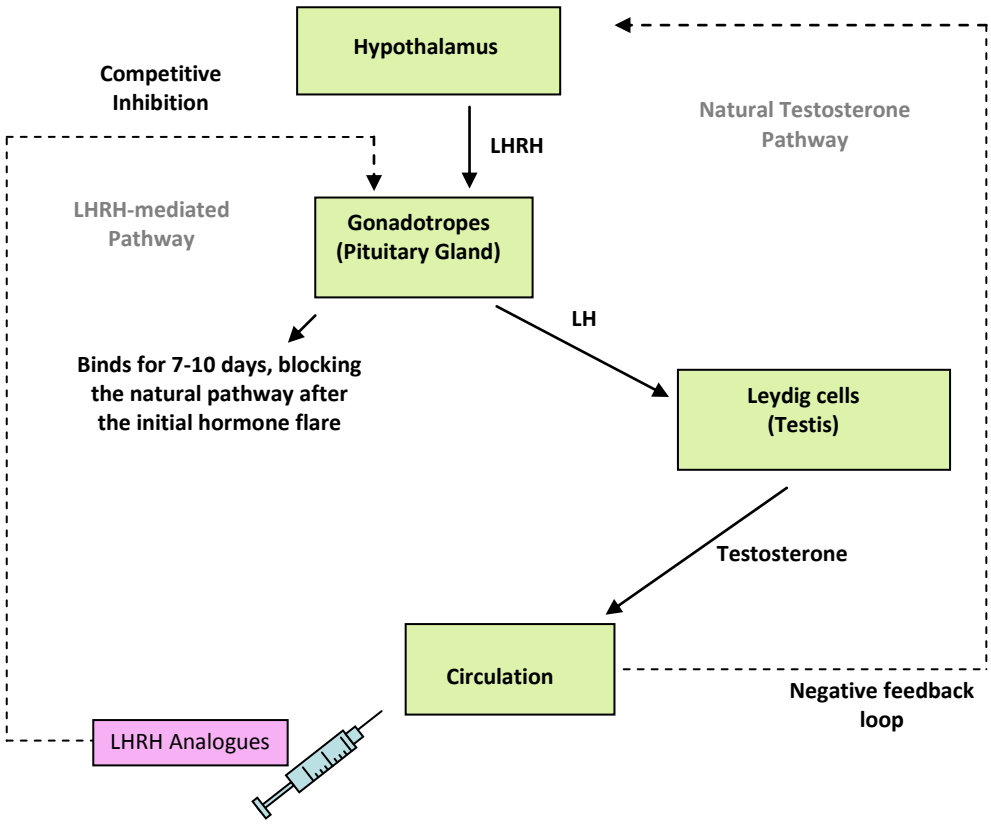

Figure 1.5: The hypothalamus secretes pulses of luteinising hormone-releasing hormone (LHRH) every 90-120 minutes, causing a chain of events that results in the production of testosterone. LHRH analogue administration binds to the gonadotropes, initially causing a hormone flare, but thereafter blocking the natural testosterone pathway, greatly reducing the level of circulating testosterone.

1.5.1.1 Hormone-Refractory PC

Fundamental changes in the AR signalling pathways occur during prostatic carcinogenesis after andogen ablation therapy, altering the suppression of growth: AR binding in the nuclei of malignant cells no longer suppresses continuous growth. Prostate cancer cells can divert stromal control and change from the paracrine pathway (Figure 1.3) to an autocrine one, whereby the cancer now neither relies on external androgens nor on androgen-induced stromal-mediated factors for its growth and survival, and the AR directly stimulates the growth of malignant cells (Figure 1.6).

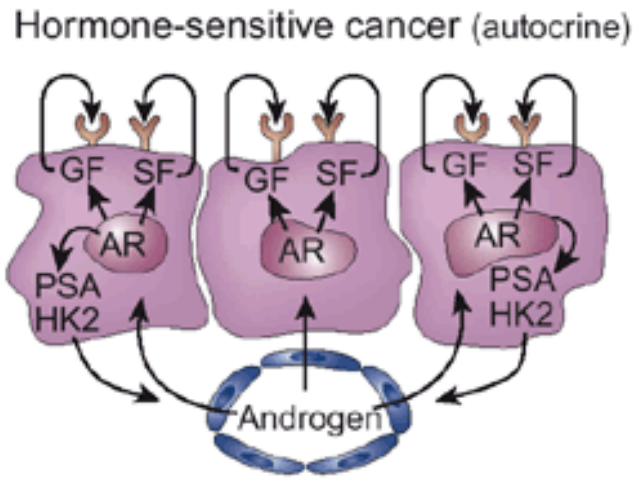

Figure 1.6: Autocrine Pathway: During the transformation to cancer, the paracrine pathway is lost and is replaced by an emergent autocrine mechanism, whereby cancer cells are less dependent on stromal cell factors. Production of growth and survival factors is directly stimulated by cancer cells when androgens interact with AR [12].

It is still not fully understood what triggers the development of AIPC, but the cancer's unique ability to rely on androgens for growth and avoid apoptosis, allowing the early formation of tumours, has been the target of many therapies. While androgen ablation therapy initially causes tumours to regress, they eventually become androgen-independent and unresponsive to the therapy. Genetic modification may be responsible for tumour progression and the emergence of AIPC. Five possible mechanisms have been proposed by which AIPC can develop: the hypersensitive, promiscuous, outlaw, bypass and lurker cell pathways (Figure 1.7).

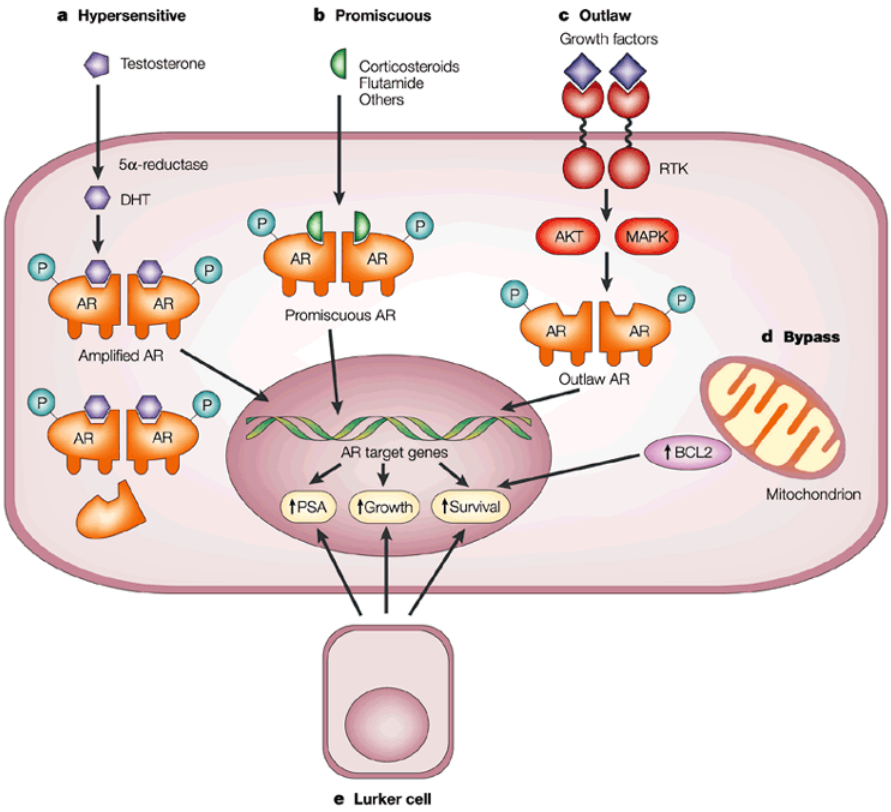

Figure 1.7: Five possible pathways to androgen independence [9], which directly or indirectly affect the activation of AR.

The hypersensitive pathway: A possible mechanism by which PC circumvents the effects of androgen ablation could be by increasing the sensitivity to low levels of androgens. Neither chemical nor surgical androgen ablation can fully prevent low levels of androgen production by the adrenal gland. The cancer exploits these low levels by amplifying its expression of AR, thereby increasing the ligand-occupied receptor content [29]. Up to 30% of tumours that have become AIPC after androgen ablation have AR genes that have been amplified over the levels observed in the primary tumours of the same patient, indicating amplification of the receptor, possibly by clonal selection. As well as amplification, increased AR sensitivity is possible, with increased stability and enhanced nuclear localisation, but also increasing the local production of androgens to compensate for the decline in circulating testosterone, by increasing the rate of conversion of testosterone to the more potent DHT via an enhanced 5α-reductase activity [9].

Reductions of 95% in serum testosterone levels have in fact been observed, though with increases in DHT concentration of only 60% [30, 31].

The promiscuous pathway: This is where genetic changes in the AR show a decrease in specificity of ligand binding and an increase in inappropriate activation by various non-androgen steroids and androgen antagonists [29]. The androgen signal is maintained by this broadening of the range of ligands that can bind and activate the receptor.

The outlaw pathway: The AR becomes activated by ligand-independent mechanisms, creating an outlaw receptor. Certain growth factors such as insulin growth factor 1, keratinocyte growth factor and epidermal growth factor have been found to bind and activate the AR. It is not clear whether these factors have a direct effect on the AR pathway, or whether the effect is a result of a downstream molecule that is induced by the signalling pathway. Receptor tyrosine kinases (RTKs) are activated, and the AR is phosphorylated, either by the AKT (member of the protein kinase B family) or the mitogen-activated protein kinase (MAPK) pathway, producing a ligand-independent AR [9].

The bypass pathway: Another possibility is, that complementary or alternative pathways can be evoked that are capable of by-passing the AR completely. The anti-apoptotic protein B-cell lymphoma 2 (BCL2) can obviate the need for AR or its ligand [29].

The lurker cell pathway: Androgen ablation fails as a result of cells that are not androgen-dependent for growth, which take over and drive the formation of the tumour in an androgen-independent manner. AIPC development has been postulated to be due to a sub-population of androgen-independent tumour cells present before any treatment was initiated; thus their rates of proliferation and death are not affected by androgen ablation, and when androgen-dependent cells began to apoptose as a result of treatment, these lurking epithelial stem cells remain viable and continue to proliferate, driving the formation of an androgen-independent tumour [32]. An example of such pathway has

been shown with neuroendocrine cells, which are widely distributed throughout the prostate gland and produce a number of bioactive substances which constitute a complex mechanism that regulates growth and differentiation of the developing prostate and secretory processes of the mature gland. Only 1% of all cases of prostate cancers exclusively contain neuroendocrine cells, they are dispersed individually or in small clusters throughout prevailing population of malignant cells. Neuropeptides such as bombesin and growth factors produced by neuroendocrine cells are thought to interact with neighbouring non-neuroendocine cells and cross activate androgen-dependent mitogenic pathways in the absence of testosterone [33]. Neuroendocrine cells do not express the AR and continue to proliferate despite androgen ablation and can be responsible for androgen-independent re-growth in PC [34].

A new pathway has recently been proposed which would help to explain proliferation and growth in androgen-independent PC. The *backdoor pathway* is the formation of DHT from progesterone, instead of from testosterone by the action of 5α-reductase. [35]. This pathway suggests that cancer cells can synthesise androgens *de novo* when androgens are not available from the bloodstream [5, 31].

1.5.1.2 Other Treatments

In the last decade, three agents have been approved by the Food and Drug Administration (FDA) in the USA for the treatment of patients with metastatic prostate cancer viz. zoledronic acid, mitoxantrone and docetaxel. Zoledronic acid and mitoxantrone provide palliative treatment without any advantage to overall survival, while docetaxel is a chemotherapeutic agent which has shown in combination with prednisone, to improve the quality of life dramatically and to improve survival rates, more so than mitoxantrone with prednisone [36].

1.5.1.3 Antibody Therapy

Antibodies were first approved for treatment of cancer in 1995. Since then five have been approved for the treatment of cancer: Campath (alemtuzumab) for chronic lymphocytic

leukaemia; Herceptin (trastuzumab) for breast cancer; Mylotarg (gemtuzumab ozogamicin) for acute myelogenous leukaemia; Panorex (edrecolomab) for colorectal cancer, and Rituxan (rituximab) for non-Hodgkin's lymphoma [37]. Many others are currently in clinical trials.

This emergence of antibodies as therapeutics was made possible with the advent of technologies designed to overcome limitations of mouse monoclonal antibodies (mAbs) such as immunogenicity, inefficient effector functions, and short half-lives. Core technologies such as chimerisation and humanisation of mouse antibodies, and direct routes to high-affinity human antibodies using phage display libraries or transgenic mice, have opened up the possibilities of using antibodies to target cancer.

Most clinically-approved antibodies and experimental antibody drugs target tumour cells directly, therefore to increase the efficacy of these antibodies, the possibility has been explored of enhancing effector functions by direct and indirect arming or pre-targeting them with pro-drugs and radionuclides. Currently the most-explored strategy is direct arming, by linking antibodies that target antigens highly expressed only on tumour cells, to toxins [Mylotarg (gemtuzumab ozogamicin)] [38] or radionuclides [Bexxar (tositumomab) and Zevalin (ibritumomab tituxetan)] [37], which target antigens more highly expressed on tumour cells than on normal cells.

Most recently, Zhang and co-workers (2010) have developed a mAb F77 which targets a unique prostate-specific glycolipid, termed prostate cancer lipid antigen (PCLA) [39]. The authors found that PCLA is expressed predominately in the prostate, in both androgen-dependent and independent PC, considerably higher levels than in normal tissue by immunohistological studies, showing intense staining correlating with tumour grade. mAb F77 has been shown to modestly initiate direct cell death in PC cells, mediating complement-dependent cytotoxicity and antibody-dependent cellular cytotoxicity as well as significantly inhibiting androgen-independent PC3 and DU145 tumour growth in cells.

Radiolabelled F77 was also shown to specifically bind PC3 tumour-bearing nude mice and represents a possible radiopharmaceutical for both imaging and therapy [39].

1.6 PROSTATE-SPECIFIC MEMBRANE ANTIGEN

PSMA is a membrane-bound type II glycoprotein[3] of approximately 100 kDa in size, with an intracellular domain (amino acids 1-18), a transmembrane domain (amino acids 19-43) and an extensive highly glycosylated extracellular domain (amino acids 44-750; Figure 1.8) [40, 41].

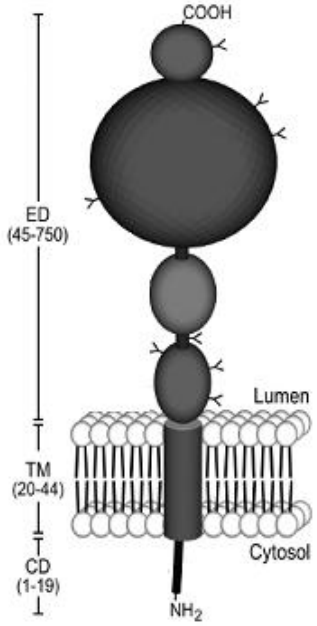

Figure 1.8: Schematic diagram of the globular nature of Prostate-Specific Membrane Antigen (PSMA). It has a small cytoplasmic domain (CD) which anchors it to the cell, a hydrophobic transmembrane domain (TM), and a large extracellular domain (ED) [40]. Y-shapes signify glycosyl groups.

PSMA, also known as folate hydrolase 1 (FOLH1), glutamate carboxypentidase II or N-acetyl-α-linked acidic dipeptidase I [42], is expressed in secretory cells within the prostatic epithelium and is absent or moderately expressed in most hyperplastic and benign tissue

[3] Bound to the cell membrane by the N-terminus

[43-45]. Although the significance of PSMA expression within the vasculature is unknown, PSMA has two unique enzymatic functions, folate hydrolase and NAALADase (cleaving the glutamate from the neurodipeptide, N-acetyl-aspasrtyl-glutamate, NAAG) [41]. NAAG is present in neuronal synapses while folypoly-γ-glutamates are present in dietary components. PSMA protein (folate hydrolase), which is located in the brush border surface of small intestine, enables the generation of folates and subsequent folate uptake [42, 46, 47]. However the specific biochemical function of PSMA in the prostate tissue and the reason for its increase in expression in PC remains unclear, in contrast to other prostate-related antigens, such as PSA and PAP, PSMA is not a secretory protein and undergoes internalisation constitutively [48]. However, at present no naturally-occurring PSMA ligand is known.

PSMA is expressed in healthy prostate [42, 49], immunohistochemistry studies have found weak to moderate staining in normal and hyperplastic tissue, restricted to the epithelial cells of the prostate [50], although the levels of expression increases considerably with PC and tumour aggressiveness, androgen-independence, metastatic disease and disease recurrence [51], Despite its name, PSMA is expressed in other tissues besides the prostate. Studies have demonstrated PSMA expression in the small intestine, proximal renal tubules and salivary glands [52]. Although present in other tissues, PSMA levels are 100-1000-fold greater in the prostate than anywhere else [43, 53]. Some minimal expression is also observed in the brain but most agents, particularly antibodies, do not penetrate the blood-brain barrier. Furthermore, PSMA is expressed in the neovasculature of numerous other solid tumours, including bladder, pancreas, lung and kidney cancers, but not in normal vasculature [45].

Mannweiler and co-workers (2009) found differences in internalisation of PSMA immunostaining that appeared to be related to the differentiation pattern of the tumour with 96% PSMA expression in primary tumours and 84% in metastasised PC [54].

PSMA has been identified as an excellent target and a good clinical biomarker for the diagnosis, detection and management of PC, because it is (i) primarily expressed in the prostate; (ii) is progressively increasingly expressed in high-grade cancers, metastatic disease and AIPC; (iii) up-regulated in metastatic disease; (iv) presented at the cell surface but not released into the circulation, and (v) internalised after antibody binding by receptor-mediated endocytosis [55, 56]. Moreover, PSMA protein is expressed as a homodimer on prostate epithelial cells and is not secreted into the circulation; therefore it exhibits an extensive extracellular domain to be readily targeted.

1.6.1 PSMA Antibodies

A number of anti-PSMA antibodies have been evaluated, a few having entered clinical trials as well as currently being under development. mAbs have the advantage of possessing specificity and high affinity for their molecular target, as well as their ability to initiate immunological effects, block receptors, or be used as vehicles to deliver highly cytotoxic radionuclides, drugs or toxins to the desired cell population [56].

Although PSMA represents an attractive antigen for therapy due to its abundance and restricted surface expression on prostate epithelial cells, in contrast to other tumour-associated antigens, there are few approaches that use PSMA. Only a few reports have appeared that propose using monoclonal antibodies and scFv that bind to cell-adherent PSMA [57-62].

The first mAb against PSMA, reported by Horoszewicz *et al* (1987), was 7E11, which recognised the internal domain of the N-terminus of PSMA [63, 64]. The first IgG1 mAb which they described, termed 7E11-C5.3, was generated using cell membranes from the cell line LNCaP to immunise mice and form hybridomas [63]. This mAb showed specific binding to PSMA presented on PC tumour tissue, benign prostatic hyperplasia (BPH)[4], and healthy prostatic tissue in immunohistochemistry analysis [43]. ProstaScint® (Capromab Pendetide, Cytogen, Philadelphia), the [^{111}In]-labelled form of 7E11, is a commercially

[4] Enlargement of the prostate, not cancerous

available monoclonal antibody conjugate. Capromab Pendetide received FDA approval in 1996 for use as an imaging agent for the detection of soft tissue metastases in PC. It is utilised either at the time of initial diagnosis or in the setting of suspected recurrent disease [65]. The radiopharmaceutical is administered by intravenous injection, and SPECT imaging is performed between 3-7 days post injection, allowing visualisation of the PC and any metastasis [66]. Questions have arisen concerning the value of *in-vivo* imaging with ProstaScint®, as the antibody only recognises the internal, cytoplasmic domain of PSMA, which is exposed only in dead or apoptosising cells, as opposed to the viable cells within the tumour; a drawback that certainly limits the value and applicability of this radiopharmaceutical, as it is important to know where new and existing tumour growth exists. Murphy and co-workers (1997) addressed this question by FACS analysis of viable LNCaP cells, and concluded that these cells specifically bound and internalised FITC-labelled 7E11-C5.3 antibody over cells of the non-PSMA expressing lines DU145 and PC3 [67]; however this antibody retains its reputation as binding to internal, cytoplasmic domain of PSMA.

Liu *et al* (1997) developed four IgG mAbs to the external domain of PSMA which were found to be reactive to vascular endothelium within a number of carcinomas, but not to normal endothelial cells [68]. One of the four, J591, showed improved reactivity over that of 7E11, and has been taken forward for a number of clinical trials with a range of radionuclides. Clinical trials have proven successful; specificity has been demonstrated to PC tumours including those in bone, soft tissue metastases, and importantly non-immunogenic [69].

In one such clinical trial, designed primarily to define dose and toxicity rather than anti-tumour response, [^{90}Y]-labelled J591 also demonstrated anti-tumour activity, reducing PSA levels by as much as 85% and measurable tumour lesions by 90% for periods of up to and beyond eight months [70]. Another group, Elsässer-Beile and co-workers [62, 66], have generated three mAbs (3/A12, 3/E7 and 3/F11) against PSMA with strong and specific affinity for the large extracellular portion. After binding, these mAbs were internalised by

PSMA-expressing PC cells, and showed immunohistochemical activity to frozen sections of prostatic tissue, but no reactivity to normal non-PSMA expressing human tissues. In preclinical studies, these mAbs have also revealed high and specific tumour uptake in PET imaging studies [66].

Although mAbs to PSMA are available, much interest has been focused on smaller antibody fragments viz. scFv, diabodies, triabodies and Fabs, which have the advantage of displaying improved tumour penetration and rapid clearance from the circulation. However, to date, only Elsässer-Beile and co-workers have published and successfully generated a PSMA-specific scFv in the form of a bispecific diabody for detection [7], and a scFv-immunotoxin for treatment [71], using respectively Quadroma Technology[5] and Phage Display. Both approaches use PSMA as the targeting antigen. For treatment, one approach employs CD3, which increases antigen-specific cytotoxicity in T-cells (potent effector cells), which on coming into contact with their target, release the cytotoxins perforin and granulysin. Perforin forms pores in the target cell's plasma membrane, allowing the entry of granulysin (a serine protease) activating the caspase cascade. The second approach utilises the immunotoxin *Pseudomonas* exotoxin A which, once internalised by the cell, catalyzes the transfer of the adenine ribosyl moiety of adenosine diphosphate from nicotinamide adenine dinucleotide to elongation factor 2, which results in the inactivation of the latter and the inhibition of protein biosynthesis [72]. Further investigation of PSMA binding is needed to exemplify its true potential as a target for therapy in PC.

As well as generating antibodies against PSMA, the possibilities of developing a vaccine for PC are currently under investigation. Dendritic cell (DC)-based vaccines hold promise as a safe therapy for PC. PSMA has been employed as a tumour-associated antigen (TAA) presented by DC-triggering naïve $CD8^+$ cytotoxic T lymphocytes, which are capable of recognising and destroying tumour cells that expose peptides derived from TAAs in

[5] Quadroma Technology is based on the somatic fusion of two different hybridoma cell lines expressing murine monoclonal antibodies with the desired specificities of the bispecific antibody.

complex with human leukocyte antigen (HLA) class I molecules [73-75]. Tumour proteins such as PSMA can be administered to the patient to stimulate DC activation, whereby PSMA is presented to T cells in the lymph nodes. Alternatively, DCs can be loaded *ex vivo* with the respective tumour antigen preparation, and injected into the patient as a DC vaccine. Garetto and co-workers have successfully selected PSMA peptides that show detectable binding to mature DC and are able to show co-localisation of PSMA and HLA class I molecules [73].

1.7 ANTIBODIES

Intact antibodies (IgG, IgM, IgA and IgE) are highly specific targeting agents. The Y-shaped multidomain protein possesses two antigen-binding sites located on the two Fab tips, and the framework Fc domain mediates the recruitment of effector functions [75]. IgGs are bivalent in their ability to bind two antigens, which increases their functional avidity and confers higher retention times on many-cell surface receptors. IgGs can be dissected into constituent domains by proteolysis using enzymes such as papain and pepsin, and recently advances in molecular biology have enabled small monovalent (Fab, single chain Fv, single variable V_H and V_L-domain) and bivalent (Fab'2, diabody and minibody) fragments to be made. Many of these smaller antibody fragments have successfully entered clinical and preclinical trials. Although they are not curative alone, many have been utilised as vehicles, conjugated to radionuclides [65, 76], toxins [56] or immunological effector cells [61] (Figure 1.9).

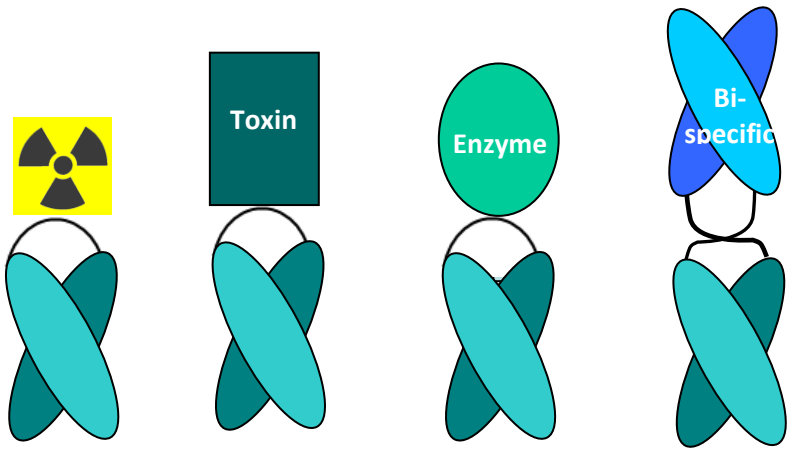

Figure 1.9: Current uses of antibodies and their analogues in cancer. Attachment to a range of derivatives can be beneficial for both imaging and therapy. This present project focuses on imaging with a radioactive isotope and the remainder of the introduction will focus on imaging using radiolabelled antibodies [77].

The present project focuses on imaging (see Figure 1.9), and the remainder of this introduction will focus on imaging using radiolabelled antibodies and peptides. mAbs however, are not ideal for imaging, due to their large size (150 kDa) and consequent poor tissue penetration. Although tumour specificity *In vivo* is observed; less than 1% of the injected dose normally reaches the tumour [77], therefore mAbs are not ideal vehicles to use for imaging with radioactive isotopes (Figure 1.10).

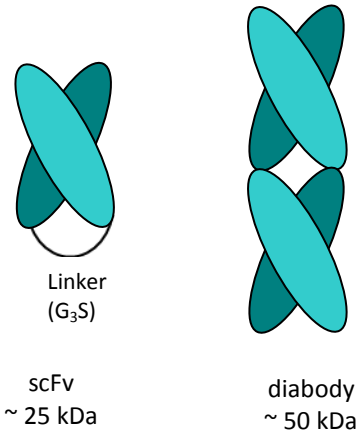

Figure 1.10: Schematic representation of scFv and diabody antibody formats, respectively ~25 and ~50 kDa. The formation of the diabody is driven by the removal of the polypeptide (glycine-serine) linker.

Single-chain Fv (scFv), ~25 kDa in size, are popular formats in which V_H and V_L domains are held together with a flexible 15-amino acid glycine-serine linker $(G_4S)_3$. ScFvs are advantageous over whole intact antibodies as they show specific binding, exhibiting improved pharmacokinetics of tissue penetration and high-affinity binding [78]. Although considerably smaller than mAbs, they retain full antibody activity and are easily cloned and expressed as functional antibody fragments on the surface of bacteriophages [77]. Manipulations of the linker by shortening, or its complete removal between the V_L and V_H domains, prevent the alignment of the V-domains into a single scFv, but allow the association and non-covalent interaction of two scFv molecules so as to form a dimer or diabody. This interaction, however, does not result in covalent linkage, and the two scFv fragments can therefore easily dissociate. Larger divalent molecules termed minibodies can be produced by fusing the gene for an scFv to that for a C_H3 domain [79]. Minibody formats confer an advantage over scFv and diabodies due to the greater stability of the protein complex.

A diabody ~50 kDa in size is a scFv dimer with two functional paratopes, which therefore has higher avidity than a single scFv alone. The association of three or four scFv fragments can respectively form a triabody or a tetravalent tetrabody. Diabodies are advantageous over scFv due to their increased binding avidity; possession of two paratopes increases the binding affinity and the increase in size slows the rate of systemic clearance from the target tissue.

1.8 PHAGE TECHNOLOGY PRINCIPLE

Smith (1985) first described Phage Display, using a non-lytic filamentous bacteriophage for the display of specific binding peptides on a phage coat [80]. Further development of the methodology was enhanced by groups such as those of Winter [81] and Wells [82]. Phage display involves the expression of proteins, including antibodies, or peptides on the

surface of filamentous phage. DNA sequences of interest can be inserted into the genome of a filamentous bacteriophage, such that the encoded protein is expressed or "displayed" on the phage surface as a fusion product to one of the phage coat-proteins [83]. This eliminates the need to genetically engineer proteins or peptide variants one-by-one and then express, purify and analyse each variant, phage display libraries containing several billion variants can be constructed simultaneously [84]. Screening of these libraries can easily select and purify phage particle bearing sequences with desired binding specificities from the non-binding variants. Antibody phage display technology allows foreign DNA inserted into the filamentous phage gene III to be expressed as a fusion protein and displayed on the surface of a phage as well as successful expression of functional antibody fragments in the periplasmic space of *E. coli* (Figure 1.11) [83].

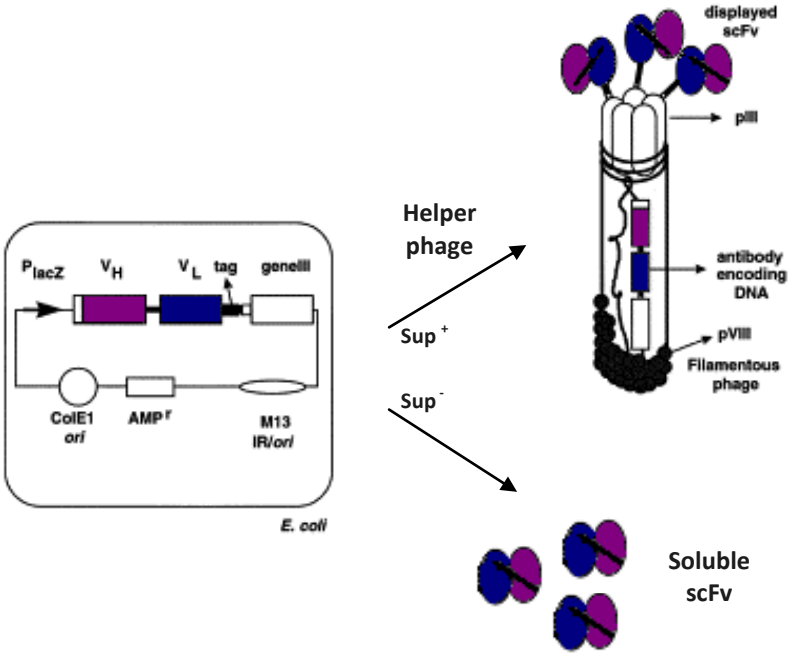

Figure 1.11: Display of scFv antibodies on filamentous phage. A phagemid encoding the V_H and V_L immunoglobulin genes fused to gene III (encoding the phage coat protein III) of a filamentous phage is superinfected (rescued) with helper phage to drive the production of phage particles expressing scFv in *E. coli* strain TG1 [a non-suppressor strain (sup+)], as a fusion product with the phage coat protein pIII on the phage surface and its encoding DNA inside (in colour). Alternatively it can be secreted as soluble fragments by the use of a non-suppressor strain [*E. coli* HB2151 (sup-); see the section Phagemid vectors below]. Key: P lacZ - the promoter that drives expression of antibody-pIII fusions; Tag - either the myc or his tag that is used in purification; AMPr – ampicillin resistance gene [85, 86].

1.8.1 Filamentous Phage – M13 Biology

M13 phages consists of a helical structure which has five types of constituent coat proteins: major coat protein pVIII, which constitutes the rod-shaped body of the phage particle and four minor coat proteins, pIII, pVI, pVII and pIX located at the ends. Incorporation of exogenous DNA into the phage genome results in display of the protein (such as scFv) on the surface of the phage particle without affecting its infectivity. The exogenous sequence is usually inserted into the gene encoding coat protein pIII, the resultant protein being anchored at the N-terminal end of the pIII coat protein [83]. This protein anchored on the viral scaffold corresponds to the insert inside the phage, therefore phage particles isolated from a library can be easily characterised by DNA sequencing (Figure 1.11). This linkage of genotype to phenotype is the fundamental aspect of phage display [87].

Infection is initiated by the attachment of pIII to the f pilus of a male *E. coli* strain such as TG1. Only the circular phage single-stranded (ssDNA) enters the bacterium, where it is converted by the host DNA replication machinery into a double-stranded plasmid-like replication form, which undergoes rolling circle replication to make ssDNA [87]. Phage progeny are assembled by packaging ssDNA into protein coats, and are then extruded through the bacterial cell membrane into the medium [83]. The genome is therefore replicated by interaction of both phage and host-derived proteins and packaged into elongated filamentous viral particles [88]. A distinctive trait of filamentous phages is that once they infect their host, they do not lyse the cell; instead, in contrast to phages such as T4 and T7, they replicate and are released through the cell membrane while the host cell continues to grow and divide.

Recombinant antibodies and folded proteins are typically expressed as pIII-fusion proteins and are displayed at the tip of the M13 phage, which enables its visualisation since after antibody binding to the target antigen; the bound phage can be detected with an HRP-labelled antibody which recognises the g8p coat protein. Amplification of the detection

signal is consequently achieved, since several thousand copies of g8p exist on the phage surface [83].

1.8.2 Phagemid Vectors

Phagemids, a popular vector for display, are hybrids of phage and plasmid vectors. Phagemid vectors are designed to contain the origins of replication[6] for both M13 phage and *E. coli* in addition to gene III, appropriate multiple cloning sites, and an antibiotic resistance gene[7]. However, they lack all the other structural and non-structural gene products required for generating a complete phage. The addition and aid of a helper phage such as M13K07 or VCSM13, provides the structural proteins that are required for generating a complete phage particle; this process is termed "phage rescue" [87].

Phagemid vectors can also be engineered for display or for secretion of free antibody by the incorporation of an *amber* stop codon between fragment and gene III. The antibody fragments are fused by pIII and displayed when the *amber* stop codon is suppressed in a suppressor strain of *E. coli* such as TG1 [89]. To produce soluble scFv, the infection of a non-suppressor strain of *E. coli* such as HB2151 with antibody-positive phage will directly produce soluble scFv (Figure 1.11) [90]. The phagemid is also designed to introduce a poly-histidine tag fused to the expressed scFv, thereby allowing the rapid and simple purification of the protein by Ni-NTA affinity chromatography [83].

Phage display selection allows *in vitro* isolation of proteins and antibodies such as Fabs and scFvs with the desired properties or selection of natural proteins from vast numbers of phage particles. Greater than 10^{12} different displayed sequences can easily be selected from at the same time, considerably more than conventional hybridomas that screen only 10^2 -10^3 clones. Since the selected phage pool can be amplified by propagation in *E. coli*, multiple rounds of selection can be carried out to select antibodies with the strongest binding affinity to a target antigen, in which the antigen of interest is either immobilised in

[6] A particular sequence in the genome at which replication is initiated
[7] Appendix I

the form of a purified protein, or as membrane-bound protein on cells. As a consequence of this, even very rare binding specificities present in large repertoires can be selected and amplified from a background of phage bearing irrelevant binding specificities [88].

1.8.3 Antibody Phage Display Libraries

In many diagnostic and therapeutic applications, phage display technology of antibody fragments is rapidly replacing the classical hybridoma technology, due to the advantages over earlier techniques. Advances in molecular biology have allowed for the use of *E. coli* to produce recombinant antibodies. By restricting the size of the antibody to either a Fab, an Fv or a linker-stabilised scFv, such fragments can not only be expressed in bacterial cells but also displayed by fusion to phage coat proteins [91].

There are a number of phage libraries available for successful antibody fragment selection to a large range of target antigens [92, 93], such as immune, single pot [94], naïve and synthetic libraries [90, 95]. Immune libraries contain variable immunoglobulin genes of B-cells from an animal or an immune patient. They are enriched in antigen-specific immunoglobulin domains, some of which have already been matured by the immune system [96]. In synthetic libraries such as the one used in this project (Tomlinson I, based on a single human framework for V_H (DP-47) and Vκ (DPK9))

[*see* www.geneservice.co.uk/products/proteomic/datasheets/tomlinsonIJ.pdf]

combinatorial diversity is introduced into a limited number of antibody scaffolds by substituting degenerate complementarity-determining regions (CDRs) within a fixed antibody sequence. The specificity of any antibody resides in the six CDRs that shape the antigen binding sites [97]. There are three CDRs on each of the variable-heavy and -light chains. Structural studies have shown that five of the six CDRs have limited structural variation. The CDR3 of the heavy chain (V_H-CDR3), the most diverse loop in composition and length is estimated to have a potential diversity of 10^{23} sequences, and it is the most central to the antigen-binding site of all CDRs [98].

To improve antibody affinity, various *in vitro* strategies have been optimised to mimic the mammalian *in vivo* process of somatic hypermutation and selection [99]. These include site-specific mutagenesis, combinatorial mutagenesis of CDRs, random mutagenesis of the entire gene, mutator strain, error-prone PCR or chain shuffling [78]. In the immune system, antibodies are produced either by plasma cells that have differentiated from naive B cells which have encountered and bound to an antigen, or by long-lived memory cells, which produce antibodies with improved binding affinity due to hypermutation [85]. Technologies for making antibodies *in vitro* by imitating the selection strategies of the immune system have emerged. The use of filamentous bacteriophages with their ability to display single antibody species on the surface have allowed the production of soluble antibody fragments, which are secreted from infected bacteria. As in the immune system, the V genes can be subjected to random mutation which may generate species with higher binding affinities for selection.

1.8.4 Generation of Small Antibody Fragments

Antibody libraries displayed on phage have successfully been used in both scFv and Fab formats. Fab fragments are usually more stable than Fv fragments, as the latter tend to dissociate because of the lack of covalent or disulphide bonds between the two chains. The expression of the scFv fragment has less toxic effects on the producing cells than larger Fab molecules, resulting in better yields and diversity in scFv libraries (Figure 1.10) [89]. Expression in *E. coli* ensures that sufficient quantities of scFv can be easily produced. Many secreted eukaryotic proteins such as antibodies require disulphide bonds for stability, and the oxidising environment of the *E. coli* periplasm, where filamentous phage assembles, provides the appropriate conditions for antibody folding [90]. For tumour imaging using immunoscintigraphic techniques, the use of whole antibodies is not ideal, due to their slow blood clearance and their uptake by the liver. Smaller antibody fragments, such as Fab and scFv, may be utilised instead, as these are cleared rapidly through the kidneys [88].

Phage display has identified a number of antibody fragments against a range of diseases. A highly characterised scFv, MFE-23, was selected using phage display by Chester and co-workers against carcinoembryonic antigen (CEA), a tumour-selective marker which is highly expressed in a range of cancers including most gastrointestinal, breast, lung and ovarian carcinomas [84]. MFE-23 scFv is the most characterised scFv and was the first to enter clinical trials. The safety and efficacy of radiolabelled MFE-23 for imaging CEA-expressing tumours in a cohort of 10 patients, was examined using [^{123}I]-MFE-23. It showed stability and rapid clearance from the blood, with specific uptake seen in the tumour, although high uptake by the kidneys was also observed [76]. Thirteen scFv have been selected against carbonic anhydrase IX (CAIX) a biomarker for the early stages of renal clear cell carcinoma (RCC) but not in corresponding normal tissue, allowing for the potential development of new immunotherapies for the treatment of RCC [100]. Phage display on LNCaP C42B cells selected scFv against intercellular adhesion molecule 1 (ICAM), which upon binding to ICAM effectively blocks prostate cancer invasions *in vitro* through extracellular matrix components [101]. A number of antigens expressed in hormone-refractory PC were screened and one identified as the activated leukocyte cell adhesion molecule (ALCA) by immunohistochemistry, its potential advantages in screening PC is still under evaluation [102]. scFv against PSMA has been successfully selected by Elsässer-Beile and co-workers and its potential for therapy has been evaluated by the conjugation of immunotoxins [56].

Despite the advent of smaller antibody fragments which provide faster delivery vehicles, mAbs are not yet redundant and are still used to target and deliver potent drugs such as ibritumomab tiuxetan (Zevalin) and [^{131}I]-tositumomab (Bexxar), and one drug conjugate, gemtuzumab ozogamicin (Mylotarg). Although mAb larger size means slower clearance from the blood supply and poor tumour delivery, they still show improved affinity over smaller antibody fragments (scFv and Fabs) [103]. A balance between high affinity binding and improved tumour penetration and rapid clearance has been addressed by the engineering of antibody fragments such as scFv, diabodies Fabs and minibodies which have shown improved tissue penetration as well as affinity.

1.9 PEPTIDES AND CANCER IMAGING

Over the last 30 years, monoclonal antibodies have been hailed as magic bullets for imaging and treating cancer. The difficulties previously experienced with the use of whole antibodies were overcome when smaller antibody fragments showing improved binding and penetration became available, and peptides have since attracted interest due to their relatively small size (1.5 kDa) and high affinity binding.

Peptides are molecules ranging from 2 to 50 amino acids in length linked together by peptide bonds. Unlike proteins, small peptides generally lack a well-defined three-dimensional tertiary structure. They can exist naturally, but more importantly can also be designed synthetically as novel molecules [104]. Due to their molecular structure and small size, peptides have a number of potential advantages over antibodies. Their hydrophilic nature and small size allow for rapid tissue permeation after systemic injection, and rapid elimination from the body by either the renal or the hepatobiliary route. They are relatively stable molecules that can withstand harsh modification and radiolabelling conditions in aqueous solution; however peptides are particularly sensitive to peptidases, which can rapidly degrade them in plasma unless modifications are introduced. They are also non immunogenic, readily radiolabelled, being suitably large enough to attach a radioactive isotope without affecting their binding ability.

1.9.1 Somatostatin Analogues

Somatostatin analogues were the first peptides to be exploited and are now commonly used for localising neuroendocrine tumours. Their high binding affinity and the subsequent internalisation of ligand-receptor complexes have proven valuable in detecting neuroendocrine tumours by nuclear medicine [105, 106].

Somatostatin is a regulatory tetradecapeptide which is endogenously produced by the hypothalamus and pancreas and has a wide spectrum of actions on multiple organs[107]. The most well defined biological activity of somatostatin is its inhibitory effect on the

secretion of numerous hormones, viz. growth hormone, thyrotropin, insulin, glucagon, vasoactive intestinal peptide and secretin and to date, radiolabelled analogues of somatostatin have been the gold standard for peptide-receptor imaging and therapeutic agents, with clinical success with [^{111}In]-DTPA-octreotide (Octreoscan® Mallinckrodt Medical Inc. USA).

1.9.2 Substance P

Substance P (SP), functions as a neurotransmitter, neuromodulator and a potent vasodilator. It is distributed through the central and peripheral nervous system and has been found in glial[8] tumours, medullary thyroid carcinoma and breast tumours. [^{111}In]-DTPA-Arg-SP has been synthesised for diagnostic imaging of SP receptor positive autoimmune diseases such as inflammatory bowel disease and arthritis as well as SP receptor positive neoplasms [108].

1.9.3 Vasoactive Intestinal Peptide

Vasoactive intestinal peptide (VIP), a neuropeptide which binds to two G-coupled receptors ($VPAC_1$-R and $VPAC_2$-R) has been identified in normal prostate cells and is over expressed in malignant prostate tissues [109]. VIP stimulates PSA and increases proliferation of prostatic epithelial cells in culture as well as increasing angiogenesis acting as a survival factor in androgen-independent PC cells. VIP induces neuroendocrine differentiation in LNCaP cells and protects from apoptosis in PC3, suggesting it is involved in prostate carcinogenesis and its evolution to a more aggressive form [110-112]. Rekasi and co-workers developed a series of analogues which have antagonistic properties (JV-1–50, JV-1–51, JV-1–52, and JV-1–53) to block the action of VIP and subsequently the proliferation of the cancer cells [113].

1.9.4 Neurotensin

Neurotensin (NT) is a 13 amino acid neuropeptide found in the brain and gut and is implicated in the regulation of LH and prolactin release. [^{125}I-Tyr^3]-NT selectively binds to

[8] Tumours of the central nervous system

endocrine pancreatic cancers over normal and chronic pancreatitis. Improved clearance was observed with [^{111}In]-DTPA [114].

1.9.5 Gastrin and Cholecystokinin

Gastrin and cholecystokinin (CCK), are gut-brain peptides with a number of roles in the gastrointestinal tract and the brain and bind with a strong affinity to CCK-B receptors. This receptor is over-expressed in a number of human tumour tissues, such as small cell lung cancers (SCLC), medullary thyroid carcinomas, gastrointestinal tumours and stromal ovarian cancers [115].

1.9.6 Bombesin Receptors

Bombesin (BN) receptors belong to the superfamily of G-protein-coupled receptors[9], characterised by the typical seven transmembrane domain [116, 117]. The bombesin receptors comprise the gastrin-releasing peptide receptor (GRP-R or BB2-receptor), the neuromedin B receptor (NMB-R or BB1-receptor) and the orphan bombesin receptor subtype-3 (BRS-3 or BB3-receptor). These receptors mediate the biological effects of bombesin related peptides. GRP-R is characterised by high binding affinity for gastrin-releasing peptide (GRP) and bombesin, whereas NMB selectively binds with only moderate affinity for NMB-R [118].

GRP-R mediates a variety of cellular responses which include modulation of smooth muscle contraction, secretion of gastric acid and pancreatic enzymes, regulation of body temperature and stimulation of cell growth [119]. GRP-R has been localised in the central nervous system and in peripheral tissue [120], and it is also expressed in a number of neuroendocrine and cancer tumours, ectopically in several human cancer cell lines such as prostate, breast, small-cell lung and colon carcinoma [116, 121, 122].

[9] G-protein-coupled receptors constitute a large and diverse family of proteins whose primary function is to transduce extracellular stimuli into intracellular signals.

Of particular clinical significance is the finding that there is a considerable receptor over-expression in neoplastic transformed prostate and breast tissue [118, 123]. After peptide binding to the GRP-R, a number of cellular signal transduction pathways are activated, such as MAPK, which result in cell proliferation and growth [124]. Extensive studies on GRP and its interaction with GRP-R have observed promotion of tumour growth in a number of normal and human cancer cell lines, both in culture and in nude mice xenografts [125, 126]. Antagonists have been developed as anticancer compounds that exhibit antitumour activity both *in vitro* and *in vivo*, by interfering with growth factor-signalling pathways such as epidermal growth factor (EFG) and vascular endothelial growth factor (VEGF) [127].

1.9.7 Bombesin Peptides

Bombesin, a tetradecapeptide, was first isolated from the skin of the European frog *Bombina bombina* in 1971 by Anastasi and colleagues [128]. The first bombesin-like peptide was isolated from porcine gastric tissue and named gastrin-releasing peptide (GRP) because of its potent gastrin-releasing action [128]. GRP belongs to the family of bombesin-like peptides neuromedin B (NMB) and amphibian bombesin (BB) [116]. GRP and bombesin share a highly-conserved 7-amino acid C-terminal sequence that is required for high-affinity binding to the GRP-preferring receptor [124]. BN-like peptides, including BN, GRP and NMB are involved in the regulation of a large number of biologic processes in the gut and central nervous system and mediate their action by binding BN receptors located on the cell membrane of target cells.

GRP is believed to function as a paracrine/autocrine growth stimulator in many cancers [129]. GRP-R is rarely detected in benign prostate hyperplasia and healthy prostate tissue [118], but high levels of these receptors have been seen in PC3 and DU145, androgen-independent cell lines from advanced stages of prostate cancer [33]. Due to the expression pattern and internalisation of GRP-R, it is potentially an early indicator of cancer and an attractive target for both radiotherapy and imaging; possibly GRP-R is an ideal target to image PC before and after treatment, to measure the course of the cancer.

GRP has also been shown to stimulate cell proliferation in PC3 cells and an antagonist of GRP-R can inhibit the growth of a number of prostatic carcinoma models [118].

Van de Wiele and co-workers first reported the radiolabelled targeting of breast and prostate cancers with a [^{99m}Tc]-bombesin conjugate, RP527 [130]. Several other bombesin radioligands have been developed and characterised both *in vitro* and *in vivo* by Volkert's group [131, 132] and the bombesin analogues Demobesins 1-6 have been developed by Nock and co-workers [116, 133].

Schroeder and co-workers [134] have determined peptide stability *in vivo*, biodistribution and GRP-R targeting potential by SPECT-CT of 5 radiolabelled bombesin analogues, antagonists PEPSIN, AMBA, MP2346 and MP2653 radiolabelled with $^{111}InCl_3$ and antagonist DB 1 radiolabelled with ^{99m}Tc. Biodistribution studies on PC3 tumour-bearing mice showed greater uptake of DB 1 than the 4 agonists, PEPSIN and AMBA were the most promising GRP antagonists with sufficient *in vivo* stabilities as well as high tumour uptake and retention. ^{177}Lu-AMBA (^{177}Lu-DO3A-CH_2CO-G-4-aminobenzoyl-Q-W-A-V-G-H-L-M-NH_2) was taken forward for phase I clinical trials. The agonist shows high affinity to GRP-R with 2-fold greater affinity to PC3 (K_d 1.02 nM) over LNCaP (K_d 0.656 nM) and DU145 (K_d 0.536 nM), promising for imaging and therapy over advanced PC [135].

1.9.8 Demobesin 4 (DB 4)

Demobesin 4, an agonist bombesin analogue, was selected for its ability to target GRP-R-positive tumours *in vivo* with rapid internalisation in PC3 cells [116], for use as a potential imaging and therapeutic agent. The hydrophilic nature of DB 4 has been demonstrated *in vivo* by its excretion via the kidney, and this combined with its specific binding to GRP-R thereby highlights its potential effectiveness in the diagnosis, staging and imaging of PC. DB 4 was modified at the N-terminal by coupling an open-chain tetra-amine framework for effective binding of ^{99m}Tc (Figure 1.15).

Tetra-amine-derivatised DB 4 was synthesised by piCHEM R&D, Graz, Austria, using solid-phase peptide synthesis (SPPS), employing 9-fluorenylmethyloxycyclocarbonyl (Fmoc) protection strategy, and supplied as a lyophilised powder at >95% purity.

Other bombesin analogues have been designed such as Demobesin 3, which is structurally similar to DB 4 as it is based on the full parent bombesin tetradecapeptide sequence after minor modifications. Demobesins 5 and 6 are truncated peptides and are more lipophilic, being based only on the essential residues needed for receptor interaction, the bombesin (7-14) motif. Both DB 4 and 6 have undergone substitution of the oxidation-sensitive methionine (Met^{14}) by norleucine (Nle^{14}) (Table 1.1) [116, 133].

Table 1.1: Analytical data for bombesin analogues, Demobesin 1 & 3-6. BB = bombesin [Pyr-Gln-Arg-Tyr-Gly-Asn-Gln-Trp-Ala-Val-Gly-His-Leu-Met-NH_2].

Peptide conjugate	Sequence	% Purity	Excretion	Interaction
Demobesin 1	[N_4-Bzdig,D-Phe^6,Leu-$NHEt^{13}$,des-Met^{14}]BB(6-14)	>96	Renal	Antagonist
Demobesin 3	[N_4^0, Pro^1,Tyr^4]BB	>98	Renal	Agonist
Demobesin 4	[N_4^0, Pro^1,Tyr^4Nle^{14}]BB	≥ 98	Renal	Agonist
Demobesin 5	[N_4-Bzdig)^0]BB(7-14)	99	Hepatobiliary	Agonist
Demobesin 6	[(N_4-Bzdig)^0), Nle^{14}]BB(7-14)	≥ 98	Hepatobiliary	Agonist

Other promising BN-analogues have been tested in preclinical studies using PC3-bearing mice include the DOTA-chelated compounds AMBA and Pesin and the DTPA-chelated compound MP2653 [136].

1.10 RADIOPHARMACEUTICALS AND CANCER

1.10.1 Therapy

Therapeutic radiopharmaceuticals are radiolabelled molecules designed to deliver therapeutic doses of ionizing radiation to targeted sites within the body. The treatment of

cancer with radiolabelled molecules has been in use for over the last 50 years [137]. Treatment of thyroid cancer, relief of bone pain associated with skeletal metastasis and neuroblastoma have been respectively treated with therapies such as [^{131}I]-sodium iodide, [^{89}Sr]-strontium chloride or [^{32}P]-sodium phosphate and [^{131}I]-metaiodobenzylguanidine (MIBG) [138].

The design and selection criteria for therapeutic radionuclides include; half-life, the types of emission (α, β, γ, auger or conversion electrons), specific activity, chemistry, internal dosimetry, radiation safety, energy and cost of production and availability. One of the most important parameters to take into consideration is the physical half-life which should be matched with the *in vivo* pharamacokinetics of the radiolabelled compound. With too short a half-life, most of the decay will have occurred before the compound reaches the target site, conversely, too long a half-life may cause unnecessary radiation dose to normal tissues during metabolism and excretion of the labeled compound [139].

The nature of the particulate emission is also important to consider, ensuring maximum therapeutic effectiveness. β-particles, α-particles and auger electrons all have different effective ranges and linear energy transfer (LET) properties. LET is the measurement of the energy deposited per unit distance over the path of the radiation (KeV/μm) [139]. β-particles are advantageous and the most popular choice as they have high energy electrons emitted from the nucleus and lower ionization density [138].

Radiation damage may occur by one of two ways; the direct action or indirect action. In the direct action, radiation may directly hit a particularly sensitive atom or molecule in the cell. The damage from this is irreparable, and the cell either dies or is caused to malfunction. In the indirect action, radiation can damage a cell indirectly by interacting with water molecules in the body causing free radicals. These free radicals can cause damage DNA. The cellular DNA damage leads to disruption in cellular function, mutation, and cancer [138].

1.10.2 Imaging

Imaging modalities can be broadly divided into primary anatomical and primary molecular imaging techniques. Computed tomography (CT), magnetic resonance imaging (MRI) and ultrasound are classed as primarily anatomical, as these techniques are limited by their inability to detect disease until the structural changes in tissue are large enough to be detected by these technologies [140].

Molecular imaging provides the visualisation, characterisation and measurement of cancer at both molecular and cellular levels. A number of new technologies directed at the diagnosis and treatment of a disease has been developed recently, which has enabled the production of internal images of the body. The use of preoperative parameters such as PSA and the Gleason score provide limited information of cancer stage and aggression, but little to no information about location or advancement and metastasis.

1.10.3 X-ray and Computed Tomography

X-rays, a form of electromagnetic radiation, are used as standard practice for skeletal imaging. The electron-dense bone and cartilage absorb most of the x-ray photons; the unabsorbed radiation generates radiographic images by photoelectric processes. This method, however, is not normally sufficiently sensitive for most soft tissues such as tumours, which may however show up as a shadowing on an x-ray film.

Computed Tomography generates 3-D images using digital geometry processing, whereby a series of 2-D x-ray images are taken around a single axis of rotation. The data obtained can be manipulated through a process known as windowing, allowing the visualisation of tumours, their depth and their location in respect to other tissues and organs.

1.10.4 Magnetic Resonance Imaging

MRI provides images similar to those obtained by CT, although with increased sensitivity, faster acquisition times and greater soft-tissue contrast. Unlike CT, it does not use ionising radiation (reduced risk to patients), but uses a powerful magnetic field to align the

nuclear magnetisation of (usually) hydrogen atoms in water in the body. Radio-frequency fields are used to systematically alter the alignment of this magnetisation causing the hydrogen nuclei to produce a rotating magnetic field detectable by the scanner; different tissues emit a more or less intense signal based on their structure and chemical composition [141]. With the combination of a paramagnetic contrast agent such as gadolinium, MRI can provide high sensitivity for the detection of vascular tissue (tumours), and permit assessment of brain perfusion in stroke patients [142]. However, concerns over the safety and toxicity of gadolinium-based contrast agents have been raised with regard to impaired kidney function.

1.10.5 Ultrasound

Ultrasound imaging has advantages over MRI and CT because of its moderate cost, real-time imaging and usefulness in making physiological measurements. It is a form of non-ionizing radiation with no known biological effects. Typical diagnostic sonographic scans operate in the range of 2-18 megahertz. A trade-off between spatial resolution of the image and imaging depth is a limitation of this procedure; although able to image soft tissues within the body, deeper structures such as the liver and kidneys have poorer resolution due to the lower frequencies employed. Improved images have recently been achieved using ultrasound Doppler techniques, which demonstrate the presence of blood flow by detecting a frequency shift in the radio-frequency signal reflected from moving blood. Ultrasound contrast agents containing encapsulated microbubbles[10] (small gas-filled microspheres with specific acoustic properties) have been used to image tumour microcirculation [140]. Microbubble contrast agents have been used to overcome problems of imaging microvasculature in the prostate [143].

Primary molecular imaging modalities such as optical imaging, positron emission tomography (PET) and single photon emission computed tomography (SPECT) offer the potential to detect molecular and cellular changes in disease, even before the tumour is

[10] Microbubbles are gas-filled agents that have a high degree of echogenicity (reflect ultrasound waves). The echogenicity between the microbubbles and surrounding soft tissue is considerable, enhancing the ultrasound backscatter, producing a sonogram with increased contrast.

large enough to cause structural changes. However these techniques do not possess very high spatial resolution, but this can be overcome by using an optimised combination of anatomical and molecular imaging modalities, such as PET-CT, PET-MRI and SPECT-CT, thereby combining the detection of pathophysiological changes in early disease by high structural resolution.

1.10.6 Positron Emission Tomography

PET, a technology which produces 3-D images of functional processes within the body, is far more sensitive than the anatomical imaging modalities previously mentioned. A tumour-targeting radiotracer is intravenously injected, and upon targeting the cancer, it emits positrons. The collision of a positron with an electron cause the release of two gamma photons at 180° to each other; this coincidence of events can be detected, reconstructed and analysed to determine the location and concentration of radiation within the body [144]. PET has been used to image a variety of different cancers, as well as neurological and cardiovascular conditions [145, 146]. PET can also detect increases in the metabolic activity of tumours with suitable radiotracers. The most common radiotracer in use is fluorine-18 bound to fluorodeoxyglucose ([^{18}F]-FDG), the principle being that tumours have an increased number of glucose transporters. These reflect the high metabolic rate of cancerous cells, due to their increased rate of cell division which is often supported by an increased level of glucose consumption in comparison with other cells [147]. Unfortunately, the uptake of ^{18}F-FDG is dependent on anabolic activity, and its incorporation into prostate cancer cells is not particularly high, because of their low metabolic activity [146].

1.10.7 Single Photon Emission Computed Tomography

Using a gamma camera, SPECT monitors the emission of single photons, acquiring 2-D images (projections) from multiple angles. These can, with the aid of specialised software, be applied to a tomographic reconstruction algorithm, yielding a 3-D dataset which can be further manipulated to show thin slices along any chosen axis of the body. The acquisition process is very similar to planar gamma camera imaging, therefore the same isotopes can

be used. The combination of SPECT and CT provide a very detailed and informative picture of the uptake of a radiolabelled ligand. CT greatly assists in orientating the uptake by certain organs, as without this, it would be much harder to know where uptake occurs, and to understand the biodistribution of the radioligand.

Improved attenuation correction, increased specificity as well as accurate depiction of the localisation of disease are many advantages of SPECT-CT. Endocrine and neuroendocrine tumours, such as pulmonary nodules can be visualised by this technology, a range of cancers including those of the lung, brain and prostate, as well as malignant and benign bone lesions and infection [148]. SPECT is also used for myocardial perfusion imaging (MPI), used for the diagnosis of ischaemic heart disease, and functional brain imaging for the diagnosis of dementia.

1.10.8 SPECT-CT and Research

Small-animal SPECT-CT has facilitated and greatly aided in the research of new radiopharmaceuticals and novel drugs. Imaging considerably reduces the number of animal models needed to obtain statistically significant data, as well as giving an insight into the biodistribution of an injected radiotracer in tumour-bearing models (Figure 1.12) [149]. Multiple pin-hole SPECT imaging provides <1 mm resolution in small animals, with good sensitivity. Fusion with CT images provides co-localisation of structural and functional information. CT images are particularly beneficial to aid in locating tumours that are growing subcutaneously [150].

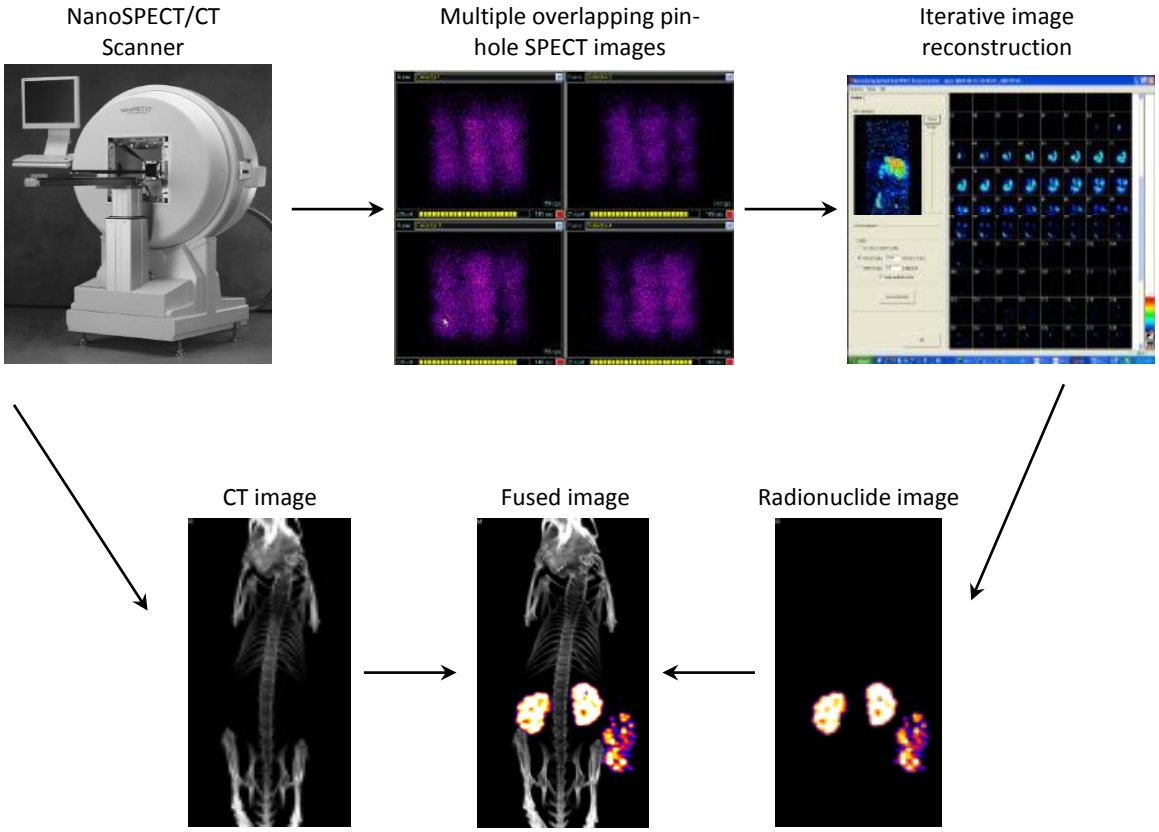

Figure 1.12: Principle of NanoSPECT-CT, showing the combination of anatomical and molecular imaging of tumour-bearing mice [150].

SPECT imaging enables visualisation of the *in vivo* distribution of the radioligand. Scanning of animal models such as mice at various times (dependent on the isotope of choice) following dosage permits visualisation of the uptake into organs and tumours.

Dynamic acquisition (continuous repetitive rotation acquisition) allows the monitoring and tracking of a radiolabelled ligand from the time of administration. It enables one to understand the kinetics of distribution and clearance of the radioligand. Typically, the mouse is placed on the SPECT bed before intravenous injection of the radioligand, then scanned over a set period of time following the injection. The data acquired can be transferred to a video format, allowing for visualisation of the behaviour of the ligand *in vivo* over time.

SPECT-CT was used for *in vivo* imaging studies with both radiolabelled antibody fragments and peptides during the course of this study.

1.11 RADIOPHARMACEUTICALS

Isotopes selected for imaging should have the following characteristics: they should be pure γ-emitters with little to no particulate emission. They should have a suitable emission-energy (typically 100-250 keV) and should be chemically reactive to allow incorporation to selected ligands. The half-life should be comparable with or less than the half-life of the pharmaceutical under study, and finally they should be non-toxic.

1.11.1 Iodine Chemistry

Radiohalogenation is one of the most commonly used procedures for radiolabelling proteins and peptides, since halogens form stable covalent bonds with carbon atoms, and there is a good understanding of halogen chemistry. Minimal alterations to peptides and proteins are caused because of the steric properties and electronic nature of halogens, enabling radiolabelling to be accomplished to high specific activities. ^{123}I, ^{125}I and ^{131}I are extensively used for scintigraphic imaging due to their relative low cost and wide availability [151].

Direct labelling of tyrosine residues is the most favoured approach to radiohalogenation of peptides, and in the absence of natural tyrosine residues, the substitution of Tyr for Phe can be incorporated to produce analogues, or Tyr can be added to the sequence at sites not critical for biological activity or receptor binding [152]. Radiohalogens must be oxidised to form an electrophilic species to enable radiolabelling. Oxidising agents such as Chloramine-T (N-monochloro-*p*-toluene-sulphonamide) [153], Iodogen[11] [154] and N-halosuccinimides (Figure 1.13) are commonly used. The reactive species generated by any of these oxidants is then incorporated into a reactive aromatic amino acid residue of the

[11] Chapter 2 - section 2.2.11.1

peptide (preferentially tyrosine). Removal of unreacted radio-iodine from the reaction mixture can be accomplished by separation techniques such as reverse- and normal-phase chromatography, and size-exclusion chromatography [151].

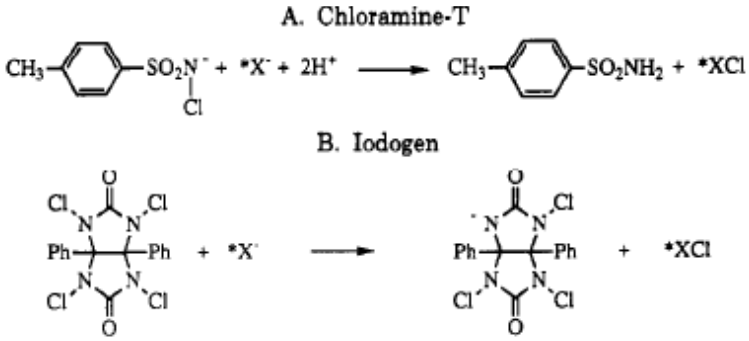

Figure 1.13: N-haloamine oxidising reagents. X = fluorine, bromine, iodine or astatine.

One disadvantage of this approach can the difficulty of obtaining a mono-iodinated product from Tyr, because the ring tends to iodinate in both the *ortho*- and *para*-positions. Furthermore, Tyr residues are prone to *in vivo* dehalogenation.

1.11.2 Technetium Chemistry

Radiolabelling with ^{99m}Technetium is one of the commonest radiolabelling processes used in nuclear medicine because it has a number of important advantages over other radiopharmaceuticals. It is readily available at low commercial cost, since it is obtained from generators on site rather than having to be obtained from an outside source. ^{99m}Tc has excellent imaging properties; it is a gamma-emitter providing high specific activity and a favourable dosimetry, producing superior images using conventional gamma cameras. As a result of its comparatively short half life (6 hours), it can be administered in relatively large doses ideal for imaging without giving a significant radiation dose to the patient [155]. Its versatile chemistry means it can be reduced to a number of different oxidation states, so it is able to react with a range of chelating agents, forming novel complexes which may then be used in different clinical applications.

^{99m}Tc, a metastable state nuclear isomer, is the immediate daughter-product of the parent isotope molybdenum-99 (Figure 1.14).

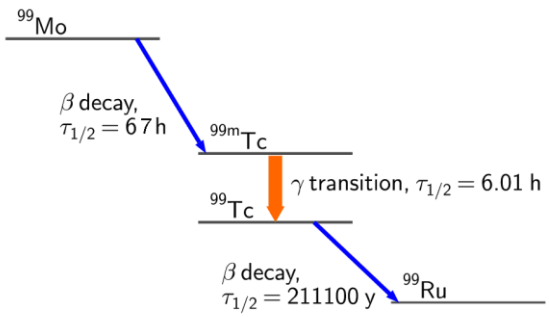

Figure 1.14: Decay scheme for ^{99}Mo and ^{99m}Tc.

^{99m}Tc has oxidation states from +7 (the highest, the most stable and the form which is eluted from the generator to -1). Radiolabelling reactions with ^{99m}Tc involve the reduction of pertechnetate ($^{99m}TcO_4^-$), which is relatively inactive chemically, to a lower oxidation state which may then be stabilised with a range of ligands, mainly N, O, S and P donors, prerequisite for the synthesis of ^{99m}Tc-labelled molecules. During reduction, the ligand stabilises the lower oxidation state, otherwise colloidal TcO_2 is formed in aqueous media. Pertechnetate, when reduced in the presence of ligands, usually does not release all its oxygen atoms, leading to complexes in which a TcO^{3+} and TcO_2^+ core is identified [156]. The most common and frequently-used technetium core is $[Tc=O]^{3+}$, which is very stable in the presence of a strong chelating ligand. $[Tc=O]^{3+}$ forms a square pyramidal oxotechnetium complex with tetradentate ligands. However, in labelling Demobesin 4, the $[O=Tc=O]^+$ core was used, as it forms an octahedral technetium complex at the polydentate liganding tetra-amine site on this analogue (Figure 1.15).

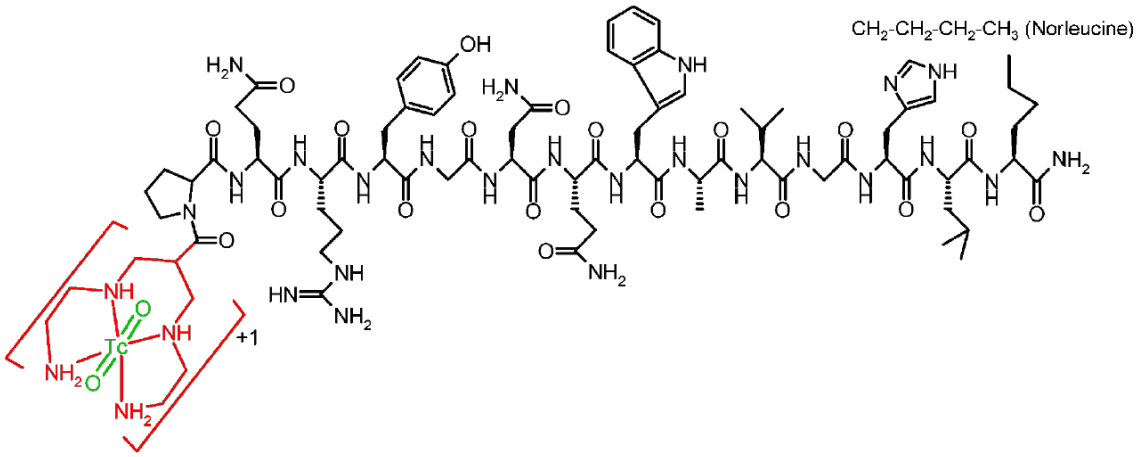

Figure 1.15: [^{99m}Tc]-DB 4 chelation via the $[O=Tc=O]^{+}$ core (green) with the tetra-amine-derivatised chelator (red). Substitution of Met^{14} by Nle^{14} was performed to produce a more oxidation-resistant analogue [116, 157]

Radiolabelling of peptides with ^{99m}Tc can be achieved by direct or indirect methods. Direct labelling with ^{99m}Tc involves the attachment of free thiol groups generated by reduction of a cysteine bridge to reduced ^{99m}Tc (Figure 1.16) [155].

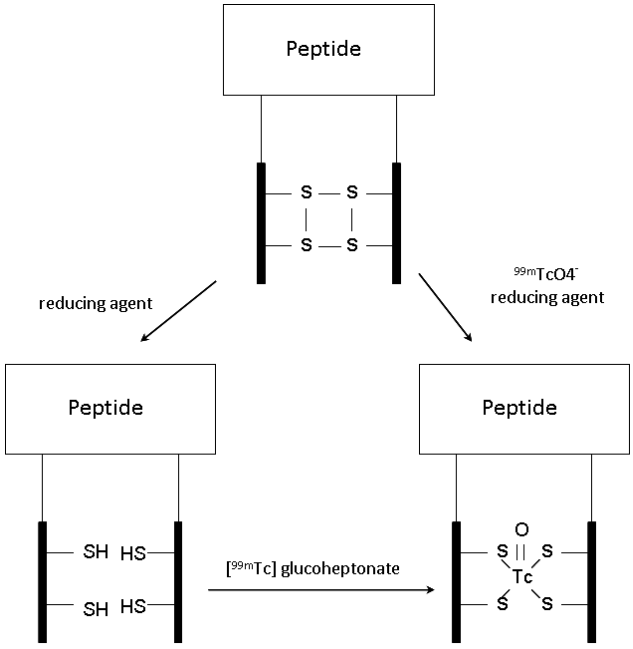

Figure 1.16: Direct labelling with 99mTc [155].

Only the peptides in which cysteine residues are cyclised are amenable to this approach; however since cyclisation of the peptide may be necessary to provide the configuration needed for receptor binding; the reduction of this peptide may inactive the peptide.

To overcome this problem, it is possible to engineer the peptide sequence to provide a technetium labelling site by extending the peptide sequence. Most tetra-peptides are able to complex technetium, and to ensure effective labelling, it is necessary to provide a site that is preferred over the rest of the peptide sequence. Normally this would be achieved by the incorporation of cysteine residues, because Tc-S bonds are extremely stable.

Another approach exploits the commonly incorporated His-tag, which is often used for the purification of such recombinant proteins by immobilised ion metal affinity chromatography [158].

Tc(I) can be prepared from pertechnetate eluted from the Tc generator and is stabilised as a tricarbonyl complex in aqueous solution which readily exchanges its water ligands for the sp^2 electrons from imidazole nitrogen atoms, resulting in complexes which are very stable [159].

This labelling approach has the advantage of avoiding the introduction of unpaired cysteines into the scFv, which present problems for routine production and storage, due to interference with generation of the disulfide bonds in the scFv fragment resulting in misfolding and leading to poor production yields and covalent aggregates [159].

Indirect labelling can be performed using a bifunctional chelating agent (BFCA). For technetium, the BFCA must follow several requirements; firstly, the binding unit should selectively stabilise technetium at an intermediate or lower oxidation state so that the complex is not subject to redox reactions; secondly, the BFCA should form a ^{99m}Tc-complex that is both thermodynamically stable and kinetically resistant to dissociation,

and thirdly, the conjugation group should be easily attached to the peptide. The post-labelling approach is a common method to label proteins and peptides; first a BFCA is attached to the peptide to form a BFCA-peptide conjugate. The BFCA can be attached to C- or N-terminus of the peptide, as well as be attached to the side chain or backbone of the peptide, providing it does not affect the receptor binding affinity (Figure 1.17) [139].

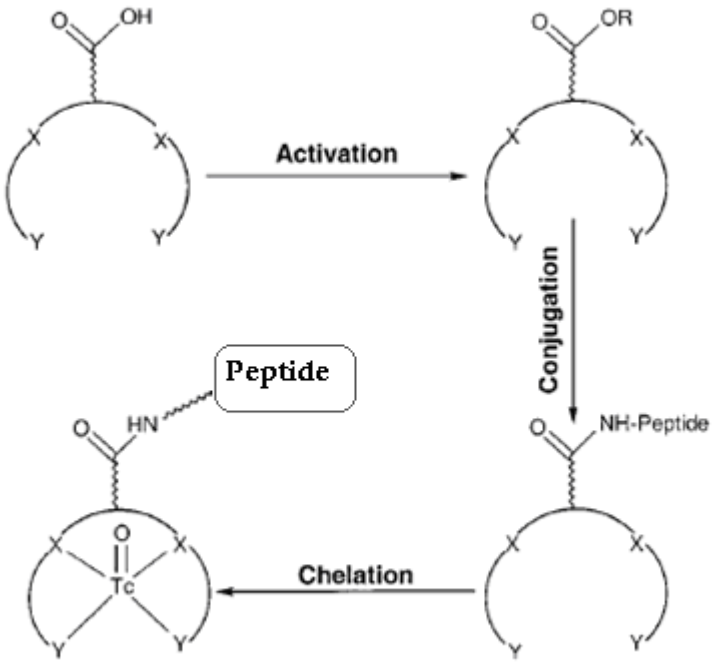

Figure 1.17: Schematic representation of indirect labelling with ^{99m}Tc, commonly employed for radiolabelling of DB 4.

Currently reagents employed for introducing bifunctional groups include diethylenetriamine-penta-acetic acid, N_2S_2 [160], N_3S [161], boronic acid adducts of technetium dioxime [162], 6-hydrazinopyridine-3-carboxylic acid (HYNIC) and the tetraamine chelator employed for DB 4 (Figure 1.15) [163, 164].

1.12 SCOPE OF PROJECT

PC remains one of the most common cancers in men. The treatment and survival rates are highly dependent on the growth-type and stage of the cancer. Currently there remains a fundamental gap in the ability to diagnose PC and to stage it effectively. The Gleason score and measurement of PSA levels do not provide detailed and accurate enough information to allow the best form of treatment to be selected for the patient during his course of treatment. In addition, it is also important to be able to screen patients for recurrent androgen-independent PC, which usually takes on a more aggressive nature (Figure 1.18).

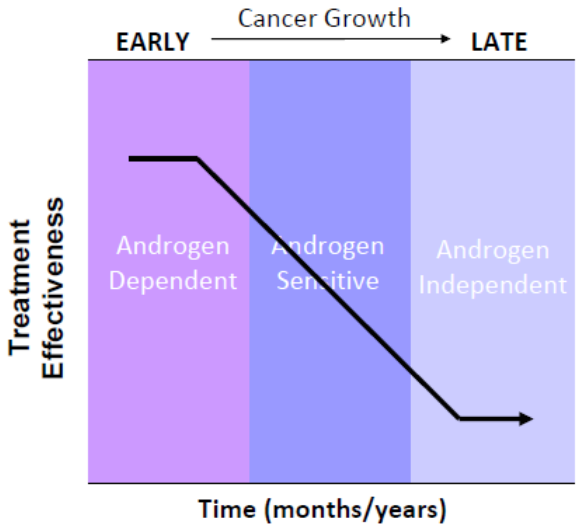

Figure 1.18: A schematic diagram showing the development of PC and the effectiveness of treatment over time.

The rationale behind this project was to design a radiopharmaceutical that would be able to bind specifically to the selected molecular target. The intention was to develop a molecule that (a) could be easily conjugated with a radioactive isotope, and upon systemic intravenous injection would target receptors or ligands that were expressed primarily by the cancerous tissue; (b) would clear the circulation rapidly, and (c) would allow imaging of the development of the cancer before and after treatment.

PSMA and GRP-R were selected as potential targets, since both are expressed preferentially in PC.

For the PSMA project the aims were to screen phage libraries for scFv against both cell-expressed PSMA and recombinant PSMA to generate diabodies from high binding clones, to radiolabel these with suitable radionuclides and finally to compare scFv and diabody pharmacokinetics and targeting efficacy.

For the GRP-R project, the main aims were to compare methods for measuring GRP-R expression in a range of PC cell lines both *in vitro* and *in vivo* and to determine changes in the levels of expression with PC advancement. The potential relationship between androgen status and GRP-R expression would also be explored. Radiolabelling and imaging *in vivo* would be performed to assess the distribution and behaviour of a peptide-based radioligand. Quantification of radiotracer uptake from imaging would be performed and its relationship with *in vitro* measures of GRP-R expression explored.

2 MATERIALS AND METHODS

2.1 MATERIALS

2.1.1 REAGENTS

Reagent	Supplier
0.25% (w/v) Trypsin – 0.53 mM EDTA solution	Cambrex
10x Tris/Glycine/SDS buffer - electrophoresis grade	National Diagnostics
2x TY media	Cancer Research UK
3,3',5,5'-tetramethylbenzidine (TMB)	Sigma-Aldrich
A	
Acetone	VWR
Acetonitrile – HPLC grade	Aldrich Chemicals Co.
Agarose	Sigma-Aldrich
Albumin, bovine	Sigma-Aldrich
Ammonium persulfate	Sigma-Aldrich
Ampicillin, sodium salt	Calbiochem
Anti-M13 HRP monoclonal conjugate	Invitrogen
AR42J (Rat pancreatic)	Clare Hall, Cancer Research
B	
Beta-actin (ACTB)	Applied Biosystems
Beta-mercaptoethanol	VWR
Bio-agar	Biogene Ltd
Bio-assay dish	Nunc
Brilliant blue R staining	Sigma-Aldrich
Bovine serum albumin (BSA)	Sigma-Aldrich
C	
SuperScript® III first-strand synthesis system	Invitrogen
Cork disc	VWR
D	
D2B	Donated by Department of Experimental Oncology, Italy
DB 4	piCHEM R&D, Graz, Austria
DU145 cell line	Donated by Dr. David Prowse, Molecular Oncology & Imaging, QMUL
E	
E.coli TG1 and HB2151	American Type Culture Collection (ATCC)
ECL ™ Western blotting detection reagent	GE Healthcare
EDTA	Sigma-Aldrich
Ethanol	BDH Laboratory
Ethidium bromide	Fisher

Express five serum-free medium	Invitrogen
F	
Foetal bovine serum	Invitrogen
First strand cDNA synthesis Kit	Invitrogen
G	
Gentamycin sulfate (Sterile -filtered, aqueous solution, cell culture tested)	Invitrogen
D-(+)-Glucose (>99.5%)	Sigma-Aldrich
Glycerol	VWR
Glycine (>99%)	Sigma-Aldrich
Goat anti-mouse alexa488 IgG (Cat no: A-11001)	Invitrogen
H	
HEPES buffer	Sigma-Aldrich
High five (Hi5) growth medium	Invitrogen
High performance chemiluminescence film	GE Healthcare
Horseradish peroxidase anti-M13 antibody	GE Healthcare
Horseradish peroxidase conjugated protein A	GE Healthcare
Horseradish peroxidase conjugated protein L	GE Healthcare
Hydrogen peroxide (30%)	VWR
I	
[^{125}I]- [D-Tyr6[^{125}I], βAla11, Phe13, Nle14]-bombesin (6-14)	Perkin Elmer
Internal standard for HPLC analysis (Murine antibody PRIAS)	Cancer Research
Isopropyl-β-D-thiogalactoside (IPTG)	Applied Biosystems
ITLC-silica gel	Pall
K	
Kanamycin sulfate	Calbiochem
KM13 helper phage	Generated in-house
L	
L-glutamine	Sigma-Aldrich
LMB_3 and FDSEQ primers	Genome Centre, QMUL
LNCaP C81, LNCaP C42B & LNCaP (androgen dependent) Cell Line	Donated by Dr. David Prowse Molecular Oncology & Imaging, QMUL
M	
Marvel milk powder	Premier International Food Ltd
Male SCID beige mice	Charles River Research Animal Diagnostic Services, London
Matrigel	BD Biosciences
Methanol (HPLC grade >99%)	BDH Laboratory
MKN45	Clare Hall, Cancer Research
Molten H-top	Clare Hall, Cancer Research
Monoclonal anti-mouse IgG (whole molecule peroxidase)	Sigma-Aldrich
Monoclonal mouse anti- PSMA (1H8H5)	Zymed, Invitrogen
N	
NaCl	VWR
Ni-NTA purification system	Invitrogen
Nitrocellulose membrane	BDH Laboratory
Nunc maxisorb immunotubes	Gibco UK

P	
Para-formaldehyde	Sigma-Aldrich
Phosphate-buffered saline (PBS)	Cancer Research
Pierce iodination tubes	Pierce
Polyacrylamide	National Diagnostics Ltd
Polyethylene glycol 6000	VWR
Ponceau solution	Sigma-Aldrich
Precision plus protein standard	BioRad
Protease inhibitors cocktail set I	Calbiochem
Protein A sepharose beads	GE Healthcare
Protein assay kit	BioRad
Q	
Quick plasmid miniprep kit	Qiagen
R	
Restriction endonucleases XhoI, SalI, HindIII & NotI	New England Biolabs
RNeasy mini kit	Qiagen
RPMI 1640 medium	Cancer Research UK
Rabbit polyclonal anti-GRP-R antibody (Ab39963)	Abcam
Rabbit polyclonal anti-GRP-R antibody (NB100-74434)	Novus Biologicals
S	
Slide-A-lyzer dialysis cassettes	Pierce
Sf9 cells	Invitrogen
Sodium [^{125}I]-iodide	Perkin Elmer
Sodium acetate trihydrate (>99%)	Sigma-Aldrich
Sodium azide reagentPlus®	Sigma-Aldrich
Sodium pertechnetate	Eluted from Amersham 'Drytec' generator, Radiopharmacy Department, St.Bartholomew's Hospital
Stannous chloride (ACH grade)	Sigma-Aldrich
Streptavidin	Invitrogen
Sucrose	Sigma-Aldrich
Sulphuric acid 95-97%	VWR
T	
Tetramethylethylenediamine (TEMED)	GE Healthcare
Taq polymerase	Invitrogen
The discovery™ DAB map™ kit	Ventana Medical Systems
Tomlinson phage library	Medical Solutions - Gene Service
Triethylamine (>99.5%)	VWR
Trifluoroacetic acid (TFA) (>(99.5)	Thermo Scientific
Triton	VWR
Tween 20	Sigma-Aldrich
Tryptone	Biogene Ltd
V	
Versene	Cancer Research UK
Visking tubing	Sigma-Aldrich
W	

W3MM Blot paper	Whatman International Ltd
Y	
Yeast extract	Biogene Ltd

2.1.2 EQUIPMENT

Equipment	Supplier
7900HT Fast real-time PCR system	Applied Biosystems
1282 CS universal gamma counter	LKB Wallac
A	
Allegra 21R centrifuge	Beckman Coulter
C	
Cyclone plus storage phosphor system (OptiQuant programme)	Perkin Elmer
D	
Developer G138i curix 60 processor	AGFA
E	
ELISA plate reader	Tecan, Magellan 4 Programme
G	
Gene pulser machine	BioRad Ltd
Graphpad prims 5 software	Graphpad Inc
H	
HPLC	Beckman
I	
In-line radioactivity detector for HPLC	Raytest
L	
Large semaphor transphor unit	GE Healthcare
M	
Mini personal thermal cycler	BioRad Ltd
Microscope (Nikon ACR-1 programme)	Axiophot - Zeiss
N	
Nano SPECT (Invivo scope programme)	Bioscan
NanoDrop 2000 S spectrophotometer	Thermo Scientific
R	
Radioisotope calibrator (CRC15R)	Capintec
Reverse-phase column, C_{18}ODS	Phenomenex
S	
Sephacryl S-200 high-resolution chromatography column	GE Healthcare
L8M shaking incubator	Beckman Coulter
Size exclusion HPLC column (Biosep-sec-s 2000)	Phenomenex
V	
Ventana discovery™ immunohistochemistry unit	Ventana Medical Systems
Vortex	Scientific Industries INC

2.1.3 BUFFERS

Buffer	Concentration/Volume	Components
FACS Buffer	0.06g	Bovine serum albumin (BSA)
200 mL	0.06g	Sodium azide
	200mL	PBS or RPMI
Loading Buffer	7.5 mL	Water
20 mL	2.5 mL	1M Tris-HCl, pH 6.8
	6.0 mL	Glycerol
	0.004 g	0.5% (w/v) Bromophenol blue
	4.0 mL	SDS (10% w/v)
Blot Buffer	100mL	Methanol
500 mL	400mL	1x Tris-glycine-SDS Buffer
TYE	15g	Bacto-Agar
1 L	8g	Sodium chloride
	10g	Tryptone
	5g	Yeast Extract
2x TY Medium	10 g	Yeast Extract
1 L	16 g	Tryptone
	5 g	Sodium Chloride
Substrate solution (To develop ELISA experiments)	100 µg/mL	Tetramethylbenzidine TMB
	100 mM	Sodium acetate buffer, pH 6.0
	0.001%	Hydrogen peroxide
5X Native Purification Buffer	250 nM	Disodium hydrogen phosphate, pH 8.0
	5 M	Sodium chloride
Native Wash Buffer	1X	Native Purification Buffer
	20 nM	Imidazole
Native Elution Buffer	1X	Native Purification Buffer
	250 mM	Imidazole
Restriction Digest Mixture	10 µL	Miniprep
(1 x - 30 µL)	0.3 µL	BSA
	1 µL	SalI
	1 µL	XhoI

	3 µL	Buffer 3 (optimal buffer for both endonucleases)
	14.7 µL	water

Demobesin 4 Labelling

Phosphate Buffer	0.25 M	$Na_2HPO_4.2H_2O$ (A)
Mix 2 parts of (A) with 1 part (B)	0.25 M	$Na_3PO_4.12H_2O$ (B)

Radiolabelling Attachment	100 mM	HEPES
Buffer	130 mM	NaCl
	5 mM	$MgCl_2$
	4.7 mM	KCl
	1 mM	EGTA
	100 µg/mL	Bacitracin
	0.1% (w/v)	BSA

Note: A superscripted M denotes that further information on the respective item can be found in the Materials section.

2.2 METHODOLOGY 1

This methodology relates to the results section in chapter 3

2.2.1 PRODUCTION OF RECOMBINANT PSMA PROTEIN

2.2.1.1 Baculovirus Expression Vector Systems

Baculoviruses (family *Baculoviridae*) form part of a large diverse group of double-stranded DNA viruses that infect many different species of insects as their natural hosts and is a popular system for production of recombinant proteins [165].

The propagation of in-house virus, using pAcGP67A Baculovirus transfer vector (donated by Pamela Bjorkman, Howard Hughes Medical Institute Laboratories, California, USA) to deliver the PSMA cDNA into the Baculovirus genome was accomplished by Dr. Stella Man, by cotransfection with linearised wild-type AcNPV DNA into Sf9[12] insect cells [42]. Only the large extracellular portion[13] (aa 44-750) of the PSMA ligand was utilised, as the smaller intracellular portion is only exposed when cells are necrotic or undergoing apoptosis.

2.2.1.2 High 5 Cell Line

For recombinant PSMA expression, viral infections were performed on High Five (Hi5) insect cells[14]. Cells were grown in Express Five serum-free medium (SFM), supplemented with L-glutamine (200 mmol/L) and gentamycin (10 µg/mL) and encased in foil because of photo-sensitivity. Cells were handled using standard tissue culture techniques. Cells were grown as a monolayer culture at 27°C. To detach them, half the medium was decanted off, and the side of the flask was tapped sharply to bring the cells into suspension.

[12] Sf9 originally established from ovarian tissues of *Spodoptera frugiperda* larvae
[13] Chapter 1 - Figure 1.8
[14] Hi5 derived from the ovarian cells of the cabbage looper *Tricholusia ni*

2.2.1.3 Protein Production Technique

To ensure even monolayers of growth, large 175 cm^2 tissue culture flasks were each seeded with 1.8 x 10^7 cells. The fluid volume was made up to 35 mL with fresh medium, and flasks were left for 30 min to allow cellular adhesion to the walls. After addition of PSMA house virus (500 µL; 10^8 PFU/mL), cultures were incubated at 27°C for 3 days. One flask was left uninfected as backup and as a point of reference to compare with infected cells.

Cells were checked daily and compared to the uninfected flask. Cells infected with the virus should become fat with a large granular nucleus, indicative of infection and protein production; there should be a visible two-fold increase in cell size. On day three, PSMA protein was harvested by centrifugation of the culture at 10,000 rpm for 5 min, and purification from the supernatant was carried out using the Ni-NTA purification system^M as per manufacturer's instructions. SDS-PAGE and Western blot were used to monitor the harvested material before and after the Ni-NTA step to ensure that the yield and purification of the protein were satisfactory.

2.2.2 SDS PAGE & WESTERN BLOT ANALYSIS

2.2.2.1 SDS-PAGE under Reducing Conditions

Protein samples or antibody fragments were analysed by SDS-PAGE using 7.5 or 15% homogeneous gels prepared from acrylamide in 0.375 M Tris-HCl, pH 8.8, containing 0.1% (w/v) SDS, 0.1% (w/v) ammonium persulfate and 0.1% (v/v) tetramethylethylenediamine (TEMED) for resolving gels, and in 0.125 M Tris-HCl, pH 6.8, containing 0.1% (w/v) SDS, 0.1% (w/v) ammonium persulfate and 0.1% (v/v) TEMED for stacking gels. Samples were heated in loading buffer^M at 95°C for 3 min to linearise proteins, and were run concurrently with a protein standard in 1 x Tris-glycine-SDS buffer, pH 8.3, at 150 V and 40 mA per gel for 1.5 h. Gels were either stained with Brilliant Blue R (0.5%, w/v) in

ethanol:acetic acid:water (9:2:9, by vol) for 2 h to visualise bands for determination of molecular weights, or were submitted to Western blot analysis.

2.2.2.2 Western Blot

PAGE gels were soaked for 20 min in blot buffer[M]. A "sandwich" in the semi-dry blotter was constructed from 2 sheets W3MM blotting paper, a nitrocellulose membrane, the gel and 2 more sheets W3MM blotting paper, all pre-soaked in blot buffer, carefully excluding air bubbles from between layers. Current was applied at 200 mA and 5-10 V for 1-1.5 h. After electro-elution, the nitrocellulose membrane was sometimes soaked with Ponceau solution to visualise bands and lanes, to check whether the transfer was successful. The nitrocellulose membrane was blocked in 2% MPBS [2% (w/v) powdered milk (Marvel) in phosphate-buffered saline (PBS)] for a minimum of 1 h at room temperature, or at 4°C overnight, then washed twice in 0.1% (w/v) Tween 20 in PBS and incubated for 1 h at room temperature, or overnight at 4°C, with the primary antibody directed at the molecule of interest, in 2% MPBS. After incubation the membrane was washed as before, adding complementary secondary antibody conjugated with horseradish peroxidase (HRP) for the same incubation times as for the primary antibody. Proteins were visualised by ECL™ Western Blotting Detection Reagent[M] as per manufacturer's instructions.

2.2.3 PHAGE DISPLAY

2.2.3.1 Selection

Selection for an antibody fragment can be performed on a number of targets such as cells and immobilised antigens. By incubating a library of phages, it is possible to select the specific phage for the target antigen. Unbound and non-specific phages are washed away during each round of selection and the specifically bound phages are eluted and amplified through further cycles to enrich the population (Figure 2.1).

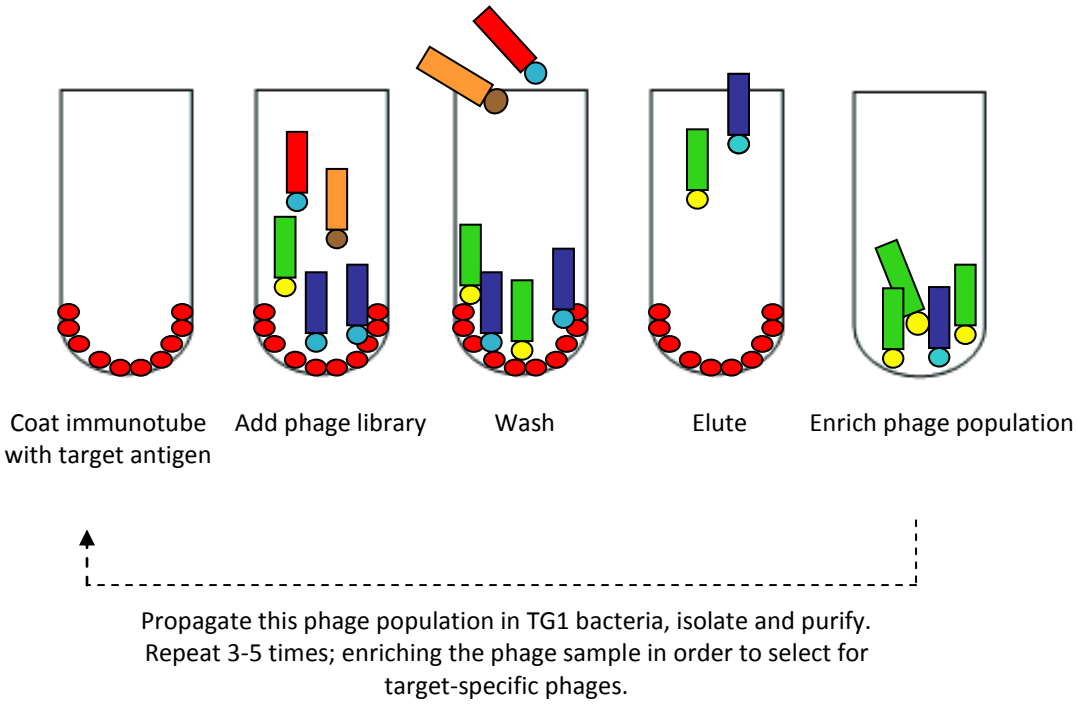

Figure 2.1: Schematic diagram of selection against a target antigen. Up to 5 rounds of selection can be performed, however 3 rounds is optimal to ensure a variety of PSMA specific binders ranging in affinity.

2.2.3.2 Production of Large Quantities of Helper Phage

A suspension of *E. coli* TG1, OD_{600} = 0.4, (200 µL) in a 27°C water bath, was infected for 30 min with 10 µL of 100-fold serial dilutions of KM13 helper phage, to ensure separated plaques. Molten H-top agar at 42°C (3 mL) was mixed with the infected bacteria and poured onto warm TYE^{M} plates containing no antibiotics, and plates were incubated overnight at 37°C. A small plaque was inoculated into 5 mL fresh TG1, OD_{600} = 0.4, and agitated (250 rpm) for 2 h at 37°C before adding to 500 mL of 2 x TY^{M} in a 2-litre flask and agitating for a further 1 h. Kanamycin[15] was added to a final concentration of 50 µg/mL and the culture was grown overnight with shaking at 30°C, then centrifuged at 9,600 rpm for 15 min. PEG/NaCl [20% (w/v) polyethylene glycol 6000/2.5 M NaCl] (100 mL) was added to 400 mL of the supernatant and left on ice for 1 h before centrifuging again for 30 min. The pellet was resuspended in 8 mL of PBS, mixed with 2 mL PEG/NaCl, and stood for a further 20 min on ice, then centrifuged for 30 min at 3,000 rpm. After discarding the

[15] Helper phage KM13 is kanamycin-resistant

supernatant, the pellet was resuspended in 5 mL of PBS to remove remaining bacterial debris, and re-centrifuged. Helper phage was stored with 15% (v/v) glycerol at -80°C as a cryoprotectant.

2.2.4 SELECTION FOR ANTI-PSMA SCFV AGAINST RECOMBINANT PSMA PROTEIN

2.2.4.1 Tomlinson Library

The Tomlinson I Phage Library is a phage antibody library (diversity of 1.47 x 10^8) which is based on a single human framework comprising the germline heavy-chain genes V3-23/DP-47 and JH4b and the κ-light chain genes O12/O2/DPK9 incorporated at position in the antigen binding site [90, 166]. The CDR3 of the heavy chain was designed to be as short as possible whilst maintaining an antigen binding surface. Library diversity was achieved by randomisation of 11 residues in key CDR2 and CDR3 positions of the heavy chain and 7 residues in the light chain. The library contains clones that were pre-selected for active folding domains by binding to protein-L and protein-A, which facilitate the capture and/or detection of the antibody fragments without interfering with antigen binding [90, 167].

2.2.4.2 Selection using Recombinant PSMA Protein

An immunotube was coated overnight with 4 mL of recombinant PSMA protein (10 µg/mL) in PBS. Next day the tube was washed 3 times with PBS, then blocked by addition of 2% MPBS, with incubation at room temperature for 2 h. Washing was repeated as before with PBS, then 1 mL of Tomlinson I Library (10^{12} to 10^{13} PFU) was added in 4 mL of 2% MPBS and incubated at room temperature, with rotation for 1 h, and stood for a further 1 h. The phage suspension was discarded and the tubes were washed several times, dependent on the number of rounds of selection; 10 (round 1) and 20 (rounds 2 and 3) times, with 0.1% (w/v) Tween 20 in PBS. After removing excess PBS, bound phage was eluted by addition of 500 µL of trypsin-PBS [trypsin (1 mg/mL) / 0.1 mM $CaCl_2$ in 5 mM Tris-HCl, pH 7.4 / PBS] and incubated at room temperature for 10 min with agitation.

Eluted phage (250 µL) was taken and incubated in 1.75 mL of exponentially growing *E. coli* TG1 (OD_{600} = 0.4) at 37°C for 30 min. (A 250 µL-portion was stored as backup at 4°C). Phage titration after each round of selection was undertaken by serially diluting phage-infected cells and spotting 10 µL of each dilution onto TYE plates containing 100 µg ampicillin/mL and 1% (w/v) glucose, and incubating overnight at 37°C. The remaining TG1 culture was centrifuged at 11,600 rpm in a micro-centrifuge for 5 min; the pellet was re-suspended in 50 µL of 2 x TY and plated on a Bio-Assay dish of TYE containing 100 µg ampicillin /mL and 1% (w/v) glucose. Plates were incubated overnight at 37°C.

2.2.4.3 Rescue with Helper Phage

After overnight incubation, 2 mL of 2 x TY containing 15% (v/v) glycerol was added, into which the growth on the plate was suspended using a glass spreader; then 50 µL of the suspension was added to 50 mL of 2 x TY containing 100 µg ampicillin/mL and 1% (w/v) glucose, and cultured with agitation (250 rpm) at 37°C until OD_{600} = 0.4 was achieved (approximately 1-2 h). The remaining suspension was stored as back-up at -80°C.

To 10 mL of the culture, KM13 helper phage ($5x10^{10}$ PFU) was added, followed by incubation at 37°C for 30 min, then centrifugation at 3,200 rpm for 10 min. The supernatant was discarded and the pellet was re-suspended in 2 x TY medium containing 100 µg ampicillin/mL, 50 µg kanamycin/mL and 0.1% (w/v) glucose, followed by incubation with shaking overnight at 30°C.

2.2.4.4 Phage purification

The overnight culture was centrifuged for 10 min at 3,200 rpm and 40 mL of the supernatant was mixed with 10 mL PEG/NaCl and held on ice at 4°C to precipitate the phage, which occurred over 1-2 h. The preparation was centrifuged for 30 min at 4°C and the pellet was re-suspended in 2 mL cold PBS, then dispensed into tubes and further centrifuged at 11,600 rpm for 2 min. A further round of selection was initiated from 1 mL of the phage suspension and the remainder was either stored at 4°C, or at -80°C after adding 15% (w/v) glycerol.

2.2.4.5 Mixed Population of Phage Particles in 96-Well Plates

A 96-well plate was inoculated with individual plaques picked from the titration plates after each round of selection and grown in 100 µL 2 x TY medium per well containing 100 µg ampicillin/mL and 1% (w/v) glucose. The plate was incubated with agitation (250 rpm) at 37°C, overnight, then 2 µL of inoculum from each well of this plate was transferred to a second 96-well plate containing 200 µL of 2 x TY with 100 µg ampicillin/mL and 1% (w/v) glucose per well, and incubated with agitation (250 rpm) for 2 h at 37°C. A glycerol stock was made with the original plate by the addition of glycerol to a final concentration of 15% and stored at -80°C until needed. After 2 h incubation, 25 µL of 2 x TY containing 100 µg ampicillin/mL, 1% (w/v) glucose and 10^9 PFU of helper phage KM13 per well was added to the plate and grown with agitation (250 rpm) at 37°C for 1 h. The plate was then centrifuged at 3,200 rpm for 10 min and the supernatants were aspirated from each well and discarded. The bacterial pellets were resuspended in 200 µL 2 x TY containing 100 µg ampicillin/mL and 50 µg kanamycin/mL, and grown with shaking (250 rpm) overnight at 30°C. The following day, the plate was spun at 3,200 rpm for 10 min and 50 µL of the supernatant was used in phage ELISA.

2.2.4.6 Phage ELISA

In a 96-well maxisorb plate, 100 µL of recombinant PSMA protein (10 µg/mL in PBS) was incubated overnight at 4°C, or for 2 h at room temperature. The plate was then washed 3 times with PBS[16] and blocked with 2% MPBS for 2 h at room temperature. Wells were washed as before, and 10 µL of PEG-precipitated phage from each round of selection in 100 µL 2% MPBS was added, and incubated for 1 h at room temperature. Phage suspension was discarded, and wells were washed 3 times with 0.1% (w/v) Tween 20-PBS, then 100 µL of HRP-anti-M13 antibody (1 : 5000, by vol.) in 2% MPBS was added followed by incubation for 1 h at room temperature. After a further wash, 100 µL of substrate solution [100 µg 3,3',5,5'-tetramethylbenzidine (TMB)/mL in 100 mM-sodium acetate, pH 6, containing 0.006% hydrogen peroxide] was added to each well, followed by incubation

[16] Plates were immersed in a shallow bath containing PBS and all wells were checked to ensure that they were filled with wash solution, to avoid creating false positives during later washes.

at room temperature for 2-15 min. Positive reactions were revealed by formation of a blue product. The reaction was stopped by the addition of 50 µL of 1 M-sulphuric acid, turning the colour product yellow. Wells were read on a plate reader at 450 nm.

For scFv ELISA, 3% BSA-PBS [3% (w/v) bovine serum albumin in PBS] was used in place of 2% MBS. The plate was handled in the same manner with the addition of Protein A-HRP (1 : 10000, by vol.) after incubation with selected scFv.

2.2.5 ANTIBODY FRAGMENTS

2.2.5.1 Production of Soluble Antibody Fragments

Strong binding clones observed in phage ELISA were subsequently sequenced, and those bearing unique and complete scFv fragments characterised by ELISA and amino-acid sequencing were taken forward to express soluble antibody fragments, and also to generate larger volumes of the desired clones.

From each round of selection for which soluble antibody fragments were required, 10 µL of eluted phage was taken and added to 200 µL of a culture of *E. coli* HB2151 cells, OD_{600} = 0.4, growing exponentially at 37°C in a water bath. (*E. coli* HB2151 is a non-suppressor strain, which, when induced, is able to give soluble expression of antibody fragments). After 30 min, serial dilutions were performed on the culture and 50 µL of each of the dilutions 10^2, 10^4 and 10^6 was spread on TYE plates containing 100 µg ampicillin/mL and 1% (w/v) glucose, and incubated overnight at 37°C. Individual colonies were picked and used to inoculate 100 µL 2 x TY 100 µg ampicillin/mL and 1% (w/v) glucose in 96-well plates and cultured with agitation (250 rpm) overnight at 37°C. From each well, 2 µL was transferred from each plate to a second containing 200 µL 2 x TY containing 100 µg ampicillin/mL and 0.1% (w/v) glucose per well, and cultured with agitation (250 rpm) at 37°C until OD_{600} = 0.9 was achieved, whereupon 25 µL 2 x TY containing 100 µg ampicillin/mL was added together with isopropyl-β-D-thiogalactoside (IPTG) to a final

concentration 1 mM, and the plate was left shaking overnight at 30°C. The following day, the plate was centrifuged at 3,200 rpm for 10 min and the supernatant was assayed by performing soluble-scFv ELISA in 3% (w/v) BSA-PBS.

2.2.5.2 Harvesting Fragments from the Periplasm

E. coli is a popular host for the production of recombinant proteins but it does not secrete the proteins into the medium; however in some instances secretion of the proteins into the periplasmic space can occur. Techniques for the recovery of periplasmic proteins include treatment with lysozyme-ethylenediaminetetraacetate (EDTA), repeated cycles of freezing and thawing, heat treatment, chemical permeabilisation using chloroform, and osmotic shock, which is advantageous for large-scale operations.

The periplasmic space is situated between the inner cytoplasmic membrane and external outer membrane of Gram-negative bacteria. It contains a loose network of peptidoglycan chains, as well as hydrolytic and degradative enzymes (Figure 2.2). To achieve osmotic shock, cells are first exposed to high concentrations of sucrose supplemented with EDTA, then centrifuged and re-suspended in cold water. As the high osmotic strength causes the cells to shrink, periplasmic proteins are released [168]. EDTA functions to release the lipopolysaccharides from the bacterial cell envelope, thus increasing the permeability of the outer membrane, and the cold water treatment, achieved by holding on ice at 4°C, causes a rapid increase in cell size which completes the release of periplasmic proteins. The addition of protease inhibitors prevents the degradation of the secreted proteins by proteases from the periplasmic space.

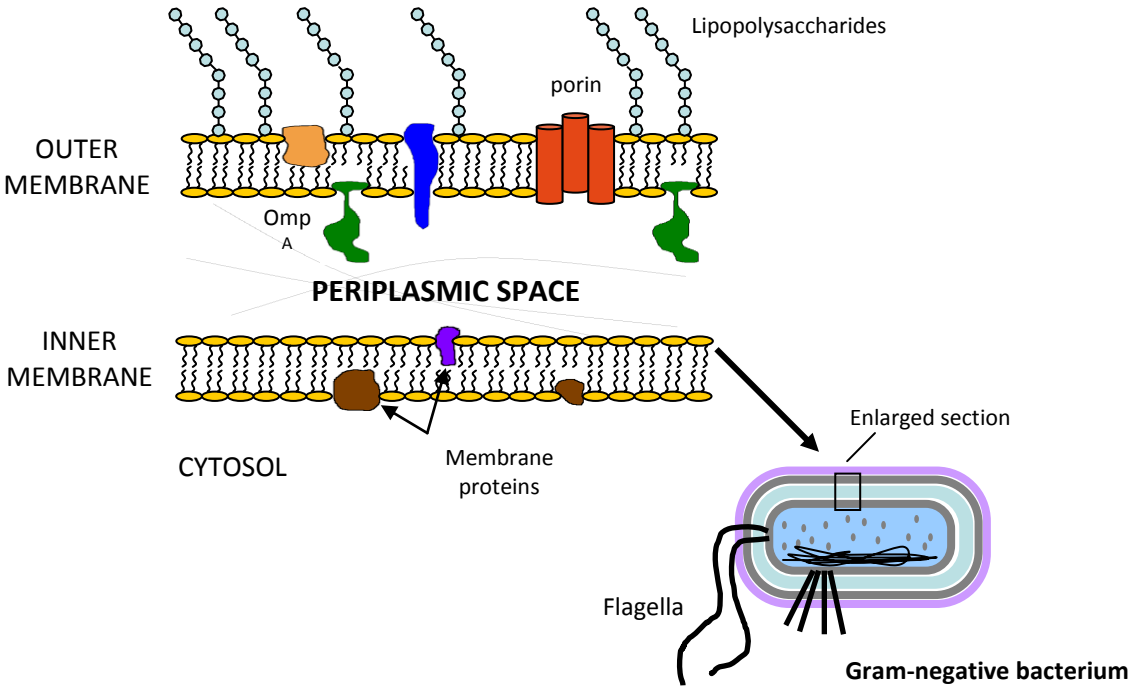

Figure 2.2: Periplasmic space of Gram-negative bacteria. This constitutes up to 40% of the total cell volume of Gram-negative bacteria.

2.2.5.3 Large Scale Production of scFv

A sample (10 µL) from a frozen stock (before addition of helper phage) was incubated in an overnight culture of *E. coli* HB2151 (1:1000) in 2 x TY containing 100 µg ampicillin/mL and 0.1% (w/v) glucose, grown at 37°C to OD_{600} = 0.9, then induced with 1 mM IPTG and cultured overnight with agitation (250 rpm) at 30°C, during which time the antibody fragments were secreted into the culture supernatant, which was collected after centrifugation at 10,800 rpm for 15 min, passed through a 0.45-µm filter and stored at 4°C until purification. The cell pellets were resuspended in 1/20 the original volume of 30 mM Tris, pH 7.0, containing 20% (w/v) sucrose and 1 mM EDTA, adding 1 mL of protease inhibitors (1% (w/v)) per 100 mL, and left on ice for 20 min. The suspension was re-centrifuged and the clear supernatant containing the periplasmic fraction was set aside for purification by column chromatography. The pellet was further resuspended in 25 mL 5 mM $MgSO_4$ and held for 20 min on ice. Following centrifugation, the supernatant (the osmotic shock fraction) was collected and combined with the periplasmic fraction, then purified immediately or frozen at -80°C until required.

2.2.6 PURIFICATION

2.2.6.1 Purification of the Periplasmic Fraction

Antibody fragments from *E. coli* periplasm or supernatant can be purified using a range of different statagies, the choice of which depends on the type of antibody fragment and the tag which is attached to it. In this case, Proteins A and L columns were used, which respectively target variable heavy and light chains, and Ni-NTA and 9E10 columns, which selectively bind his-tag and myc-tag. Purification should be undertaken at 4°C if possible or on ice, to prevent proteases from cleaving the antibody fragments.

2.2.6.2 Protein A Chromatography

Protein A-Sepharose can be used to purify antibody fragments encoded by V_H segments from the VH_3 family [169]. Protein A-Sepharose was pre-swollen overnight and washed several times in PBS. To a 10-mL glass column (pre-washed in concentrated HCl and distilled water), a 1-mL bed volume of Protein A-Sepharose beads was added and equilibrated with 50 mL sterile PBS. The periplasmic fraction was applied to the column and allowed to pass through, and the emergent fluid was recycled through the column a further two times to ensure quantitative binding of scFv to the beads. The column was then washed 5 times with the following filter-sterilised buffers, decreasing in pH: PBS, pH 7.0; 0.5 M PBS-NaCl, pH 7.0; 0.2 M glycine, pH 6.0, and finally 0.2 M glycine, pH 5.0. Protein was eluted with 3 column volumes of 0.2 M glycine, pH 3.0 (filter-sterilised), collecting 1 mL fractions into 200 µL 1 M Tris-HCl, pH 7.4 (filter-sterilised), with immediate mixing. After determining the protein content by measurement of A_{280}, protein fractions were dialysed overnight in PBS in Slide-A-Lyzer dialysis cassettes (molecular weight cut-off, 10 kDa). SDS-PAGE of eluted fractions was performed on 15% polyacrylamide gels to ensure that purification was successful and scFv was not lost.

2.2.6.3 Ni-NTA Chromatography

Ni-NTA columns exploit the his-tag present on scFv and are used to extract the antibody fragment from a protein mixture. Imidazole is added to buffers to minimise binding of

untagged and contaminating proteins, therefore increasing the purity of the target protein with fewer wash steps [170]. However, too high a concentration of imidazole can actually compete with the binding of the scFv.

The periplasmic fraction was dialysed overnight in Visking tubing (molecular weight cut-off, 10 kDa) in 1 x native purification buffer^{M}. Swollen Ni-NTA-agarose (5 mL), washed twice in 25 mL of sterile water and again twice with 25 mL of binding buffer, then equilibrated in the buffer, was dispensed in 5-mL portions into 50-mL falcon tubes. After adding 40 mL of the dialysed periplasmic fraction, the tubes were placed on a roller either overnight at 4°C or for 2 h at 37°C.

After incubation, the suspended beads were transferred into a cleaned glass column, collecting the flow-through before passing and collecting five 25-mL fractions of wash buffer through the column. To elute the protein, 15 mL of elution buffer was applied to the beads and 1-mL fractions were collected. To monitor the purification, the eluates, together with the flow-through and wash fractions, were submitted to SDS-PAGE on 15% polyacrylamide gels, checking for the presence of the expected 25-kDa scFv band. Protein concentrations were determined by measurement of A_{280} in sterile cuvettes, before aliquoting and storage at -80°C.

2.2.6.4 Sequencing

Strong binding observed by monoclonal ELISA with purified scFvs can be checked, by sequencing, for the presence of full-length V_H and V_L inserts in individual clones. Primers LMB_3 and FDSEQ were used (Figure 2.3). Correct bands were visible at 1018 bp, indicative of whole scFv.

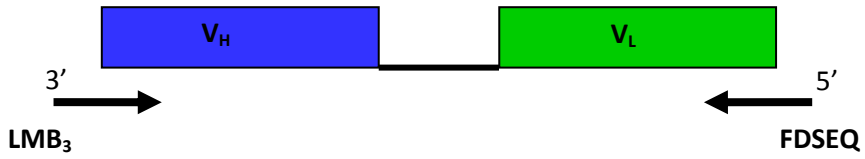

Figure 2.3: LMB_3 reads from 3' end and FDSEQ reads from the 5' end. The combined size of the PCR product is 1018 bp, the size of the complete scFv fragment.

2.2.6.5 Clonal Polymerase Chain Reaction (PCR)

Individual specific clones were picked from the glycerol stock plate with a sterile pipette tip. Preparation of the PCR master mixture for each reaction was performed on ice (Table 2.1).

Table 2.1: PCR components

Components	**Volume (µL per reaction tube)**
10x PCR Buffer	5
$MgCl_2$	2.5
LMB_3 primer	2.5
Fdseq primer	2.5
Deoxyribonucleotide triphosphate (dNTP)	2.5
water	34.0
Taq polymerase	1.0

Taq polymerase, kept at -20°C until needed, was added last to the master mixture. Both a positive (Original Library) and a negative control (PCR master-mix alone with no clone) were included, the negative control being important to ensure that there was no contamination of the master-mix during preparation, and the positive control to ensure the procedure has been successful.

The following primers were used:

LMB_3: - CAG GAA ACA GCT ATG AC

Fdseq: - GAA TTT TCT GTA TGA GG

PCR was run on the following programme:

95°C – 10 min

95°C – 1 min
60°C – 1 min } x 29 cycles

72°C – 2 min

4°C – indefinitely

Agarose gel was prepared by heating 1 g agarose powder in 100 mL 1 x Tris/Borate/EDTA (TBE) buffer until dissolved. After cooling, ethidium bromide[17] (2 µL) was added prior to casting the gel. Samples (5 µL) mixed with loading buffer (2 µL) were loaded and the gel was run at 100 V in 1x TBE solution. Bands were visualised under UV light to identify clones yielding the correct size of band, which were submitted to sequencing.

BigDye 3.1 chemistry with visualisation on an ABI 3700 Automated DNA Sequencer was used to generate read-lengths of up to 850 bp.

2.2.7 CELL LINES

Table 2.2: Prostate Cancer (PC) cell lines

Cell line	Description	Species
PC3	PC bone metastasis	Human
DU145	PC brain metastasis	Human
LNCaP C42B	PC bone metastasis	Human xenograft
LNCaP C81	PC lymph node metastasis	Human

[17] Ethidium bromide fluoresces under UV light when intercalated into DNA (or RNA)

Cells were grown in RPMI 1640 / 10% foetal bovine serum (FBS) medium. Cells were handled using standard tissue culture techniques: briefly, after growth medium was removed, the cell layer was rinsed with 5 mL of sterile PBS and 3 mL of 0.25% (w/v) Trypsin / 0.53 mM EDTA solution to remove all traces of serum, which contains trypsin inhibitor. Cells were incubated at 37°C for 2 min to facilitate detachment, then RPMI 1640 medium (10 mL) was added, and gentle pipetting was applied to separate cell clumps so as to obtain a single-cell suspension. Appropriate aliquots of the cell suspension were transferred to new tissue-culture flasks, which were then incubated at 37°C under 5% (v/v) CO_2 /air.

2.2.8 FACS ANALYSIS USING PURIFIED SCFV PREPARATIONS ON CELLS

Flow cytometry simultaneously measures and analyses multiple physical characteristics of cells as they flow in a fluid stream through a beam of light. It depends on the use of a fluorescent marker, e.g. fluorescein isothiocyanate (FITC), which is conjugated to a monoclonal antibody that specifically binds to the primary antibody bound to the target of interest (Figure 2.4).

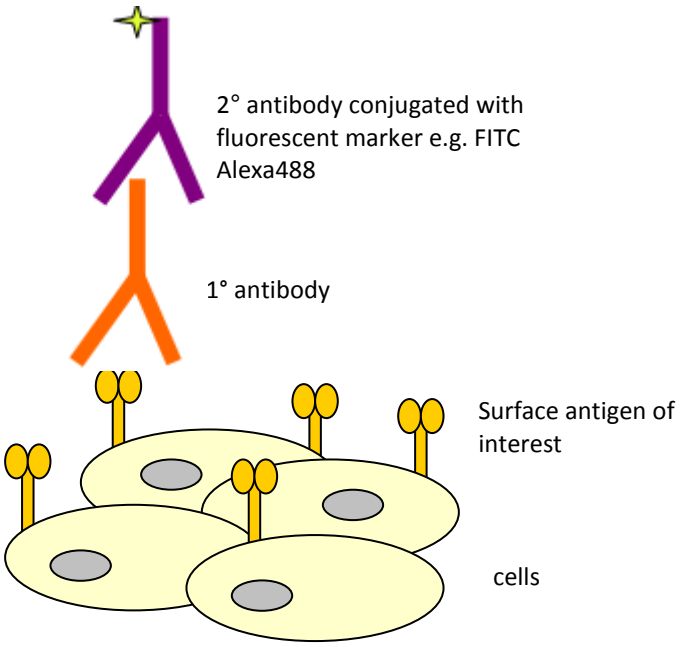

Figure 2.4: Schematic diagram of binding steps in FACS analysis. Washing after each incubation step is essential to prevent non-specific binding.

Flow cytometry can measure the relative size of the cells, their relative granularity or internal complexity, and their relative fluorescence intensity [171]. The results can be represented graphically (Figure 2.5).

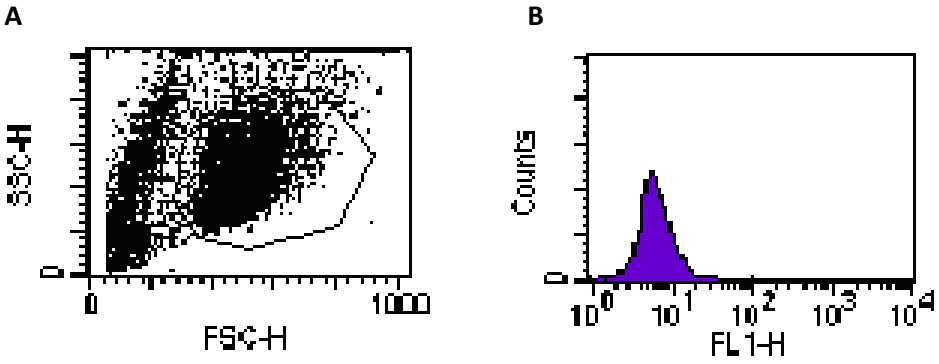

Figure 2.5: Graphical representation of a FACS analysis from a single population of cells.

Histogram A illustrates the entire population of cells present in a sample. This graph plots the side scatter (SSC-H), which is a measure of the cells' granularity and general shape,

against forward scatter (FSC-H), a measure of cell size. Being able to view the entire population enables the gating and separation of sub-populations that one wishes to analyse. Apoptosing cells and cell debris are indicated at the bottom left and can be excluded from analysis by the gating system.

Histogram B illustrates the level of fluorescence due to cell-associated FITC (FL1-H), measured in the cells that have been gated in histogram A. With increasing fluorescence, the peak will shift from the left to the right, indicating positive cells for the target of interest. Negative cells do not possess the fluorescent marker and thus remain on the left-hand side.

Selected cells were detached using Versene[18] and then neutralised with fresh medium. After centrifugation at 1200 rpm, the supernatant was discarded and the cells were washed with cold PBS, then kept on ice throughout the remaining procedure to prevent internalisation of the antibodies.

Cells were washed once in FACS buffer^{M} and re-suspended at 4 x 10^6 cells/mL. For the detection of surface molecules of interest, 50-µL portions of the primary antibody (10 µg/mL) were delivered into a V-bottomed 96-well plate, avoiding every other well to prevent contamination, followed by 50 µL of cell suspension, with gentle tapping to the side of the plate to ensure even mixing. The plate was incubated for 40 min at 4 °C. A non-specific cell line and non-specific antibody were used as negative controls. Cells were washed twice with FACS buffer. For each wash, cells were centrifuged in a plate-spinner at 1200 rpm for 3 min, and the supernatant was gently ejected. FACS buffer (150 µL) was added to each well and mixed with the cells. After re-centrifugation, the final supernatant was ejected and the pellets were each resuspended in 50 µL secondary antibody (1:500) conjugated with a fluorescent marker (goat-anti-mouse, alexa488-conjugated). Due to the

[18] Versene was used instead of 0.25% (w/v) trypsin / 0.53 mM EDTA solution because the latter sometimes cleaves the surface markers

photosensitive nature of the secondary antibody, cells were incubated for 30 min at 4°C in the dark, before washing the plate twice as previously described.

Re-suspended cell pellets in 100 µL of FACS buffer were transferred to FACS tubes pre-cooled on ice, each containing 400 µL of FACS buffer. Cells were then analysed with single-colour (green) analysis using a CellQuest / LSR-1 Flow Cytometer.

2.2.9 PRODUCTION OF DIABODIES

Manipulation of the glycine-serine linker prevents the natural folding of the variable light and heavy chains which normally fold and interact with each other to give rise to the antigen-binding site of the scFv. By manipulation or even the complete removal of this linker, the variable light and heavy chains are unable to fold and are held in place rigidly, which renders the scFv ineffective because the creation of the binding pocket is prevented. It is only by interaction with a complementary scFv to form a diabody that two binding sites can be formed (Figure 2.6).

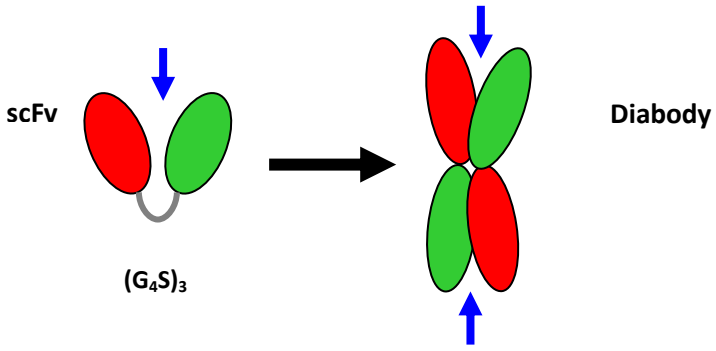

Figure 2.6: Schematic diagram of scFv and diabody antibody fragment. Red and green represent variable light and heavy chains respectively. Blue arrows indicate the binding domains which interact with specific antigen.

The manipulation of this linker can be effected by the many restriction enzyme sites present on the genetic map, which can cut at various places on the vector, depending on the endonuclease used[19].

2.2.9.1 Extraction of DNA

DNA was extracted from overnight cultures of selected clones grown in 2 x TY containing 100 µg ampicillin/mL and 1% (w/v) glucose, using a Quick Plasmid Miniprep Kit[M], according to the manufacturer's instructions. To ensure successful extraction, 5 µL of the extracted DNA mixed with 3 µL running buffer was applied to and run on a 0.8% agarose gel. A successful DNA extract revealed two bands, one of supercoiled DNA and the second of circular DNA.

2.2.9.2 Restriction Digest

The complete removal of the linker was achieved using the restriction enzymes XhoI and SalI (Figure 2.7), which were selected to cut at points before and after the linker, linearising the vector and ensuring complete removal of the linker.

Figure 2.7: Schematic representation of the cutting abilities of XhoI and SalI restriction enzymes.

XhoI and SalI cut at various points on the vector, creating "sticky or cohesive ends", where each restriction endonuclease has cut the DNA and caused a four-base overhang in one strand and a complementary terminus in the other. These ends can be joined by a ligase.

[19] Appendix I

Extracted DNA (10 µL per clone) was incubated with restriction digest mixture^{M} (20 µL) in duplicate at 37°C for 2 h. Remaining extracted DNA was stored at -20°C as back-up. To verify whether the digestion had been successful, another agarose gel was run, loaded with the pooled digestion reaction and 10 µL of loading buffer, split between two wells. Bands were visualised under a UV light, and excised and treated with QIAquick gel extraction to remove the agarose. A further verification to check for quantitative DNA recovery was performed by running 10 µL of the DNA extract on 1% agarose gel.

2.2.9.3 Ligation

After removal of the linker the newly-formed sticky ends were ligated. Reaction mixtures containing 5 µL of the digested DNA for each clone were incubated at 16°C overnight; negative controls were set up lacking ligase.

2.2.9.4 Preparation of Electroporation-Competent Cells

To prepare electroporation-competent cells, 1 L of 2 x TY medium containing 100 µg ampicillin/mL was inoculated with a 1:100 dilution of an overnight culture of *E. coli* HB2151 and incubated at 37°C with agitation (250 rpm). An inoculum of 10 mL from the overnight culture was added to 1 L of 2 x TY medium containing 100 µg ampicillin/mL and incubated again until OD_{600} = 0.5-0.7 was attained, after which the flask was cooled on ice for 15-30 min and centrifuged at 5000 rpm at 4°C. The pellet was resuspended in the original volume of ice-cold sterile 1 mM 4-(2-hydroxyethyl)-1-piperazineethanesulfonic acid (HEPES) buffer, pH 7.0, re-centrifuged, washed again in half the original volume of the same buffer, and centrifuged once more. The cells were resuspended in 20 mL 10% (w/v) glycerol, pelleted and finally resuspended in 2-3 mL 10% (w/v) glycerol to a final concentration of $3x10^{10}$ cells/mL) and stored at -80°C until needed.

2.2.9.5 Electroporation

For soluble expression of antibody fragments from pIT2, the non-suppressor strain *E. coli* HB2151 was used. Electroporation-competent bacteria, thawed on ice, (50 µL) were transferred to a pre-chilled 0.2-cm cuvette, mixed with 2 µL ligation mixture and left to

stand on ice for 1 min. Using a Gene Pulser machine at 25 µF, 2.5 kV, the reaction mixture was irradiated with the pulse set to 200 ohms. The resultant pores formed in the membrane allowed the reformed vector to enter the cells and be replicated. The culture was plated in 10-µL and 100-µL portions onto separate TYE plates and incubated overnight at 37°C.

Individual colonies were picked and incubated overnight with agitation (250 rpm) in 2 mL of 2 x TY with 100 µg ampicillin/mL and 1% (w/v) glucose. Mini-preps were prepared from the cultures, backing up the remainder as glycerol stocks. Removal of the linker was confirmed by performing digestions at various restriction sites, including those used originally, the rationale being that if the linker had been removed, the vector would no longer possess XhoI and SalI cut-sites, because they would have been lost along with the linker. XhoI and SalI were used in conjunction with two further restriction enzymes that would cut the DNA at different sites to yield fragments of differing size; thus two distinct bands would be visualised on the gel. If the linker were absent, XhoI and SalI combined with either HindIII or NotI would yield only one band, but two would be generated if XhoI and SalI were combined with both HindIII and NotI, or if the linker were present. Samples were analysed as before on 0.8% agarose gel.

2.2.10 COLUMN CHROMATOGRAPHY ANALYSIS OF ANTIBODY FRAGMENTS

2.2.10.1 High Pressure Liquid Chromatography (HPLC)

Size-exclusion HPLC is used to separate soluble compounds of different sizes. The HPL chromatograph consists of a reservoir of mobile phase, a pump, an injector, a separation column and a detector. After injecting a sample mixture onto the column, the different-sized components in the mixture pass through the column at different rates due to differential filtration through the stationary phase, the largest species emerging first. Samples were run using mobile phases of 0.1 M phosphate buffer, pH 7.0, containing 10%

(v/v) ethanol[20], and 0.1 M phosphate buffer, pH 7.0, containing 2 mM EDTA. Eluates were monitored from 220 nm to 280 nm.

2.2.10.2 Fast Protein Liquid Chromatography (FPLC) – ÄKTA ™

Unlike HPLC, FPLC allows the separation of compounds under low pressure, and can be used to determine the molecular weight of the sample injected; but it can also be used as a purification method for quantities of proteins that are too large for HPLC to handle. Gel filtration by FPLC was performed using a Sephacryl S-200 high-resolution column with spectrophotometric monitoring of the eluate at 280 nm.

Prior to use, the column was washed with filter-sterilised 20% (v/v) ethanol and water, and equilibrated with sterile PBS. Fractions (500 µL) of diabody and scFv fragments purified by Protein A chromatography were collected by elution with PBS as per the manufacturer's instructions.

2.2.11 RADIOLABELLING OF SCFV AND DIABODY USING SODIUM [^{125}I]-IODIDE

2.2.11.1 Sodium [^{125}I]-Iodide and Iodogen

Iodine-125[21] is used to radiolabel antibody fragments, reacting with tyrosine and some histidine residues in proteins or peptides by electrophilic substitution [172]. For efficient labelling of antibody fragments, iodinations were conducted in glass tubes (12 x 75 mm) coated at the bottom with the oxidant iodogen 1,3,4,6-tetrachloro-3α, 6α-diphenylglycoluril for the activation of ^{125}I. One possible drawback of this technique is that the iodogen can cause oxidative damage to the sample being labelled.

The procedure was performed in a fume hood. To the iodogen tube, 50 µL of PBS was added, followed by approximately 2 MBq of sodium [^{125}I]-iodide, and finally 20 µg of the

[20] Ethanol improves recovery without affecting retention times
[21] ^{125}I half life = 60 days

antibody fragment. After mixing, the tube was incubated at room temperature for 10 min before the addition of 100 µL of PBS and transfer into a storage cryovial, then stored at 4°C. Confirmation of successful labelling was achieved by Instant Thin Layer Chromatography (ITLC) of the samples.

2.2.11.2 Instant Thin Layer Chromatography (ITLC)

Samples on ITLC-Silica Gel (ITLC-SG) strips (1 x 8 cm) were developed in duplicate, in 85% methanol. A 1 µL fraction of labelled antibody fragment was spotted onto strips, which were developed to within 1 cm of the top. Strips were removed from the solvent tank, dried, and the labelled antibody fragments were visualised using a phosphor imager. The percentage of the radioactivity in each part of each strip was calculated.

2.2.11.3 Radioimmunoassay

Immunoreactivity can be used either to compare the binding ability of radiolabelled antibody with that of the unlabelled starting material, or to measure the proportion of the radiolabelled antibody able to bind to the target antigen [172]. Both methods are used to assess the antibody's ability to bind to the target antigen.

To determine whether the ability of antibody fragments to bind to the antigen has been damaged or compromised by the addition of the radioisotope, the ability of the radioactive antibody fragment to bind to the antigen-expressing cells was measured.

LNCaP C81 cells ($3x10^7$) were trypsinised and resuspended in 5 mL of cold 1% BSA-PBS, then washed and resuspended in 3 mL of the same buffer. After diluting the suspension to 8 x 10^6 cells/mL, 0.5 mL aliquots were transferred into a duplicate series of 5 tubes and serially diluted 1:2 with PBS. Two further tubes each containing $4x10^6$ cells in 0.5 mL were labelled as non-specific binding (NSB) samples, and to these, 50 µL of the unlabelled antibody fragment was added with brief vortexing.

Radiolabelled antibody was diluted to a final concentration of 50 ng/mL with cold 0.1% BSA-PBS, and 250 µL thereof was dispensed to all the tubes and a further two tubes

labelled "T" (to measure total activity). Tubes were incubated with rotation either for 2 h at room temperature or for 3 h at 4°C.

After incubation, tubes were centrifuged at 13,000 rpm in a micro-centrifuge for 2 min and supernatants were carefully removed and collected into new tubes. Cell pellets were washed twice with 500 µL of cold 0.1% BSA-PBS per tube and re-pelleted by centrifugation as before. The supernatants from the washing steps were also collected and pooled with the previous wash samples to determine whether bound antibody was lost by washing. Tubes were submitted to the gamma counter, together with those labelled "T", and the immunoreactivity was determined.

2.2.12 IMAGING OF SODIUM [^{125}I]-IODIDE-LABELLED ANTIBODY FRAGMENTS IN TUMOUR-BEARING MICE

The characteristics and behaviour of the antibody fragments established *in vitro* needed to be demonstrated *in vivo* to conclude with absolute certainty that the fragments targeted and bound specifically to the target antigen – PSMA. Many new factors, such as concentration, pH and affinity, come into play *in vivo*, and can cause fragments to dissociate, rendering them ineffective.

Ten male SCID Beige mice[M22] aged 4-6 weeks were each injected subcutaneously on both hind-leg flanks with 10 million LNCaP C81 cells mixed with Matrigel[23] in a 1:1 ratio by volume, in a total volume of 200 µL. Tumours approximately 5 mm^3 in size became visible beneath the fur about 5 weeks post injection. Mice were injected intravenously in the tail (100 µL total volume) with 7 MBq (10 µg) of ^{125}I-labelled scFv or diabody, and uptake and

[22] Congenic mice that possess both autosomal recessive mutations SCID(Prkdc^{SCID}) and beige (Lyst^{BG}). The SCID mutation results in the severe combined immunodeficiency affecting both T and B lymphocytes. The beige mutation results in defective natural killer (NK) cells.

[23] Matrigel contains structural proteins such as laminin and collagen which provide additional support to the cells in a form of a growth matrix, which increases vascularisation.

distribution was measured by SPECT[24] at various time points; 30 min, 4 h and 34 h after injection of the radiolabelled antibody fragments. Images obtained allowed visualisation of uptake and clearance of labelled antibody fragments from the tumours and other organs. Uptake and retention in certain organs helps to understand the behaviour of labelled antibody fragments.

2.2.13 SINGLE PHOTON EMISSION COMPUTED TOMOGRAPHY (SPECT)

For CT scans, mice were scanned feet-first for approximately 6-7.5 min/180 projections. CT data was reconstructed using CT Reconstruction on the Bioscan InVivoScope (IVS) software, using standard reconstruction resolution. For SPECT images, 1.4-mm pinhole collimators were used and mice were scanned feet-first for approximately 30 min/24 projections. Images were reconstructed in a 256 x 256 matrix using HiSPECT, a reconstruction software package, and were fused with CT images using proprietary Bioscan IVS software.

[24] Chapter 1 - Section 1.11.7

2.3 METHODOLOGY 2

This methodology relates to the results section in chapter 4

2.3.1 RADIOLABELLING

2.3.1.1 Radiolabelling Demobesin 4 (DB 4)

Technetium was provided by the Radiopharmacy Department, St. Bartholomew's Hospital. On the day of the experiment, ^{99m}Tc (present chemically as pertechnetate) was eluted from the molybdenum-99 generator, from which the isotope ^{99m}Tc is continuously formed by nuclear decay. Pertechnetate is separated off from molybdenum-99 by washing with isotonic sodium chloride solution.

Almost all technetium-labelled pharmaceuticals are prepared by reducing pertechnetate from +7 to a lower oxidation state, usually +4. Once in this reduced state, technetium will readily bind to chelating agents and other compounds. This reaction can be achieved by the addition, with the ligand, of several labelling components that facilitate the reaction, together with stabilisers and buffers.

2.3.1.2 Stannous Chloride

A reducing agent commonly used in ligand binding reactions is stannous (Sn^{2+}) chloride. Stannous ions reduce pertechnetate (Figure 2.8) which binds to the ligand. A short incubation at room temperature completes the reaction.

$$2\ ^{99m}TcO_4^- + 16H^+ + 8Sn^{2+} \longleftrightarrow 2\ ^{99m}Tc^{4+} + 8Sn^{4+} + 8H_2O$$

Figure 2.8: Equation for reduction of technetium with stannous chloride [172].

Stannous chloride is added in excess, so minimising the amount of unbound pertechnetate, and the reaction is performed in nitrogen-purged vials to prevent the re-

oxidisation of technetium ions, thereby limiting the amount of unbound and reduced technetium released by hydrolysis [172].

2.3.1.3 Binding Components and Labelling of DB 4

In addition to stannous chloride, other components are added to the reaction mixture which facilitate binding of Tc and reduce the formation of unwanted by-products. Trisodium citrate is a weak chelator for technetium which chemically stabilises the isotope and prevents the formation of Tc-colloids (TcO_2 and insoluble hydroxides, formed at neutral/alkaline pH). The reaction is buffered with phosphate and the addition of ethanol reduces hydrophobic interactions of Tc compounds with the polypropylene vial used.

Into a lead-shielded polypropylene vial, the following components were added in the following order: 100 µL 0.25 M phosphate buffer^{M}, 5 µL 0.1 M trisodium citrate, and 400 µL $^{99m}Tc^{4+}$ solution at the desired radiochemical activity. DB 4 (10 µg) was added prior to stannous chloride (60 µg (w/v), in ethanol, freshly prepared), followed by 40 µL ethanol. After thoroughly mixing, the reaction was allowed to proceed at room temperature for 30 min while the labelling took place.

2.3.2 QUALITY CONTROL ANALYSIS

2.3.2.1 Instant Thin Layer Chromatography (ITLC)

Subsequent to the labelling reaction, it is important to determine the radiochemical purity of Tc-labelled DB 4, i.e. how much labelled peptide is present in comparison with undesirable by-products. Both ITLC and HPLC analysis can be used to determine the success of the labelling. ITLC is a rapid, simple method of determining labelling efficiency; for DB 4, ITLC was carried out using two solvents, acetone and methanol : 1 M ammonium acetate (1:1, by vol.) which resolve the radiolabelled peptide from other products (Figure 2.9).

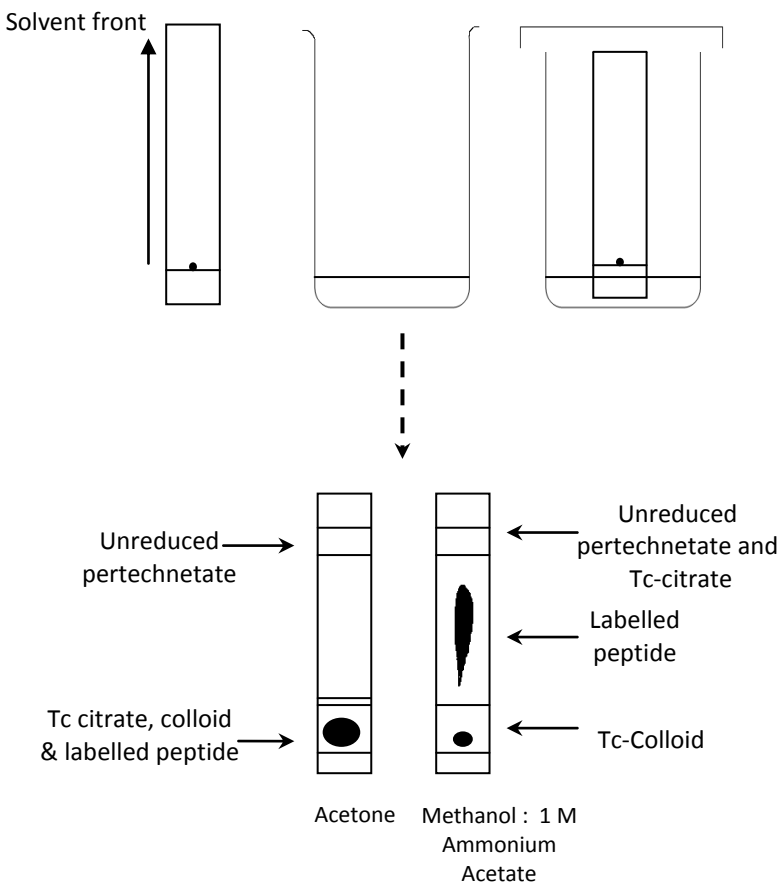

Figure 2.9: Schematic diagram of ITLC resolved in acetone and methanol:ammonium acetate. The two strips were run concurrently, one in each solvent.

ITLC performed in acetone allows for the resolution of remaining free pertechnetate. Using methanol : 1 M ammonium acetate, the radiolabelled peptide is resolved from Tc-colloids and Tc citrate. ITLC strips were exposed for varying times to phosphor imager screens from which images were obtained by scanning them on a Cyclone Plus Storage Phosphor System, using the programme OptiQuant™, which calculates the percentages of the labelled peptide and other radiolabelled components present.

2.3.2.2 High Pressure Liquid Chromatography (HPLC)

There are a number of limitations associated with HPLC analysis of Tc radiopharmaceuticals, as the method relies on the complete elution of all the radioactive species injected onto the column, which is not possible when the sample contains

colloidal or reduced TcO_2, because these components become trapped on the column and therefore over-estimations of sample purity occur. Therefore this method is best used in conjunction with ITLC analysis. HPLC is advantageous over ITLC because it enables recovery of the purified fraction.

HPLC was carried out on a reverse-phase column, C_{18}ODS, using a gradient of aqueous 0.1% (v/v) trifluoroacetic acid (TFA)[25] (solvent A) and acetonitrile (solvent B). UV detection was performed at 160-280 nm and radioactivity was detected using an in-line gamma-detector.

The gradient system used for analysis was as follows: 40% A : 60% B for 25 min, then B was increased linearly to 100% over the next 5 min to elute lipophilic impurities, and reduced to 0% (i.e. A was increased to 100%) linearly thereafter over 5 min. The flow rate was 1 mL/min. Solvent A was passed through the column for ten minutes between injections to allow re-equilibration. The radiolabelled peptide was diluted 1:1 in PBS before injecting 20 - 30 µL samples.

Unbound pertechnetate eluted from the column within a few minutes, in 40% A : 60% B, followed by the radiolabelled peptide (Tc-DB 4), usually towards the end of the 40% A : 60% B mixture, at just over 20 min.

2.3.3 CELL LINES

Prostate cancer cell lines and negative control cell lines for gastrin-releasing peptide receptor (GRP-R) expression experiments are shown in Table 2.3 .

[25] TFA facilitates the release of peptides from solid-phase resins

Table 2.3: Prostate cancer cell lines and negative control cell lines for GRP-R expression experiments. *GRP-R negative, ** GRP-R positive.

Cell line	Description	Species	Androgen Dependence
PC3	PC bone metastasis	Human	Independent
DU145	PC brain metastasis	Human	Independent
LNCaP	PC	Human	Dependent
LNCaP C42B	PC bone metastasis	Human xenograft	Independent
LNCaP C81	PC lymph node metastasis	Human	Independent
MKN45 *	Stomach adenocarcinoma	Human	N/A
AR42J **	Pancreatic neuroendocrine tumour	Rat	N/A

Cells were handled using standard tissue culture techniques[26]. In conjunction with these cell lines, LNCaP C42B and C81 were also sub-cultured in androgen-deprived media, and are denoted as LNCaP C42B and C81 androgen-deprived in future experiments. RPMI phenol red-free medium was used (phenol red can bind to the androgen receptor and activate it through the promiscuous pathway[27]), and supplemented with 8% (w/v) charcoal-stripped FBS (CS-FBS) and 2% (w/v) regular FBS. CS-FBS, which is commercially available, is used to elucidate the effects of hormones within media that are used in a variety of *in vitro* systems. Activated carbon is used to remove non-polar, lipophilic materials such as growth factors, hormones and cytokines from the medium without affecting the salt, glucose and amino-acid content. However cells were unable to grow in CS-FBS alone, probably due to removal of essential growth factors, therefore they were grown in the lowest concentration (8% CS-FBS with 2% FBS) that ensured healthy growth, but were switched to total CS-FBS 24 h prior to experiments.

[26] Chapter 2 - Section 2.2.7
[27] Chapter 1 - Section 1.2.2

2.3.4 RADIOLIGAND BINDING ASSAY

Once the peptide has been successfully radiolabelled, it is important to determine whether it has retained its receptor-binding affinity, and that this has not been compromised in any way. The ability of the labelled peptide to bind to a receptor preparation is measured in a radioligand binding assay (saturation assay; Figure 2.10).

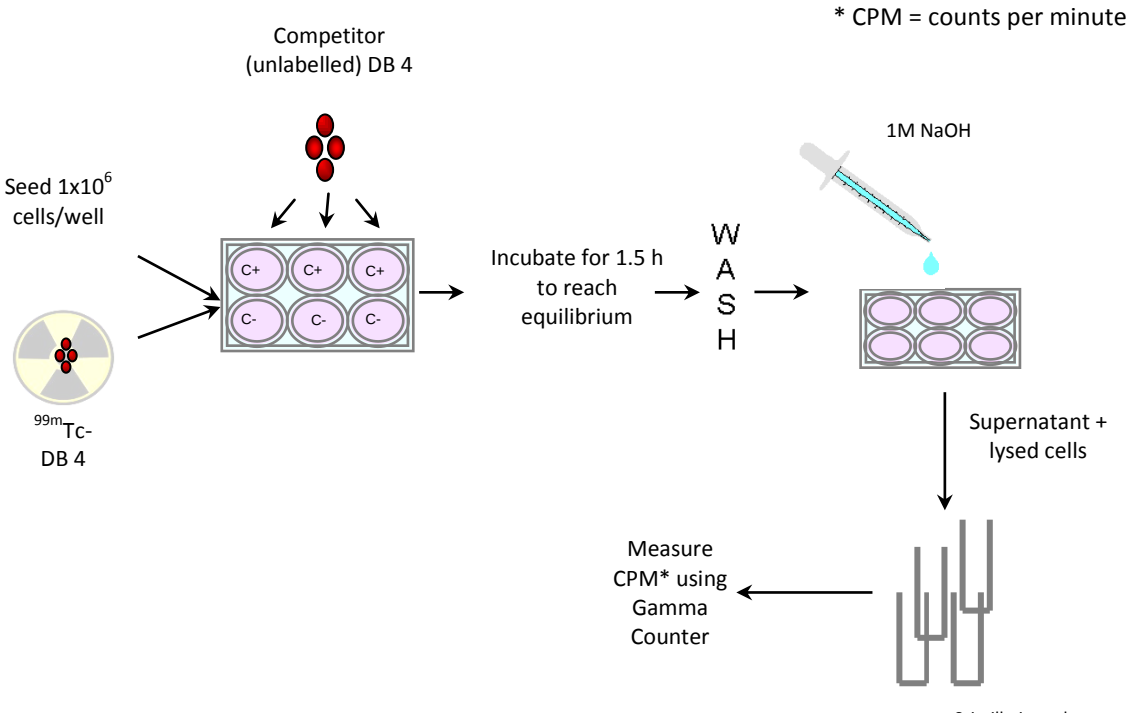

Experiments were performed on all cell lines in triplicate and repeated three times on separate occasions

Figure 2.10: Schematic representation of each step in a radioligand binding assay. C+ and C- = with and without the addition of competitor (unlabelled DB 4). With competitor measures non-specific binding; without measures total binding (non-specific and specific binding).

The receptor preparation is normally in the form of cells (or cell membranes), and serial dilutions of the radiolabelled peptide are incubated with the cells at either 37 or 4°C for 1.5 h in order for binding equilibrium to be reached. As well as specific binding to the receptors, non-specific binding can also occur due to hydrophobic and ionic interactions with other sites on the cell surface, and it is important to identify the proportions that are specific and non-specific from the total binding observed.

2.3.4.1 Preparation of Cells

Forty-eight hours prior to the experiment, adherent cells ($1x10^6$ per well), in 2 mL of cell growth medium (RPMI 10% FBS) per well, were seeded in a 6-well plate. One plate was prepared for each of the following concentrations of radioligand: 25, 10, 7.5, 5, 2.5, 1 and 0.1 nM.

Prior to experimentation, cells in the plates were checked to ensure they had fully adhered to the wells and were not over-confluent. The medium was aspirated carefully to avoid disturbing the cells, which were washed twice in PBS to remove any that were not adhering. Fresh medium (1.2 mL/well) containing 1% (w/v) FBS and 0.1% (w/v) sodium azide[28] was added and plates were returned to the incubator until needed. The remaining medium was kept at 4°C.

2.3.4.2 Radioligand

DB 4 was radiolabelled and the radiochemical purity determined[29]. The radioligand was prepared at 10x the concentration ultimately required. Assays were performed in triplicate, and for each concentration of radiolabelled peptide, a duplicate well containing unlabelled competitor was set up. Competitor wells received, in 1% PBS-BSA, 150 µL of unlabelled DB 4 at a final concentration of 1 mM. The corresponding non-competitor wells received 150 µL 1% PBS-BSA to bring the protein concentration and volume to the same values. All wells received 150 µL of the appropriate concentration of labelled DB 4, added dropwise to the contents of each well, avoiding contact with the walls to prevent non-specific binding to the plastic. Plates were gently swirled to ensure even dispersion of the radioligand, then incubated at 37°C under 5% (v/v) CO_2/air for 90 min.

[28] Sodium azide prevents the internalisation of the bound radioligand because the uptake is driven by active (energy-dependent) transport - which is inhibited. If the peptide was internalised, the radioisotope would be deposited in the cell, the peptide broken down by peptidase action, and the receptor recycled and re-presented on the cell ready to be bound again. This would give high readings due to the accumulation of the radioisotope rather than to binding.

[29] Chapter 2 - Section 2.3.2

After incubation, the medium was aspirated and the cells washed twice in 1% FBS, then in medium containing 0.1% (w/v) sodium azide, and finally in ice cold PBS, taking care not to disturb the cells. To each well, 1 mL of 1 M NaOH was added to lyse the cells and left until lysis became apparent (10 min).

Thereafter, three 5 µL-aliquots per well were transferred to a 96-well plate for determination of protein concentration. Protein was assayed using the Bio-Rad Protein Assay Kit^{M}, as per manufacturer's instructions, and the plate was measured on the plate reader at 595 nm. The remaining supernatant samples were transferred into scintillation tubes, together with the washings from two 1-mL fractions of PBS for each well, and the tubes were then counted on the gamma counter. This experiment was performed three separate times for each cell line to allow for statistical analysis.

2.3.5 BIODISTRIBUTION

Once successful *in vitro* experiments have been undertaken, *in vivo* analysis is essential to determine parameters such as biodistribution into tissues, target-to-background ratios, and the clearance times from the blood and body. These factors are determined by the stability of Tc- labelled DB 4 complex *in vivo.* Animal models, commonly immunodeficient mice, are used for these biodistribution studies. Animals are injected with cancer cells to form tumours, then injected with the radiolabelled ligand of interest, and at varying times thereafter are culled, the organs are excised and radiochemical activity is measured using a gamma counter.

2.3.6 IMAGING

2.3.6.1 Single Photon Emission Computed Tomography (SPECT)

SPECT is a nuclear medicine tomographic imaging technique using gamma rays. By imaging through sections, 3D images can be generated [30].

2.3.6.2 Preparation of Mice

Groups of 12 male beige SCIDS mice aged 4-6 weeks were used for the imaging and biodistribution studies. Subcutaneous inoculations of the desired cells (10^6) on both hind-leg flanks were made with and without Matrigel (1:1) and grown until tumours were visible beneath the fur.

DB 4, labelled and verified for radiochemical purity, was drawn up in 100-µL doses into identical insulin syringes, one per animal and an additional dose as a control. The radiochemical activity of all syringes was measured in the isotope calibrator, and their activity and weights were recorded to enable calculation of the injected dose later. Animals were injected via the tail veins, collecting any wipes used to dab the wound into individual scintillation counting tubes. As a control to standardise the experiment, a 100-µL dose (assuming an injected dose of that volume) was dispensed into a polypropylene 15-mL falcon tube containing 9.9 mL of 1% PBS-BSA[31]. Injection times and the weights of empty syringes were recorded. Groups of 3 or more mice were used per time point, to allow for statistical analysis, and were either scanned or culled at 1, 2.5 and 4 h post injection, depending whether they were to be imaged or used for biodistribution analysis respectively.

The amount of activity varied per experiment, however approximately 40 MBq of Tc-DB 4 per mouse for imaging, and 2-4 MBq per mouse for biodistribution studies, was injected intravenously.

[30] Chapter 2 - Section 2.2.13

[31] BSA was used to minimise non-specific binding to the tube

For biodistribution studies, the empty scintillation tubes were weighed with their lids prior to the experiment, and reweighed after filling to obtain the weights of the excised tissue. Tissue samples (within the scintillation tubes) were counted in the gamma counter together with three 1-mL fractions from the 10-mL control sample, neat and after dilution (1:10 and 1:100). The counts obtained from the counted tissues were compared with counts obtained from the control standards which were corrected for dilution to obtain CPM per mL and the percentage of injected dose per gram of tissue was calculated.

2.3.7 AUTORADIOGRAPHY

2.3.7.1 Preparation of Tumours

Tumours were grown subcutaneously in the same manner as for biodistribution and imaging studies, until notable beneath the fur, then excised, mounted onto 2-cm-diameter cork discs covered with Optimal Cutting Temperature (OCT) Gel, which when frozen becomes a solid white protective layer over the embedded tissue. The tumour was completely covered in OCT Gel before snap-freezing in *iso*-pentane pre-cooled in liquid nitrogen. Once completely frozen, tumours were cut at 20 µm thickness onto slides and stored at -80°C until needed.

Slides were thawed at room temperature for 10 min and photographed over a Perspex sheet bearing a small square grid (of size approximately 0.3 mm), in order to orientate the location of the tumour after autoradiography (Figure 2.11).

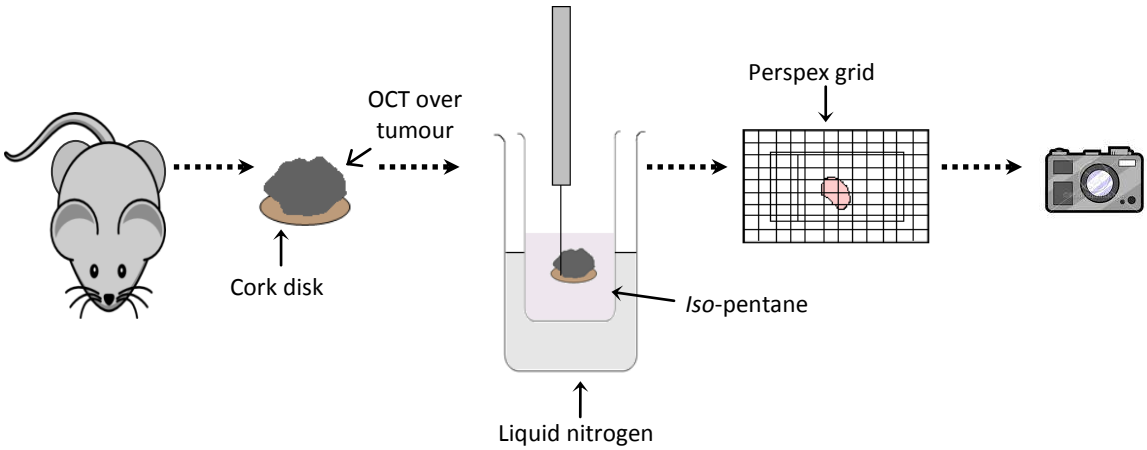

Figure 2.11: Schematic representation of preparation of tumours ready to perform autoradiography.

Slides were pre-incubated in 10 mM HEPES, pH 7.4, for 5 min at room temperature, followed by incubation in radiolabelling attachment buffer $(RA)^M$ containing radiolabelled DB 4 for 1 h at room temperature. Slides were washed four times in 10 mM HEPES, pH 7.4 / 0.1% BSA at 4°C, rinsed twice in ice-cold distilled water for 5 s, and dried fully before exposure to the phosphor imager plate for 24 h. Autoradiography on each cell line was performed in duplicate, with and without competitor, to establish specific binding.

Serially-diluted samples of radioligand were spotted in 5-µL fractions onto a glass slide and allowed to dry before exposing alongside the tumour sections. Samples of these dilutions were also placed in scintillation tubes and counted on the gamma counter.

2.3.8 REAL-TIME PCR (QUANTITATIVE PCR)

Real-time PCR (RT-PCR) or quantitative PCR is a method for determining the amount of a target sequence or gene that is present in a sample. It monitors the progress of PCR as it occurs; data is collected throughout the PCR process rather than at the end, allowing a more quantitative study of gene expression. Reactions are characterised by the point in time during cycling when amplification of a target is first detected, rather than the amount of target accumulated after a fixed number of cycles.

There are two types of RT-PCR; absolute quantification and relative quantification. In the present experiments, the latter was utilised. Relative quantification determines the change in expression of a nucleic acid sequence (target) in a test sample relative to the same sequence in a calibrator sample, which in this instance was a non-GRP-R-expressing cell line, MKN45. Also run in parallel was an endogenous control gene, which was the housekeeping gene for β-actin. Its expression occurs in all the samples at consistent levels and for this reason is commonly used as a reference in RT-PCR reactions [173]. The endogenous control allows one to normalise quantification of the cDNA target for differences in the amount of cDNA added to each reaction.

A singleplex reaction (a single primer pair per reaction) was performed against the target (GRP-R) with β-actin as the endogenous control for each of the cell lines. A two-step reaction was performed, whereby total RNA was first transcribed into cDNA, which was then amplified by PCR.

The RT-PCR reaction occurs in a four-step process (Figure 2.12). The oligonucleotide probe has a fluorescent reporter dye attached to the 5' end and a quencher at the 3' end. The quencher greatly reduces the fluorescence emitted by the reporter dye when the probe is intact. When the probe finds the target sequence, it anneals between primer sites and is cleaved, removing the probe from the target strand and separating the reporter dye from the quencher, thereby increasing the reporter signal. Cleavage allows primer extension to continue to the end of the template strand. For the GRP-R transcript, the TaqMan® Gene Expression Assay was used, an already optimised and ready-to-use 5' nuclease assay. The probe was labelled at the 5' end with FAM™ as the reporter dye, and a non-florescent quencher combined with a minor groove binder (MGB) moiety[32] at the 3' end.

[32] The MGB stabilises the hybridised probe.

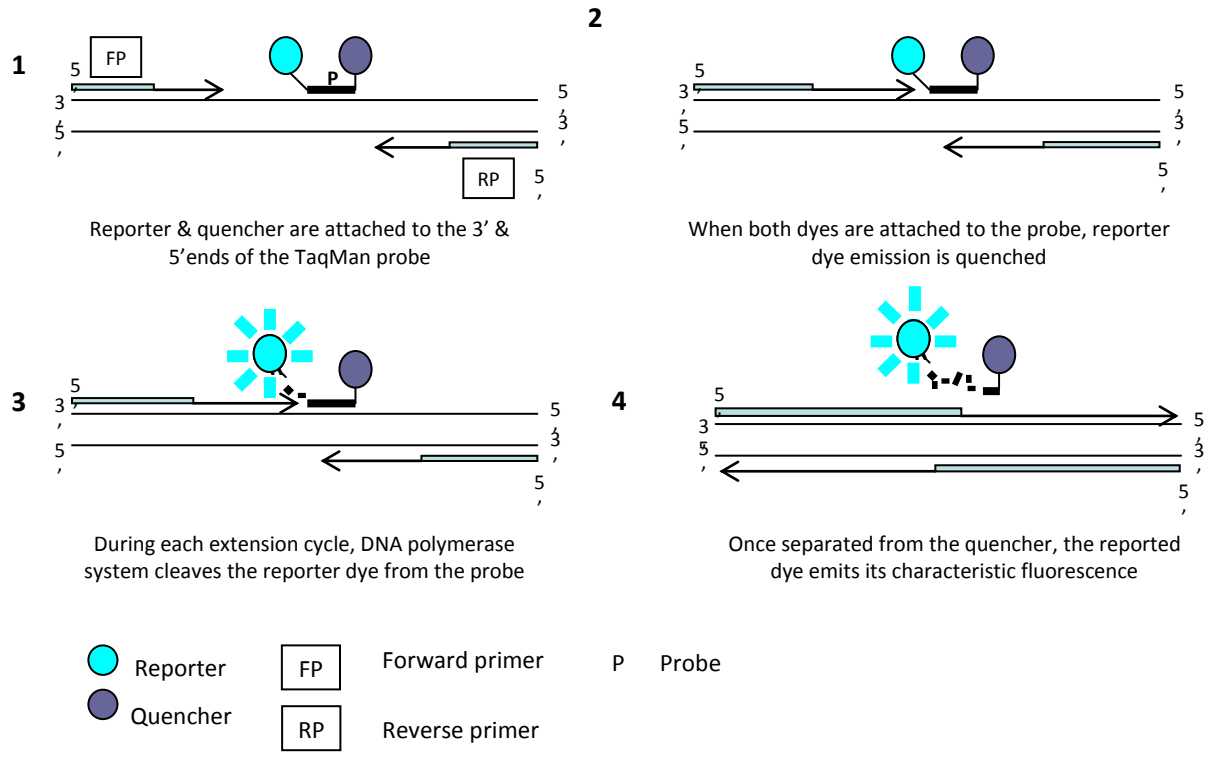

Figure 2.12: Four-step schematic representation of the 5' nuclease chemistry uses a fluorogenic probe to enable detection of a specific PCR product.

2.3.8.1 RNA Isolation

Cells were detached from the flask using Versene instead of 0.25% (w/v) Trypsin / 0.53 mM EDTA solution, to eliminate any possibility that the expressed receptor was cleaved. Detached cells were washed twice in PBS and the pellet was taken forward for RNA isolation using the RNeasy Mini Kit^{M} as per manufacturer's instructions. A negative GRP-R cell-line served as the control. The kit comprises a spin column which allows up to 100 µg of total RNA of minimum length 200 bases (mainly mRNA) to bind to a silica-gel membrane, with the aid of a specialised high-salt buffer. The addition of ethanol ensures the binding of total RNA to the column membrane, and contaminants are efficiently washed away.

Briefly; the pellet, comprising $5x10^{6}$ cells, was homogenised in 350 µL of lysis buffer containing guanidine thiocyanate, and β-mercaptoethanol (10% of final volume) to inactivate RNase. Thorough mixture of cells and buffer was achieved by pipetting

followed by vortexing for 1 min. To the homogenised lysate, 350 µL of 70% (v/v) ethanol was added and mixed well, before transferring all the lysate, including any precipitate that formed, to an RNeasy mini-column equipped with a 2-mL collection tube, and centrifuging for 15 s at 8000 g. The flow-through was discarded, and the column was washed. DNase I was applied to the column membrane and incubated at room temperature for 15 min, followed by wash buffer (350 µL). The column was re-centrifuged, again discarding the flow-through, then washed again twice with the appropriate buffer before being transferred to a new collection tube. RNase free-water (50 µL) was applied directly onto the membrane and the column was centrifuged for 1 min at 8000 g to recover the eluted RNA. RNA yield and purity was determined spectrophotometrically using a NanoDrop spectrophotometer at 260 and 280 nm. Recovered total RNA gave A_{260}/A_{280} >1.9. Samples were stored at -80°C until needed or taken forward for cDNA synthesis.

2.3.8.2 cDNA Synthesis

cDNA synthesis was performed using a cDNA synthesis kit[M] as per manufacturer's instructions. Briefly, defrosted RNA samples were placed on ice with other kit components. The concentration of RNA was measured again to ensure that the freeze-thawing process had not damaged it. In a 0.5 mL tube, the following components (Table 2.4) were mixed to generate the RNA/primer mixture:

Table 2.4: RNA/primer mixture

Components	Volume (µL)
5 µg total RNA	x
random hexamers	1
10 mM dNTP mix	1
RNase free water	To a total of 10

Random hexamers are a mixture of oligonucleotides representing all possible sequences for a hexamer. x varied between 1 and 7 µL.

After mixture, samples were incubated at 65 °C for 5 min, then placed on ice for a minimum of 1 min. A cDNA synthesis mixture was prepared, adding each component in the order shown in Table 2.5.

Table 2.5: cDNA synthesis mixture.

Components	Volumes (µL)
10x RT buffer	2
25 mM $MgCl_2$	4
0.1 M DTT	2
RNaseOUT™	1
SuperScript™ III	1

RT Buffer comprised of 200 mM Tris-HCl, pH 8.4 / 500 mM KCl, RNaseOUT safeguards against degradation of target RNA due to ribonuclease contamination and SuperScript III RT is used to synthesise first-strand cDNA.

cDNA synthesis mixture (10 µL) was mixed gently with the RNA/primer mixture, then incubated on the thermo-cycler at 25°C for 10 min, followed by 50°C for 50 min, and finally 85°C for 5 min, after which samples were chilled on ice. In parallel, a reverse-transcriptase control without RNA was also prepared. Brief centrifugation ensured collection of each sample without any air bubbles before the addition of 1 µL of RNase H solution to each tube and incubation at 37°C for 20 min. Samples were used for PCR immediately or stored at -20°C in aliquots to minimise repeat freeze-thaw cycles.

2.3.8.3 Real-Time PCR – Experimental Protocol

RT-PCR was performed by setting up PCR master mix for a 20 µL reaction, for both the tested gene and the endogenous (β-actin) control (

Table **2.6**)

Table 2.6: Master Mix for RT-PCR

Master Mix		
Components	**Tested Gene (µL per reaction tube)**	**Endogenous Control (µL per reaction tube)**
TaqMan	10.0	10.0
TaqMan Gene	1.25	-
β-Actin Gene	-	1.25
Water	4.75	4.75

The PCR master mixture was distributed in 16-µL aliquots into the wells of a RT-PCR plate at room temperature. To this, 4 µL of cDNA template was added and mixed by pipetting. The plate was briefly centrifuged to collect the contents at the bottoms of the wells, then stored on ice until used.

The plate was placed in the RT-PCR instrument and incubated, using the following settings (Table 2.7).

Table 2.7: RT-PCR Instrument Settings

RT-PCR Settings			
	Repetitions	**Temperature (°C)**	**Time**
Reverse Transcription	1	50	2 min
Enzyme Activation	1	95	10 min
PCR Cycle (melt)	40	95	15 s
PCR Cycle (anneal & Extend)	40	60	1 min

An amplification plot for each sample was obtained and further analysis was performed on the threshold cycle (C_T) values acquired. An example of an amplification plot (Figure 2.13) attained in RT-PCR, shows how C_T values are derived. C_T is the intersection between an amplification curve and a threshold line (automatically determined; it is set above the baseline, but sufficiently low to be within the exponential growth region of the

amplification curve). It is a relative measure of the concentration of the target in the PCR reaction. A no-template control (NTC) sample that does not contain template is performed to verify amplification quality.

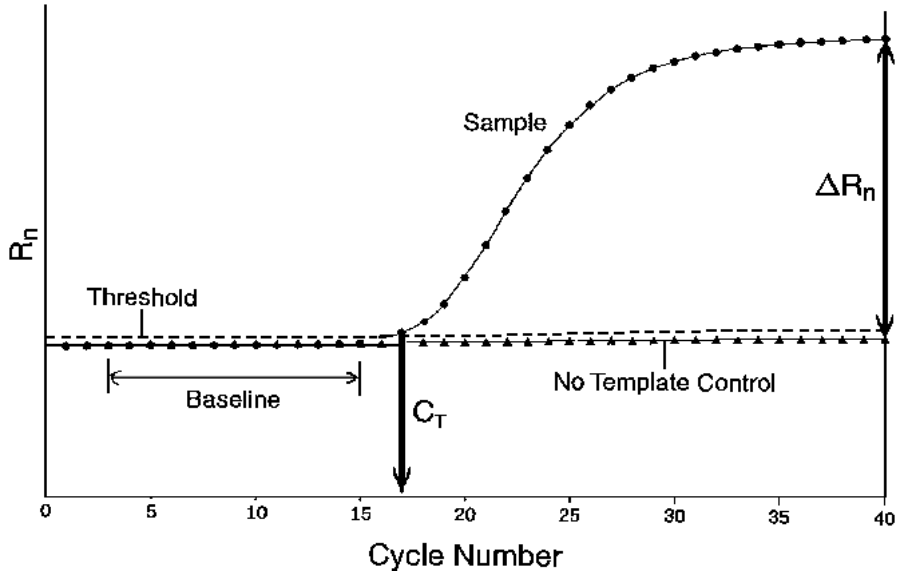

Figure 2.13: A representation of an amplification plot. R_n = the ratio of the fluorescence emission intensity of the reporter dye to the fluorescence emission intensity of the passive reference dye. ΔR_n = the magnitude of the signal generated by the specified set of PCR conditions ($\Delta R_n = R_n$ - baseline).

2.3.9 IMMUNOHISTOCHEMISTRY ON TUMOUR SECTIONS

Immunohistochemistry (IHC), in the present context, is the localisation of antigens in tissue sections by the use of labelled antibodies as specific reagents through antigen-antibody interactions. These are visualised by use of a marker such as a fluorescent dye, an enzyme, a radioactive element, or colloidal gold.

Tumours were processed by the pathology services at the Institute of Cancer, Queen Mary University, using the Ventana Discovery™ Immunohistochemistry Unit, which stains samples automatically and performs IHC under controlled conditions, minimising technique-dependent errors and increasing reproducibility and productivity. Slides were

treated with the Discovery™ DAB Map™ Kit, designed for antigen localisation in cytological preparations, frozen sections, or formaldehyde-fixed, paraffin-embedded tissue sections. The kit is based on peroxidase detection using 3,3-diaminobenzidine (DAB), an insoluble, light-insensitive chromogenic substrate for peroxidase product, which stains antigen-antibody sites brown, and contrasts well with the blue nuclear counterstain, haematoxylin. It ensures sensitive and specific antibody detection by incorporating streptavidin-biotin technology for the detection of antibodies (in a number of applications), and reduces background staining.

Optimisation of the commercially available anti-GRP-R antibody (Abcam 39963) was performed on human pancreatic tissue. A range of antibody dilutions were tested and a 1:100 dilution was found to be the optimal concentration, yielding good staining on tissue sections. Tumour sections were viewed under a standard light microscope.

All tumour sections were stained for GRP-R expression and compared both the positive control (pancreatic tissue) and negative control (no antibody).

3 PSMA STUDY

3.1 AIMS AND OBJECTIVE

Recognising the shortage of PC radiopharmaceuticals to image and stage PC, it was the aim of this study to explore new approaches to identify new ligands as potential targets for PC imaging.

PSMA was selected as a promising clinical biomarker target for diagnosis, detection and management of PC. The aim of this project was to develop a PSMA-specific scFv and successfully radiolabel to develop a radiopharmaceutical that could image all stages of PC growth.

The objectives were to;

1. To screen phage display libraries against both cell-expressed PSMA and recombinant PSMA protein.
2. To construct diabody fragments and assess binding specificity against svFv.
3. To apply established radiolabeling techniques appropriate for different imaging approaches using the selected scFv and diabodies with low and high affinity and compare their pharmacokinetics and efficacy to each other.

3.2 PSMA STUDY RESULTS

3.2.1 PHAGE DISPLAY

3.2.1.1 Selection for Anti-PSMA Phage on PSMA-Expressing Cells

Selection for anti-PSMA scFv was performed using phage display. Two approaches were taken to select for anti-PSMA scFv; one performed on cells naturally expressing PSMA, and the second approach using in-house-generated recombinant PSMA protein. The rationale behind this was to enable the selection of scFv that bound to the target antigen - PSMA.

Selection on PSMA-expressing cells was considered to be the preferred approach, as phage would recognise the naturally-occurring PSMA that bears the typical conformation and glycosylation patterns[33]. Using the Tomlinson I Library [90], selection for anti-PSMA-specific phage was therefore performed on the non-PSMA and PSMA-expressing cell lines, DU145 and LNCaP C81 respectively[34] (Figure 3.1).

[33] Glycosylation is an enzymic process which, as well as producing fundamental components of all cells, also provides a co-translational and post-translational modification mechanism that modulates the structure and function of the membrane and secreted proteins.

[34] LNCaP C81 and DU145 cells are respectively derived from human lymph node metastasis and human brain metastasis.

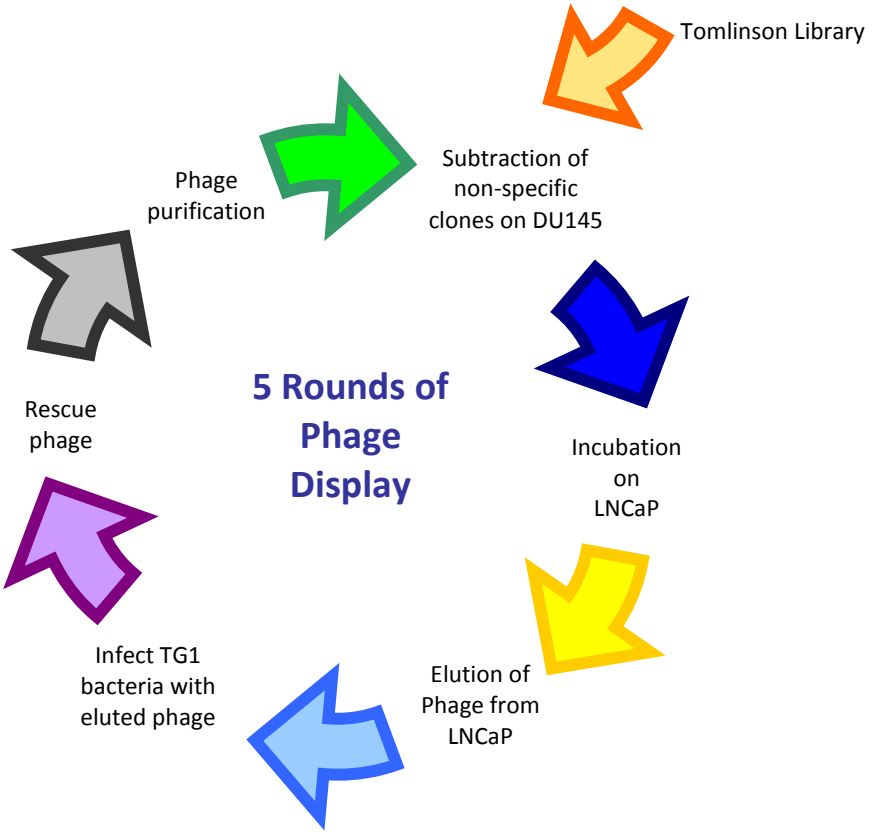

Figure 3.1 Schematic representation of selection performed on cells. DU145 are PSMA negative and were used to subtract non-specific clones before incubation on PSMA-positive cells, LNCaP C81. A total of 5 rounds of selection were performed.

The selection of recombinant antibodies using PSMA-expressing whole cells provides a means of cloning antibody fragments that react selectively with cell-surface antigens. One drawback of this method is the possibility of selecting for another receptor or marker heavily expressed by the LNCaP C81 cells. Therefore each round of phage display was performed on whole adherent LNCaP C81 cells after subtraction of non-specific phage on the PSMA-negative cell line (DU145) which lacked the desired target antigen but are otherwise similar to the selection cells, thereby greatly increasing selection efficiency. Positive phage clones (those that bound to the positive cell line) were eluted from the

cells and the whole process was repeated on this enriched population a further four times. Selection was monitored using ELISA which was performed after each round, indicating the presence of positively-binding phage clones (Figure 3.2).

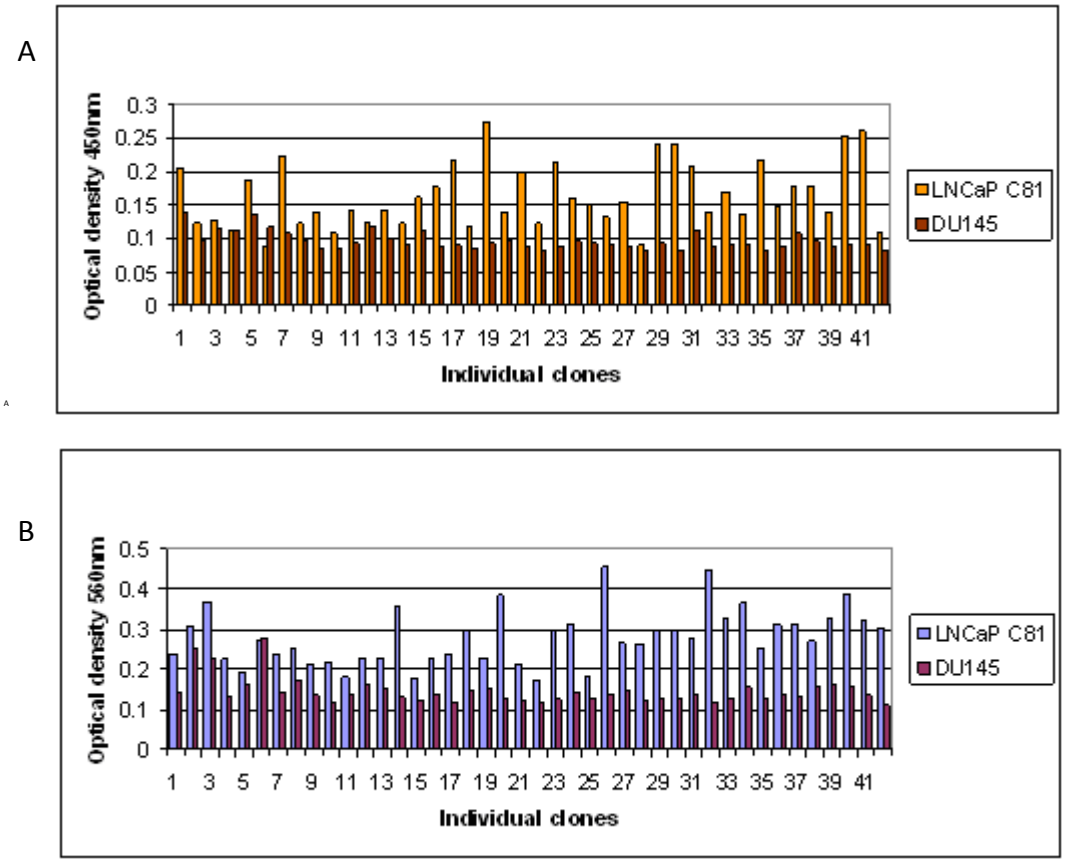

Figure 3.2: Monoclonal ELISA after rounds 4 (A) and 5 (B). Increase in PSMA-specific clones binding to LNCaP.

PSMA-positive phage clones were taken forward for further study after the last round of panning by expressing the soluble scFv and evaluating the specificity of binding, in particular to ensure that the binding seen was specific via the scFv to PSMA, rather than non-specific binding to the phage body. Positive scFv clones were therefore subjected to a number of verification analysis including FACS, ELISA and immunoprecipitation. Five potential clones were identified; however analysis showed that the specificity and affinity of the selected clones was not optimal. FACS failed to differentiate between positive and negative cell lines (
Figure **3.3**) and ELISA revealed poor binding to recombinant PSMA.

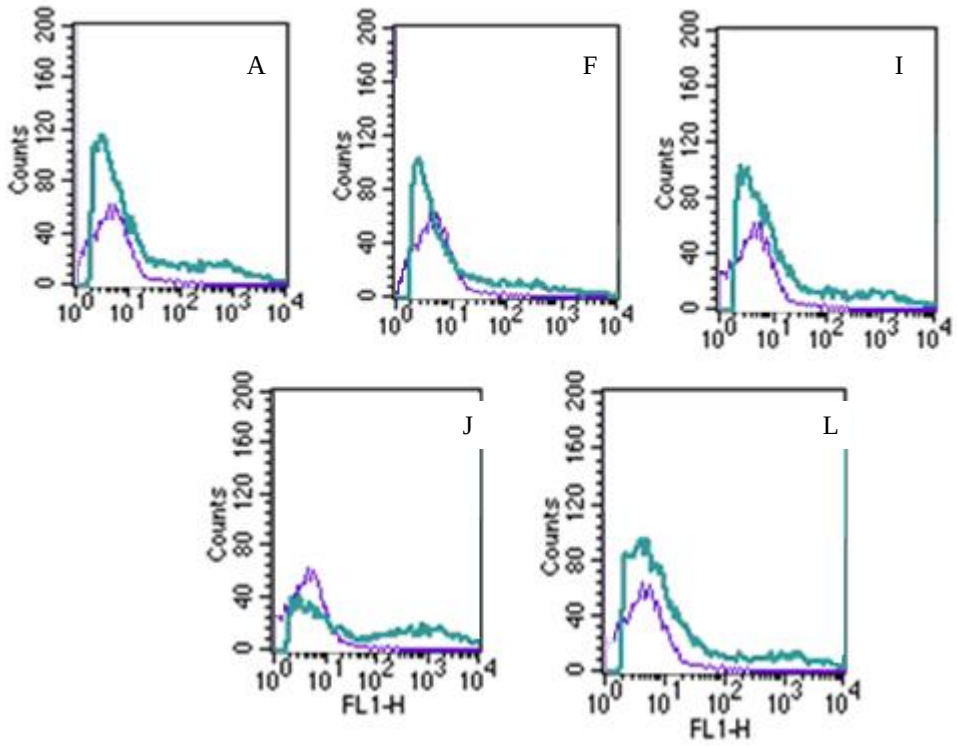

Figure 3.3: FACS analysis using the 5 positive phage clones on PSMA-positive cells (LNCaP - blue) and PSMA-negative cells (DU145 - purple). Binding was not conclusive, as poor binding observed with LNCaP cells.

Clones seemed to weakly bind to PSMA specifically in preference to other proteins (BSA) or non-PSMA-expressing cells, but only marginally so, and their affinity was considered too low; therefore this approach and the selected scFv were not pursued further.

Selection for anti-PSMA scFv was performed using phage display. Two approaches were taken to select for anti-PSMA scFv; one performed on cells naturally expressing PSMA, and the second approach using in-house-generated recombinant PSMA protein. The rationale behind this was to enable the selection of scFv that bound to the target antigen - PSMA.

Selection on PSMA-expressing cells was first investigated and considered to be advantageous, as phage would be able to bind *in vivo* to naturally-occurring PSMA that

bears the typical conformation and glycosylation patterns[35]. Using the Tomlinson I Library [90], selection for anti-PSMA-specific phage was therefore performed on the non-PSMA and PSMA-expressing cell lines, DU145 and LNCaP C81 respectively[36]. The selection of recombinant antibodies using PSMA-expressing whole cells provides a means of cloning antibody fragments that react selectively with cell-surface antigens. One drawback of this method is the possibility of selecting for another receptor or marker heavily expressed by the LNCaP C81 cells. Therefore each round of phage display was performed on whole adherent LNCaP C81 cells after subtraction of non-specific phage on the PSMA-negative cell line (DU145) which lacked the desired target antigen but are otherwise similar to the selection cells, thereby greatly increasing selection efficiency. Positive phage clones (those that bound to the positive cell line) were eluted from the cells and this enriched population was resubmitted to the whole process a further four times. Selection was monitored using ELISA which was performed after each round. PSMA-positive phage clones were taken forward for further analysis after the last round of panning by expressing the soluble scFv and evaluating in terms of the stability and specificity of binding, i.e. that the binding seen was specific via the scFv to PSMA, rather than non-specific binding to the phage body. To do this, positive scFv clones were subjected to a number of verification analysis including FACS, ELISA and immunoprecipitation. However, these studies showed that the specificity and affinity of the selected clones was not optimal. Clones seemed to bind to PSMA specifically in preference to other proteins or non-PSMA-expressing cells, but only marginally so, and their affinity was considered too low; therefore this approach and the selected scFv were not pursued further.

[35] Glycosylation is an enzymatic process which, as well as producing fundamental components of all cells, also provides a co-translational and post-translational modification mechanism that modulates the structure and function of the membrane and secreted proteins.

[36] LNCaP C81 and DU145 cells are respectively derived from human lymph node metastasis and human brain metastasis.

3.2.2 PRODUCTION OF RECOMBINANT PSMA PROTEIN

3.2.2.1 Baculovirus Expression Vector System

Using the Baculovirus Expression Vector System, the large extracellular portion of PSMA was generated in Hi5 cells[37]. Cells were infected with the in-house virus and left at 27°C for 3 days. A negative control flask was left uninfected to allow comparison and establish whether infection had been successful (Figure 3.4).

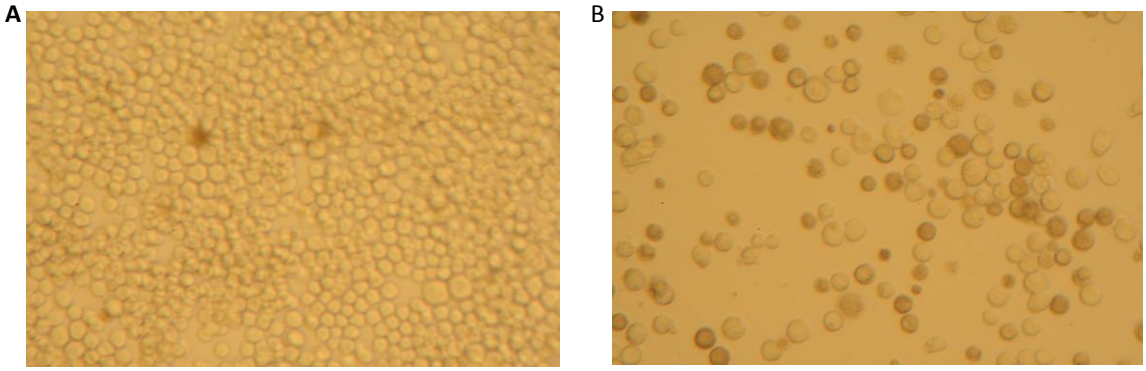

Figure 3.4: Comparison of uninfected and infected Hi5 cell monolayers. A – Uninfected Hi5 cells, B – Hi5 cells infected with in-house virus.

Hi5 cells that were incubated with in-house virus were grown to allow for infection, production and secretion of the recombinant protein into the medium. A notable difference in morphology was observed in comparison with the uninfected cells which grew in parallel. Infected cells swelled to become much larger than uninfected cells, contained enlarged nuclei, stopped dividing, and often became detached from the flask.

3.2.2.2 Verification of Recombinant PSMA Protein Production

Prior to purification, samples of supernatants were checked by SDS-PAGE to determine whether the 90 kDa band was present, corresponding to the large extracellular portion of the recombinant PSMA protein (Figure 3.5).

[37] Chapter 2 - section (Baculovirus)

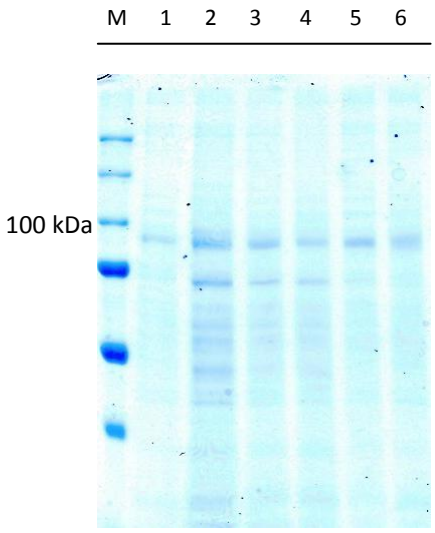

Figure 3.5: SDS-PAGE with supernatant harvested 3 days after infection with in-house virus. Each lane (numbered 1-6) was loaded with the material from one of the large 175cm^2 flasks.

The mobilities of the reference standard proteins (lane 1) in SDS-PAGE, plotted against log molecular weight, are shown in Figure 3.6.

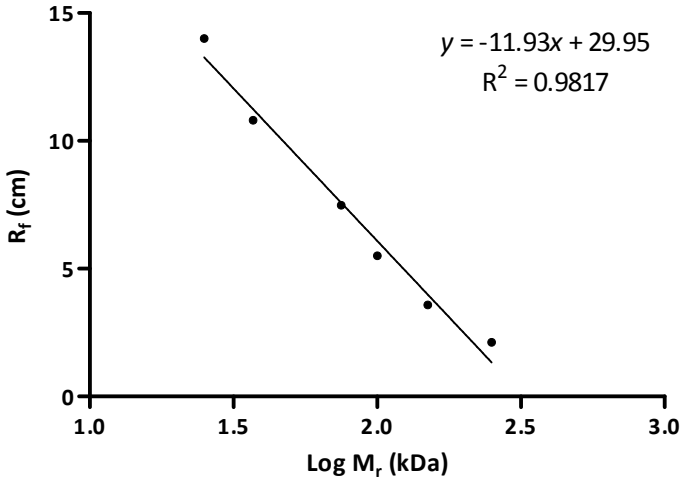

Figure 3.6: Log molecular weight of markers versus their mobility.

Table 3.1: Molecular weight of the major protein in each sample

Lane	Mobility (R_f) (cm)	Log M_r	M_r (kDa)
2	6.2	1.989	97
3	6.4	1.972	94
4	6.4	1.972	94
5	6.34	1.977	95
6	6.34	1.977	95
7	6.28	1.982	96

From this plot, the molecular weight of the major protein in each sample was determined (Table 3.1). Values were slightly in excess of that expected (90 kDa, indicative of the large extracellular PSMA portion), due to slight distortion of the banding in the gel, but were close to the expected value. Having confirmed recombinant PSMA protein production by SDS-PAGE, Western blot analysis was also performed to check whether commercial anti-PSMA antibody (1H8H5) recognised the recombinant protein. Cell lysate (LNCaP C81) was used as positive control (Figure 3.7).

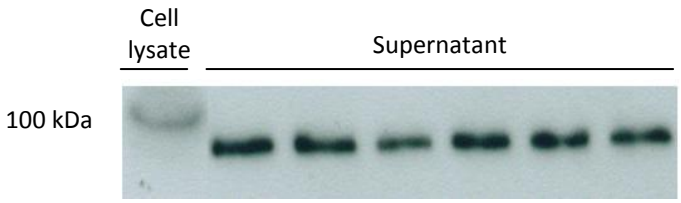

Figure 3.7: Western blot of recombinant PSMA protein generated using Hi5 cells. Bands at 90 kDa were seen with each sample of supernatant representative of each flask. The positive control (cell lysate) revealed a band at 100 kDa, confirming that only the large extracellular portion of PSMA protein was generated. Five minute exposure.

Both SDS-PAGE and Western blot analysis substantiated the production of recombinant PSMA protein, which was purified from the supernatants using Ni-NTA kits. The purified recombinant PSMA protein was used for selection and verification experiments.

3.2.2.3 Selection For Anti –PSMA Phage on Recombinant PSMA Protein

Selection on recombinant PSMA protein was initially run in parallel to the presently-reported work by Dr. Stella Man, who had propagated in-house recombinant PSMA protein using the Baculovirus system[38] and performed 3 rounds of phage display against the recombinant PSMA. Positive binders were then used in this project and taken forward for further analysis. Using recombinant PSMA was potentially advantageous over selection on cells because the Tomlinson phage library was screened against considerably higher concentrations of the target protein than that naturally found on cells *in vivo*. Also the protein was designed to be composed of only the large extracellular portion of the PSMA molecule, eliminating the smaller intracellular portion only exposed once cells became necrotic or apoptotic[39]. A potential disadvantage of this technique was that, although the protein was generated using the Baculovirus system which produces proteins with similar glycosylation patterns to those found in humans, it may not be exactly the same as found naturally *in vivo*.

Three rounds of phage display on PSMA-coated immunotubes were performed in total[40]. The progress of selection can be readily monitored after each round by measuring phage titre; titre was expected to increase with each round of selection as the population was being enriched towards the target antigen (Table 3.2).

Table 3.2: Phage titre after each round of selection

Selection Round	Titre
1	8×10^5
2	6×10^6
3	2×10^7

Increase in phage titre was a quick validation that each round of selection had been successful and the phage population was being enriched towards the target antigen.

[38] Baculovirus system is a versatile method of producing large quantities of biological active and functional recombinant protein using cultured insect cells.
[39] Chapter 1 - Figure 1.8
[40] Chapter 2 - Section 2.2.3.1

Selection using immobilised recombinant PSMA protein was more successful than that performed on cells, and yielded a number of PSMA-specific phage clones that showed improved binding in ELISA on recombinant PSMA protein. These selected clones were further subjected to several validating experiments to ensure that the phage selected contained a complete, unique scFv sequence, and bound selectively with high affinity to PSMA expressed both *in vitro* and *in vivo*.

3.2.2.4 Sequencing of Phage Clones

Phage clones showing high binding in ELISA (results not shown) were chosen and sequenced to examine variability and ensure the presence of the complete scFv sequence.

Table 3.3: Sequencing results of selected phages. Sequences were read with FDSEQ and LMB_3, obtaining the CDR2 & 3 for both heavy and light chains. * represents stop codons in the gene - the sequences below are of amino-acids.

Phage Clone	V_H-CDR2	V_H-CDR3	V_L-CDR2	V_L-CDR3
A1	TISYDGSGTAYADSVKG	NGSSFDY	SASYLQS	QQSADNPA
A5	NIDYAGNYTAYADSVKG	TNDNFDY	YASSLQS	QQSADNPA
C4	SIAYDGDGTGYADSVKG	GTATFDY	TASSLQS	QQGNYGPA
C6	YISDNGNATDYADSVKG	NTASFDY	AASTLQS	QQANADPT
D2	DISSSGSTT*YADSVKG	SYSYFDY	SASSLQS	QQNSANPG
D4	SIAYDGDGTGYADSVKG	GTATFDY	TASSLQS	QQGNYGPA
D6	DISSSGSTT*YADSVKG	SYSYFDY	SASSLQS	QQNSANPG
E3	DISSSGSTT*YADSVKG	SYSYFDY	SASTLQS	QQSTNAPN
G7	TIAYDGTATSYADSVKG	NGASFDY	GASYLQS	QQANYGPA

ScFv sequences were present in all the clones tested. Sequences with stop codons present in the V_H-CDR2 sequence indicated possible sequencing errors.

3.2.3 BINDING STUDIES ON PSMA-EXPRESSING CELLS

3.2.3.1 FACS Using Selected Phage Clones

Binding studies of those phage clones with a full unique scFv sequence and high binding affinity in ELISA were then performed on whole LNCaP and DU145 cells using FACS analysis. An anti-PSMA monoclonal antibody, D2B antibody, kindly provided by a collaborative research group at the Department of Experimental Oncology, Instituto Nazionale per la Studio e la Cura dei Tumori, Milano, Italy, was used as a positive control, and the unselected Tomlinson I library as the negative control.

FACS on selected phage clones was performed as in previous experiments[41], with the addition of an extra incubation step with anti-M13 monoclonal antibody[42] (Figure 3.8).

[41] Chapter 2 - Section 2.2.8

[42] Monoclonal anti-M13 pIII recognises non-reduced and denatured reduced forms of wild type pIII or pIII fusions in ELISA, immunoblotting and FACS.

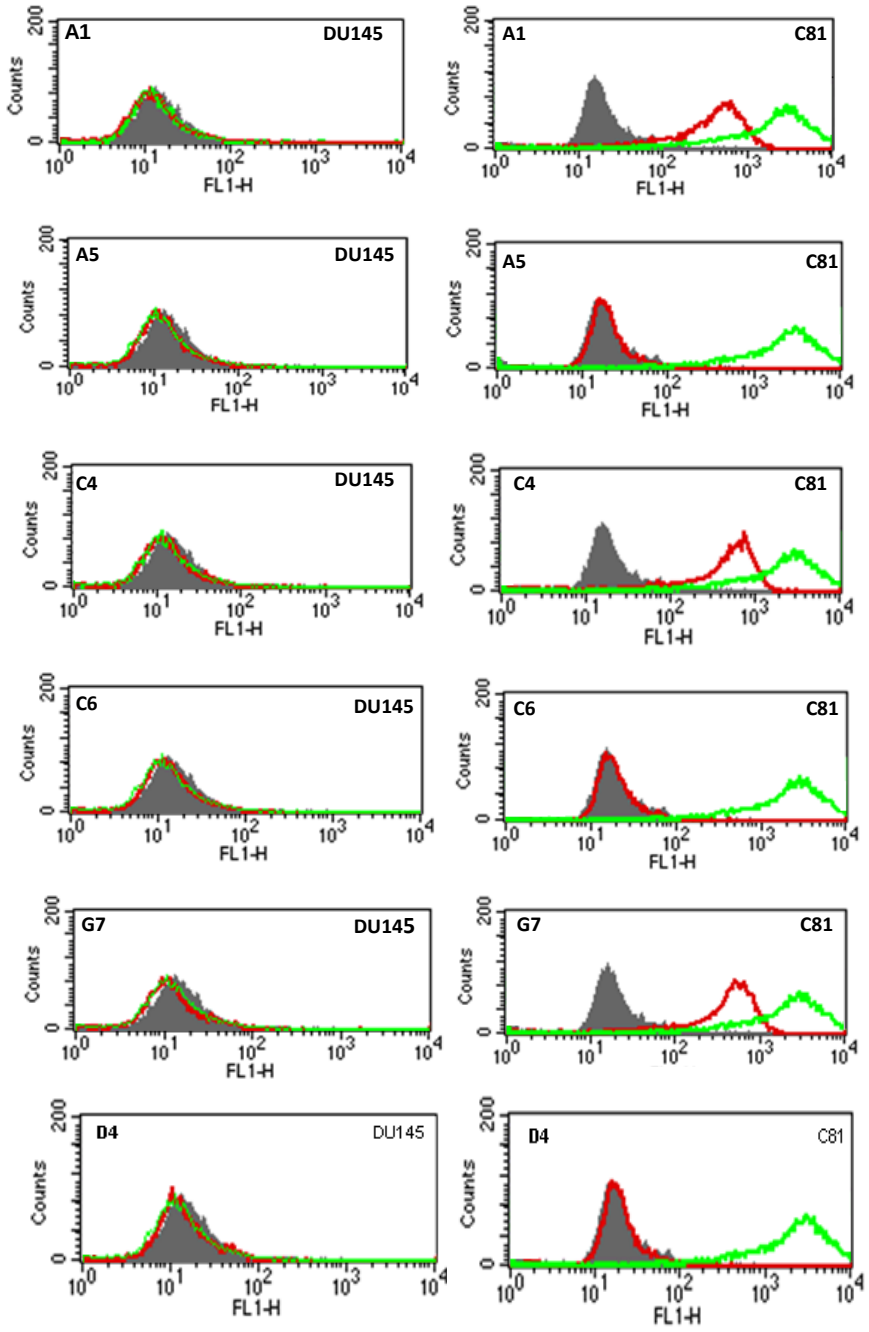

Figure 3.8: Incubation of selected phage clones on DU145 and LNCaP C81 cell lines differentiating between positive and negative anti-PSMA phage. The identity of the phage clone is denoted on the top left hand corner of each graph and cell line tested is identified on the right. Solid grey: Negative control – Tomlinson I Library; Green line: Positive control – D2B anti-PSMA antibody; Red line: Tested phage clone.

Promising results were obtained in FACS: approximately half of clones tested selectively bound more strongly to LNCaP cells than DU145, suggestive of anti-PSMA phage clones. No binding with the unselected Tomlinson I library was observed in either cell line,

whereas the positive control antibody, D2B, bound selectively to LNCaP C81 cells compared to DU145. The clone names were derived from the 96-well plate, which was numbered 1-12 as well as lettered A-H, allowing for the designation of the phage clone to a known well.

3.2.4 EXPRESSION OF SOLUBLE SINGLE-CHAIN FV

ELISA was performed on secreted scFv supernatant from binding phage clones from both rounds 2 and 3[43] (Figure 3.6).

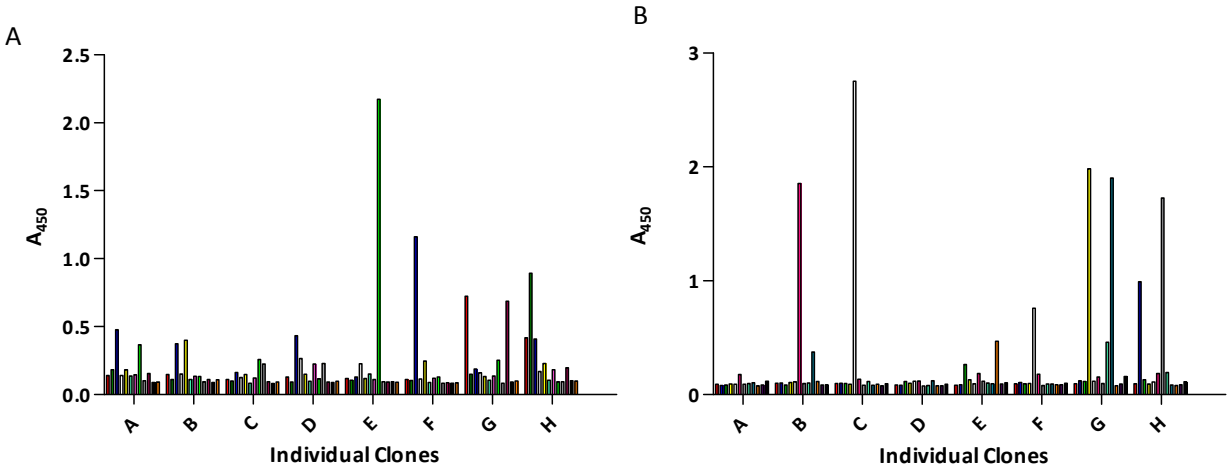

Figure 3.9: ELISA of soluble scFv tested against immobilised recombinant PSMA protein. (A) Round 2 of selection; (B) round 3 of selection.

Antibody fragments exhibiting high levels of binding to the recombinant PSMA protein from both rounds 2 and 3 were selected and put forward for sequencing to ensure that the selected scFv was complete and that a diverse repertoire was selected (Table 3.4).

[43] Chapter 2 - Section 2.2.4.6

Table 3.4: Sequencing results of high-binding soluble scFv from the results of the ELISA. Sequences were checked to ensure that they were complete and that the scFv were undeleted, as well as representing a diverse population from rounds 2 and 3. ND = no data obtained.

scFv Clone	ELISA (A_{450})	V_H-CDR2	V_H-CDR3	V_L-CDR2	V_L-CDR3
R3B6	1.853	ATGGSGDATSYADSVKG	AATGFDY	DASSLQS	QQYSAYPT
R3C5	2.752	SISGYGSTTAYADSVKG	NAASFDY	TASSLQS	QQANSY
R2E8	2.175	AISTYGSYTSYADSVKG	NYTDFDY	SASSLQS	QQAYNYPS
R2F3	1.161	SIAYDGDGTGYADSVKG	GTATFDY	TASSLQS	QQGNYGPX
R3F5	0.761	SIAYDGDGTGYADSVKG	GTATFDY	TASSLQS	QQGNYGPA
R3G4	1.983	AISTAGAATAYADSVKG	NTAAFDY	ASYLQS	QQTYSTPT
R2G10	0.686	TISYDGSGTAYADSVKG	NGSSFDY	SASYLQS	ND
R2H2	0.892	TIAYDGTATSYADSVKG	NGASFDY	GASYLQS	QQANYGPA

The numbering system was set such that R2 or R3 denoted the selection number followed by the location on the 96-well plate as with the phage clone number system. Sequencing results obtained revealed that only two identical clones were present (R2F3 and R3F5) and the remainder had yielded complete and diverse scFv. Clone R2G10 sequence had failed to read V_L-CDR3, possibly due to an error during sequencing, although the A_{450} reading from the ELISA results showed relatively high binding to the recombinant PSMA protein.

3.2.4.1 FACS Analysis of Purified Selected Clones

To further confirm the high binding affinity observed in ELISA, FACS analysis was performed. For this purpose, a small fraction of each clone was purified using Sepharose A chromatography (Figure 3.10).

FACS analysis of the purified scFv was performed on both LNCaP C81 and DU145 cell lines to determine whether the positive, selective binding observed with the phage clones was still present with the scFv alone. A comparison of anti-his and anti-myc monoclonal IgG antibodies as secondary layers was performed; anti-myc demonstrated improved binding over anti-his antibody and this was used thereafter.

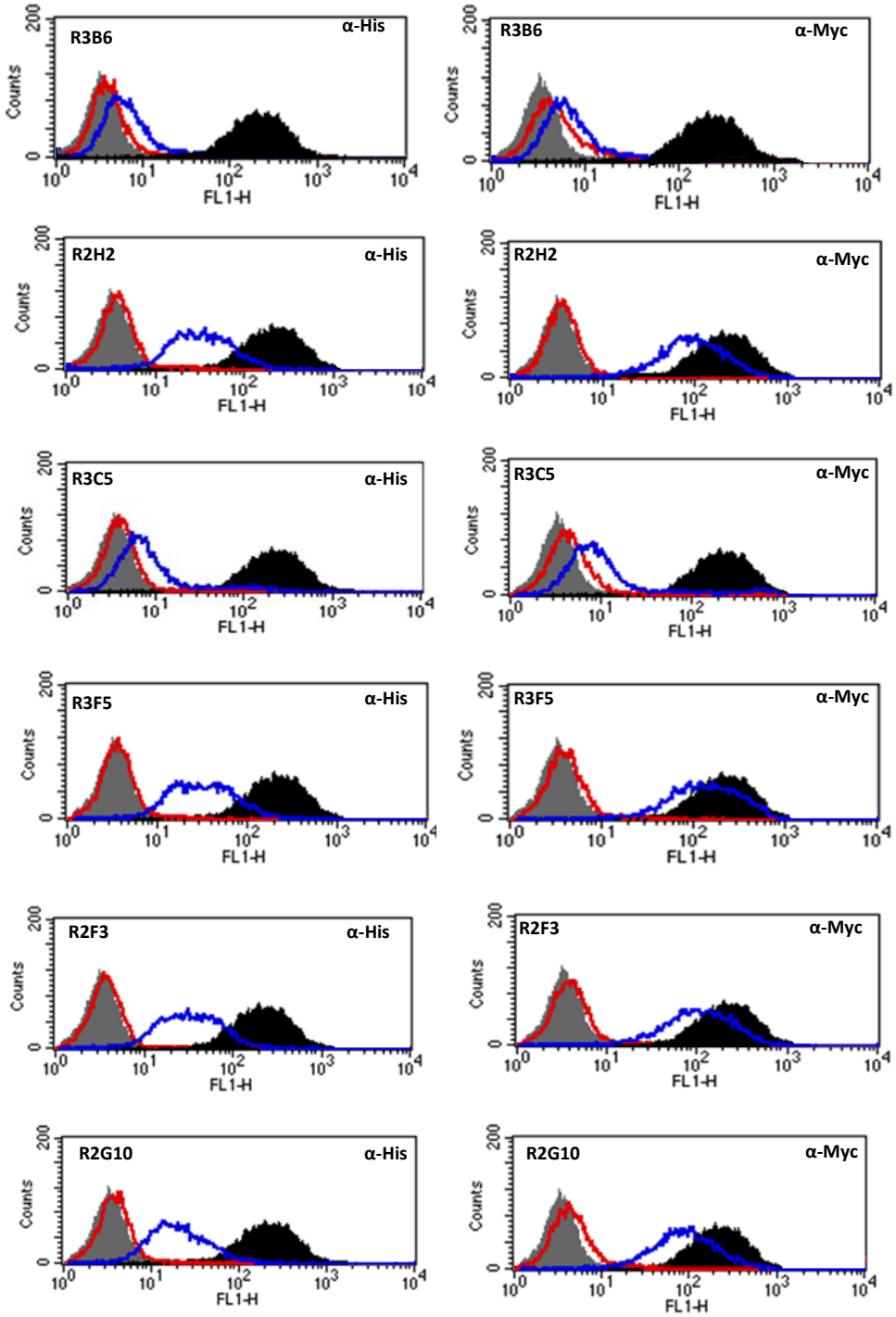

Figure 3.10: Incubation of purified scFv with LNCaP C81 and DU145 cell lines, differentiating between positive and negative anti-PSMA phage. Solid grey: Negative control – DU145 with D2B anti-PSMA antibody; Solid black: positive control - LNCaP C81 with D2B anti-PSMA antibody; Red line: DU145 tested with scFv; Blue line: LNCaP C81 tested with scFv.

Selective binding was observed with all the tested clones, however R3B6 and R3C5 which showed very high readings in ELISA, did not mirror this in FACS and were therefore not pursued further. Remaining lower-binding scFv clones were also examined to ensure that improved affinity scFv clones were not lost[44]. R2F3, R2G10, R2H2 and R3F5 were selected as the most promising candidates with good binding affinity demonstrated in both ELISA and FACS. The two clones with identical amino acid sequences (R2F3 and R3F5) were both selected to see whether they behaved in the same manner.

3.2.4.2 Purification of scFv

Larger scale purification of the selected scFv clones was then performed. The periplasmic fraction obtained during production of the soluble scFv needed to be purified to remove other proteins secreted during osmotic shock[45]. The purification profile obtained by Protein A chromatography[46] was compared with that obtained by chromatography on Ni-NTA[47] (Figure 3.11).

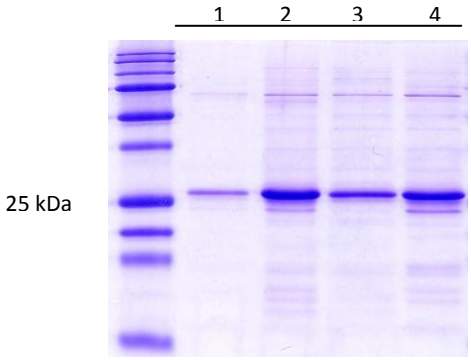

Figure 3.11: SDS-PAGE of selected scFv antibody fragments recovered after Protein A-Sepharose purification. 1 - R2F3, 2 - R2G10, 3 - R2H2, 4 - R3F5

[44] Appendix II
[45] Chapter 2 - Section 2.2.5.2
[46] Protein A chromatography can be used to purify antibody fragments encoded by V_H segments from the V_H3 family
[47] Ni-NTA binds to his-tagged proteins

Purification by chromatography on Protein A-Sepharose yielded clean 25 kDa-bands indicative of scFv. Bands could be seen at both higher and lower molecular weights, but those observed were faint and considered as inconsequential (Figure 3.12).

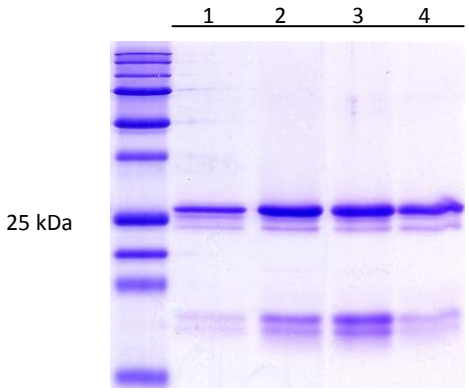

Figure 3.12: SDS-PAGE of selected scFv antibody fragments recovered after Ni-NTA purification.
1 - R2F3, 2 - R2G10, 3 - R2H2, 4 - R3F5

Purification using Ni-NTA failed to purify the antibody as efficiently as the protein A-Sepharose column (Figure 3.12). Substantial bands of lower molecular weight were observed between 15 and 10 kDa, and the 25 kDa-bands looked to be slightly fragmented, possibly due to degradation of the antibody fragments.

3.2.4.3 Protein Concentration

Protein concentrations of the purified scFv were obtained by measurement of $A_{280\ nm}$ following dialysis (Table 3.5). Protein concentration was estimated on the basis 1 $A_{280\ nm}$ unit ≡ 800 μg/mL, an approximation derived from the method of Warburg and Christian [174].

Table 3.5: Concentrations of scFv antibody fragments after Protein A-Sepharose chromatography.

Sample	Elution Fraction	$A_{280\ nm}$	Protein concentration (µg/mL)
R2F3	E1	0.1	80
	E2	1.33	1065
	E3	0.39	313
R2G10	E1	0.47	374
	E2	2.04	1628
	E3	0.60	481
R2H2	E1	0.84	674
	E2	0.53	426
	E3	0.11	89
R3F5	E1	0.39	309
	E2	1.09	874
	E3	0.42	366

Elution fractions represent 1 mL volumes of eluted protein from the column. All the elution fractions were measured to establish which fraction held the largest concentration of protein. Fractions with similar concentrations were pooled together before aliquoting into smaller fractions and for storage at -80°C.

The purified clones were re-tested by FACS to confirm that specific binding observed still remained (results not shown). The most promising clones from ELISA and FACS results, R2F3, R2H2, R2G10 and R3F5, were then selected for conversion into diabodies.

3.2.5 PRODUCTION AND ANALYSIS OF DIABODIES

ScFv antibodies are genetically-engineered fusion proteins containing variable heavy- and variable light-chain domains joined by a polypeptide linker. To facilitate the formation of an intermolecular antigen binding site, artificial linkers such as glycine-serine $(G_4S)_3$ have been utilised in various scFvs, because such linkers do not contribute to the formation of any specific secondary structure [175]. The length of the flexible linker dictates the final

structure; linkers longer than 12 residues are predominately monomers, whereas scFvs with shorter linkers form dimeric or multimeric molecules [176].

Manipulation of the glycine-serine linker can therefore be performed to prevent the natural folding of the variable heavy and variable light chains[48]. The complete removal of the linker was carried out by utilising the many restriction sites present in the genetic map[49].

3.2.5.1 Extraction of DNA

Extraction of DNA from all four clones (R2F3, R2H2, R2G10 and R3F5) was successful, as verified by agarose-gel electrophoresis (Figure 3.13) In each case, two bands were visualised; one representing the circular DNA and the second denoting supercoiled DNA.

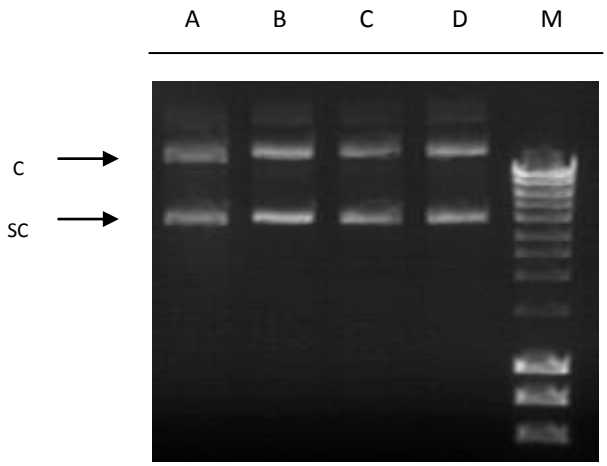

Figure 3.13: Confirmation of successful DNA extraction. A - D – clones R2F3, R2G10, R2H2 & R3F5 respectively, M – 1 Kb DNA marker. Two bands were visualised in all four clones; SC - supercoiled, and C - circular, indicative of successful DNA extraction.

[48] Chapter 2 - Section 2.2.9
[49] Appendix I

3.2.5.2 Restriction Digest

Linearisation of the pIT2 vector was achieved by restriction digestion using SalI and XhoI, which act on sites situated either side of the glycine-serine linker. Digestion was performed and verification of successful linearisation was observed by agarose-gel electrophoresis, where one clear band could be seen to be recovered from all four clones. The removed linker was too small in size to be seen on the gel[50]. Bands (linearised vector) were cut out and the DNA was extracted using QIAquick gel extraction. To ensure DNA had not been lost during this process, samples were run again. Single clear bands could be seen in all four clones, indicating that the extraction from the agarose had been successful (Figure 3.14), although the bands were not as sharp as expected, symptomatic of overloading the wells.

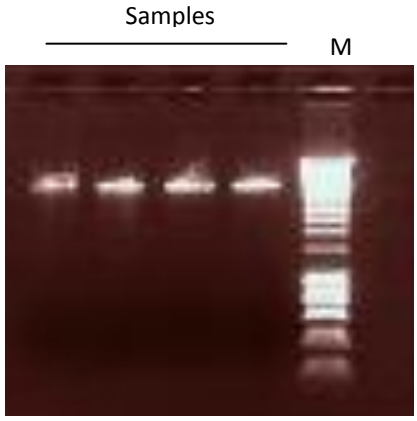

Figure 3.14: Linearisation of pIT2 vector in all four clones. M - 1 Kb DNA ladder run in parallel.

3.2.5.3 Ligation

Rejoining of the linear vector was performed by ligation[51]. Several methods to confirm successful removal of the linker between V_H and V_L after ligation were investigated to ensure that the SalI and XhoI restriction sites had been removed from newly-formed vector, indicating complete removal of the linker. Verification of successful removal was seen in several digestions using SalI, XhoI, HindIII and NotI (Figure 3.15). Digestions with

[50] Appendix III
[51] Chapter 2 - Section 2.2.9.3

the combination SalI or XhoI (acting on the removed restriction sites) with either HindIII or NotI yielded one band, as only one restriction site was present and therefore the cut had been made in one place only. Combination of HindIII and NotI together yielded two bands, since both these enzymes were able to cut the DNA in separate places to yield two bands.

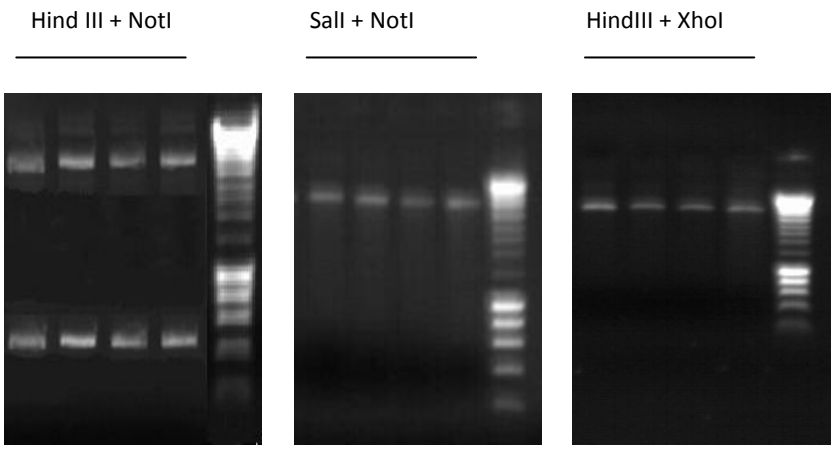

Figure 3.15: Different combinations of restriction enzymes were used to verify that the linker had been effectively removed. HindIII with NotI was selected as the sites for these were present on the genetic map and the fragments generated were of different sizes, enabling them to be easily visualised.

Final confirmation was obtained by sequencing, which revealed full and complete removal of the glycine-serine linker (results not shown).

3.2.5.4 ELISA of The Dimeric Periplasmic Fraction

As a rapid means of verifying that dimeric expression was successful, ELISA on recombinant PSMA protein was performed on the periplasmic fraction, before undertaking purification. This method gave an indication of the specific binding of the dimeric antibody fragments to the target antigen, as well as non-specific binding to BSA (Figure 3.16).

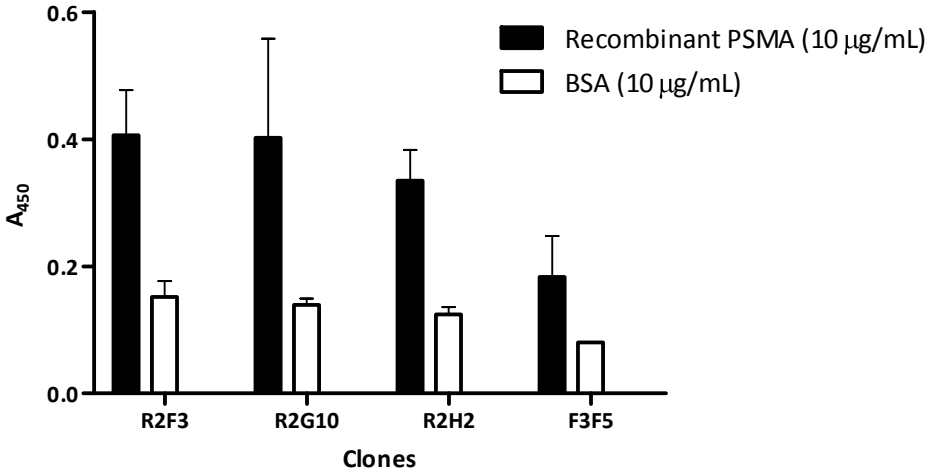

Figure 3.16: ELISA performed on recombinant PSMA- and BSA-coated plates. Periplasmic fractions from all four clones were incubated to check for specific binding affinity to the immobilised targets. Binding assays were performed in triplicate.

Clear differences between all four clones could be seen in the extent of binding to PSMA protein compared with binding to BSA, with a minimal difference seen between the R2F3 and R2G10 clones. A significant difference in the extent of binding was observed between R2F3 and R3F5. Even though these had the same scFv sequence, this could be due to different levels of expression. Encouragingly, the binding observed validated the production of the dimeric antibody fragments.

As a means of ensuring that the production of the antibody fragments was successful, the levels of expression of the four clones were also measured by adsorbing the periplasmic fraction and supernatant material to a Maxisorb plate, and performing an ELISA[52] (Figure 3.17).

[52] Chapter 2 - Section 2.2.4.6

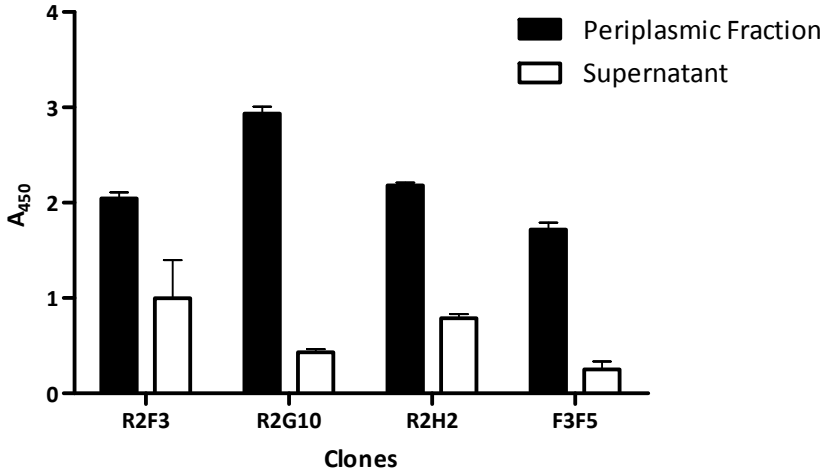

Figure 3.17: Expression levels measured of the four clones pre-purification. The periplasmic fraction showed higher levels of expression than the supernatant.

Expression was observed in all the clones. The periplasmic fraction yielded higher values than the supernatant, due to retention of scFv predominantly in the periplasmic space, with only a small amount 'leaking' into the medium[53]. Both ELISA experiments confirmed positive production of the dimeric antibody fragments, and showed higher levels of expression in the periplasmic fraction over the supernatant; therefore validating the purification of the periplasmic fraction, which was performed in the same manner as for the monomeric antibody fragments. Interestingly little difference could be observed between the levels of expression between R2F3 and R3F5, indicating the difference in binding seen was not due to expression differences.

3.2.5.5 ELISA of Purified Diabodies

After production and purification of the diabodies (as with scFv purification), a further ELISA experiment was performed to ensure that expression and specificity towards PSMA protein still remained (Figure 3.18). Preliminary results revealed an acceptable level of expression with moderate specificity for the recombinant PSMA protein.

[53] Chapter 2 - Section 2.2.5.2

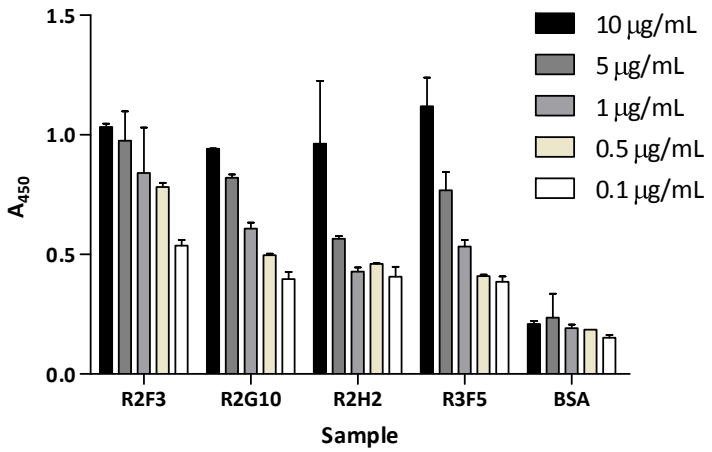

Figure 3.18: ELISA was performed on decreasing concentrations of adsorbed recombinant PSMA protein in order to assess specific and selective binding of purified dimeric antibody fragments

Specific binding was observed in a dose-dependent manner with all four clones. R2F3 displayed better binding than the other clones.

3.2.5.6 FACS Analysis of Purified Diabodies

Specificity of the diabodies to naturally-expressed PSMA was examined by FACS analysis. Initial results showed specific binding to PSMA-expressing cells, with differentiation between LNCaP C81 and DU145 cell lines (Figure 3.19).

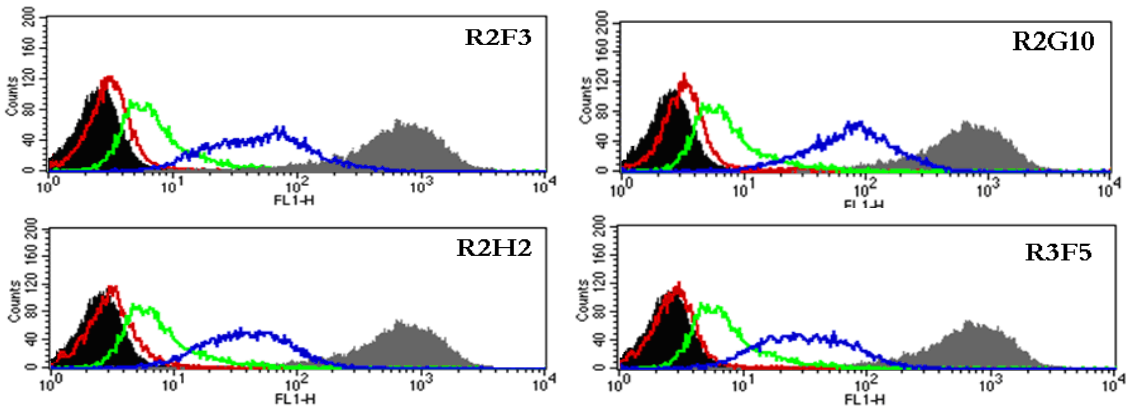

Figure 3.19: FACS analysis using newly generated diabodies (20 µg/mL) showed positive and selective binding to PSMA-expressing cells (LNCaP C81). Black solid: Negative control - DU145 + D2B anti-PSMA antibody; Grey solid: Positive Control - LNCaP C81 + D2B anti-PSMA antibody; Red line: DU145 + tested purified dimeric clone; Blue line: LNCaP C81 + tested purified dimeric clone; Green line: Negative control – LNCaP C81 + alpha V beta 6 diabody[54]

Selective binding to PSMA on LNCaP C81 by all four generated diabodies was observed (blue trace in Figure 3.19); however this peak appeared to be broader than the other peaks in the trace, possibly due to a the presence of a heterogeneous mixture of both monomeric, i.e. scFv, and dimeric i.e. diabody fragments. The 'negative' diabody alpha v beta 6 did not appear to be as unreactive as originally thought, which has prompted further examination (by another research group).

3.2.6 COMPARISON BETWEEN SCFV AND DIABODIES

3.2.6.1 FACS Analysis – scFv vs. Diabodies

The rationale for forming diabodies was to attempt to increase the affinity of the selected clones to the target antigen, PSMA, since the presence of two binding sites should increase their ability to bind to the target. FACS analysis was therefore performed to compare the binding affinities of scFv with those of the diabodies. FACS was performed on DU145 and LNCaP C81 with clones R2G10 and R2H2 over a range of antibody

[54] Alpha V beta 6 was provided as a negative diabody control from a colleague, Dr. John Marshall, Tumour Biology. It was believed that it would be unreactive because it predominately binds to skin, mouth and breast carcinomas.

concentrations, viz. 10, 5, 1, 0.5 and 0.1 μg/mL (Figure 3.20). Overlaying the histogram results for all the variables allowed direct, qualitative comparison between the binding of scFv and the diabodies.

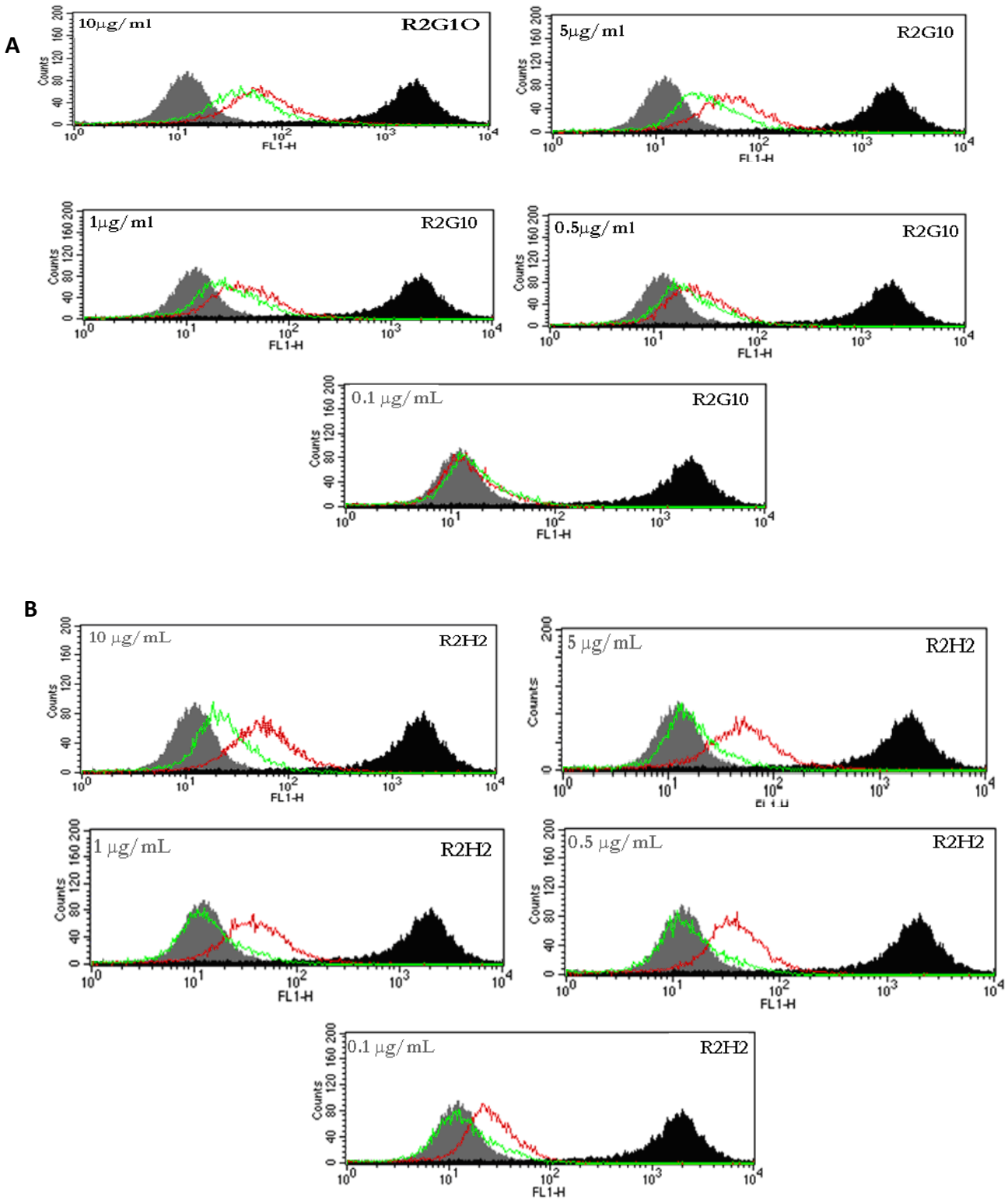

Figure 3.20: FACS analysis to determine binding affinity between scFv and diabodies. Grey solid: Negative control - DU145 + D2B anti-PSMA antibody; Black solid: Positive control - LNCaP C81 + D2B anti-PSMA antibody; Green line: Purified scFv clone; Red line: Purified diabody clone. A - R2G10 and B - R2H2.

With decreasing concentrations of antibody fragments, binding decreased in a corresponding manner. Greater binding of the diabody than the scFv could be observed in both clones; R2H2 still showed noticeably better binding than R2G10 at lower concentrations.

Mean fluorescence intensities (MFIs) obtained from the FACS analysis were plotted against antibody concentration to allow a more quantitative means of directly comparing scFv and diabody binding affinities. Improved binding with the diabodies was seen for both clones, with R2H2 demonstrating improved binding at lower concentrations, suggesting enhanced affinity over that of R2G10 (Figure 3.21).

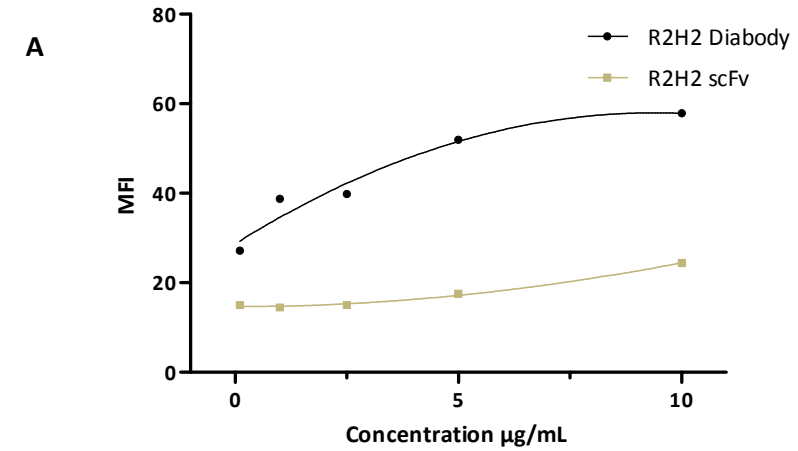

Diabody: $y = -0.3314x^2 + 6.231x + 28.70$ $R^2 = 0.9523$
ScFv: $y = 0.09459x^2 + 0.03781x + 14.66$ $R^2 = 0.9935$

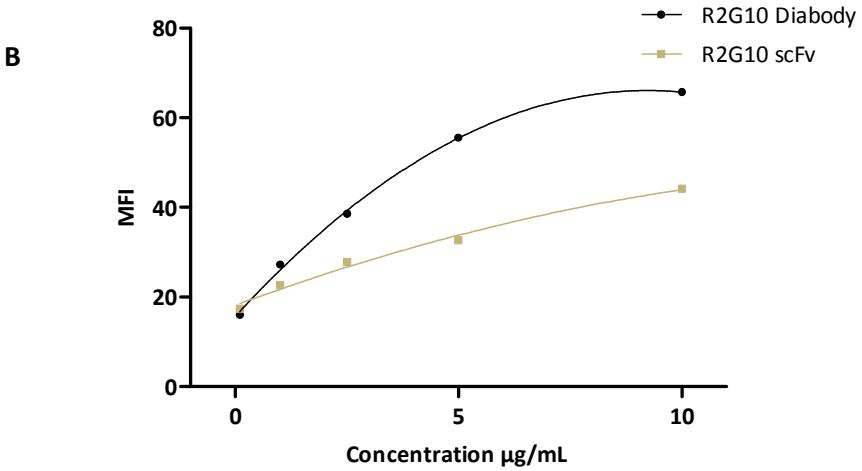

Diabody: $y = -0.5915x^2 + 10.93x + 15.62$ $R^2 = 0.9984$
ScFv: $y = -0.1090x^2 + 3.671x + 18.15$ $R^2 = 0.9881$

Figure 3.21: FACS analysis showing mean fluorescence intensity for a range of antibody concentrations for clones R2H2 (A) and R2G10 (B). Polynomial (2nd order) regression line fitted.

3.2.6.2 HPLC Analysis of scFv and Diabodies

The lack of covalent bonds between the two scFv molecules which form the diabodies means that diabodies can dissociate, giving rise to a heterogeneous mixture of the two molecular species. However, these scFv can no longer fold as they would naturally, due to the removal of the flexible linker, therefore preventing the formation of the antigen binding pocket/site, and ultimately rendering them ineffective. A number of factors can contribute to the dissociation of diabodies, such as temperature, the freeze/thawing

process, and pH. Dissociation is not the only factor to take into consideration; because scFv and diabodies can also aggregate to form triabodies and even tetrabodies, this will subsequently affect their binding abilities and interaction with the target antigen. It was important that the stability of the diabodies was investigated to ensure reproducibility of future results.

Since SDS-PAGE dissociates diabodies under the harsh conditions employed, i.e. the presence of the detergent sodium dodecyl sulphate (SDS), and heating the samples to 100°C, Size-Exclusion HPLC was utilised to investigate this problem. This enabled direct comparison between the two types of antibody fragments, and also the size of the molecules to be determined by measuring their retention times from a column calibrated against known standards (Figure 3.22).

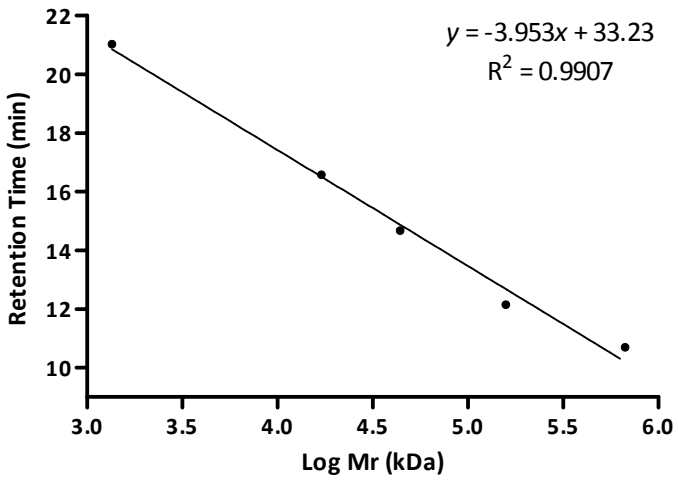

Figure 3.22: Calibration plot constructed for HPLC from standards of known molecular weight.

HPLC analysis yielded multiple peaks for both the scFv and diabody fragments, indicating both aggregation and dissociation of the fragments. To assess reproducibility the analysis was repeated several times with and without an internal standard. The internal standard used was an intact antibody molecule of a known size (150-kDa murine antibody PRIAS) and stability. Figure 3.23 shows scFv and diabody chromatograms for R2G10; chromatograms for other clones are shown in Appendix IV.

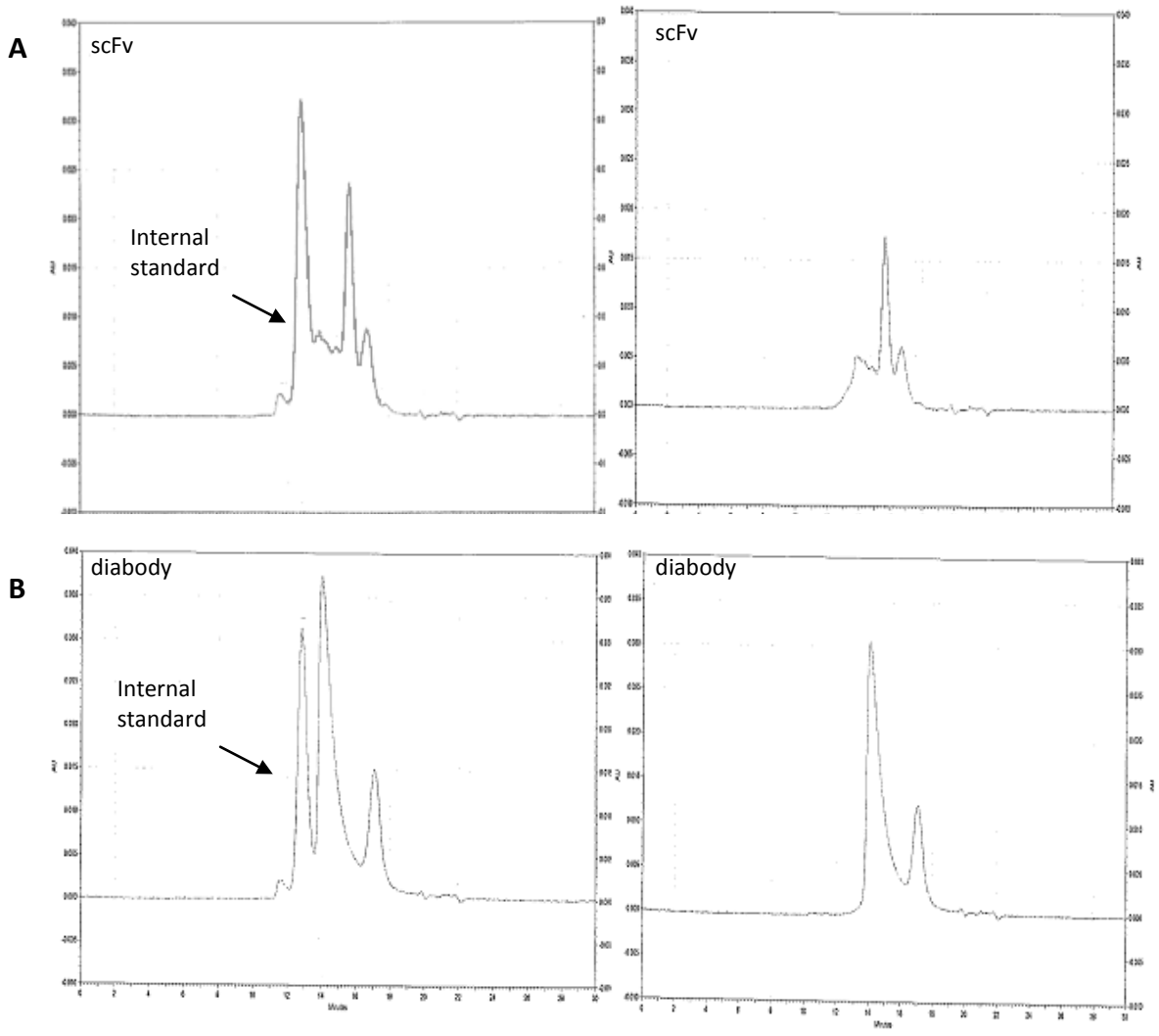

Figure 3.23: HPLC chromatograms for R2G10 scFv (A) and diabody (B). Left with, and right without, internal standard.

HPLC chromatograms of both dimeric and monomeric antibody fragments were obtained in combination with the internal standard or alone. The chromatograms of the antibody fragments alone were directly compared with those containing the internal standard, and (apart from the extra peak from the standard) very little difference could be seen between them, thus showing good reproducibility.

The size of the proteins eluting in the various peaks, determined by comparison with the retention times of the calibration plot, and the integrated peak areas are shown in Table 3.6 and Table 3.7.

Table 3.6: Molecular weight and percentage peak area calculated from all scFv peaks from each run, with calculated means.

Sample	Peak Number (left to right)	scFv					
		Run 1		Run 2		Mean	
		kDa	Integrated peak area (%)	kDa	Integrated peak area (%)	kDa	Integrated peak area (%)
R2F3	1	74	52	72	30	**73**	41
	2	34	48	34	41	**34**	45
	3	-	-	20	29	**-**	-
R2G10	**1**	80	24	81	28	81	26
	2	45	10	46	9	46	10
	3	28	44	29	42	29	43
	4	15	22	15	21	15	21
R2H2	**1**	76	31	71	33	**74**	32
	2	31	49	31	47	**31**	48
	3	17	20	17	20	**17**	20
R3F5	**1**	72	32	73	32	**73**	32
	2	32	44	33	46	**33**	45
	3	19	24	19	22	**19**	23

Table 3.7: Molecular weight and percentage peak area calculated from all diabody peaks from each run, with calculated means. ND = no data

Sample	Peak Number (left to right)	Diabody					
		Run 1		Run 2		Mean	
		kDa	Integrated peak area (%)	kDa	Integrated peak area (%)	kDa	Integrated peak area (%)
R2F3	1	150	98	92	92	**121**	95
	2	15	2	15	8	**15**	5
R2G10	**1**	76	78	73	81	**75**	80
	2	12	22	13	19	**13**	20
R2H2	**1**	34	54	36	54	**35**	54
	2	12	46	12	46	**12**	46
R3F5	**1**	-	-	95	83	**-**	-
	2	15	89	15	17	**15**	ND

The molecular weights calculated from the peaks of the HPLC chromatograms do not correlate exactly with their predicted weights; 25 kDa for monomers and 50 kDa for dimers.

HPLC analysis thus indicates that both antibody preparations were a heterogeneous mixture of several components as indicated by the separation of the sample into components that eluted with retention times indirectly proportional to the molecular weights (i.e. the higher the molecular weights, the faster the components eluted from the column). The diabody preparations for R2G10 appeared to contain approximately 80% dimeric fragments and 20% smaller dissociated fragments, whereas the scFv preparations contained a mixture of aggregated and dissociated fragments (10 and 21%), 26 % dimeric and 43% monomeric fragments. The peak area determined for the different molecular weight components were expressed as a percentage of total integrated peak areas in each chromatogram.

To confirm these results, size-exclusion chromatography using an alternative methodology was used.

3.2.6.3 Fast protein liquid chromatography (FPLC) (ÄKTA ™) on scFv and Diabodies

ÄKTA™ - FPLC was utilised to analyse the samples and to assess whether the results were comparable with the chromatograms obtained by HPLC. FPLC, unlike HPLC, allows the antibody fragments to pass through the column at lower pressures, which would eliminate any fear that the antibody fragments were dissociating due to shear forces. A fresh batch of both antibody fragments was generated, and both FPLC and HPLC were performed after purification on Protein A-Sepharose beads and prior to freezing, to establish whether freeze-thawing process also had an effect on the stability of the fragments (Figure 3.24).

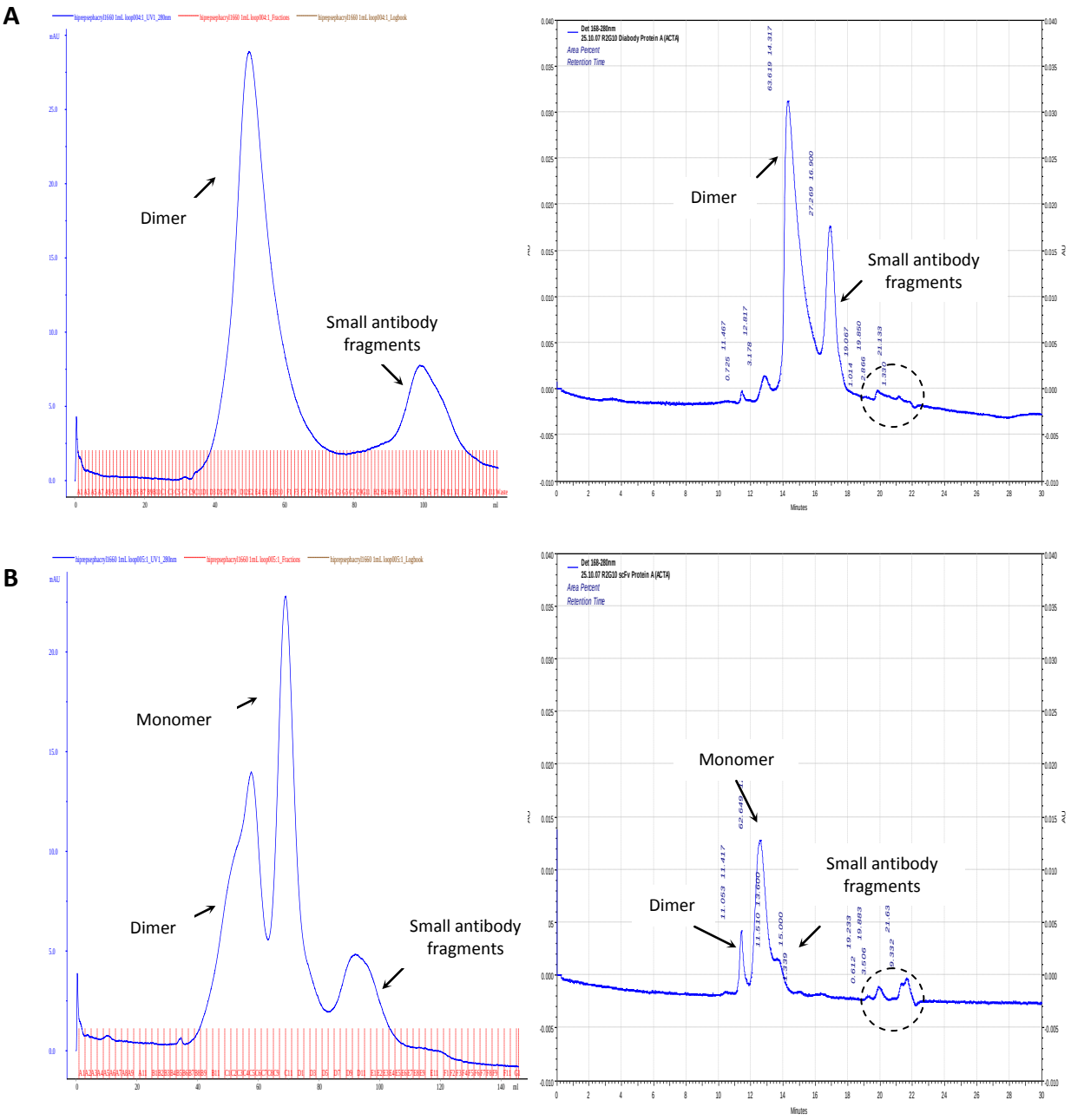

Figure 3.24: R2G10 scFv and diabody were analysed by FPLC (left) and HPLC (right) to enable direct comparison between the two techniques. A: Dimeric diabody fraction; B: scFv fraction. Dashed circle indicating buffer salts.

Chromatograms from both FPLC and HPLC were similar. HPLC also showed small peaks at later retention times caused by buffer salts: this is more evident in the chromatogram of the scFv fraction. As with HPLC, the sizes of the antibody fragments were determined by reference to the calibration plot of known standards (Figure 3.25).

To obtain the standard curve for FPLC, calibration of the gel filtration column was first performed using a low molecular weight gel filtration kit, which consisted of five individual lyophilised proteins ranging in molecular weights and Blue Dextran 2000. Blue Dextran 2000 was run separately to determine the void volume of the column.

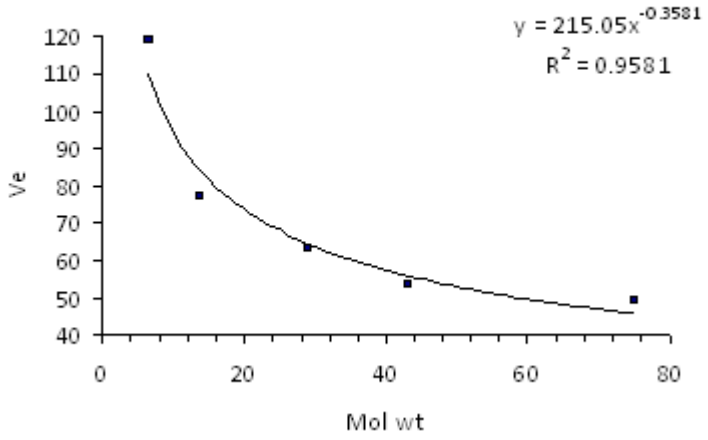

Figure 3.25: Calibration plot constructed using standard of proteins of a known molecular weight. Ve - elution volume.

From the calibration plot (Figure 3.25), the molecular weights of both the dimeric and monomeric fragments for R2G10 were calculated (Table 3.8).

Table 3.8: Molecular weights of peaks from FPLC chromatograms of components from R2G10

Sample	V_e	Molecular Weight (kDa) FPLC	Molecular Weight (kDa) HPLC
Diabody – Peak 1	49.96	**59**	**62**
Diabody – Peak 2	98.82	**9**	**13**
scFv – Peak 1	57.76	**39**	**38**
scFv - Peak 2	69.07	**24**	**29**
scFv – Peak 3	91.92	**11**	**16**

As observed with HPLC, both diabody and scFv were not a homogeneous preparation but they comprised of a mix of differently-sized antibody fragments. The diabody in Figure 3.24 (A) analysed by both FPLC and HPLC, revealed two clear peaks, the larger

representing 59 and 62 kDa species, and the smaller 9 and 13 kDa species. In B, the scFv yielded three peaks; 39, 24 and 11 kDa species in FPLC and 38, 29 and 16 kDa species for HPLC. Results obtained from FPLC thus gave very similar results to those from HPLC, which confirmed the heterogeneity of the antibody samples. Results compared with previous HPLC chromatograms (Figure 3.23) also revealed little difference between the chromatograms from samples that had been thawed a number of times, indicating that freeze-thawing was not a major contributor to the heterogeneity of the samples.

This, however, gave rise to questions regarding the purity of the samples. Was the heterogeneity observed in both monomeric and dimeric fractions due to the instability of the antibody fragments *in vitro*, or a result of insufficient purification? Purification of these scFv and diabody preparations has been performed by Protein A chromatography and post-purification analysis performed by SDS-PAGE.

3.2.6.4 SDS-PAGE Analysis

In addition to the expected bands at 25 kDa, SDS-PAGE gels often but not always (see pages 113) showed some bands at lower molecular weights, but the purity has been considered sufficiently high for FACS and ELISA. The results of HPLC and FPLC analyses agreed with these from SDS-PAGE, which also showed the presence of lower molecular-weight impurities (Figure 3.26).

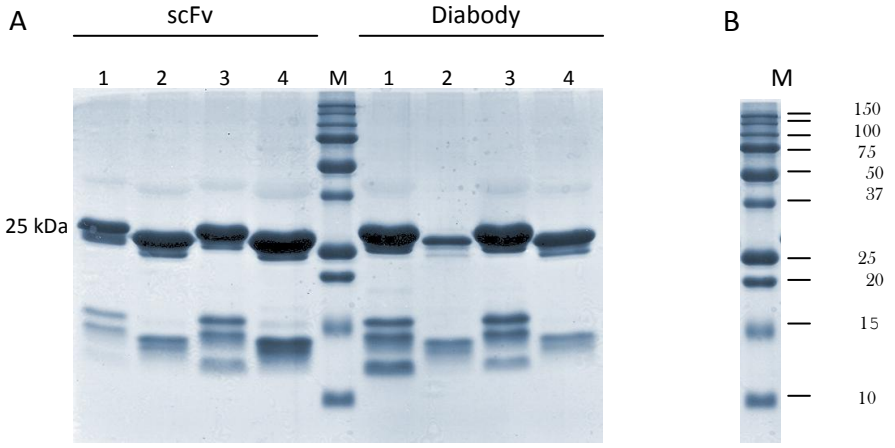

Figure 3.26: A: SDS-PAGE of antibody fragments after Protein A purification. Samples of eluate from each clone (20 µL) were loaded. 1 - R2F3, 2 – R2G10, 3 – R2H2 and 4 - R3F5. B: M – molecular weight marker and corresponding weights (kDa) both scFv and diabody.

Bands at 25 kDa corresponded to scFv; these bands were present even in the samples of the diabodies, as the gel was run under reducing conditions, and the diabody subunits were not covalently bound. Bands at 15-10 kDa showed low molecular-weight impurities, which were also visible in HPLC chromatograms.

It was therefore necessary to determine whether the lower molecular-weight peaks seen on HPLC corresponded to the small bands seen in SDS-PAGE, or whether the antibody fragments were themselves dissociating. It was also considered necessary to achieve a higher level of purity of the preparations prior to *in vivo* use. Therefore a more efficient purification method that removed the lower molecular-weight contaminants from the antibody preparations was sought.

3.2.7 FURTHER PURIFICATION

3.2.7.1 Protein A and Ni-NTA Columns

Antibodies purified initially by Protein A chromatography were therefore further purified by Ni-NTA chromatography. SDS-PAGE of samples purified using Protein A alone and Protein A with Ni-NTA chromatography were compared (Figure 3.27).

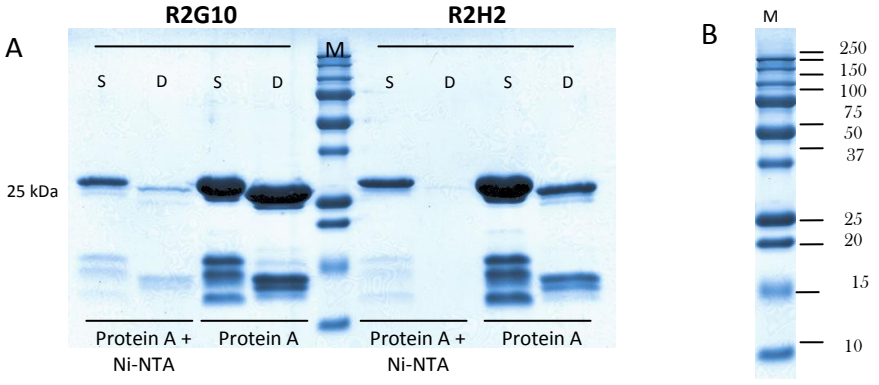

Figure 3.27: A: SDS-PAGE of antibody fragments of two clones R2G10 and R2H2 were purified using Protein A with Ni-NTA chromatography, and using Protein A alone. S – scFv, D – diabody. B: M – molecular weight marker with corresponding weights (kDa).

Bands of lower molecular-weight material detected after purification with Protein A were noticeably reduced after chromatography on Ni-NTA; however the intensity of the 25 kDa-band was greatly reduced, which showed that further Ni-NTA purification of samples derived from chromatography on Protein A removed lower-molecular weight bands, but also reduced the antibody yield by approximately 50%. Previous purification experiments (results not shown) using Ni-NTA chromatography alone had also generated low yields of purified antibody protein, and the procedure had therefore been discounted as a potential purification method; these results therefore confirmed the initial findings. In addition to the removal of the lower molecular weight bands, purification using both protein A and Ni-NTA also ensured the purification of complete scFv.

3.2.7.2 Protein L Columns

Protein L[55] chromatography was then tested for its ability to remove the low-molecular weight fragments and ensure complete scFv purification. R2G10 scFv and diabody purified by Protein A were subjected to a further round of purification using this system, and SDS-PAGE was performed as before (Figure 3.28).

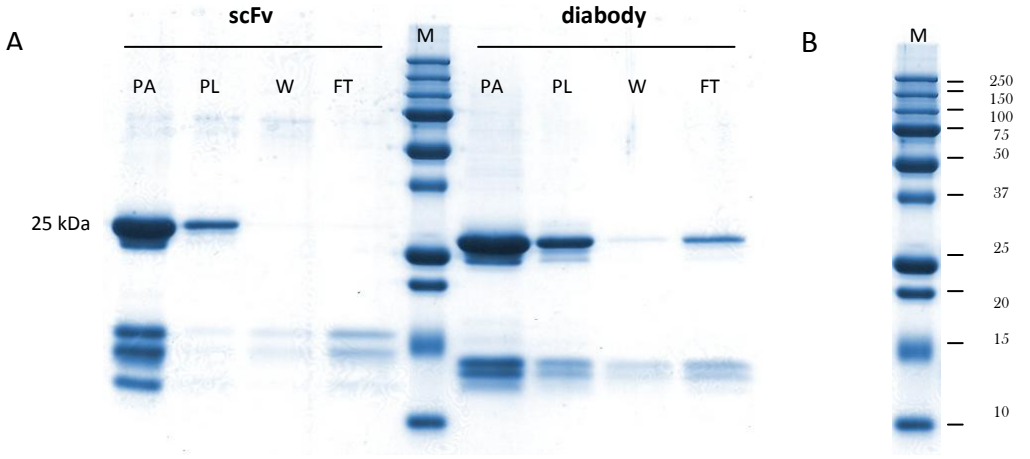

Figure 3.28: A: SDS-PAGE of antibody fragments purified by Protein A (PA) and Protein L (PL) chromatography. The wash (W) and flow-through (FT) fractions from protein L chromatography were analysed to determine whether protein was lost. B: Molecular weight marker with corresponding weights (kDa).

[55] Protein L binds immunoglobulins through interactions with the light chains

Removal of bands in the lower molecular-weight range was again observed with the scFv samples after purification with protein L; however, as with Ni-NTA chromatography, the intensity of 25-kDa bands was considerably diminished after protein L chromatography, indicating loss of protein. With the diabody fraction, bands at 15 kDa were still present after purification though fainter, but so were the 25 kDa-antibody bands. Analysis of the flow-through sample indicated some diabody loss, but subsequent washes of the columns from both scFv and diabody were clear.

As with Ni-NTA, Protein L purification therefore removed the smaller fragments, but considerably reduced the yield of the intact antibody fragment. Although this reduction could be attributed to fragmented scFv, the difference was considered too large to be due to this alone. While over half of the antibody present after Protein A purification was lost after Protein L purification, very little was seen in either the flow-through or wash samples, indicating that the protein was most probably still attached to the Sepharose beads. With this in mind, a sample of the beads was removed from the column, boiled in 20 µL of SDS-PAGE running buffer, and the supernatant was analysed by SDS-PAGE. Intense bands for both the scFv and diabody were visible, confirming that protein had remained bound to the beads, and but not eluted (Figure 3.29, lane H).

3.2.7.3 Elution Strategies

Various elution buffers were therefore investigated in an attempt to improve the elution efficiency of the antibody fragments from Protein L-Sepharose beads. The buffers selected were those previously used in other applications [169, 177] to elute protein from various columns and beads, and were considered to provide conditions that were stringent enough to elute the protein, but mild enough not to damage the antibody fragments.

Varying concentrations of NaCl were first examined. In addition, 10% (w/w) SDS and 6 M guanidine were tested to see whether the protein could be removed from the beads under denaturing conditions. SDS-PAGE was performed on all eluted products, and a

sample of the beads was boiled in running buffer as a control representing total bound protein.

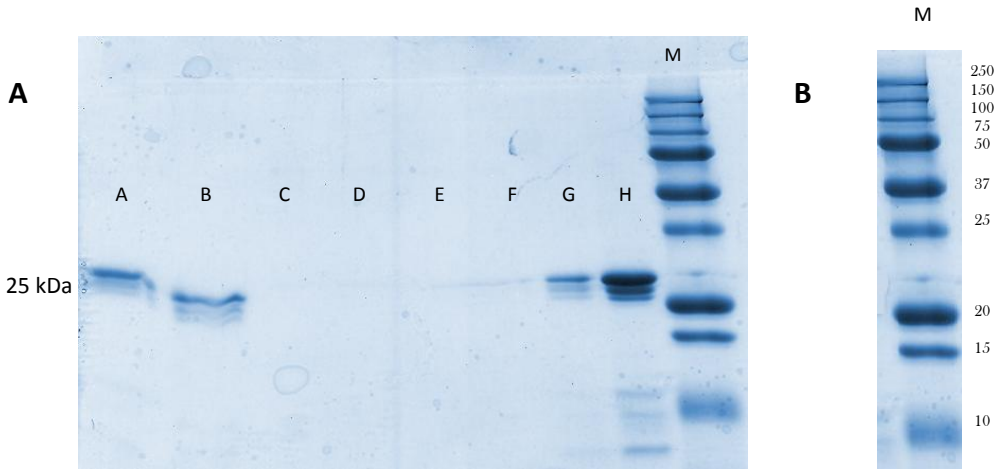

Figure 3.29: (A) SDS-PAGE of samples recovered using various elution buffers of high pH and/or high salt concentration. Beads (10 µL) were incubated for 10 min with buffers at room temperature. A - 10% (w/v) SDS B - 6 M guanidine, C - 125 mM sodium borate, pH 10 / 0.5 M NaCl, D - 125 mM sodium borate, pH 10 / 1 M NaCl, E - 125 mM sodium borate, pH 10 / 2.5 M NaCl, F - 250 mM sodium borate, pH 10, G – 0.2 M glycine, pH 3.0, H – Antibody protein from beads boiled in SDS-PAGE running buffer. B: M – molecular weight marker and corresponding weights (kDa) both scFv and diabody.

The selected elution buffers all failed to elute scFv protein from the Protein L beads. SDS (10% w/w) and 6 M guanidine did elute protein, but would have denatured it, and were therefore not considered suitable for purification. Since sodium borate pH 10, did not seem to be effective, other buffers were investigated in an attempt to elute as much of the antibody as possible from the Sepharose beads without damaging it (Figure 3.30).

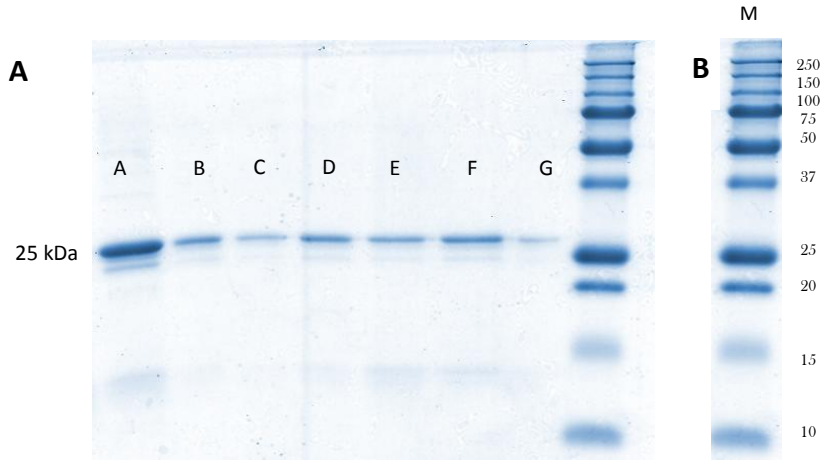

Figure 3.30: A: SDS-PAGE of protein eluted from Protein L beads bearing attached R2G10 scFv. A - Boiled protein (antibody) from beads, B - 0.1 M glycine, C - 0.5 M glycine, D - 1 M glycine, E - 100 mM triethylamine, F - 200 mM triethylamine, G - best elution from a Protein L purification. Glycine buffers were pH 2.0, and triethylamine buffers pH 11.0. B: M – molecular weight marker and corresponding weights (kDa) both scFv and diabody.

The gel revealed weak bands with all elution buffers used; however none of the buffers used yielded a band of the same intensity as from the boiled beads, indicating that most of the scFv was still retained on the beads. Band F, obtained with 200 mM triethylamine, pH 11, appeared to contain some eluted scFv. This buffer is commonly used in cell selection to elute phage bound to cells [94] and is thus believed not to damage the antibody fragment, therefore it was further investigated. It was possible that by increasing the concentration, this buffer might elute more of the protein (Figure 3.31).

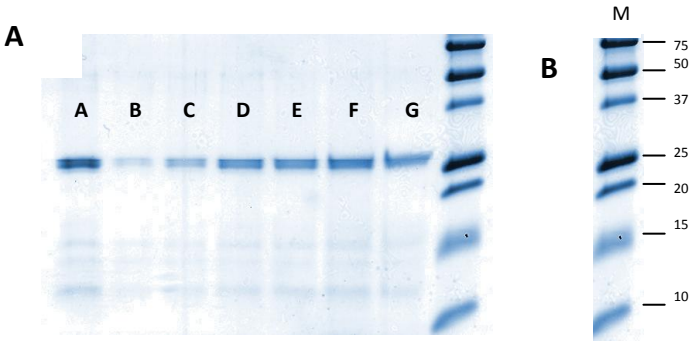

Figure 3.31: A: SDS-PAGE of protein eluted from Protein L beads binding R2G10 scFv. Beads were incubated with increasing concentrations of triethylamine. A - Boiled beads, B -100 mM, C - 200 mM, D-500 mM, E - 1 M, F- 2 M, G - 3 M. B: M – molecular weight marker and corresponding weights (kDa) both scFv and diabody.

The use of increasing triethylamine concentrations appeared to elute more scFv from the beads, with the optimal concentration between 0.5 and 2 M. As very little difference could be seen between the two concentrations, 500 mM triethylamine, pH 11 was used to elute the scFv and diabody from Protein L after Protein A purification.

A summary of the range of buffers used during the attempt to elute the scFv bound to Protein L is shown in Table 3.9.

Table 3.9: Elution of scFv and diabody from Protein L-Sepharose beads using a number of solvents of varying pH and sodium ion concentration

Elution Buffer	Concentration	Previous application	Eluting protein
Glycine pH 2	0.1 M	Elution from Protein A Sepharose beads	Faint bands were observed, but these buffers failed to elute the protein
	0.5 M		
	1 M		
Sodium Borate pH 10	250 nM NaCl	Elution of protein from Proteins A and G	Increasing concentrations of salt failed to elute the protein
	0.5 M NaCl		
	1 M NaCl		
	2.5 M NaCl		
Potassium thiocyanate	1 M and 3 M	Disrupting antibody - antigen interactions	Failed to elute protein
Guanidine hydrochloride pH 3	6M	To clean Protein G - Sepharose beads	Eluted protein, but high pH probably damaged antibody fragments
10% (w/v) SDS		Reducing agent in SDS-PAGE	Eluted a moderate amount of protein; probable damage to antibody fragments
Triethylamine pH 11	100 mM	Used in phage display to elute bound phage from cells	Weak elution of protein
	200 mM		
	500 mM		Strong elution of protein, close to that eluted from boiled beads
	1 M		
	2 M		
	3 M		Weak elution of protein; probable damage to antibody fragments

In conclusion from these experiments, scFv and diabody periplasmic fractions were purified using Protein A, followed by Protein L chromatography, and eluted with 500 mM triethylamine, pH 11. This method ensured complete purification and removal of all lower molecular-weight contaminants, although it also compromised the yield of protein eluted.

3.2.8 RADIOLABELLING OF SCFV AND DIABODY USING SODIUM [^{125}I] IODIDE

3.2.8.1 Labelling antibody fragments with Sodium [^{125}I] Iodide using Iodogen tubes

Both monomeric and dimeric antibody fragments were radiolabelled with sodium [^{125}I]-iodide[56]. ITLC, performed to measure the percentage bound, showed radiolabelling efficacy always to be greater than 90%.

3.2.8.2 Radioimmunoassay

Cell-binding assays were carried out on both LNCaP C81 and DU145 cells with [^{125}I]-iodine-labelled R2G10 scFv and diabody. These assays were repeated several times whilst varying the incubation time and temperature; however no assays showed specific binding to the LNCaP C81 cells. This raised questions as to whether radiolabelling interfered with the binding sites on scFv and the diabody, and prompted analysis of the binding of antibody fragments labelled with non-radioactive (stable) iodine (^{127}I) by FACS (Figure 3.32). Stable isotope ^{127}I was used to allow analysis by FACS which would not be possible with its radioactive counterpart. As the stable isotope behaves chemically in the same way as radioactive iodine, if conjugation of the isotope to the antibody fragment was interfering with the binding domain, this would be highlighted in the FACS analysis. It was also a safer and more economical method; limiting the experimenter's exposure time and utilising a more readily available product.

3.2.8.3 FACS Analysis to Test for Oxidative Damage

The antibody fragments were labelled as before, substituting $^{125}I^-$ with the stable isotope $^{127}I^-$ to ascertain whether labelling interfered with the antigen binding site. The antibody fragments were also incubated in the iodogen tubes alone, to assess whether the oxidative environment damaged them. FACS analysis was performed with ^{127}I-labelled antibody fragments and 'oxidised' antibody fragments, and their binding affinity was compared with that of the antibody fragments alone.

[56] Chapter 2 - Section 2.2.11

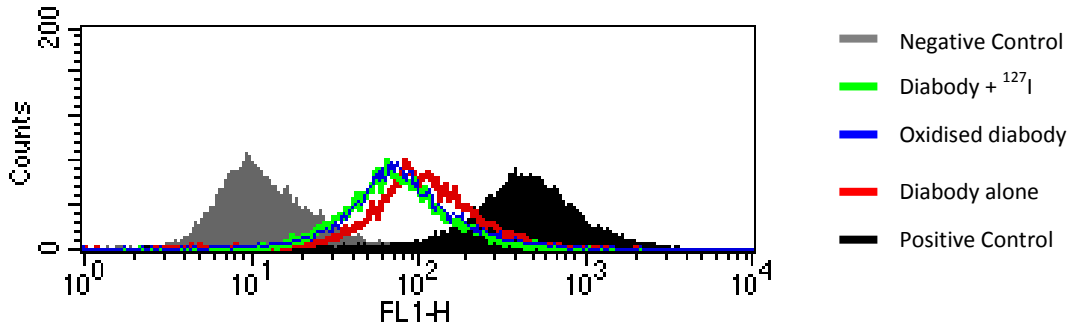

Figure 3.32: FACS analysis on PSMA-expressing cells LNCaP C81. Overlay of histograms using 5 µg of diabody. Negative control – no antibody fragment, just secondary antibody[57] and FITC, positive control – commercially-available anti-PSMA antibody.

Usually, the labelling process does not damage the antigen-binding ability of the antibody, but occasionally oxidative damage may occur during binding or attachment of the isotope to the antigen-binding site if the latter is tyrosine-rich. The experiment was carried out under the same conditions as in previous FACS analysis[58]. The binding affinity of the dimeric antibody fraction was compared with that of unlabelled diabody, and oxidised diabody resulting from treatment in the iodogen tube in the absence of iodine. Very little difference was seen between the behaviour of any of the samples treated under all the conditions. The unprocessed diabody showed a slight improvement in binding, but this difference was not regarded as significant.

This experiment was also performed on scFv fractions and, as with the dimeric fractions, little difference in binding efficacy was seen, suggesting that the labelling process, oxidation and the substitution of the radioisotope did not affect the binding site. The reason for the apparent decrease in antibody binding after labelling with sodium [^{125}I]-iodide was unknown and an *in vivo* experiment was performed in one last attempt to test the antibody fragments' specificity.

[57] 9E10 - c-Myc antibody
[58] Chapter 2 - Section 2.2.8

3.2.9 *IN VIVO* BINDING

Although radioimmunoassay failed to show any specific antibody binding to LNCaP C81 FACS showed that ^{127}I-labelled diabody selectively bound to PSMA-expressing cells, with no significant difference observed between the labelled and unlabelled species. Therefore it was thought worthwhile to assess the behaviour of the antibody fragments *in vivo*. Five weeks prior to the experiment, 10 male SCID beige mice were injected subcutaneously with 10^6 LNCaP C81 cells in a 1:1 mix with Matrigel in the left hind leg at the level of the pelvis, and left to grow until tumours became visible under the skin. R2G10 scFv and diabody were selected for the initial *in vivo* experiment, and were radiolabelled with sodium [^{125}I]-iodide. The percentage radiolabelling efficiency, determined by ITLC, was greater than 98%.

Radiolabelled antibody fragments were administered by intravenous tail injections, and scanned using SPECT at several times post injection; 30 min, 4 h and 24 h (Figure 3.33). These times were chosen to allow monitoring of the distribution and both specific and non-specific uptake of the radioligand.

A

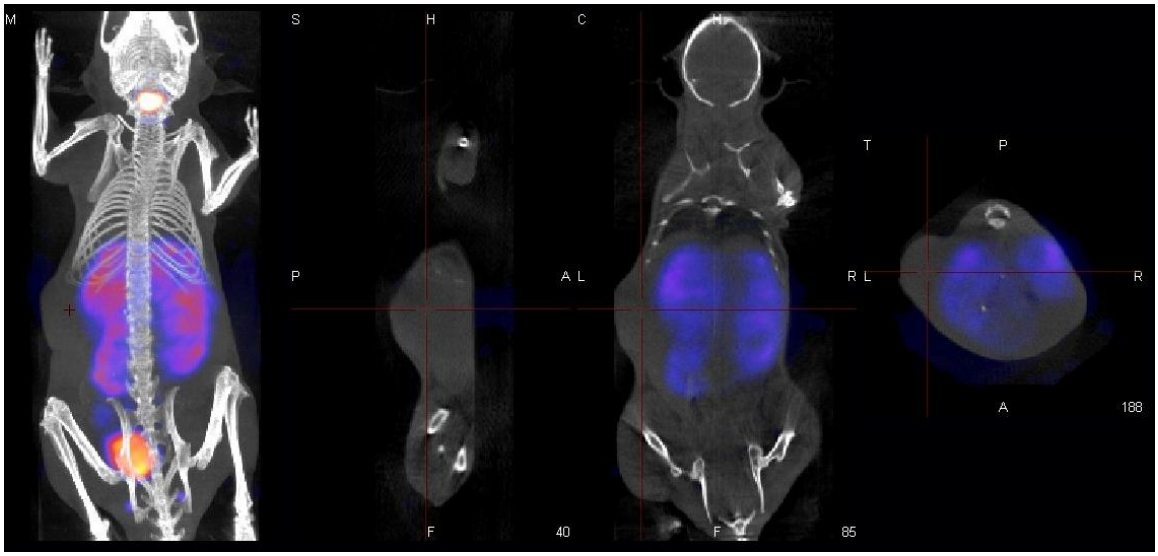

B

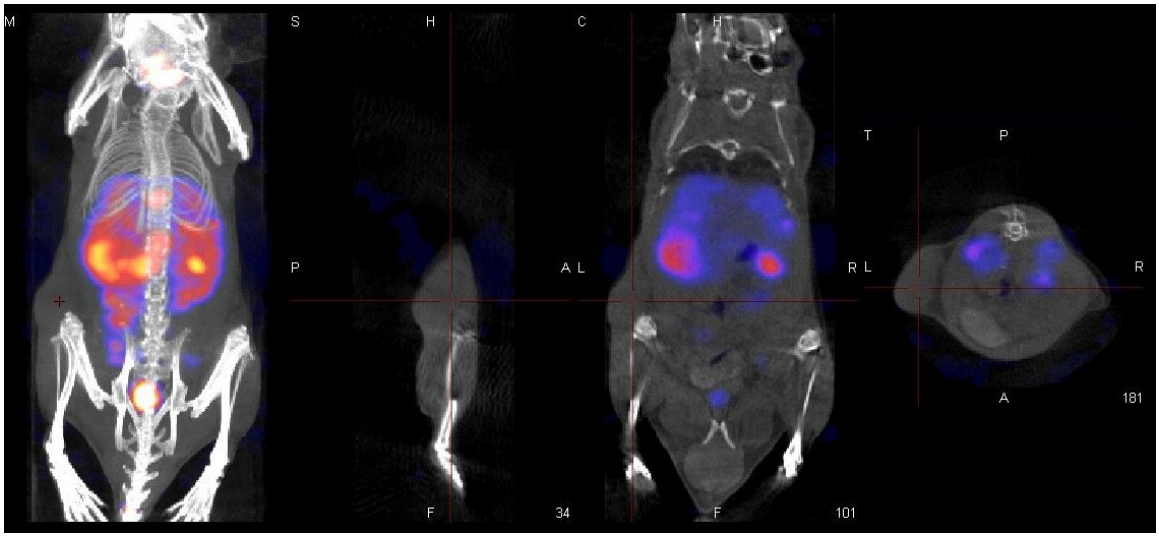

Figure 3.33: SPECT images of mice 4 h after injection. A – 7 MBq of [^{125}I]-iodine - labelled R2G10 diabody; B – 7 MBq of [^{125}I]-iodine - labelled R2G10 scFv.

The tumours grew to approximately 5 mm in diameter and were readily apparent in the CT images in both mice, in longitudinal and transverse sections. In the SPECT images, the thyroid was clearly visible due to the uptake of [^{125}I]-iodine, as well as the kidneys, liver and gall bladder; however, no uptake of either scFv or diabody by the tumour was seen in injected mice at any of the sampling times, raising questions about the specificity of the antibody fragments and the labelling technique employed.

3.3 DISCUSSION

3.3.1 PSMA ANTIBODIES

3.3.1.1 PSMA Antibodies

Monoclonal antibodies (mAb) are highly specific and versatile for targeting cells and in the last decade much research has been undertaken for treating a range of human diseases including cancer. PSMA has attracted a lot of interest due to its potential at being both a diagnostic and therapeutic target [45, 66].

3.3.1.2 Selection for Anti-PSMA Phage on PSMA-Expressing Cells

In the present investigation, the use of phage display technology to generate anti-PSMA antibody fragments represented a promising and quick alternative to the conventional immunisation approaches employed to produce polyclonal and monoclonal antibodies. The use of a synthetic phage library in this work enabled the isolation of scFv specific to PSMA, without the need for immunisation.

Selection for anti-PSMA scFv was first performed on the cell line LNCaP C81, which naturally expresses PSMA. The rationale behind this approach was that the scFv raised against PSMA would recognise the naturally expressed PSMA, because the selection was being performed on the form of PSMA found *in vivo*, bearing the typical conformation and glycosylation patterns, rather than that of synthetically generated PSMA. Five rounds of selection performed on the cells yielded 5 clones that were deemed PSMA-specific and were taken forward for a number of validating experiments. However, this approach ultimately did not yield high-affinity PSMA-specific scFv, and was subsequently abandoned.

A possible modification of this approach, which might have been more successful, would have been to alternate selection between the PSMA-expressing cells and the recombinant PSMA protein developed in-house in parallel to cell selection. That would enhance the

enrichment of the phage population to PSMA because of the greater concentration of PSMA protein, and yet still ensure specificity toward the naturally-expressed PSMA. Conversely this approach could equally be emulated by transfecting either the LNCaP or DU145 cell line with PSMA, to enable selection to be performed on cells that expressed PSMA in considerably higher concentrations.

3.3.2 PRODUCTION OF RECOMBINANT PROTEIN

Recombinant PSMA protein was generated using the Baculovirus Expression Vector System in insect (Hi5) cells. The advantage of generating the protein in this way (established by Dr. Stella Man) enabled only the large, extracellular portion of the molecule (the ectodomain) to be generated, without the smaller intracellular portion, which is only exposed once the cell has undergone apoptosis. Using this system, high yields of PSMA were obtained. A his-tag having been inserted next to the ectodomain, purification was then facilitated by chromatography on Ni-NTA Sepharose, which shows high affinity and selectivity for 6xHis-tagged recombinant fusion proteins; and purity was confirmed by Western blot analysis, which revealed bands at the expected molecular weight of 90 kDa.

3.3.2.1 Selection using Recombinant PSMA Protein

The three rounds of selection performed on the recombinant protein were considered sufficient, because selection was performed using considerably higher concentrations of PSMA than that naturally expressed on cells, and performing too many rounds risked amplifying only a few highly-expressed phages, with the potential to lose less-prevalent but higher-affinity phages.

This procedure might have been improved by biotinylation of the protein at the N-terminus, so that during subsequent assay in immunotubes or 96-well plates coated with

streptavidin, the protein would have been bound so as to maximise exposure to binding, rather than adhering in a randomised manner to the plastic.

3.3.2.2 Sequencing of Phage Clones

Amino-acid and nucleotide sequence alignments have been compiled for all functional V, D and J segments of the immunoglobulin in the program V Base, The Database for Human Genes Medical Research Council (MRC). Using this program, sequences from selected clones were analysed against the corresponding V_H and V_L sequences, DP47 from V_H3 and DP-k9, respectively. Here, comparison of the fixed framework was used to find the scFv sequence and verify it by analysis of the CDRs 2 & 3 of both the heavy and light chains, to determine whether the selected phage clones possessed unique and complete sequences. Sequences from screened phage clones revealed a diverse range of PSMA-specific scFv.

During phage enrichment and amplification to PSMA, deletions in antibody gIII fusions can occur which result in the surface expression of only part of the antibody fragment. Such species are often "sticky"; they can interact non-specifically with the solid phase and can co-elute with antigen-specific phages [178]. It is therefore important to perform PCR on single bacterial colonies infected with eluted phage and then to sequence them to determine the proportion of phages containing the full scFv insert. This, combined with ELISA and phage titration, allows monitoring after each round of selection and provides a first hint of progress.

3.3.2.3 FACS Using Selected Phage Clones

It was crucial, at an early stage of screening, to determine whether PSMA-specific phages shown to bind the recombinant PSMA protein also bound to PSMA naturally expressed on cell surfaces, thereby confirming similarities in conformation between the recombinant protein and PSMA expressed *in vivo*. FACS analysis enabled measurement of the binding of the positive phage clones and their ability to discriminate between the PSMA-positive and -negative cell lines, respectively LNCaP C81 and DU145, and ensured that clones bound PSMA specifically, not by "sticky" interactions. The Tomlinson I Library [90] was

employed as the negative control, to ensure that binding was not due to the reactivity towards the PSMA of an enriched population of different PSMA-binding phages present in the original library.

FACS analysis revealed that 50% of the phage clones from selection rounds 2 and 3 bound specifically to LNCaP C81, and not to DU145. Accordingly, cells of the non-suppressor strain *E. coli* HB2151 were infected with these clones to prompt the expression of the soluble scFv alone, but the binding affinity of these phage clones never approached that of the positive control D2B.

3.3.3 EXPRESSION OF SOLUBLE SINGLE-CHAIN FV

Soluble scFv expression was carried out on clones from both rounds 2 and 3 because a diverse scFv population giving both high expression and strong binding was required for further analysis. Soluble scFv was expressed and secreted by the non-suppressor strain, *E. coli* HB2151, instead of the originally-used strain, *E. coli* TG1, because although a small proportion of soluble scFv is produced by this organism (since suppression is never fully achieved), HB2151 cells secrete soluble antibody fragments quantitatively into the periplasm[59] and the supernatant because an *amber* stop codon is present at the junction of the antibody gene and gIII[60]. The *lacZ* promoter drives the expression of the scFv gene, which is induced by IPTG. Due to expression sometimes occurring in the absence of IPTG, glucose is added to the growth medium to inhibit expression of the scFv gene until IPTG is added, which is why the glucose concentration is reduced from 1% (w/v) to 0.1% to ensure that it has been completely metabolised by the time IPTG is added [179, 180]. Recovery of the scFv fragments is then easily achieved.

[59] Chapter 2 - Section 2.2.5.2
[60] Appendix I

3.3.3.1 FACS Analysis of Purified Selected Clones

FACS analysis on the purified, secreted scFv was performed again to determine whether the selected scFv retained the binding and specificity towards PSMA of the original phage clones, and the ability to discriminate between PSMA-expressing and non-expressing cells. The results confirmed that selection to the target PSMA had been successful, and that the observed binding was indeed due to specific interactions between scFv and PSMA, and not to non-specific interactions via the phage body.

As well as ascertaining the PSMA-specificity of the scFv, optimisation of the secondary antibody was also performed, by targeting both the myc- and his-tags using anti-myc and anti-his monoclonal antibodies respectively. These tags, incorporated into the vector, offered a range of sites for assay and purification procedures [181, 182]. For reasons unknown (perhaps stronger affinity), anti-myc yielded better results than anti-his, and was thereafter used routinely.

The peaks obtained in the FACS histograms (Figure 3.10) for the scFvs were not as sharp as those of the positive and negative controls. Their breadth suggested heterogeneity, possibly indicating the formation of di-, tri- or even tetrabodies by interaction of the fragments with one another.

3.3.3.2 Purification of scFv

Purification of scFvs from the periplasm and supernatant can be achieved by use of a number of different columns, depending on the choice of target, viz. the myc- and his-tags incorporated into the pIT2 vector, or the V_H3 family and V_L chains of the scFv, which bind to Proteins A and L, respectively. Compared with Ni-NTA chromatography, initial purification on Protein A-Sepharose gave high yields of purified scFv from the periplasmic and supernatant fractions, as verified by SDS-PAGE, and was therefore selected as the method of choice.

Four scFv clones were selected for further analysis; R2F3, R2G10, R2H2 and R3F5. These all exhibited good binding both to PSMA naturally expressed in cells (as shown by FACS) and also to the recombinant protein (shown by ELISA). Analysis showed that R2F3 and R3F5 possessed the same scFv sequence, and were at first selected in error; however, both clones were retained as it was thought interesting to see whether differences in binding or expression were nonetheless observed (see below).

3.3.3.3 Production of Diabodies

Diabodies were produced in an attempt to increase avidity for the target antigen by combining two antigen-binding sites. Diabodies are known to have an advantage over scFvs for *in vivo* applications due to this increase in avidity, and because dimerisation reduces the rate of clearance from the circulation [180]. Complete removal of the flexible glycine-serine linker was performed by exploiting the two restriction sites, SalI and XhoI[3], on either side of the linker. After cutting and ligation, removal of the linker was verified by using other restriction sites present on the vector, viz. HindIII and NotI. As expected, digestions with the combination SalI or XhoI (acting on the removed restriction sites) with either HindIII or NotI yielded only one band, since only one restriction site remained. The combination of both HindIII and NotI resulted in two bands, due to both sites being cut on the vector (Figure 3.15).

Diabody production was confirmed by ELISA using immobilised recombinant periplasmic-fraction PSMA protein, and BSA as a non-specific control. The results were encouraging; all the diabodies generated discriminated between PSMA and BSA, indicative of specific binding.

Diabodies from the supernatant and periplasmic fractions were also compared by performing ELISAs in Maxisorb 96-well plates[61], which revealed dimeric antibody fragments in both fractions. Removal of the glycine-serine linker resulted in the attachment of the C-terminal residue of the V_H domain directly to the N-terminal residue

[61] Chapter 2 - Section 2.2.9

of the V_L domain, so sterically preventing the two sites from coming together to form the natural antigen binding site of which scFv fragments were capable; therefore the observed binding could only occur with dimeric molecules (possibly also with triabodies and tetrabodies [180]).

Hudson *et al* (1999) [180] showed that when the linker is reduced in length to a small number of residues, it is possible to predict the interactions and aggregation of antibody fragments. Reduction to two glycine residues increases the probability of triabody formation, whereas limiting the linker to 3-5 residues usually favours diabody production [180].

As well as confirming successful diabody production, ELISA also showed that the periplasmic fraction contained two or three times more soluble antibody material than the supernatant, therefore confirming the value of purifying the periplasmic fraction rather than the supernatant.

3.3.3.4 ELISA of Purified Diabodies

Diabody purification was performed (as with scFvs) using Protein A-Sepharose, and binding analysis was likewise performed on the purified fractions to ensure that the specificity remained. Purified diabodies specifically bound to the recombinant PSMA in a concentration-dependent manner; minimal binding was observed with the same concentrations of BSA (Figure 3.16).

3.3.3.5 FACS Analysis of Purified Diabodies

The four diabodies were further examined to see whether they retained the specificity of the parent scFvs to PSMA naturally expressed by cells. As with purified scFvs, FACS histograms again showed broad peaks, possibly due to heterogeneity of the dimer fractions that may have also contained triabodies and tetrabodies. Nonetheless, selective binding took place with LNCaP C81 cells, compared to DU145, confirming specificity towards PSMA. This, together with the ELISA results obtained with recombinant PSMA

protein, confirmed successful manipulation of the linker to drive the formation of dimeric fragments.

It was also important to determine whether diabody binding showed greater avidity over that achieved with scFv. A range of concentrations of both scFv fragments and diabodies was compared by FACS, taking the mean fluorescence intensity for both scFv and diabody clones as the measure of binding. For all clones, significantly improved diabody binding was seen compared with the parent scFvs. Binding decreased in a concentration-dependent manner, with R2H2 exhibiting the greatest avidity. The apparent improvement in binding shown by the diabodies may have partly been due to the two myc-tags present on the V_L chain of each scFv molecule (Figure 3.20), each of which bound more of the secondary antibody via the anti-myc sites, thereby enhancing the fluorescence signal. However, if the enhanced fluorescence were due to this amplification alone, then there would maximally have been a two-fold increase in fluorescence yield over that of the corresponding scFv, but the increase with R2H2 diabody was three-fold.

Due to its rigid structure and small size, it is unlikely that the diabody could bind two PSMA ligands simultaneously [183]. The antigen binding sites of diabodies lie at opposite ends of the molecule, but unlike normal antibodies and Fab antibody fragments, in which binding sites can take up a range of orientations and spacings, the structure of diabodies is more compact and rigid due to the shortening or complete removal of the linker, which separates the binding sites by 6.5 nm and limits possible movement from their mean position to only 30° [183, 184].

Nevertheless, FACS analysis confirmed successful manipulation of the scFv fragments to drive the formation of dimers, which still exhibited PSMA-specific binding. The benefits of diabody formation would be more evident in *in vivo* applications than *in vitro,* as the increase in size of the antibody fragment would diminish the rate of antibody clearance from the circulation, thereby maintaining a higher concentration at the target site [180]. Diabodies are known to possess significantly lower dissociation rates (K_{off}) than the

parental scFv molecules, and are therefore more attractive molecules for *in vivo* imaging of tumours [184].

3.3.3.6 HPLC and FPLC Analysis of scFv and Diabodies

The two scFv molecules that form a diabody are not linked covalently, hence they can readily dissociate when changes in environmental conditions such as pH or temperature occur, or during freeze/thawing. The regenerated scFv molecules cannot themselves bind to antigen due to the rigidity resulting from the removal of their linker.

HPLC analysis was employed to examine the heterogeneity of diabody and scFv preparations consequent on their tendency to aggregate to generate diabodies, triabodies and even tetrabodies, which display different binding abilities and interactions with the target antigen. Therefore it was important that the stability of the diabodies was investigated to determine whether they would behave reproducibly in future experiments, or in the long term. Size-exclusion chromatography revealed a mixture of molecules ranging from small fragments to species the size of triabodies (Figure 3.23, Table 3.6 and Table 3.7). To ensure comparability of the results, samples were run with an internal standard, an intact antibody of mol. wt. 150 kDa, that did not interact with other proteins in the mixture and was adequately resolved from them during elution [185].

Chromatograms were reproducible and demonstrated a mixture of scFv and diabody fragments. Molecular weights did not correlate exactly with their predicted values (25 kDa for scFvs and 50 kDa for diabodies), but manipulated proteins such as engineered antibody fragments have a more open tertiary structure than naturally-produced proteins of the same molecular weight [186] because the environment in which a protein is synthesised and allowed to fold is a significant determinant of its final shape. Therefore, in size-exclusion chromatography, such proteins pass through at a faster rate than those with more compact structures and register higher apparent molecular weights than expected, which is a limitation of the method [187]. Lower molecular-weight contaminants may have persisted because of inefficient purification, or could have arisen

due to degradation by proteases because protease inhibitors were not added during purification, which in hindsight may have been advantageous.

The integrated areas of the chromatography peaks shown below (Figure 3.34) demonstrate the heterogeneity of the samples.

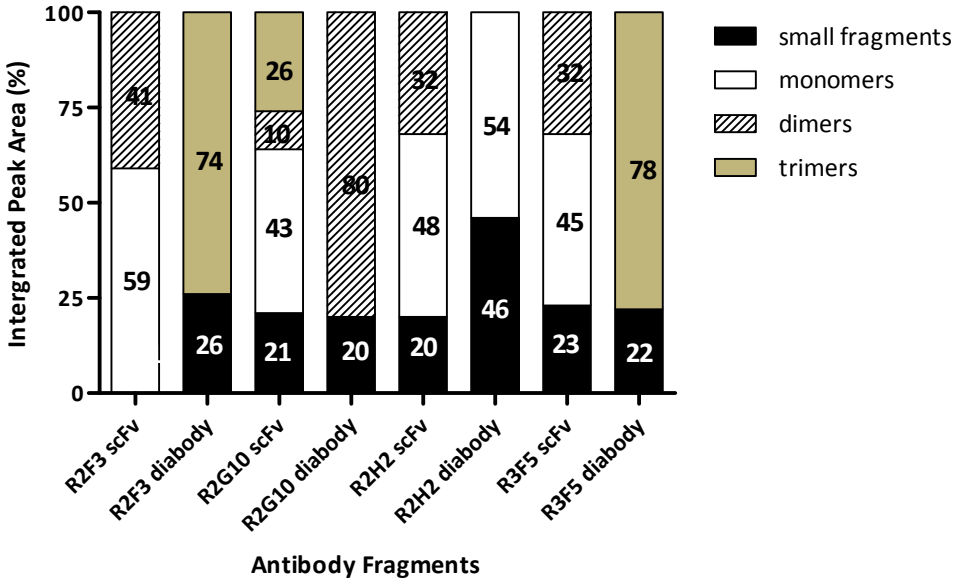

Figure 3.34: Heterogeneity of scFv and diabody preparations demonstrated by HPLC analysis. Mean integrated peak areas were calculated for both antibody preparations for all the clones.

These results showed a decidedly heterogeneous mix of antibody fragments. Small molecules of less than 15 kDa, present in both diabody and scFv preparations, were possibly generated by protease action. The antibody preparations from the R2G10 clone had already been established as the most promising, having shown selective binding with both recombinant and naturally-expressed PSMA, respectively by ELISA and FACS analysis, and size-exclusion chromatography showed that the R2G10 diabody generated the most stable dimeric preparation. It is not known why the other clones yielded so little dimeric material, perhaps due to the instability of the dimers, disaggregation driven by protease action on intact diabodies, or to the complete removal of the linker favouring triabody formation over diabody [180].

The behaviour of R2G10 diabody and scFv fragments on HPLC was also compared with their elution pattern on FPLC, because it was possible that the shear forces applied during HPLC were causing loosely-associated dimeric fragments to dissociate. The chromatograms of both the scFv and diabody obtained by FPLC were very similar to those obtained by HPLC, showing very little difference in the proportions or sizes of components, further confirming the stability of the dimeric fragment, and demonstrating that the heterogeneity of the antibody preparations was not an analytical artefact.

3.3.3.7 Purification

Throughout the analysis, several new batches of antibodies were generated and divided into smaller portions in preparation for further analysis. Each new batch was purified using Protein A-Sepharose and then analysed by SDS-PAGE. Although sometimes this procedure resulted in high purity, on other occasions significant levels of fragments of size <15 kDa remained. It was important, firstly, to achieve the highest level of purity for *in vivo* applications, and secondly to see if the low molecular-weight fragments seen in HPLC analysis corresponded to these seen in SDS-PAGE. It was not clear whether these small molecules originated in the periplasmic fraction and had not been fully removed during the purification step, or whether they resulted from enzymatic degradation of antibody.

Other purification techniques were explored to remove the small fragments whilst ensuring high yields of purified protein. Ni-NTA chromatography proved inefficient at removing these contaminants and also reduced the yield of purified protein by 50%, so was therefore discounted. Protein L-Sepharose, which has an affinity for kappa-light chains, was trialled after initial purification using Protein A-Sepharose, but although the lower molecular-weight fragments were removed, the yield of protein was diminished. The loss of protein prompted further analysis to establish the cause. Neither the flow-through samples nor the washes contained any protein, which indicated that it still remained on the beads, from which it can be released by boiling in buffer, as demonstrated by subsequent SDS-PAGE analysis. The reason for the failure to elute from the beads is unclear. In an attempt to release the antibody without damaging it, a range

of elution buffers was explored in which NaCl concentration and pH were varied. Normally, during affinity chromatography, proteins bind to beads when they have a greater or significantly lower charge than the bead, therefore elution buffers must alter this charge in order to release the protein efficiently; this can be done either by decreasing the pH or by increasing the NaCl concentration [188].

These buffers failed to elute the protein, so others were employed. Triethylamine, a moderately strong base, also used previously in cell selection to elute bound phage, was thought to be sufficiently basic to disrupt the interaction between the antibody fragment and the beads, and was known not to denature the antibody itself [178]. The optimal triethylamine concentration for successful elution was 500 mM, pH 11, which was used thereafter for elution from Protein L, in conjunction with the purification step using Protein A-Sepharose.

3.3.4 RADIOLABELLING OF SCFV AND DIABODY USING SODIUM [^{125}I]-IODIDE

Radiolabelling of both the monomeric and dimeric R2G10 antibody fragments was achieved using sodium [^{125}I]-iodide in iodogen tubes[62], with an efficiency of >90%.

To determine whether the binding affinity of R2G10 antibodies had remained unaffected by labelling, a direct radioimmunoassay was performed to measure the immunoreactivity of the labelled fragments, i.e. the proportion of radioactive antibody fragments having the ability to bind the antigen [144]. However this failed to yield any positive results; no specific binding to LNCaP C81 cells was observed, implying that radiolabelling had interfered with the antigen binding site. [^{125}I]-Iodide reacts with tyrosine residues by electrophilic substitution in the phenolic side-chain[63], therefore if the antigen-binding site is rich in tyrosine, [^{125}I]-iodide might bind and interfere with the avidity of the fragment,

[62] Chapter 2 - Section 2.2.11
[63] Chapter 1 - Section 1.11.1

however the sequence that makes up the binding site is known, and contains no tyrosine residues, thus eliminating this possibility. Alternatively the antibody-binding ability of the fragments could be damaged by the labelling procedure itself, notably during the period of residence in the oxidative environment of the iodogen tube. This possibility was explored by FACS analysis. R2G10 antibody was accordingly either labelled with stable iodide [$^{127}I^-$], using iodogen, or incubated in iodogen tubes alone to determine whether the oxidative environment was the cause. The resultant preparations showed no significant difference in behaviour from untreated dimeric antibody. Although the labelling procedure was shown not to affect the immunological activity of the fragments, it remains unclear why binding ability was lost after radiolabelling. Labelling experiments with both sodium [^{125}I]-iodide and stable iodide [^{127}I] were repeated on several occasions and with new R2G10 scFv preparations, but all failed to reveal the cause of the loss of binding.

It is however important to consider the differences between the two assays which could account for the differences in binding behaviour. Although the radioimmunoassay was performed at 4°C to prevent internalisation, the binding buffer did not, unlike the FACS buffer, contain sodium azide. If the radiolabelled antibody were internalised, it would be metabolised, the iodide released and secreted from the cell into the supernatant, so that subsequent analysis would reveal no evidence of binding. To ensure that the loss of any weakly-binding material in the wash steps was detected, the washes were also collected and assayed, but no activity was found, therefore no bound material was lost during these steps.

Furthermore, binding studies conducted by FACS analysis were routinely performed with approximately 800-fold greater antibody concentrations than those used in the radioimmunoassay, which could explain why no binding was observed. Although concentrations were later increased, they still fell well short of the normal values used in FACS and a low binding affinity of the antibody fragments could explain the lack of observable binding by radioimmunoassay.

Although the labelling procedure appears not to have been responsible, other techniques could be employed to radiolabel the antibody fragments effectively, such as the enzyme-catalysed methods using lactoperoxidase or glucose oxidase, which proceed under much milder conditions, though with diminished labelling efficiency. Alternatively, one could employ a reaction that attaches the iodine to a different amino-acid; e.g., the Bolton and Hunter reagent [N-succimidyl 3-(4-hydroxyphenyl) propionate] results in iodination of lysine residues [144], but again with lower labelling efficiencies than using iodogen tubes.

^{125}I was employed initially to verify binding efficiency of the antibody fragments once radiolabelled. The benefits of iodination with this radionuclide include the relative ease of the methodology, the long half-life of the isotope which allows repeated study on the same preparation, minimal losses of protein, and most importantly, it allows the radiolabelling of low protein concentrations, which was crucial as antibody production was only performed on a micro-scale.

An intrinsic drawback of iodination is the possibility of deiodination resulting in the generation of free iodide. Deiodination of the radiolabelled antibody fragments *in vivo* would result in iodide being taken up by the thyroid and other iodide-transporter expressing tissues. More importantly, as PSMA is internalised into the cell, deiodination could occur once inside and be released from the cell, resulting in poor images due to high background or even complete loss of the released iodide which would fail to generate any images of uptake. Deiodination could also occur *in-vitro* if the radioligand is internalised by PSMA-expressing cells after which the free iodine can be released from the cell resulting in poor retention of the radiolabel. To ensure that this did not happen in the *in vitro* experiments described above and to assess the whether the extent of deiodination, TCA precipitation of the supernatant was performed to ensure that the majority of the radioiodine remained in a protein-bound form with minimal free iodide, this however cannot be performed for *in vivo* analysis.

3.3.5 *IN VIVO* STUDIES

Despite negative results from the cell-binding studies, a limited exploration of *in vivo* targeting was undertaken, however no uptake in the tumour was observed.

The failure of this *in vivo* study with tumour-bearing mice to demonstrate any specific binding of radiolabelled antibody could have been due to a number of factors. The stability of the labelled antibody as a function of temperature was not fully examined to determine whether the binding ability of the complex remained stable at 37°C for a time period matching that of the experiment. Binding capacity can be diminished by up to 25% over 24 h [61]. Plasma stability analysis, whereby radiolabelled antibody is incubated in human or murine blood at 37°C and then analysed by reverse-phase HPLC [189], would have determined whether the labelled preparation remained intact *in vivo* long enough to target the PSMA expressed on the tumour cells. However it was concluded that although PSMA-specific, positive binding had been seen *in vitro* by FACS and ELISA, the binding efficacy of the antibody fragments appeared to be too low to justify further analysis.

3.4 SUMMARY & CONCLUSION

3.4.1 Generating scFv Antibody Fragments

Using phage display technology two attempts to generate PSMA specific scFv were made; firstly on PSMA expressing cells and secondly on in-house generated recombinant PSMA protein.

Attempt one

A total of 5 rounds of selection were performed and 5 ‘positive’ candidates were selected and taken forward for further validating experiments, using a range of techniques viz.

FACS, ELISA and immunoprecipitation. Results however did not show high affinity to PSMA and questions arose to their specificity to the PSMA target, subsequently, this approach was abandoned.

Attempt two

In-house recombinant PSMA protein provided a high concentration of target to which 3 rounds of selection was performed. Several PSMA-specific clones were selected and soluble scFv molecules expressed.

Binding specificity was measured by ELISA and FACS and the 4 selected clones were able to discriminate between the target with non-specific proteins and non-PSMA expressing cells.

To increase avidity, the formation of diabodies was performed on the selected clones, molecular biology techniques allowed for the complete removal of the flexible linker, driving the spontaneous formation of dimeric molecules. Improved binding could also be observed over the scFv antibody fragments.

The stability and heterogeneity of the fragments were also measured using both HPLC and FPLC. Dimeric fragments were not as unstable as feared and results from HPLC were reproducible and further confirmed in FPLC.

Optimisation of purification techniques were also studied and issues overcome. High purity of both the scFv and diabodies was established by combination of Protein A and L chromatography, with the use of optimal elution buffer to elute the protein without damage to the antigen binding site.

Radiolabelling of the antibody fragments yielded in excess of 90% efficiency, however the specific binding previously observed was lost. Investigation into why binding was lost did not reveal a conclusive answer; with antibody preparation concentration and binding

affinity a possible cause, however it confirmed that labelling of the radiotracer did not interfere with the antigen binding site and the antibody fragments were not damaged by oxidative stress during the labelling procedure.

In vivo analysis to tumour bearing mice did not reveal specific binding to the PSMA expressing cells and although PSMA specific clones were successfully selected using phage display, both the scFv and diabodies did not posses high enough affinity to justify further radio-imaging studies.

4 DEMOBESIN 4 STUDY

Small peptides are currently being investigated for their ability to bind to cell surface receptors, over-expressed in a wide variety of malignant tissues. They are potentially useful for radionuclide-mediated detection and therapy, and could serve as ideal delivery vehicles for toxins or drugs to act against tumours. The clinical utility of using radiolabelled receptor-avid peptides is readily exemplified by the current use of [^{111}In]-DTPA-octreotide (Octreoscan® Mallinckrodt Medical Inc. USA)[64] [190] and other radiolabelled octrotide analogues that bind cancer cells expressing somatostatin receptors.

GRP and somatostatin receptors share some similarities and there is increased interest in GRP-R expression in a number of cancers, including prostate cancer. The incidence of GRP-R and its density on prostate cell surfaces was investigated in this project using Demobesin 4 (DB 4), an analogue of Bombesin, to establish its clinical potential and application as a radiopharmaceutical.

4.1 AIMS

The aims of this project were four-fold:

1. Compare methods for the measurement of GRP-R expression by prostate cancer cell lines
2. Compare expression levels *in vitro vs. in vivo*
3. Determine whether imaging *in-vivo* is able to quantify the level of GRP-R expression
4. Assess the relationship between androgen status and GRP-R expression

[64] ["'I]-DTPA-pentetreotide (Octreoscan®) - a somatostatin receptor radiopharmaceutical, for the detection of somatostatin-positive tumours.

4.2 DEMOBESIN 4 STUDY RESULTS

4.2.1 *IN VITRO* STUDIES WITH ^{99M}TC – LABELLED DB 4

4.2.1.1 Radioligand Binding Assay

Assays were performed at various concentrations of ^{99m}Tc-labelled DB 4 to measure the specific radioligand binding to cells at equilibrium, and to determine both the receptor numbers (B_{max}) and the binding affinity (K_d).

B_{max} and K_d were determined for all cell lines. Before the advent of non-linear regression programmes, data obtained from these experiments was transformed into a linear form, such as a Scatchard plot (more accurately attributed to Rosenthal) (Figure 4.1 (A)).

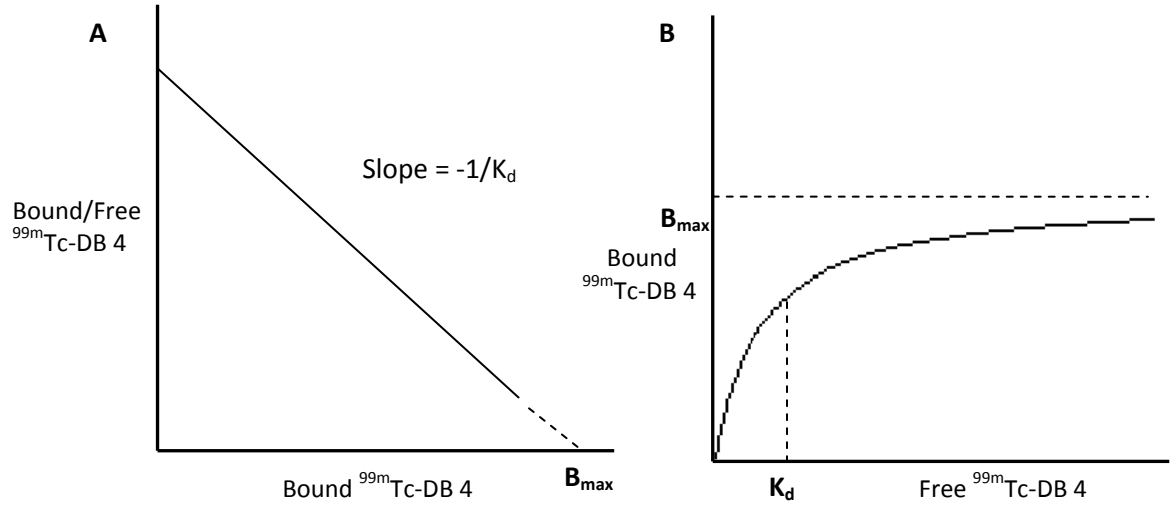

Figure 4.1: Schematic diagram of Scatchard plot (A) and non-linear regression plot (B) [191].

The Scatchard plot allows the estimation of B_{max} and K_d; respectively the *x* intercept and negative reciprocal of the slope [191], however the Scatchard transformation distorts the experimental error and may transform data far from their true values, therefore non-linear regression is now widely used. Graphpad Prism 5, a statistical program was used to perform non-linear regression plots.

The ligand binding assay was first performed on AR42J rat pancreatic cells, the positive control known to express GRP-R [192] . Non-specific binding, measured using unlabelled DB 4 as the competitor, was subtracted from the total binding to obtain the specific binding (Figure 4.1 (B)). Non-specific binding is almost always a linear function of the ligand concentration, so a straight line can be drawn that best fits the non-specific values without the need to measure non-specific binding at every radioligand concentration. A range of radioligand concentrations was investigated to obtain the full curve and reach saturation; when most of the receptors are occupied by the radioligand. Radioligand concentrations of 0.1, 1, 2.5, 5, 7.5, 10 and 25 nM were investigated; normally saturation is reached prior to the highest concentration (Figure 4.2).

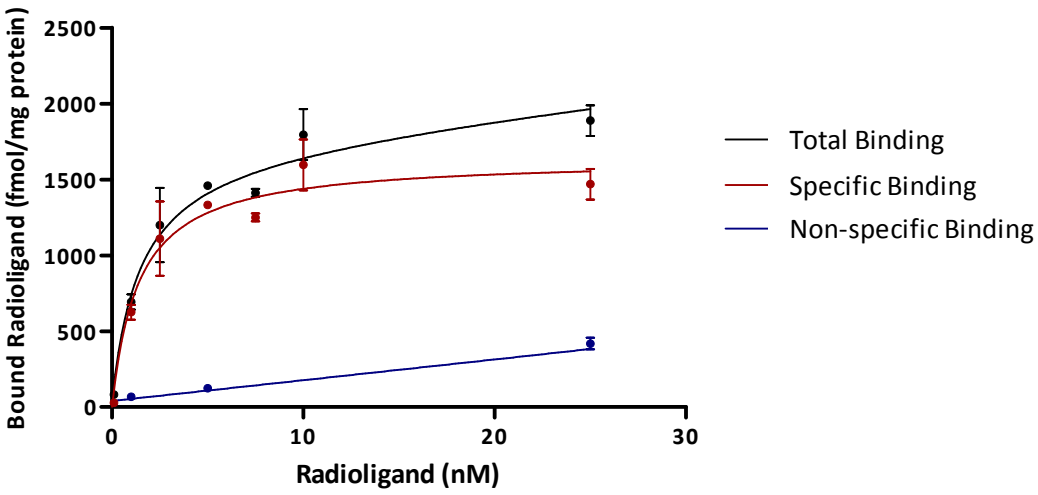

Figure 4.2: Non-linear regression graph of radioligand binding assay for AR42J cells. Experiment performed in triplicate on 3 separate occasions (n=9)

Specific binding levelled off at higher radioligand concentrations after incubation for 1.5 h at 37°C, by which time the reaction had reached equilibrium.

The results of the radioligand binding assay on all cell lines[65], including LNCaP C81 and C42B, grown in androgen-reduced media[66], are shown in Figure 4.3. B_{max} and K_d were calculated for each cell line tested (Table 4.1).

[65] Appendix V
[66] Chapter 2 - Section 2.3.3

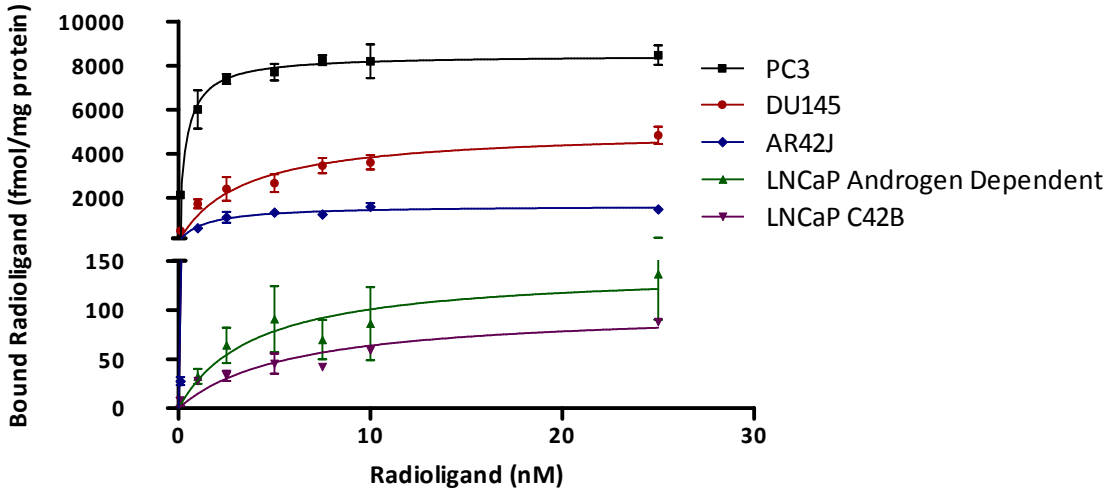

Figure 4.3: Results of radioligand binding assay for all prostate cancer cell lines tested. AR42J - positive control known to highly express GRP-R. Experiments were performed in triplicate on 3 separate occasions for each cell line (n=9).

Elevated levels of GRP-R were observed in PC3 and DU145 above that of the positive control AR42J. LNCaP, the only androgen-dependent cell line, also showed GRP-R expression but to a lesser extent than that of PC3 and DU145. LNCaP C81, LNCaP C81 (androgen-deprived) and C42B (androgen-deprived) [results not displayed in Figure 4.3] did not show receptor expression, or the level of expression was below the sensitivity of the assay.

Table 4.1: B_{max} and K_d values with standard deviations for all PC cell lines obtained from radioligand-binding assays. N/A - not applicable (AR42J is a rat pancreatic cell line).

Cell line	Androgen Dependence	B_{max} (fmol/mg protein)	K_d (nM) ± SE
AR42J	N/A	1108 ± 477	1.361 ± 0.183
PC3	Independent	8345 ± 426	0.356 ± 0.108
DU145	Independent	4182 ± 624	2.24 ± 2.200
LNCaP	Dependent	104 ± 70	1.509 ± 0.814
LNCaP C81	Independent	No specific binding observed	No specific binding observed
LNCaP C42B	Independent	57 ± 19	1.229 ± 0.517
LNCaP C81 (*androgen-reduced medium)*	Independent	No specific binding observed	No specific binding observed
LNCaP C42B (*androgen-reduced medium)*	Independent	No specific binding observed	No specific binding observed

A range of B_{max} and K_d values was obtained for the cell lines tested. Some androgen-independent cell lines showed receptor expression, with some at levels greater than that of the positive control. The androgen-dependent cell line LNCaP showed GRP-R expression but at lower levels than the independent cell lines PC3 and DU145. GRP-R expression thus seemed to be up-regulated with later stages of cancer (Figure 4.4).

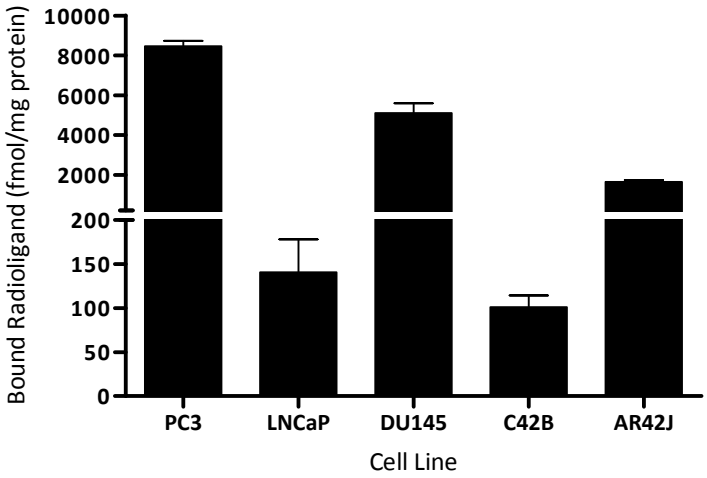

Figure 4.4: Comparison of B_{max} values obtained for all tested cell lines. AR42J - positive control cell line. Experiments were performed in triplicate on 3 separate occasions for each cell line (n=9).

Very similar K_d values were found, with minimal differences observed between cell lines; any differences observed were found not to be significantly different when t-test analysis was performed with a P value = >0.05.

4.2.2 HIGH- AND LOW-PASSAGE NUMBERS IN THE LNCAP C42B CELL LINE

4.2.2.1 Increased Passage Number

Over-subculturing *in vitro* is widely known to change cell lines' properties over time. Cell lines that have been passaged too many times experience alterations in cell morphology, responses to stimuli, growth rates, protein expression, transfection and signalling compared to cells that have been passaged fewer times [193, 194]. LNCaP cells are known to display markedly divergent responses to androgens, which can drive androgen-dependent cells to become androgen-independent.

With this in mind, it was important to ascertain whether the *in vitro* results obtained and relationships inferred were in fact a true representation of the natural behaviour of these cells *in vivo.* Although there is considerable literature to support the fact that over-subculturing cells has an effect on their growth and behaviour, not much is known as to why and how this occurs. Nutrient stress is one possibility which might account for this phenomenon. Selecting LNCaP C42B as a representative example, a comparison of radioligand binding was made between cells that had been passaged a few times and cells passaged many times. Passage numbers below 30 were classed as *low-passage number*; numbers greater than this were classed as *high-passage number* (Figure 4.5).

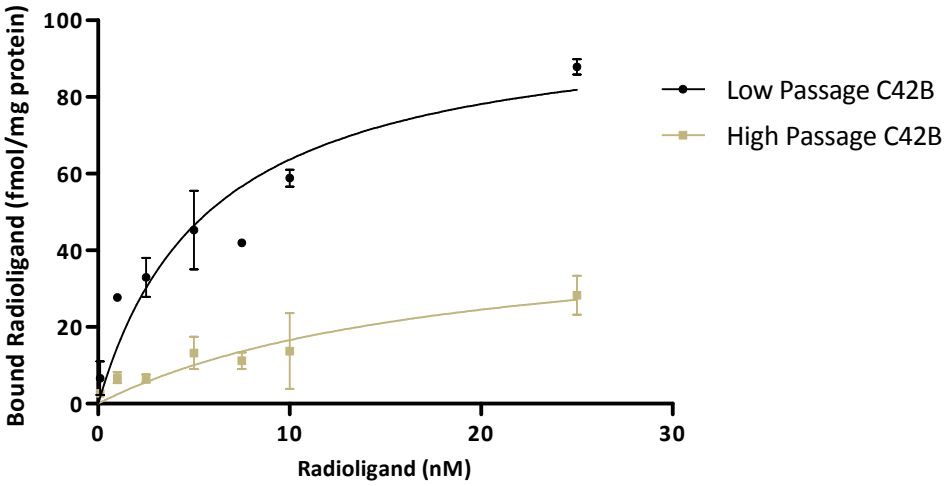

Figure 4.5: Radioligand binding assay on high- and low-passage LNCaP C42B cells. The experiment was performed in triplicate on 3 separate occasions (n=9).

Results obtained revealed a notable difference between high- and low-passage LNCaP C42B cells, which confirmed the hypothesis that cells with a higher passage number behaved in an abnormal way, and although there is no gold standard that defines an upper limit to passage numbers (since passage levels considered high for one cell line may not give rise to abnormal effects in another) all the cell lines used in both *in vitro* and *in vivo* experiments were limited to those of passage numbers <30.

4.2.2.2 RT-PCR – Relative Quantification

A quantification assay using RT-PCR was performed to measure the amount of GRP-R mRNA present in the range of cell lines studied (representing both early and late stages of prostate cancer growth) and to see whether similar expression levels observed with radioligand binding assays were found. This experiment sought to determine the extent to which each cell line (representing different stages of PC growth and thus of androgen-dependence) expressed the GRP-R gene, and also whether external factors such as passage number and culture conditions influenced the expression in comparison with a non-expressing cell line.

Total RNA was extracted from the cell lines of interest, from which cDNA was generated for the acquisition of C_t[67] values which were quantified and compared with those derived from a calibrator, here the non-GRP-R expressing cell line, MKN45. Results were expressed in terms of the ratio of the level of expression of the base sequence in a given cell line to that found in the calibrator.

The comparative C_t method is also known as the $2^{-\Delta\Delta Ct}$ method[68], where:

$$\Delta\Delta C_t = \Delta C_{t\ sample} - \Delta C_{t\ reference}$$

Here $\Delta C_{t,sample}$ is the C_t value for the tested cell line normalised to the endogenous housekeeping gene (Beta-actin-ACTB), and $\Delta C_{t,\ reference}$ is the C_t value for the calibrator also normalised to the endogenous housekeeping gene.

For the $\Delta\Delta C_t$ calculation to be valid, the amplification efficiencies of the target and the endogenous reference must be approximately equal. This was established by observing how ΔC_t varied with template dilution[69]. Relative quantification RT-PCR was performed on all the PC cell lines, and GRP-R expression was compared with that from the calibrator (Figure 4.6).

[67] C_t (threshold cycle) - the intersection between an amplification curve and a threshold line. Chapter 2 - Section 2.3.8.3

[68] For 100% efficient PCR, doubling of product is obtained at every cycle, which is raised to the negative power of the $\Delta\Delta C_t$ in order to transform these $\Delta\Delta C_t$ values into a -fold change.

[69] Appendix VI

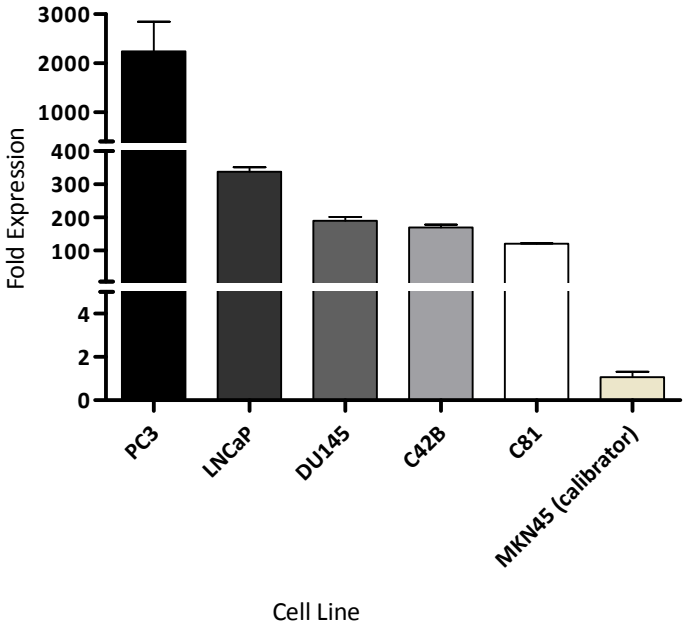

Figure 4.6: Quantitative RT-PCR for GRP-R expression over MKN45 (calibrator) in all prostate cancer cell lines. The expression level of MKN45 was set equal to 1. Values are the mean ± standard error for three separately performed studies (n=3).

All cell lines tested expressed GRP-R mRNA significantly more than MKN45. The highest-expressing cell line was PC3, which gave levels considerably greater than any other line. The remaining lines all expressed GRP-R within a four-fold difference among them. This experiment confirmed the expression of GRP-R in all the lines tested, especially in the androgen-independent PC3.

Further investigations were performed to elucidate the effects of androgens on the expression of GRP-R in cells by reducing the levels of androgens and growth factors in the growth medium, and to examine the effects of over-subculturing the cells on the expression of the receptor (Figure 4.7).

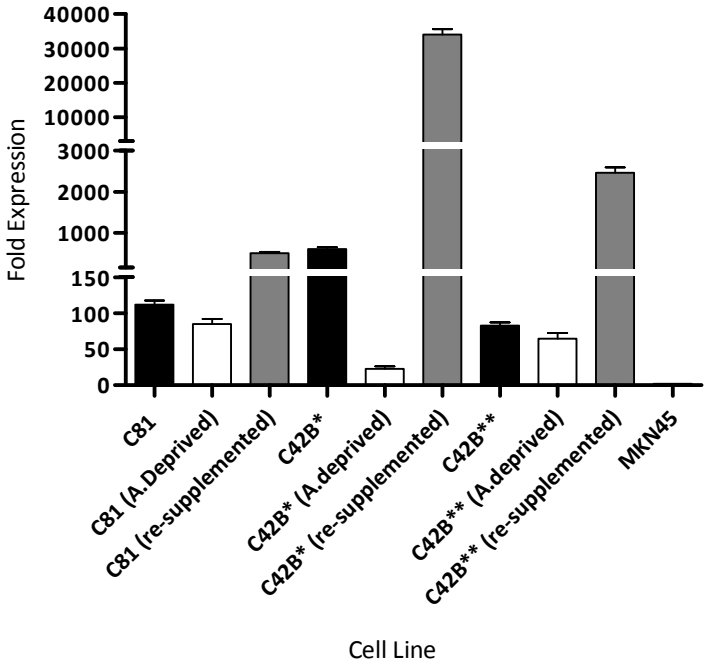

Figure 4.7: Quantitative RT-PCR on LNCaP lines grown under different conditions. The expression level of MKN45 was set equal to 1. *LNCaP C42B underwent <30 passages; **LNCaP C42B underwent >50 passages. A. deprived means androgen-deprived, ie. grown on reduced levels of androgen; Re-supplemented means growth in medium supplemented with androgen after androgen deprivation. Androgen-deprived medium was supplemented with 8% CS-FBS and 2% FBS, and was re-supplemented with 10% FBS. Values are the mean ± standard error for three separately performed studies (n=3).

Cells grown in 10% FBS were subcultured in 8% CS-FBS with 2% FBS[70], and back into 10% FBS, remaining in each growth medium for 1 week. Significant differences were seen in the level of GRP-R expression in cells cultured in the different types of medium, and between cells of high- and low-passage number. LNCaP C42B lines of high- and low-passage numbers both showed a reduction in expression after androgen deprivation, and over-expression of the target receptor once supplementation was restored. High-passage LNCaP C42B showed a smaller reduction than did the low-passage line, as seen in Figure 4.6, a relationship previously observed in the radioligand binding assay[71] whereby low-passage LNCaP C42B revealed a higher receptor density (B_{max} = 101 fmol/mg protein) compared with high-passage LNCaP C42B (B_{max} = 47.1 fmol/mg protein). A considerably increased level of expression of GRP-R was observed in all three cell lines after re-

[70] The use of CS-FBS alone caused cells to die, probably because essential growth nutrients were withheld, therefore an 80:20 mix of CS-FBS and FBS was used.
[71] Chapter 2 - Section 2.3.4

supplementation of the standard FBS, indicating a physiological change within the cells which caused an up-regulation of GRP-R expression.

4.2.2.3 GRP-R Expression by FACS

GRP-R expression *in vitro* was examined by FACS analysis using the commercially-available rabbit-polyclonal anti-gastrin-releasing peptide receptor antibodies (Novus Biologicals NB100-74434 and Abcam Ab39963) on all the prostate cancer cell lines. Varying concentrations (10, 5, 2.5, 1 and 0.1 μg of GRP-R/mL) were evaluated. No binding with either was observed with any of the cell lines.

Cells were detached from tissue culture flasks with Versene instead of 0.25% (w/v) Trypsin / 0.53 mM EDTA solution to reduce any possibility of cleaving the receptor during the detachment process. Neither antibody was recommended for FACS and it was concluded that they were unsuitable for this purpose.

4.2.3 *EX VIVO* STUDIES

4.2.3.1 Autoradiography Optimisation Study with ^{99m}Tc

The methodology for autoradiography used throughout this thesis was developed and refined using ^{99m}Tc-DB 4[72]. Radiolabelling components, technique and phosphor imager screens were all standardised or calibrated in order to optimise procedures.

The radiolabel content of tissue samples was quantified using phosphor screens, which store energy in photostimulable crystals. There are several types of screen available, ranging in sensitivity. Sensitivities to ^{99m}Tc of the super resolution screens (formulated from fine-grain crystals) and the durable multipurpose screen were measured and calibrated.

[72] Chapter 1 - Section 1.9.8

To determine the comparative responses of these screens, twelve 5-µL spots of serially-diluted samples of the isotope were spotted onto a glass cover slip. Each type of screen was exposed to the source for 30 min and scanned in a Cyclone Plus Phosphor Imager at 600 dpi resolution. Quantification of the responses was performed using OptiQuant software, which recorded the readings in terms of digital light units (DLU)[73]. Identical elliptical regions were drawn around each spot of radioactivity, and a series of identically-sized regions were similarly circumscribed in background areas; the measurements from these were subtracted from those of the standards. In parallel, duplicate spots of the serial dilutions were measured in a gamma counter to quantify these standards in terms of CPM.

The radioactivity (CPM) was plotted against the phosphor-imager output (DLU) (Figure 4.8). This relationship was linear, therefore the slope of the line was used as the conversion factor from DLU to MBq.

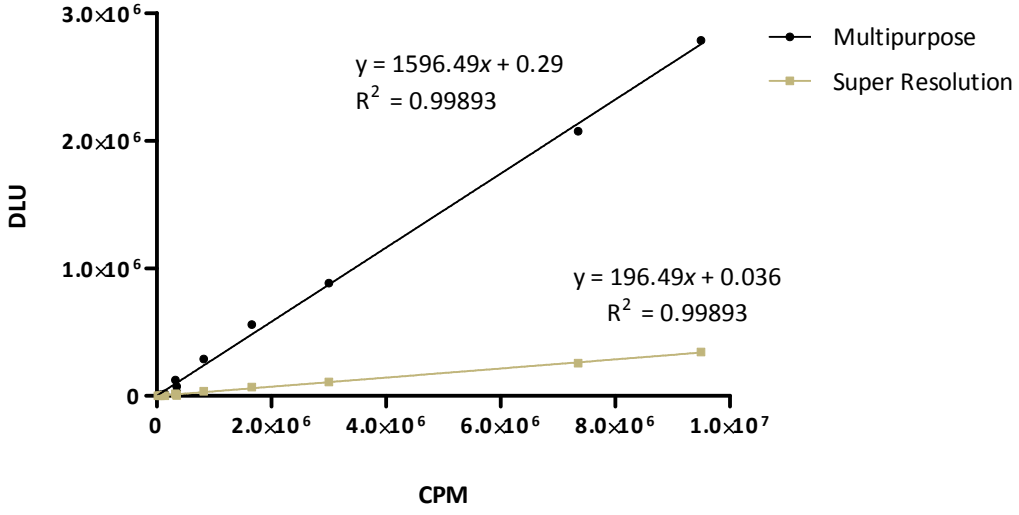

Figure 4.8: Correlation of DLU values and CPM readings as recorded using the multipurpose and super resolution screens after 30 min exposure to various quantities of ^{99m}Tc.

[73] A measure of luminosity

Sections of tumour xenografts which had been incubated with ^{99m}Tc-DB 4 (see Section 2.3.7) were then exposed to the phosphor imaging plates using the same experimental conditions. However, poor results were obtained, as shown in Figure 4.9, because of insufficient contrast between sample and background. In order to overcome this problem and increase the level of specific binding, the effects of increasing exposure times and radioactivity levels on the calibration were studied. The results are shown in Figure 4.10. It can be seen that the linear relationship between radioactivity and the DLU generated was lost, and that the plates became saturated under these conditions.

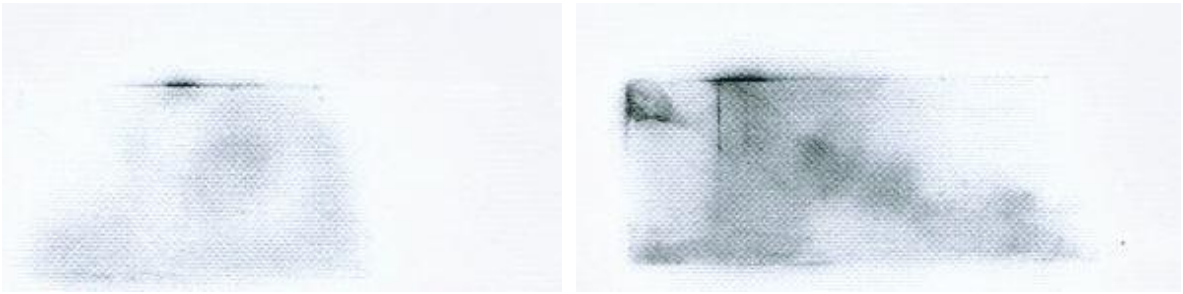

With competitor Without competitor

Figure 4.9: Autoradiography performed on PC3 tumour sections using ^{99m}Tc-DB 4 with and without the addition of the competitor, unlabelled DB 4, showing the impossibility of successfully orientating the location of tumour sections mounted on the glass slide.

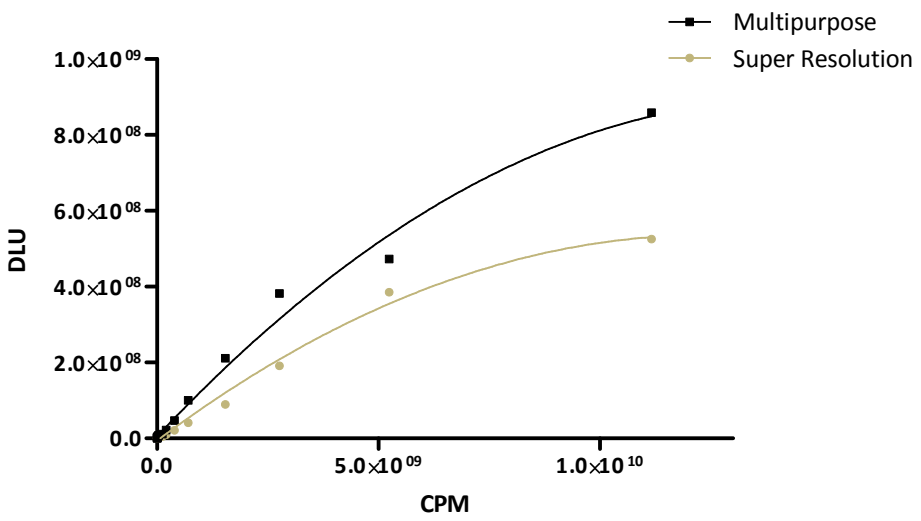

Figure 4.10: Overnight exposure (10 hours) of multipurpose and super-resolution screens to ^{99m}Tc. Binomial regression was plotted for each screen. For the mulipurpose screen, R^2 = 0.9892; for the super resolution screen, R^2 = 0.9927.

Autoradiographic analysis using radionuclides with short half-lives is difficult because their rapid decay restricts sensitivity unless very high activities are used, which in turn gives rise to the problems shown. Long exposure times heighten the contrast between sample and background, but over-exposure reduces sensitivity. For this reason, the use of sodium [^{125}I]-iodide as a radiolabel was explored because longer exposure times to tumour sections could potentially be achieved with lower levels of radioactivity, due to its longer half-life (60 days).

4.2.3.2 Autoradiography Optimisation Study with [^{125}I]-Bombesin Analogue [[^{125}I]-D-Tyr^{6}, β-Ala^{11}, Phe^{13}, Nle^{14}-Bombesin

Optimisation with two screens were therefore performed using a commercially available [^{125}I]-D-Tyr^{6}, β-Ala^{11}, Phe^{13}, Nle^{14}-Bombesin. Exposure times of 24 and 48 h were tested (Figure 4.11).

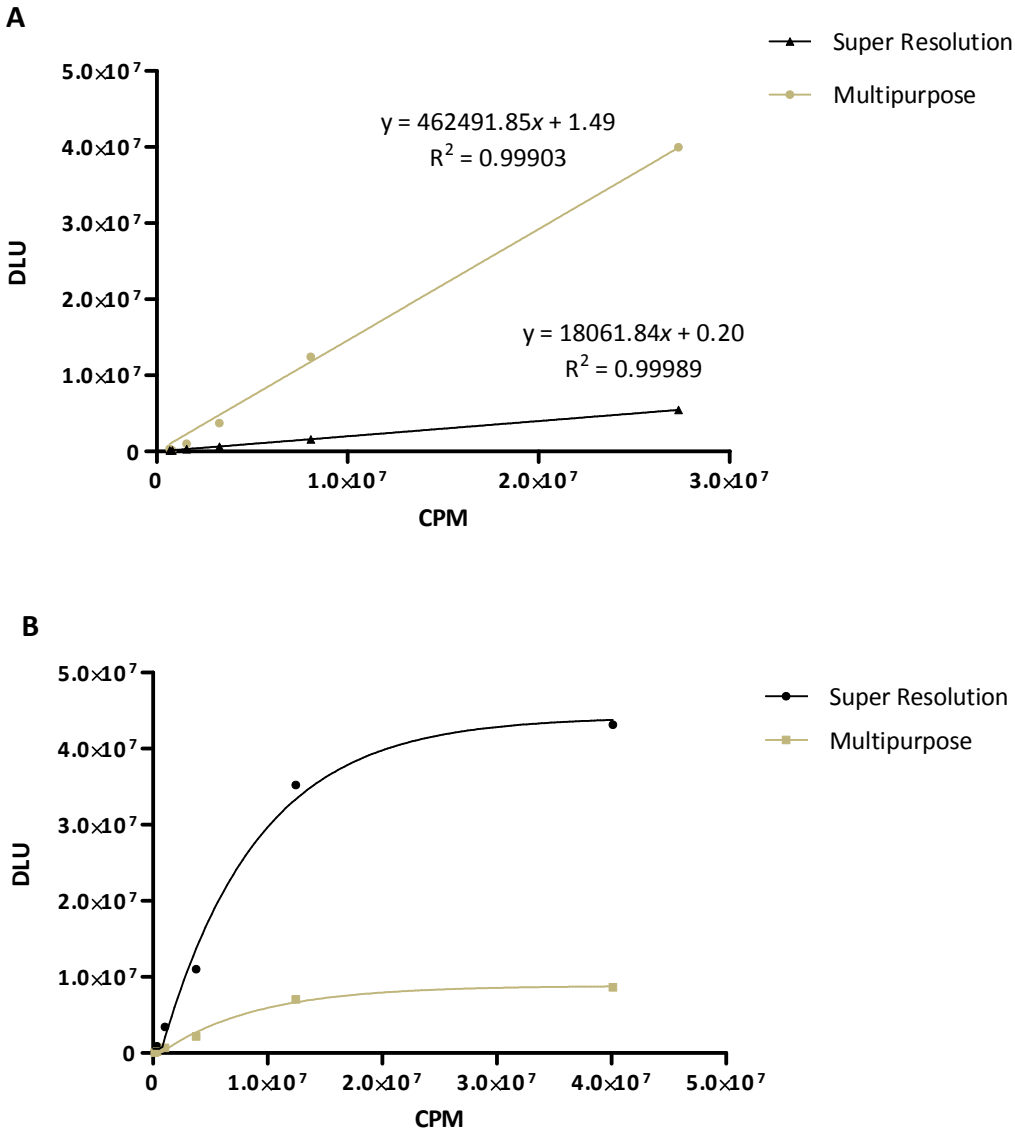

Figure 4.11: (A) 24 h exposure and (B) 48 h exposure to [^{125}I]-Bombesin Analogue [[^{125}I]-D-Tyr^{6}, β-Ala^{11}, Phe^{13}, Nle^{14}-Bombesin of the multipurpose and super resolution screens.

As with ^{99m}Tc, the multipurpose screen showed greater sensitivity than the super resolution screen. Exposure times longer than 24 hours saw saturation of the phosphor imager screens (B), whereas exposure for 24 hours maintained a linear relationship (A). The multipurpose screens were therefore used in subsequent autoradiographic studies, with a maximum exposure of 24 h.

Sample preparations of all prostate cancer tumours, as well as a non-GRP receptor-expressing tumour were incubated with [^{125}I]-Bombesin Analogue [[^{125}I]-D-Tyr^{6}, β-Ala^{11}, Phe^{13}, Nle^{14}-Bombesin in the absence and presence of an excess of the competitor, 1000 μM-unlabelled DB 4, for 1 h. Unbound and non-specifically bound radioligand was removed by wash steps prior to exposing samples to the multipurpose phosphor imager screen for 24 h (Figure 4.12).

With competitor Without competitor

Figure 4.12: Example of autoradiography on PC3 tumour sections using [^{125}I]-D-Tyr^{6}, β-Ala^{11}, Phe^{13}, Nle^{14}-BB, with and without competitor, unlabelled DB 4. Regions of interest were drawn around the tumour sections and DLU obtained.

Compared with ^{99m}Tc-DB 4, autoradiography performed with [^{125}I]-D-Tyr^{6}, β-Ala^{11}, Phe^{13}, Nle^{14}-BB showed improved binding and contrast between sample and background, as shown in Figure 4.12. Autoradiography was therefore performed on the other excised tumours to see whether the binding observed correlated with the binding seen both *in vitro* and *in vivo*.

Slides directly cut one after the other were used to prepare a series of sections as similar as possible to each other. Serial dilutions of the stock radioligand were used as standards, spotted onto a glass slide and placed side-by-side with the tumour sections, which were then autoradiographed together. Duplicate dilutions of the standard were also measured on the gamma counter to obtain CPM values. Prior to exposing to screens, slides and standards were dried completely to minimise contamination.

Specific binding was determined by subtracting the non-specific binding (measured in the presence of the competitor) from the total binding (measured without competitor) (Figure 4.13). The following equation was used to calculate the percentage of [^{125}I]-Bombesin Analogue [[^{125}I]-D-Tyr^{6}, β-Ala^{11}, Phe^{13}, Nle^{14}-Bombesin specifically bound:

$$\frac{x-y}{x}\times 100$$

Where *x* is the total bound (without competitor) and *y* is the amount bound non-specifically (with competitor).

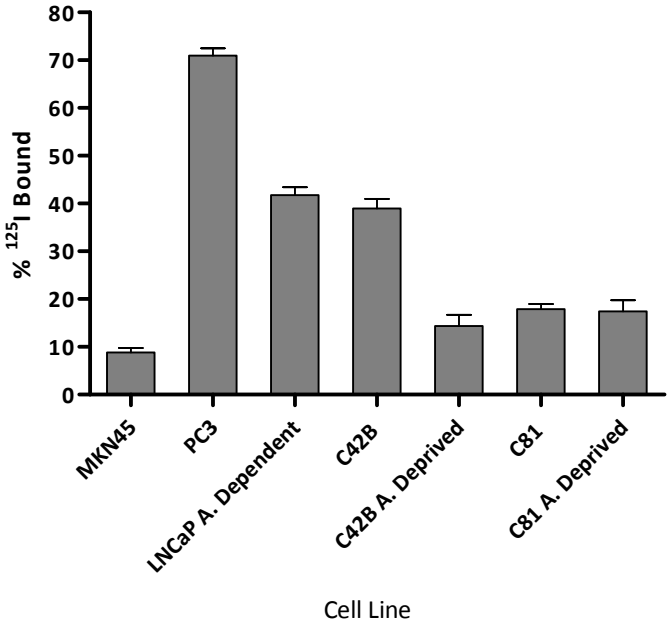

Figure 4.13: Autoradiographic studies performed tumours derived from a range of prostate cancer cell lines, varying in stages of development. MKN45 is a negative (non-expressing) GRP-R cell line. A. Deprived means androgen-deprived, ie. grown on reduced levels of androgen. Values are the mean ± standard error for three separately performed autoradiography studies (n=3).

Among the cell lines, PC3 tumours yielded the highest GRP-R expression, followed by those from LNCaP androgen-dependent and LNCaP C42B.

LNCaP C42B and C81 cells grown in reduced levels of androgen[74] were also subjected to autoradiography. Cells injected into male, non-castrated mice took substantially longer to establish tumours, compared with their parent cell line grown in regular FBS medium, but were of course exposed to circulating androgens once within the body. This experiment was performed to see whether the results would concur with those obtained *in vitro*, where a difference in GRP-R expression was observed. There was a definite decrease in expression of GRP-R in LNCaP C42B, but no significant difference between LNCaP C81 and LNCaP C81 androgen-deprived cells was detected.

4.2.3.3 Immunohistochemistry

Prior to the analysis of GRP-R expression by immunohistochemistry, optimisation of the use of the commercial antibody rabbit polyclonal anti-GRP-R (Abcam 39963) was performed. Human pancreatic tissue, donated by Pathology Services, Institute of Cancer, Queen Mary, University of London, was used as the positive GRP-R-expressing tissue, and a range of anti-GPR-R antibody concentrations was tested to select for the optimal concentration (Figure 4.14).

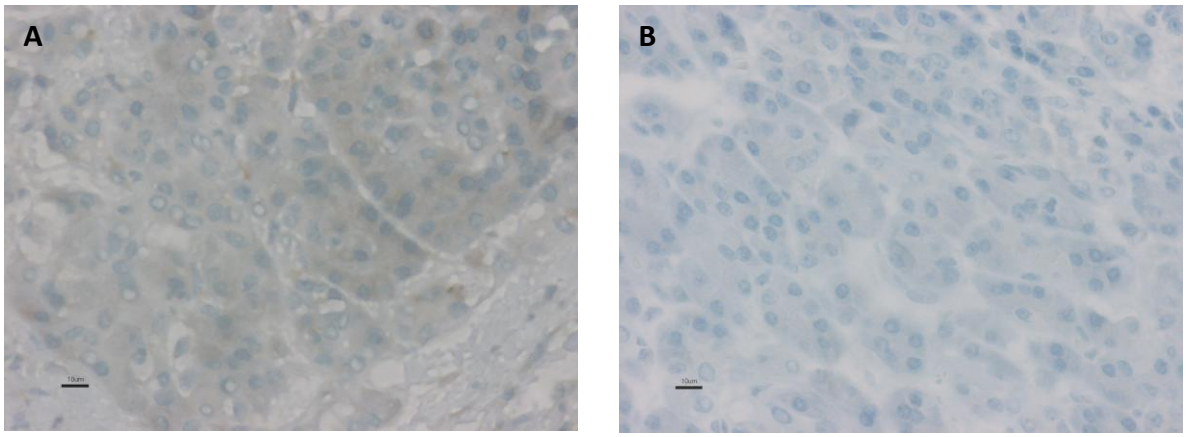

Figure 4.14: Optimisation study performed on human pancreatic tissue. (A) Stained in the presence of a 1:100 dilution of anti-GRP-R antibody; (B) without primary antibody. Slides were imaged under a light microscope at x40 magnification. Bar = 1 µm.

[74] Chapter 2 - Section 2.3.3

Weak positive staining for GRP-R expression was seen as indicated in Figure 4.14 (A), where the chromogenic substrate stained the antigen-antibody interactions brown throughout the tissue section, indicating antibody binding. Little or no non-specific binding occurred in the tissue stained without primary antibody [Figure 4.14 (B)]. A 1:100 dilution was selected as the optimum antibody concentration from a range of concentrations tested [1:10, 1:30, 1:50, 1:500, 1:1000 and 1:10,000]. Tumour sections of all the PC cell lines were then stained for GRP-R expression (Figure 4.15 and Figure 4.17).

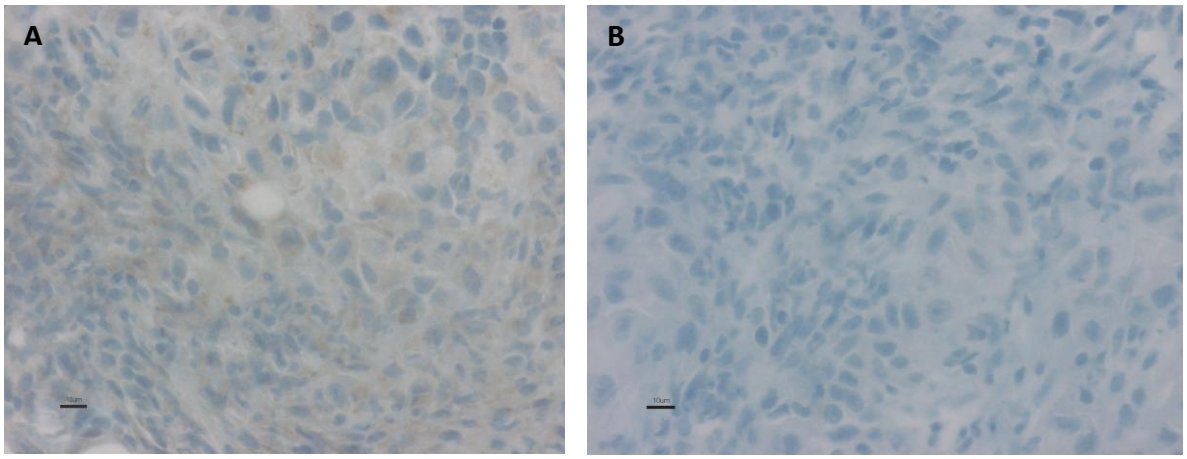

Figure 4.15: PC3 tumour sections stained (A) with and (B) without anti-GRP-R antibody. Slides were imaged under a light microscope at x40 magnification. Bar = 1 µm.

Results obtained with PC3 revealed a similar level of weak staining for GRP-R expression, with a distribution of the chromogenic substrate similar to that seen in human pancreas. Without primary antibody (Figure 4.15 B), there was little or no staining, confirming that binding was due to the primary antibody (Figure 4.15 A). However, in addition to staining of the tumour, staining also occurred in skeletal muscle, which does not express GRP-R, therefore indicating non-specific binding (Figure 4.16).

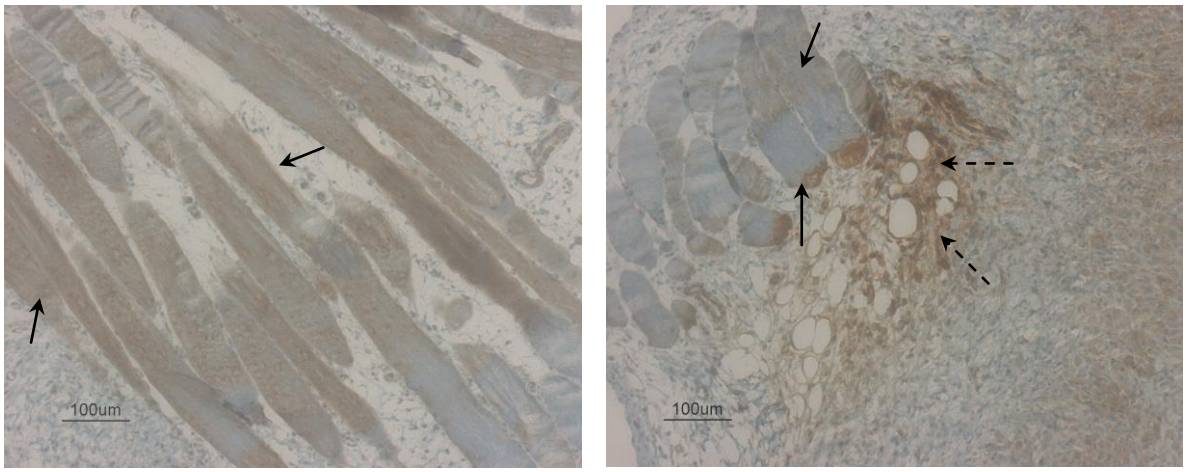

Figure 4.16: Different areas within a section of PC3 tumour. Non-specific staining of skeletal muscle is seen in the finger-like projections (arrowed) which were not GRP-R positive. Dashed arrows indicate tumour tissue. Faint staining on blood vessels was also observed (not shown). Slides at x 40 magnification.

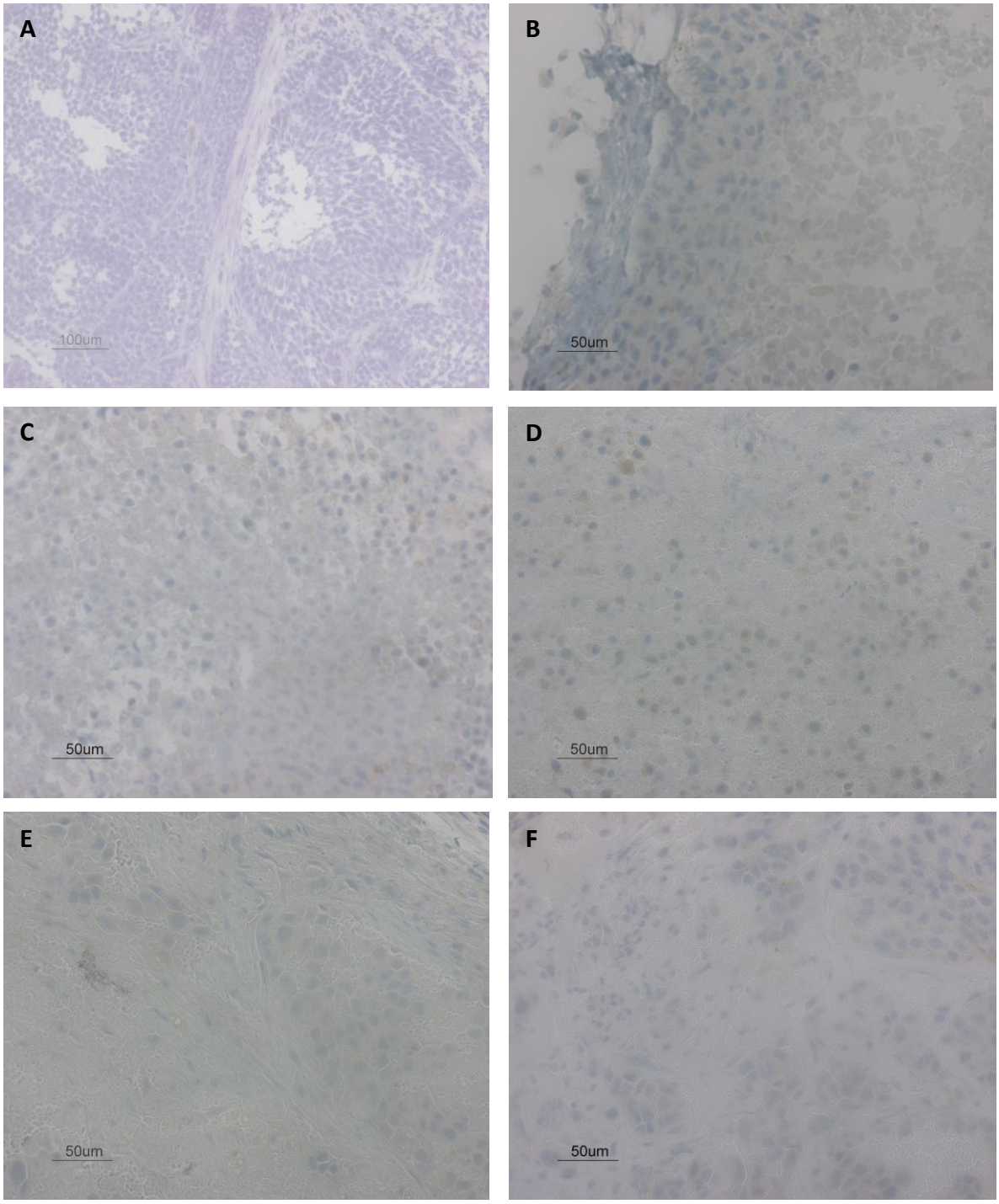

Figure 4.17: Immunohistochemistry performed on all the remaining cell lines to investigate GRP-R expression. (A) - MKN45 (GRP-R-negative cell line), (B) - LNCaP androgen-dependent, (C) LNCaP C42B (androgen-deprived), (D) - LNCaP C81 (androgen-deprived), (E) - LNCaP C42B (androgen-independent) and (F) - LNCaP C81 (androgen-independent). Slides at x20 magnification.

No significant staining was observed in the other tumour lines, although compared with the negative cell line, MKN45, there was some minimal brown, granular cytoplasmic staining, which was generally neither convincing nor significant, especially in comparison with the high degree of non-specific binding observed in the PC3 tumour sections.

4.2.4 *IN VIVO* STUDIES

4.2.4.1 Radiolabelling and ^{99m}Tc - Quality Control Analysis

ITLC

After radiolabelling, it is important to ascertain the percentage of radiolabelled peptide, free pertechnetate and ^{99m}Tc by-products. For quality control purposes, labelling efficiency was measured using both ITLC and HPLC.

Using acetone as the mobile phase, unreduced and free pertechnetate, which migrated with the solvent front, was resolved by ITLC from other radiolabelled components, including unwanted by-products, which remained at the origin. Acetone, however, was unable to resolve further the radiolabelled components; these were separated using methanol : 1 M ammonium acetate as the mobile phase. Here ^{99m}Tc-colloids remained at the origin while the radiolabelled peptide and unreduced pertechnetate travelled up the strip.

Figure 4.18 shows an example of ITLC analysis of [^{99m}Tc]-DB 4 after the labelling procedure, together with data obtained from the phosphor imager. Data acquired was subtracted from background readings, and analysis performed by OptiQuant enabled the percentage of radiolabelled DB 4 to be calculated.

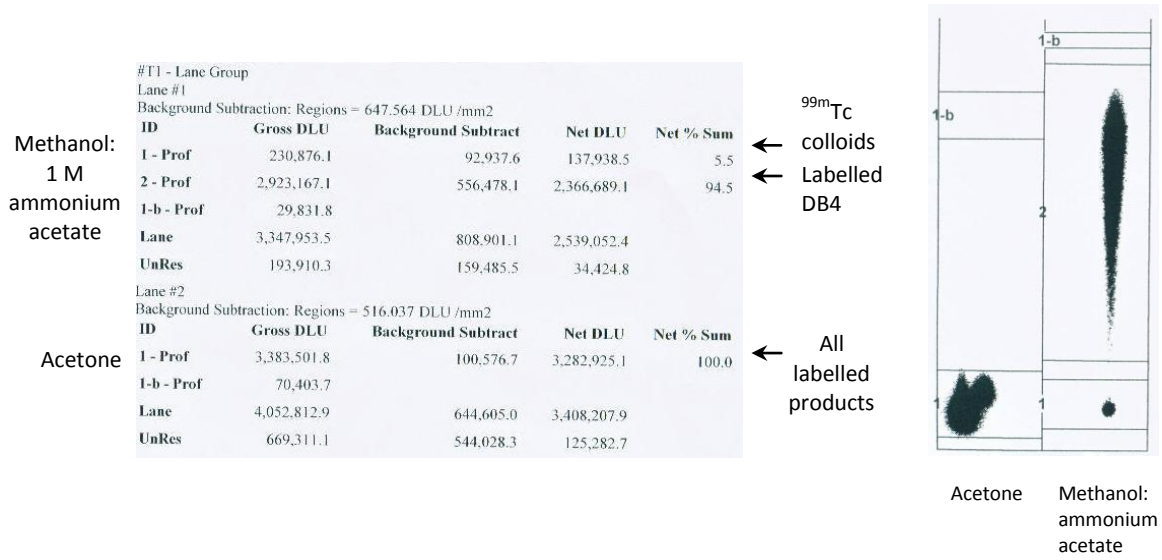

Figure 4.18: Analysis of the radiolabelled product using ITLC-SG strips run in acetone and methanol: 1 M ammonium acetate.

The quality of this sample was particularly good; no free pertechnetate was present in the radiolabelling mixture. In Table 4.2, ITLC results obtained from a representative selection of other radiolabeling procedures demonstrate the stability of the product and the reproducibility of the labelling procedure.

Table 4.2: ITLC analysis from a number of quality control procedures performed after radiolabelling. Data were obtained by exposure of ITLC-SG strips to phosphor imager screens for 30 s.

ITLC Analysis	% Free Pertechnetate	% ^{99m}Tc-Colloids	% ^{99m}Tc-DB 4
1	0	5	95
2	2	4	94
3	0	4	96
4	1	6	93
5	2	7	91
6	0	2	98
7	0	8	92
8	3	3	94
9	2	5	93
10	0	4	96

To further confirm results obtained by ITLC, reverse-phase HPLC was run in parallel. The HPLC chromatogram in Figure 4.19 shows a successful labelling procedure, in which one clean, sharp peak of ^{99m}Tc-DB 4 has eluted at approximately 21 min, and no additional peaks of free or unreduced pertechnetate have appeared near the solvent front. The absence of peaks eluting before or after 21 min indicate that the peptide has not undergone complexation or dissociation.

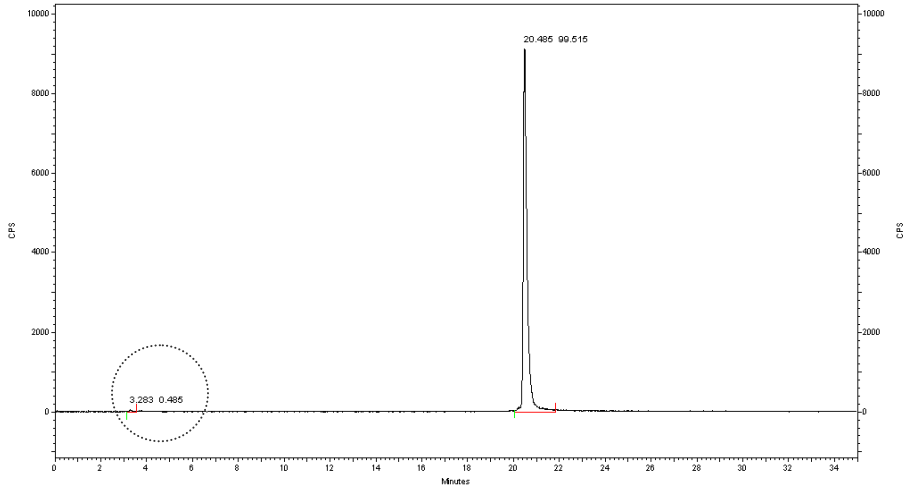

Figure 4.19: HPLC chromatogram of radiolabelled DB 4. [^{99m}Tc-DB 4] eluted from the column in the region of 21 min. Circled section indicates the position of unbound pertechnetate. This chromatogram indicates excellent labelling with >99% labelling efficiency.

The circled region on the graph indicates where unwanted soluble impurities such as unreduced pertechnetate would elute. It is essential that significant amounts of free pertechnetate are not present in the preparation, to optimise the targeting of the radionuclide. As with ITLC analysis, HPLC analysis showed that the reproducibility of the radiolabelling procedure was good (Table 4.3).

Table 4.3: HPLC analysis of a number of chromatograms performed after the radiolabelling procedure.

HPLC Chromatograms	% ^{99m}Tc-DB 4	Soluble impurities
1	99.5	0.5
2	99.4	0.6
3	100.0	0
4	100.0	0
5	100.0	0
6	98.0	2.0
7	99.5	0.5
8	99.0	1.0
9	99.3	0.7
10	99.5	0.5

4.2.4.2 Biodistribution Studies on PC3 Tumour-Bearing Mice

In vivo analysis was performed on all the cell lines tested to see whether the relationships and specific binding observed *in vitro* were replicated *in vivo*. Groups of tumour-bearing mice were therefore tested to examine the distribution, specific uptake and clearance of ^{99m}Tc-DB 4.

For *in vivo* analysis, mice were injected subcutaneously on both hind-leg flanks with 10 million cancer cells, in the right flank with cells alone, and in the left flank with cells mixed in a 1:1 ratio by volume with Matrigel, which was used to promote tumour growth. With certain cell lines, tumour formation was particularly difficult to achieve; PC3 and AR42J were faster growing cell lines (approximately 2 weeks) LNCaP cells alone took approximately 8 weeks and androgen deprived up to 12 weeks.

Initially biodistribution studies were performed in mice bearing PC3 tumours at three time points; 1, 2.5 and 4 hours post injection. These time points were thought to provide a sufficient window of observation as to how the radiotracer was behaving within the mouse. Groups of 3-4 mice were used per time point, since it is important to note that there is a degree of variability when using these biological models.

At each time point, mice were culled, and organs and tissue were excised and collected into pre-weighed scintillation tubes to be measured on the gamma counter. The counts obtained were then used to calculate the uptake of radioactivity per g of tissue (% ID/g) (Figure 4.20).

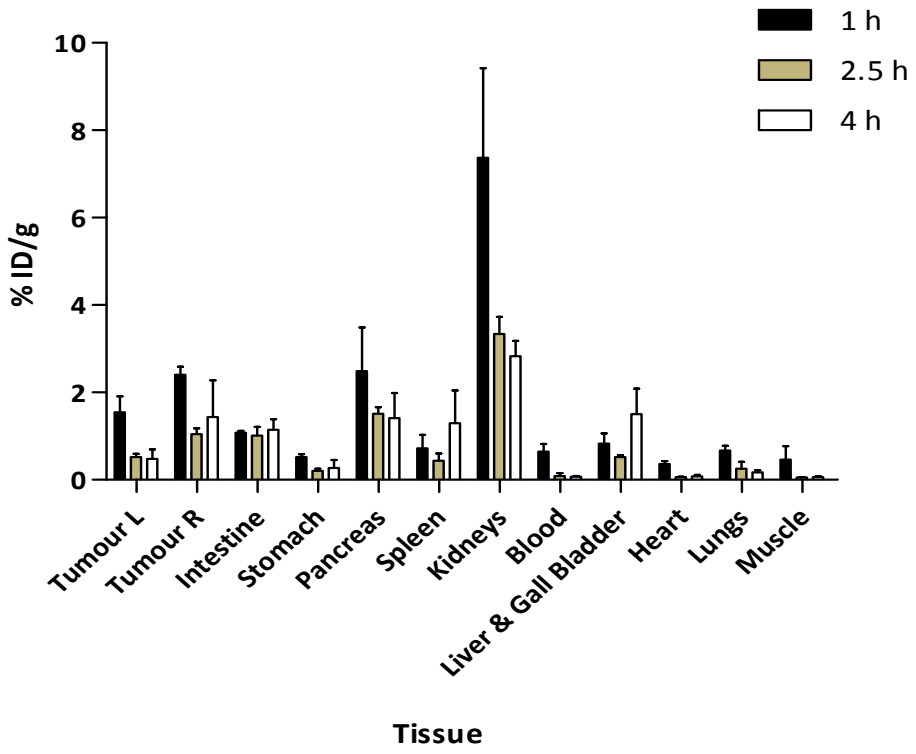

Figure 4.20: Biodistribution of [^{99m}Tc]-DB 4 in PC3 tumour-bearing mice. The average amount of radiotracer measured in three mice, per time point, is shown with standard deviations. % ID/g = % uptake of injected dose per g of tissue. Left tumour - with Matrigel, right tumour without Matrigel.

Relatively high uptake was seen in those tissues with known GRP-R expression, in particular tumour, intestine and pancreas. Increased binding was observed in the right tumour (no Matrigel) over the left tumour (with Matrigel). Growth rates in the flanks differed significantly with time, with the left flank showing palpable tumours before the right, due to the addition of Matrigel. At times the mice were left an additional day or two for the tumour to form in the right flank, therefore it is probable that the higher binding observed is due to the right tumour still being within the exponential growth phase and

cellular metabolism being more active than in the left tumour. Lower levels of uptake were seen in receptor-negative tissue such as heart, lungs and muscle. The highest uptake was observed in the kidney, which provides the major excretory route for this hydrophilic radiopharmaceutical. A decrease in uptake was seen in all tissues between 1 h and 2.5 h, with little change thereafter.

4.2.4.3 Blocking Study

To determine whether the uptake in GRP-R positive tissue observed was specific and not as a result of non-specific binding or hydrophobic interactions, a blocking study was performed.

PC3 tumour-bearing mice were split into two groups of four. One group was injected with ^{99m}Tc-DB 4, and the second with ^{99m}Tc-DB 4 in the presence of excess competitor, unlabelled DB 4, at 10 µg per mouse, sufficient to bind and occupy/block all the GRP receptors. Mice were culled at 4 h post injection, and organs were excised for biodistribution analysis (Figure 4.21).

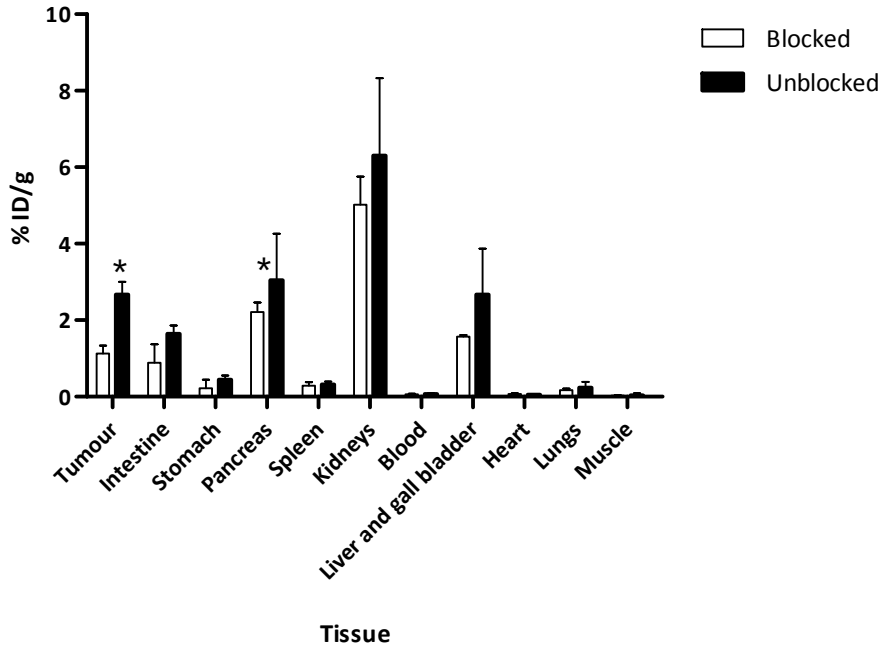

Figure 4.21: Biodistribution analysis of the blocking study, 4 h post injection. % ID/g = % uptake of injected dose per g of tissue. * t-test showed no significant difference between blocked and unblocked samples for all tissues, apart from the tumour and pancreas, which showed a significant difference (P >0.05).

A reduction in binding was observed within the GRP-R-expressing tissues viz. tumours, intestine and pancreas. The percentage differences between the blocked and unblocked tissues were respectively 58, 46 and 28%, however t-test analysis showed the difference to be statistically significant only in tumour and pancreas. Bombesin-binding sites have been identified throughout the small and large intestine [120]. Smaller differences were seen between the groups in any of the other tissues examined, indicating low levels of specific binding in them. Some reduction was seen in kidney uptake but the level of uptake varied greatly in this organ, perhaps as a result of differing rates of excretion between the animals. This experiment confirmed that a significant proportion of uptake initially observed with PC3 tumours was indeed due to specific binding to expressed GRP-R but also that a significant level of non-specific uptake also occurred.

4.2.4.4 Biodistribution Studies on Other Cell Lines

Biodistribution studies were also performed with the remaining PC cell lines to assess the uptake of ^{99m}Tc-DB 4[75] by these tumours. Uptake seen in tumours was compared with that in non-expressing tissue (muscle) and also clearance via kidneys (Table 4.4).

Table 4.4: Biodistribution studies on prostate cancer cell lines. *AR42J is the rat neuroendocrine cell line.

Tissue	Time (h)	Ar42J*	PC3	LNCaP Androgen-dependent	LNCaP C81	LNCaP C81 (androgen-deprived)	LNCaP C42B	LNCaP C42B (androgen-deprived)
		% ID/g ± SD						
Tumour	1	1.89 ± 0.56	1.55 ± 0.36	1.98 ± 1.16	0.86 ± 0.33	2.16 ± 0.48	0.78 ± 0.49	0.41 ± 0.17
	2.5	1.31 ± 0.44	0.52 ± 0.08	2.41 ± 0.39	0.75 ± 0.36	1.72 ± 1.03	0.62 ± 0.66	0.14 ± 0.12
	4	1.88 ± 0.47	0.48 ± 0.22	1.35 ± 0.58	1.02 ± 0.36	0.36 ± 0.04	0.43 ± 0.16	0.44 ± 0.52
Kidney	1	13.58 ± 1.44	7.37 ± 2.05	16.92 ± 1.44	11.11 ± 3.12	8.46 ± 2.47	3.82 ± 1.89	5.87 ± 2.51
	2.5	8.53 ± 0.50	3.34 ± 0.39	10.10 ± 3.22	7.77 ± 2.48	8.10 ± 4.55	5.10 ± 1.50	1.67 ± 1.27
	4	9.65 ± 2.74	2.83 ± 0.35	3.96 ± 1.32	4.43 ± 1.12	3.42 ± 0.67	5.11 ± 0.37	6.42 ± 3.70
Muscle	1	0.11 ± 0.03	0.46 ± 0.31	0.22 ± 0.04	0.19 ± 0.10	0.29 ± 0.15	0.09 ± 0.01	0.07 ± 0.02
	2.5	0.16 ± 0.12	0.05 ± 0.01	0.12 ± 0.02	0.14 ± 0.04	0.21 ± 0.06	0.13 ± 0.09	0.01 ± 0.00
	4	0.08 ± 0.04	0.06 ± 0.02	0.02 ± 0.01	0.11 ± 0.04	0.06 ± 0.05	0.03 ± 0.01	0.23 ± 0.38

Tumour uptake and specific binding was observed in the majority of the cell lines tested, but minimal or no significant binding was observed in both LNCaP C81 and C42B. The greatest level of uptake was observed by the androgen-dependent LNCaP line which, like the positive control AR42J, showed uptake at just under 2%, which was retained for up to 4 h post injection. PC3 tumours also showed a high uptake, and interestingly, specific binding was increased in androgen-deprived LNCaP C81, but not androgen-deprived C42B (Figure 4.31 on page 210). Uptake levels in the PC tumour cell lines were variable but were

[75] Appendix VII

always significantly greater than in muscle. In general, uptake declined with time, but not always.

4.2.4.5 Imaging with ^{99m}Tc-DB 4 in all Prostate Cancer Cell Lines

As well as biodistribution studies, mice were also imaged using a Nano SPECT/CT scanner.

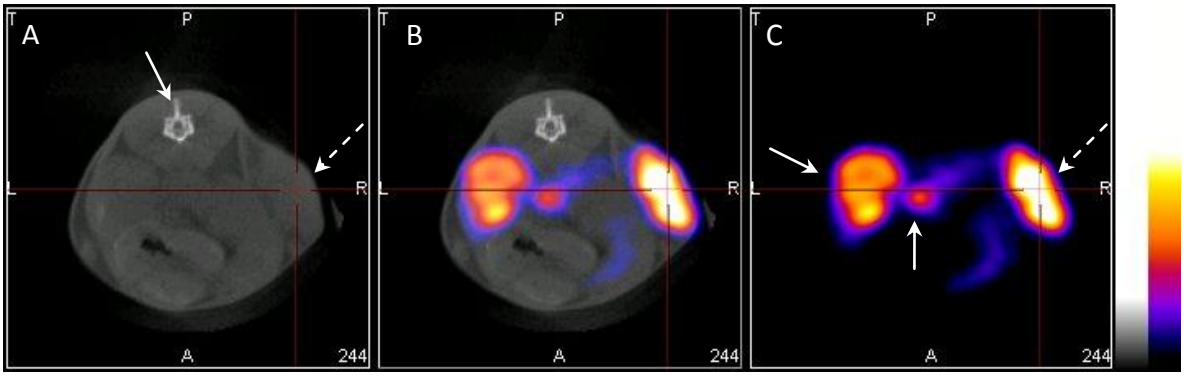

CT CT & SPECT Combined SPECT

Figure 4.22: Transverse images of a PC3 tumour-bearing mouse. (A) CT image - arrow shows the dense vertebra, indicating the back of the mouse. Dashed arrow indicates the right PC3 tumour. (B) Combined CT and SPECT images. (C) SPECT image alone - arrows indicate the left kidney (larger area) and intestine (smaller area) uptake. Dashed arrow indicates the right PC3 tumour.

CT imaging facilitates the location and orientation of the tumour [Figure 4.22 (A)]: as the cancer cells were injected subcutaneously, tumour formation occurred just beneath the skin, and a solid mass was easily identified in the CT image, which could be overlaid on the SPECT image, ensuring that the activity measured was due to uptake by the tumour, and not other adjacent tissues (Figure 4.22 B & C). Although activity was observable in the SPECT image alone, without the CT image it was difficult to orientate and attribute the uptake.

4.2.4.5.1 Dynamic Acquisition

Dynamic acquisition was performed on an AR42J tumour-bearing mouse. [^{99m}Tc]-DB 4 was injected intravenously into a mouse, which was scanned continuously by the Nano SPECT/CT over the next hour to allow visualisation of the distribution, clearance, and specific and non-specific binding of the radiopharmaceutical (Figure 4.23). Dynamic

acquisition showed the total spread of the radiopharmaceutical throughout the body and a rapid clearance from the blood and receptor negative tissues. High levels of uptake were seen in the kidneys and bladder, due to the hydrophilic nature of the peptide and its rapid renal clearance. Heterogeneous uptake was observed in the tumour tissue.

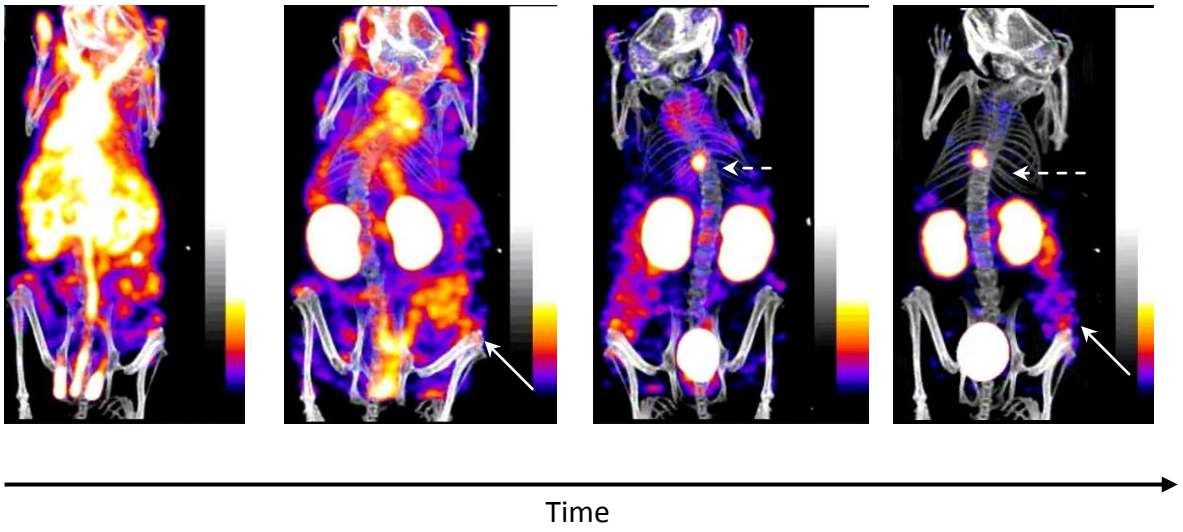

Figure 4.23: Dynamic acquisition of an AR42J tumour-bearing mouse, injected with [^{99m}Tc]-DB 4 and scanned continuously for 1 hour. White arrow indicates tumour, dashed arrow, indicates gall bladder.

4.2.4.5.2 Static Imaging

Static images of the mice were acquired 1, 2.5 and 4 h after injection of [^{99m}Tc]-DB 4. High levels of activity were observed in the ventral body cavity in the mice at all time points, mainly due to clearance via the kidneys and the bladder, as well as some uptake in the intestines, but this activity diminished over time as the radiotracer was excreted (Figure 4.24). Uptake was seen in the gall bladder of earlier time points, suggesting a small proportion cleared via the liver.

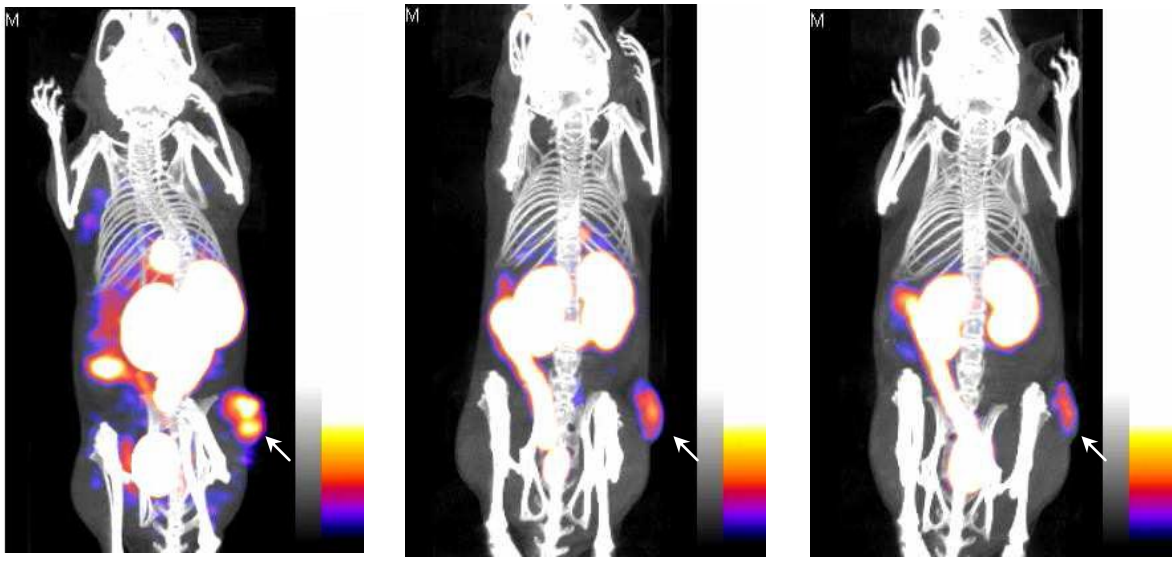

1 h 2.5 h 4 h

Figure 4.24: Coronal images of PC3 tumour-bearing mouse no. 1 of three imaged over the three time points. Uptake and clearance by the various organs and tissues was observed. Arrows indicate the PC3 tumour on the right flank. Images were scaled the same to allow for direct comparison.

Heterogeneous specific binding (not a uniform distribution of uptake) was observed in the right tumour, with several small 'hot spots', which were retained there in excess of 4 h. No obvious sites of necrosis, which would appear as black non-specific regions in the centres of tumours, were observed. Imaging data was obtained for all PC cell lines, at all the time points tested[76]. Uptake also occurred into the left tumour, but a lesser extent than the right.

4.2.4.5.3 Quantification

From SPECT data, it is possible to obtain quantitative as well as qualitative information. Using the SPECT-analysis programme, In Vivo Scope™, elliptical regions of interest (ROIs) were manually drawn around target tissue from imaged mice. Tumours on both the left and right flank were measured as well as the kidneys for all three time points (1, 2.5 and 4 h) post injection (Figure 4.25).

[76] Appendix VI

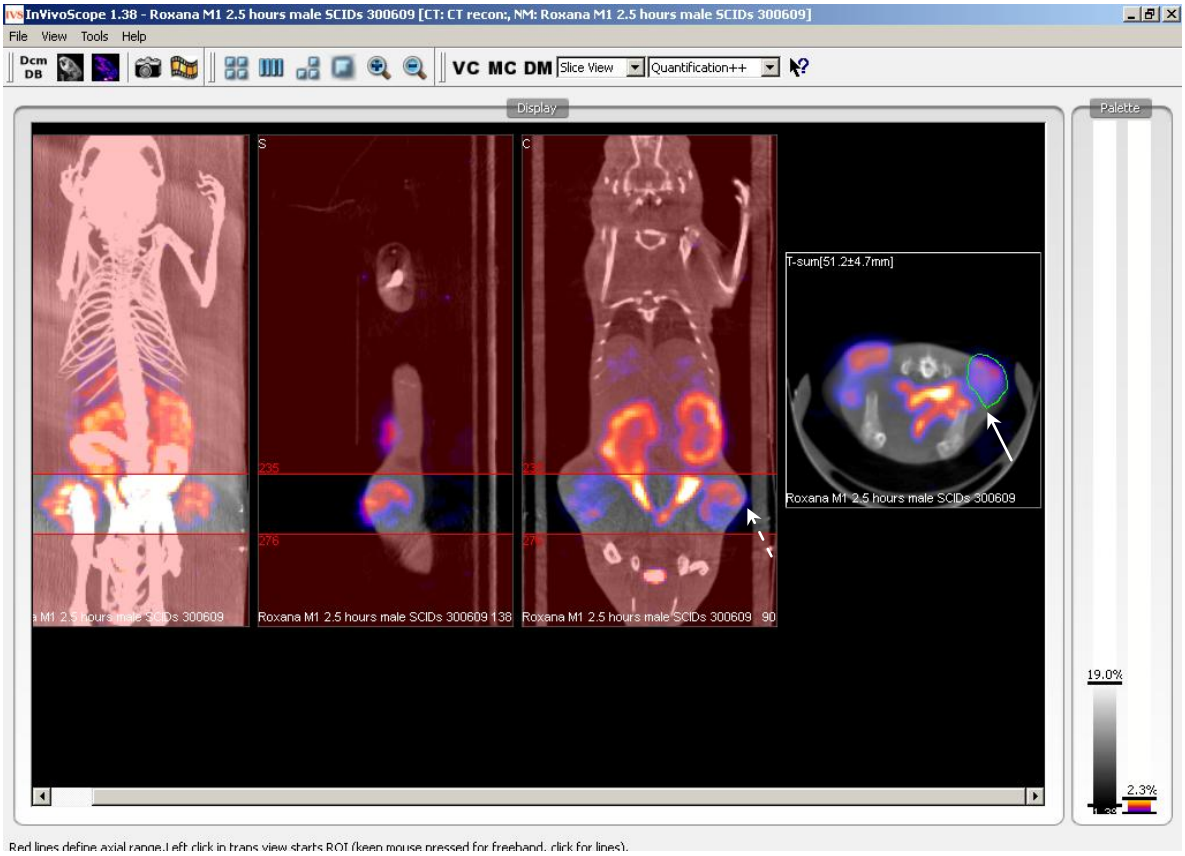

Figure 4.25: Example of the acquisition of quantification data, using the In Vivo Scope™ SPECT-analysis programme. White dashed arrow - indicating the tissue of interest (right tumour). White arrow - highlighting the ROI (green) which was manually drawn around the tumour.

The ROI was manually drawn around the tumour or kidney in the transverse section, although all views were used to locate the tissue of interest. Data obtained from the ROIs drawn was expressed in terms of MBq/mm^3, and the percentage of the injected dose in the total ROI was calculated by dividing this by the total radioactivity injected. The uptake obtained from the imaged data was compared with that obtained from biodistribution analysis for PC3 tumours. Data was normalised to correct for decay, to ensure that results were directly comparable.

Difficulties were encountered in drawing the boundaries around ROIs of the tumours and kidneys without including unwanted surrounding tissue, especially at the 1 h time point. With the tumours, unwanted muscle tissue was sometimes selected; however as minimal

radioactive uptake was observed in muscle, this was not seen as a significant problem. The kidneys however are in close proximity to a number of organs which also showed uptake of ^{99m}Tc-DB 4, such as the intestines, stomach and liver, so great care was taken to ensure that the ROI of the kidney was defined without incorporating any unwanted tissue (Figure 4.25).

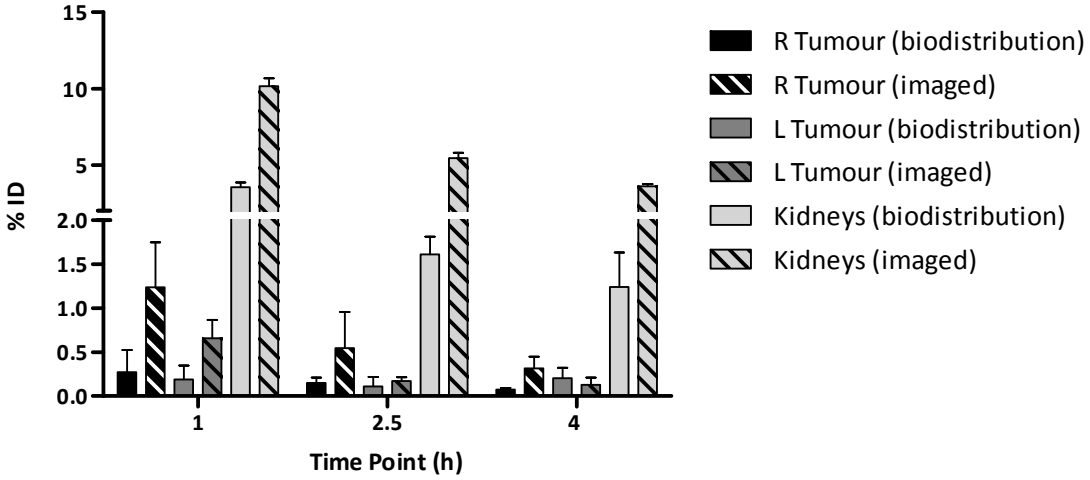

Figure 4.26: Comparison of % ID values in tissues obtained via quantification from imaged data and biodistribution data for the PC3 line.

Figure 4.26 compares the averaged % ID values obtained from the imaging and biodistribution data. Only the 4-h time points are directly comparable, as the mice imaged at this point were culled for the 4-h biodistribution point. The % ID values of the tumours were similar for the later time points, but not for the 1 hr time point, when the uptake from the imaging data appeared to be much higher at 1 h. This is thought to be due to a higher background in normal tissues giving tumours a larger appearance than in the later images, therefore resulting in a higher estimation of uptake. Significant differences in kidney uptake between the two methods can also be observed which may be attributable to difficulties in obtaining an exact ROI without including the activity from the intestine. A smaller ROI could be drawn within a region of the selected tissue and then multiplied to derive a value for the total tissue mass; however although that would eliminate the issue of taking in unwanted surrounding tissue, it also makes the assumption

that the uptake and binding was homogenous, which examination of the images showed was not the case.

Another way of graphically representing these results was to compare the activity recorded by the two techniques and to observe whether there was a linear relationship between them (Figure 4.27).

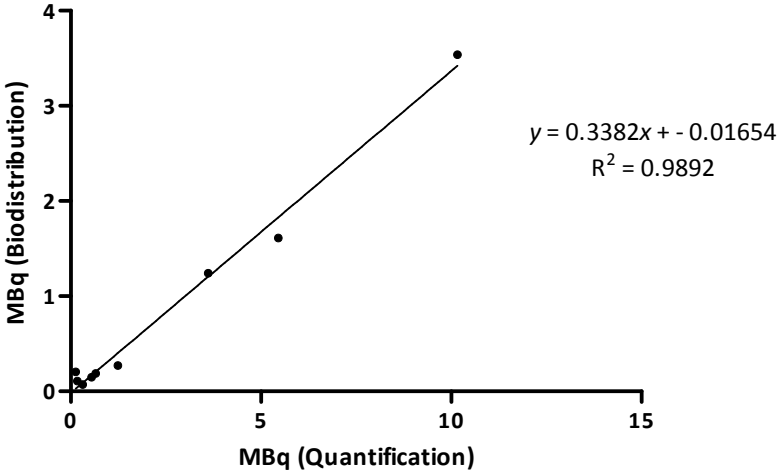

Figure 4.27: Comparison of tissue uptake in MBq: biodistribution versus quantification.

It is clear that there is a linear relationship between the uptake values obtained by biodistribution and those determined by image quantification. The line of best fit shows a good correlation between the two methods. However the slope of the line is 0.3382 rather than 1 as would be expected from a perfect correlation. This suggests that the differences are not due to experimental variability but to a fundamental flaw in one or both of the calculation methods.

In order to overcome the problem of drawing the ROI on the early, 1-hour image, ROIs were drawn from the CT image rather than SPECT image, which ensures that the ROI was drawn round the tumour only, eliminating any possible background activity (Figure 4.28).

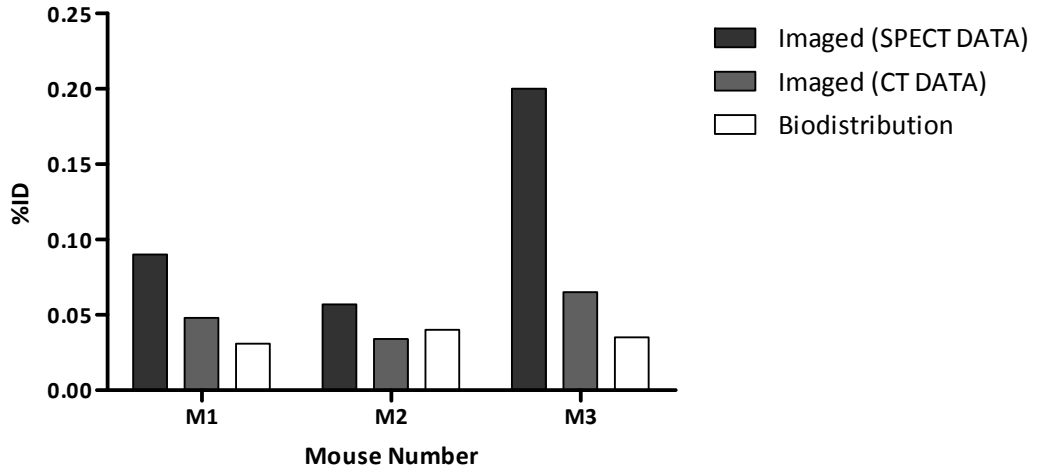

Figure 4.28: Comparison between tumour uptake obtained from biodistribution measurements and imaging procedures. ROI were drawn on CT and SPECT images to compare the difference. Data taken from right PC3 tumours from 3 imaged mice, 1 h post injection.

It can be seen that there is a closer correlation between the data obtained from the CT ROIs than the SPECT ROIs, indicating that assigning accurate ROIs may be a source of error.

4.2.4.5.4 Specific Activity

Specific activity was investigated as another cause of this discrepancy, since as the binding capacity of receptors *in vivo* can be as low as a few nanomoles, a low concentration of labelled ligand is essential. It was considered important to determine the effect of changes in specific activity because the non-radioactive substrate (DB 4) may competitively bind to the GRP-R and thus prevent the binding of the labelled ligand.

The differences in uptake were measured in PC3 tumour-bearing mice, mice were split into two groups; half of which were administered with an imaging dose of approximately 1000 pmol, and the other half with a biodistribution dose of 50 pmol; a 20-fold difference. Biodistribution was carried out 2.5 h post injection and organs and tissues were excised and measured (Figure 4.29).

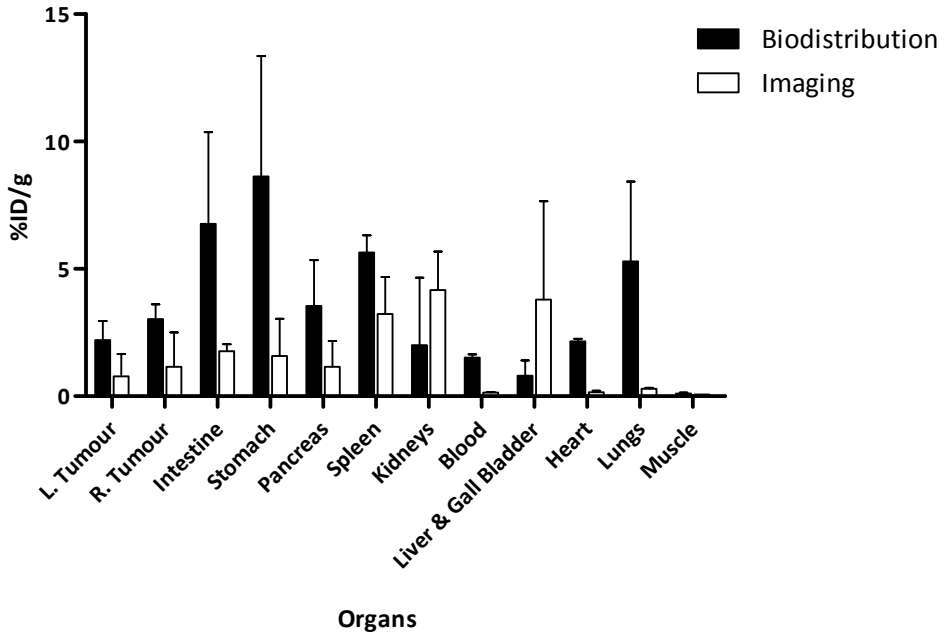

Figure 4.29: Biodistribution of PC3 tumour-bearing mice injected with either a biodistribution dose (50 pmol) or an imaging dose (1000 pmol). The average amount of label bound in three mice, taken per group at 2.5 h post injection, is shown with standard deviations. % ID/g = % uptake of injected dose per g of tissue.

A difference in uptake can be observed between the mice receiving the biodistribution and the imaging doses. Differences were seen in GRP-R expressing tissue such as tumour, intestine, pancreas and stomach. However differences were also seen in lungs, heart, liver and spleen, non-GRP-R expressing tissues.

4.2.4.5.5 Quantification of Other Cell Lines

The data shown above was obtained from mice bearing PC3 tumours. Quantification was also performed on mice bearing tumours from the other PC cell lines. A comparison of % ID/g values obtained from imaging and biodistribution analysis was performed. Data was again normalised to correct for decay and the 4 h time point was analysed to allow for direct comparison between the datasets (Figure 4.30).

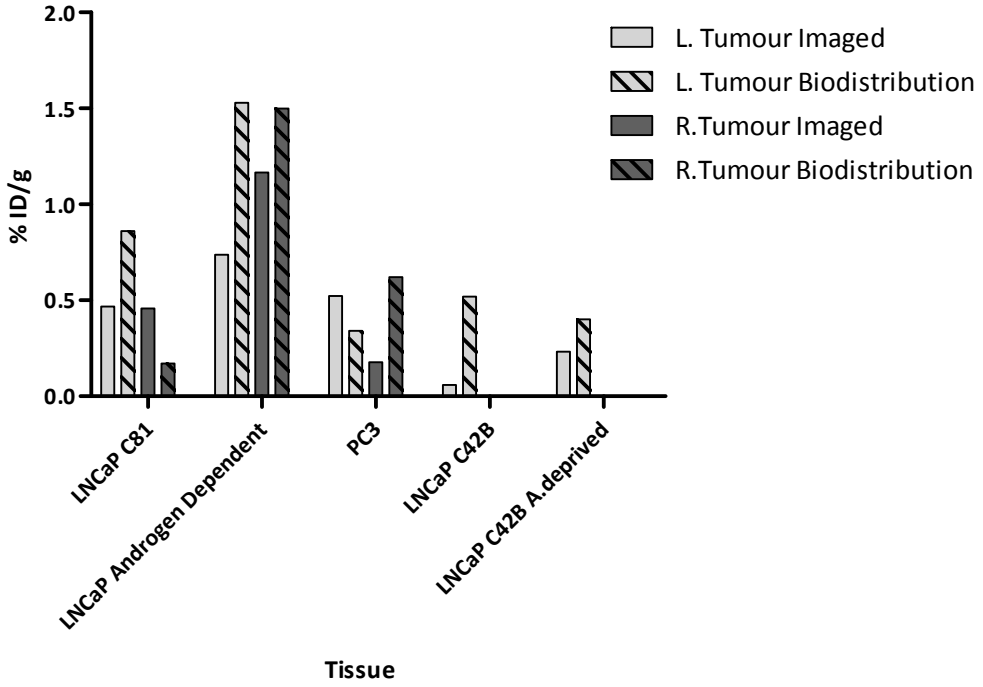

Figure 4.30: Comparison of % ID/g values in tumours obtained via quantification from imaged data and biodistribution data. Cell lines C42B & C42B androgen-deprived did not grow any tumours on the right flank.

The results obtained show a similar % ID/g uptake by the tumours in some of the cell lines tested, with LNCaP androgen dependent showing highest GRP-R expression in both imaging and biodistribution. However LNCaP C42B showed greater variability between the two methods.

4.3 DISCUSSION

Interest in radiopharmaceuticals has increased considerably over the last decade, with radiolabelled receptor-binding peptides emerging as a new class of radiopharmaceuticals. Peptides show a number of favourable characteristics; they are readily synthesised, inexpensive, and can withstand harsh chemical conditions for modification and radiolabelling. Furthermore, they offer several advantages over antibodies, being less likely to induce immunogenic responses, having improved pharmacokinetic profiles inherent in fast blood clearance, better tissue penetration, higher tumour uptake and therefore offering a more favourable tumour-to-background ratio [195].

The transition from androgen-dependent to androgen-independent (hormone-refractory) metastatic tumour type poses a major challenge for PC treatment. Molecules that are differentially expressed throughout this transition are likely to play important roles in imparting PC cells with the ability to grow in a hormone-deprived environment, and are therefore likely targets for diagnostic and therapeutic intervention. GRP-R expression has been reported in early stages of PC when tumour-growth is androgen-dependent as well as in prostatic intraepithelial neoplasia, a possible precursor to PC [9]. Expression levels at later stages of PC especially androgen-independent have been investigated and reports of receptor expression have been observed in androgen-independent PC3. During the emergence of an androgen-independent cancer, molecular changes occur and cancer-specific surface receptors and ligands are upregulated [196]. Imaging radiopharmaceuticals can potentially exploit these changes, allowing an insight to the development of the cancer, and also its response to treatment [116]. DB 4, a peptide binding to GRP-R was used to study GRP-R expression in a range of PC cell lines (from androgen-dependent to independent) in order to explore its potential as a radiopharmaceutical.

4.3.1 Prostate Cancer Cell Lines

The LNCaP cell line is one of the most widely studied cell lines in prostate cancer research because the cells express AR and behave much like early prostate cancer by being androgen-sensitive and having the ability to be transformed into androgen-independent cell lines both *in vivo* and *in vitro* [197]. LNCaP C42B and C81, cell lines derived from LNCaP show features of progressed disease such as metastatic capabilities and androgen independence, although androgen-sensitivity is also sometimes observed [198].

The two "classical" cell lines DU145 and PC3 are reported to be androgen insensitive and have been used extensively as a model for androgen-independent PC. They are however not regarded as optimal PC cell lines as they lack androgen receptor expression despite the presence of an apparently normal androgen receptor gene [199, 200]. Contradictory reports in the literature concerning the expression of AR mRNA and protein have been observed in these cells by a number of research groups [200, 201]. It remains an area of uncertainty as to whether these cells are AR negative or not, however it must be considered as a possibility.

De Visser and co-workers addressed this issue by measuring GRP-R expression in a range of human prostate tumour xenograft models [202]. A unique panel of human prostate tumour xenograft models had been established and reviewed by Van Weerden *et al* [203] which represented the various aspects of human PC and De Visser *et al* were therefore able to study the PC progression from androgen-dependence to androgen-independence stages. They found GRP-R expression in androgen-dependent PC, but minimal to no binding observed in androgen-responsive and androgen-independent PC, suggesting that GRP-R expression is regulated by androgens.

This aims of this project were to measure GRP-R expression in a number of PC cell lines ranging in androgen sensitivity by a number of different techniques and to compare expression both *in vitro* and *in vivo* with [^{99m}Tc]-DB 4. It was considered important to see whether results were comparable over a range of different techniques.

4.3.2 Radioligand Binding Assays

Radiolabelled peptides must retain their receptor-binding capacity if they are to function as effective radiopharmaceuticals and this was confirmed on the positive control cell line AR42J, a rat pancreatic tumour. Radioligand binding assays were then performed on all the PC cell lines in order to obtain both the receptor number (B_{max}) and the binding affinity (K_d) of DB 4, by analysis of non-specific binding and total binding.

Non-specific binding, importantly, occurs in many types of binding assay. In addition to specific binding to target receptors, radioligands may also bind non-specifically to other sites, notably the cell membrane. The details of the molecular interactions remain unclear, but charge and hydrophobicity of the ligand are involved, more so than sequence-specific structure. Non-specific interactions may also occur to other receptors and transporters expressed on the surface of the cell membrane, and is usually directly proportional to the concentration of the radioligand (the addition of twice the concentration of radioligand doubles the amount non-specifically bound) [191].

Unlabelled DB 4 was used as the competitor to measure non-specific binding to ensure that all the target receptors were occupied, so that any binding observed would be to other receptors, or be due to interactions with the cell membrane. The concentration used (1000 μM) was adequate to block all the receptors.

Measurable B_{max} and K_d values were obtained for PC3, DU145, LNCaP (androgen-dependent), LNCaP C42B and AR42J but LNCaP C81 and androgen-deprived LNCaPs C81 and C42B failed to generate any conclusive data, possibly due to lack of expression of GRP-R; or more likely, expression at levels below the sensitivity range of the assay.

Although androgen-dependent lines, showed a high level of expression of GRP-R, the androgen-independent lines, PC3 and DU145 revealed substantially higher levels of expression, even greater than of AR42J, the positive control (Table 4.1).

Aprikian and co-workers [204] found B_{max} values for GRP-R of 47600, 1500 and 1000 fmol in PC3, DU145 and LNCaP respectively using [^{125}I]-Tyr^4-bombesin. These values differ considerably from ours (8345, 4182 and 104 fmol respectively) but the order of level of expression (PC3>DU145> LNCaP) remains the same. This discrepancy may be explained by the effects of passage number and culture conditions described below.

Others have also shown GRP-R expression in these cell lines [204, 205] including increased expression in more advanced cancer [118]. The B_{max} values obtained from the cell lines thus demonstrated expression of the GRP receptor over a range of different stages of prostate cancer growth, especially in some of the more advanced androgen-independent forms; but they also show a reduction or loss of expression levels in the androgen-independent strains of LNCaP. K_d values were obtained for DB 4 from the tested cell lines and fell between a range of 0.3 – 2.2 nM, similar to those observed with a BN-analogue, [^{125}I]Tyr^4-bombesin on the PC3, DU145 and LNCaP, respectively 1.5, 1.1 and 3.6 nM [206].

The radioligand binding assay thus confirmed the expression of GRP-R in some of the prostate cancer cell lines tested, including androgen-independent PC3 and DU145 but with no receptor expression being observed in 3 lines.

4.3.3 High- and Low-Passage Numbers in LNCaP and C42B cell line

4.3.3.1 Increased Passage Number

It is essential to handle cell lines in a manner that maintains their usual phenotype. Androgen-dependent LNCaP cells that are used in experimental analysis should be maintained at as low a passage number as possible, and grown in media that maintain their growth and androgen dependency for as long as possible. The use of charcoal stripped-FBS (CS-FBS) is preferred, and media should be free of phenol red, since this

indicator is known to bind to androgen receptors [207] and elicit the same responses as do androgens, via the promiscuous pathway [9]. A main focus of research is aimed at understanding why after androgen ablation there is a switch in cell growth from a paracrine pathway to a newly-emergent autocrine pathway. A number of hypotheses and possible explanations concerning the role of androgen receptor expression and behaviour have been advanced to account for this [12, 208, 209]. One should also consider that the levels of expression of other receptors may also be up- or down-regulated *in vitro* due to factors such as increased passage number and nutrients within the media.

This change in behaviour was observed with high- and low-passage LNCaP C42B cells. All cell lines were passaged, and media changed in accordance with each line's requirements; however, working stocks of cells were regularly replaced with cells from frozen stocks of lower passage number to maintain a supply with as low a passage number as possible. Radioligand binding assays were performed on both low- and high passage-number stocks of LNCaP C42B which had been handled in the same manner. The difference observed between the two confirmed that passage number had an effect on the levels of expression of GRP-R, and validated the need to continue maintaining cell lines at low passage numbers. The precise reason for this effect is unclear, but perhaps the stress associated with the passaging of cells is causing the cells to evolve and behave differently from what is normal, or the gradual adaptation to their artificial environment, which is different from what naturally occurs *in vivo*. This observation was further confirmed in a comparison between high- and low-passage LNCaP C42B mRNA by RT-PCR. High-passage C42B expressed significantly lower levels than low-passage cells (explained in further detail in section 4.2.2.1).

4.3.4 RT-PCR – Relative Quantification

GRP-R expression was determined in androgen-dependent and -independent PC cell lines by relative quantification and -fold expression compared with MKN45, the non-expressing cell line. All cell lines tested revealed expression of GRP-R mRNA; in PC3 considerably

more than in any other cell line. It was not possible to obtain a value for GRP-R expression by the rat pancreatic cell line AR42J due to the use of probes and primers designed for human transcripts. The results obtained were comparable in some respects to those from the radioligand binding assays, PC3, DU145 and LNCaP showed the highest level of expression and the androgen-independent LNCaP lines the lowest. However the order of expression was PC3>LNCaP>DU145>C42B>C81 compared to PC3>DU145>LNCaP>C42B>C81 for the radioligand binding assays. Similar patterns of GRP-R expression have been observed in PC3 and DU145 as well as LNCaP using standard PCR [210].

To assess whether androgens and the AR had an affect on GRP-R expression as previously observed by De Visser *et al*, LNCaP cells were transferred from regular FBS into CS-FBS and back into regular FBS. These exhibited changes in GRP-R expression. Decreased expression was first observed when the medium was supplemented with CS-FBS (lacking androgens and growth factors), however once cells were transferred back to standard FBS, recovery of GRP-R expression and sometimes enhanced-expression was observed in all the cell lines.

Schroeder *et al* [211] have also observed this effect in androgen-dependent prostate cancer *in vivo*. The authors investigated GRP-R regulation in 3 androgen-dependent human PC xenograft models representing the early androgen-responsive state of PC. RT-PCR of mRNA from the tumour tissue was performed to evaluate the changes in mRNA expression of GRP-R during androgen manipulation. After androgen ablation, the relative level of GRP-R expression dropped considerably, but partially recovered after re-supplementation with testosterone. Autoradiographic analysis also revealed reduced binding after androgen ablation by up to 95% reduction in androgen-dependent cell lines. Biodistribution studies demonstrated a similar response, but to a lesser extent.

Future work would beneficially be directed at attaining fundamental knowledge of the hormonal regulation of GRP-R; essential information for the clinical use of GRP-R-based technologies.

4.3.5 GRP-R Expression Examined using FACS

FACS analysis of GRP-R expression was not successful using either of the commercially available anti-GRP-R antibodies (Novus or Abcam) on the PC cell lines. As no positive control antibody was available, optimisation of the assay was not possible, therefore it was difficult to know for certain whether the negative results obtained were the result of the absence of binding, or a fault of the assay method. Neither of the commercially available antibodies had been optimised for FACS, and currently there is no FACS data published on GRP-R expression.

4.3.6 Autoradiography

Autoradiography was performed as another means of measuring GRP-R expression, but also to assess whether the levels of expression observed *in vitro* were maintained *ex vivo*.

Autoradiography was first attempted with ^{99m}Tc but was found to be not an ideal isotope for this procedure. ^{99m}Tc is not a β-emitter, therefore autoradiography depends on the activity of Auger and internal conversion electrons, which have a lower and broader energy spectrum than β-particles. When an electron is removed from an atom leaving a vacancy (leaving the atom in an energetic ionised state), an electron from a higher energy level may fall into the vacancy, which results in a release of energy; this energy can be emitted in either the form of a photon or an Auger electron [172]. Internal conversion is a radioactive decay process where an excited nucleus is de-excited by interaction with an electron from one of the lower atomic orbitals, causing an internal conversion electron to be emitted from the atom [172].

Because of difficulties in obtaining reproducible results using ^{99m}Tc, optimisation studies were performed. Due to the small tumour sections used, a high specific activity was required to label the DB 4 peptide, to limit competition between unlabelled and labelled DB 4 for the GRP-receptors. High levels of activity are also necessary to detect a signal in a short exposure time because of the short half-life of ^{99m}Tc, however, use of higher activity levels of ^{99m}Tc was found to cause saturation of the screens. For these reasons, results obtained were of poor quality and it was not possible to clearly differentiate between tumour sections incubated with and without competitor (unlabelled DB 4), due to low tumour-to-background signal ratios. Since the use of ^{99m}Tc-DB 4 failed to give conclusive answers, the technique was adapted for use with the [^{125}I]-Bombesin analogue [^{125}I] -D-Tyr^{6}, β-Ala^{11}, Phe^{13}, Nle^{14} BB in place of ^{99m}Tc.

This radioligand yielded much clearer results, facilitating the distinction between non-specific and total binding, which allowed specific binding to be measured. The relatively long half-life allowed for longer exposure times, which heightened the contrast between the tumour and the background. The results obtained from this assay mirrored those obtained by *in vitro* analysis (radioligand binding assays and relative quantification by RT-PCR), and showed that the PC3 cell line gave the greatest level of GRP-R expression, followed by LNCaP androgen-dependent, LNCaP C42B and LNCaP C81. No sites of necrosis were observed, confirming good vascularisation of the tumours. Autoradiography of GRP-R has also been performed by Maddalena and co-workers in both LNCaP and PC3 cells confirming receptor expression *ex vivo* [135].

Autoradiography studies of GRP-R expression in a range of prostatic tissue from patients with PC have been performed by Marwalder and Reubi [118]. Four types of tissue were investigated: invasive prostatic carcinoma; high-grade PIN; prostatic hyperplasia, in which prostatic stroma and GRP-R frequency and intensity were measured. Their main findings were a high incidence and high density of GRP-R in not only invasive prostatic carcinomas, but also in the earliest phase of neoplastic transformation. Little to no expression was seen in non-neoplastic prostatic tissue, such as benign prostatic hyperplasia. The

autoradiography results obtained in the present work are similar to these documented findings, in that high levels of GRP-R expression were observed in early PC growth (in LNCaP androgen-dependent), when cells proliferate and differentiate via a paracrine pathway. High levels of GRP-R were also observed in advanced PC such as in the PC3 cell line.

A slight drop in GRP-R expression was observed when cells were grown in androgen-deprived medium, however autoradiographic study of these tumours does not provide a true representation of the effects of complete androgen removal, as cells were injected into intact male mice, and therefore were exposed to circulating androgens, thus nullifying the effect of the androgen-deprived environment that the cells were previously grown in. Nonetheless, androgen deprivation did have an effect on the growth of the tumours, because compared with the same cell lines grown in 10% FBS, the androgen-deprived line took 2 to 3 times longer to grow *in vivo*, suggesting a possible link between the level of GRP-R expression and rate of cell proliferation.

4.3.7 Immunohistochemistry

Immunohistochemistry failed to fully reveal specific GRP-R binding in the prostate cancer cell lines studied. PC3, was the only line that stained positively, visually nearing that of pancreatic tissue, the positive control. However upon closer inspection, other types of non-expressing cell, such as skeletal muscle, also appeared to exhibit positive staining. Therefore PC3 probably displayed a certain degree of non-specific binding, though a proportion of the staining may still be attributed to specific binding.

The remaining prostate cancer cell lines all failed to reveal any specific binding with anti-GRP-R antibody. Diffuse staining was observed with all lines, and although it was not observed with the negative line MKN45, that was not sufficient evidence to corroborate specific binding.

The minimal level of specific binding seen in all the sections of tumour tissue tested could be attributed to a number of possible causes; firstly, the antibody, which had to meet the

requirements of both IHC and FACS analysis. There are very few commercially-available human anti-GRP-R antibodies. The first antibody considered, Novus Biologicals NLS830, failed at the optimisation stage of the experiment. No specific binding even to the positive control, pancreatic tissue, was seen. The second, Abcam 39963, yielded better results, however the specificity of the antibody may still have been the cause of the little specific binding observed in the range of cell lines. It was possible that this antibody was not optimal for this procedure, and the levels of expression in these cells were lower than the sensitivity of the assay and that only the high expressing PC3 tissue sections was stained successfully. Secondly, the epitopes on the receptors may also have been damaged during the processing, embedding and sectioning of the paraffin samples.

Schultz and co-workers were successful in positively staining GRP-R in a number of GRP-R expressing cancer cell lines, such as prostate and breast with their novel antipeptide antibodies [212]. GRP-R protein has also been successfully detected in colon cancer by immunohistochemisty [213] and with weak and diffuse staining in breast cancer tissue with a commercially available antibody [214]. Both the results obtained and data in the literature indicate that commercially available antibodies towards GRP-R give a diffuse positive-staining which is open to interpretation.

4.3.8 Imaging

4.3.8.1 Radiolabelling with ^{99m}Tc - Quality Control Analysis

Radiolabelling efficency was measured for each batch of labelled DB 4 by ITLC and confirmed by HPLC analysis; an important step before commencing any experiment to ensure the quality of the labelled product. Both ITLC and HPLC routinely indicated a labelling efficiency >98%, therefore further purification was not necessary.

4.3.8.2 Biodistribution Studies on PC3 Tumour-Bearing Mice

The jump in experimentation from the *in vitro* to the *in vivo* environment is considerable, and many new factors come into play, such as the stability of the radiotracer, pharmacokinetics, temperature (stability at 37 °C), pH, non-specific binding to proteins and its general ability to interact with the biological environment [215].

Both left and right flanks of the mice were injected with PC3 cancer cells, the left with a 50:50 mix of Matrigel[77], and the right with cells alone. Matrigel was used to encourage tumour growth; however it was not known whether this would affect the imaging and biodistribution studies. In both imaging and biodistribution studies, the Matrigel tumours did not show as high levels of specific binding as observed with the tumours grown with no Matrigel. This could be for one of two reasons; either a direct effect on GRP-R expression or, more probably, on the rate of tumour growth. Matrigel tumours always grew much more rapidly than non-Matrigel tumours, so it is possible that they outstripped their supply of nutrients and became senescent or underwent apoptosis and necrosis.

Biodistribution studies in PC3 tumour-expressing mice showed increased levels of uptake in both left- and right-flank tumours, with right tumours exhibiting higher binding than the left. Rapid clearance from the circulation was observed with minimal ^{99m}Tc-DB 4 background seen after 1 h post injection. Very little non-specific binding was observed in non-GRP-R-expressing tissue including muscle, heart and lungs. Activity observed in the stomach could be due to the degradation of the ^{99m}Tc-DB 4 complex or to possible low levels of GRP-R expression [216]. A degree of binding would also be expected in the intestine and pancreas, which express lower levels of GRP-R. High uptake by the kidneys was due to the hydrophilic nature of this radiopharmaceutical, which was accordingly excreted renally. The decrease in uptake observed at later time points was indicative of washout from the tissue and clearance from the body.

[77] Matrigel contains structural proteins such as laminin and collagen which provide additional support to the cells in a form of a growth matrix, which increases vascularisation

4.3.9 Blocking Study

Prior to the commencement of the *in vivo* imaging study, it was important to ensure that the binding observed was specific, therefore a blocking study was performed to validate this. Some degree of non-specific binding is expected due to hydrophobic and ionic interactions with other sites on the cell surface [144]; however this percentage must be low enough to allow specific binding to be observed.

The results showed a decrease in binding of ^{99m}Tc-DB 4 when blocked with 10 µg of unlabelled DB 4. A reduction of only ~50% was observed. This residual uptake may be non-specific or possibly due to GRP-R not being fully blocked by unlabelled DB 4. A blocking dose of 10 µg was used, considerably lower than other groups who used a dose of 250 µg and showed a reduction in PC3 tumour uptake of DB 4 from 5.19 to 0.55 %ID/g at 4 hours [206]. The 10 µg blocking dose chosen was influenced by toxic effects seen after injection of higher doses of bombesin analogous in these mice.

Cescato [206] have also studied the distribution of ^{99m}Tc-DB 4 in PC3 tumour-bearing mice, and found higher uptake by the tumour, with better retention extending over longer periods of time, with % ID/g values for tumour uptake of 9.37, 5.19 and 2.67 at 1, 4 and 24 h respectively post injection was observed. However, they also showed greater uptake by the pancreas at 38.90, 34.80 and 14.43%; substantially higher (pancreas at 1, 2.5 and 4 h showed 2.49, 1.51 and 1.41%) than the uptake observed in any of the cell lines tested in the present work. Although the experimental conditions were the same, significant differences were observed between the two sets of data which can perhaps be attributed to differences in cell culturing techniques, which may affect GRP-R expression in tumours, but not pancreas. Other factors which may account for these differences are the age, sex and strain of murine models used. All our biodistribution studies were performed on male, SCID mice aged 6-8 weeks. Although Cescato *et al* also used SCID mice, the age and sex is not known. Administered dose could not be a contributing factor, since these were the same, and the reason for this high pancreatic uptake remains unclear.

4.3.10 Biodistribution Studies on Other Cell Lines

Biodistribution studies were performed on the remaining PC cell lines to assess their GRP-R expression and to see whether they followed the same level of expression as previously observed in both *in vitro* and *ex vivo* analysis. These results are summarised in Figure 4.31.

A range of uptake across the cell lines tested was seen, with LNCaP androgen-dependent showing higher uptake than all the other lines, including PC3. No correlation was observed between *in vivo* uptake and the level of receptor expression shown by *in vivo* and *ex vivo* analysis. However, the results are difficult to interpret, because in some instances the uptake observed did not always decrease with time, and in some cell lines (AR42J, LNCaP C42B androgen deprived and LNCaP C81) increases in uptake were observed at later times (Figure 4.31).

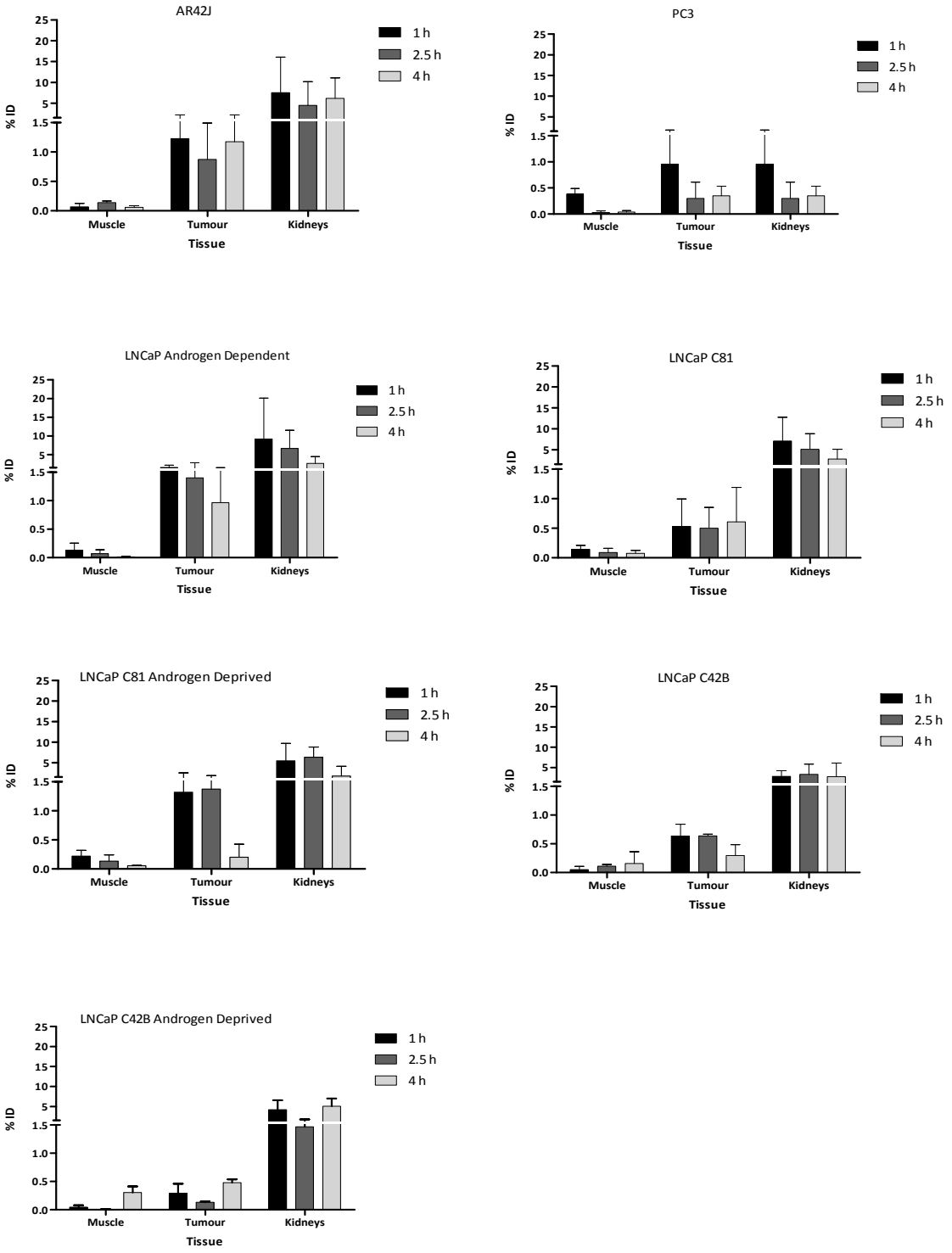

Figure 4.31: Biodistribution of % ID/g uptake of [^{99m}Tc]-DB 4 in a range of PC cell lines over 1, 2.5 and 4 h in muscle (non-specific binding), tumour (specific binding) and kidneys (renal clearance). Values are the mean ± standard error for each tested tissue (n=3).

A possible reason for the lack of correlation is the fact that the different tumours were often of quite different sizes. The use of Matrigel-assisted and non-Matrigel-assisted tumours in opposite flanks often resulted in a non-ideal combination of tumour sizes, with the Matrigel-tumours being too large and the non-Matrigel tumours being too small. This meant that factors such as the level of necrosis (in large tumours) or variations in blood supply (in small tumours) could have an influence on the level of uptake independent of the level of receptor expression.

4.3.11 Specific Activity

The effect of the difference in specific activity between the biodistribution and imaging studies was evaluated. A difference in uptake can be observed between the mice receiving the biodistribution and the imaging doses, probably due to a proportion of competing unlabelled DB 4, blocking the GRP-R in the imaging dose mice. However, although this trend was observed in all the GRP-R-positive tissues such as tumour, intestine and stomach, non-GRP-R expressing tissues also showed a blocking effecti such as the spleen, blood, heart and lungs, which would not be expected. This anomaly needs to be clarified by further work, but the difference between the two doses may explain in part the poor correlation between biodistribution and quantification shown in Figure 4.27, where the slope of the line of best fit does not equal 1.

4.3.12 Imaging with [^{99m}Tc]-DB 4 in all Prostate Cancer Cell Lines

Imaging provides both qualitative and quantitative information allowing the visualisation of the uptake, clearance and interaction with biological systems in real-time. It also reduces the numbers needed in animal studies. Two to three mice bearing each tumour type were selected for imaging. It was considered important to select mice with tumours that were not too advanced (too large), because it was important to try to capture growth in the initial growth phase, with good vascularisation but minimal necrotic sites. These mice were injected at 40-min delay intervals to allow for Nano SPECT and CT analysis, and were subsequently scanned at 1, 2.5 and 4 h post injection. The images showed uptake in the tumour in all the cell lines to varying degrees, LNCaP C81 androgen-deprived showed

the least visual uptake, with AR42J, PC3 and LNCaP androgen-dependent showing greater uptake than the other cell lines[78]. As well as uptake at the sites of tumour, imaging allowed an assessment of how long the radiopharmaceutical was maintained at the tumour sites, as well as an indication of any uptake in other tissues. Kidney uptake decreased over time as the radiopharmaceutical cleared from the system, but was also dependent on the rate of excretion by individual mice. Uptake was also observed by the intestines partly due to the GRP-R expression present there and partly, perhaps to excretion[119].

The behaviour of [^{99m}Tc]-DB 4 was encouraging as the radionuclide:peptide complex appeared to remain intact, since no activity was observed in the thyroid, which would have indicated the presence of free pertechnetate, and the spleen, which would have accumulated [^{99m}Tc]-colloids.

4.3.13 Quantification

ROI analysis was performed to obtain quantitative information from the SPECT images and to see whether the results obtained by Nano SPECT/CT were comparable with the biodistribution data. Quantification analysis was performed on the PC3 images at the three time points studied and compared with the biodistribution data for the same time points. However, only the 4-hour time point was directly comparable because the imaged mice were the same as those used for the 4 h biodistribution time point. Figure 4.26 shows that similar uptakes for both left and right tumours were obtained for the time points 2.5 and 4 h. Uptakes at 1 h were not as similar, possibly because of the greater background uptake in normal tissues. This gives the tumour a larger appearance on the SPECT images than the CT scans (Figure 4.28). Uptake in kidneys was not comparable either due to difference in excretion between the two sets of mice or the difficulties in drawing accurate ROIs round the tissues of interest.

[78] Appendix X

When the imaging results were plotted against the biodistribution results, a linear relationship was observed, but the slope of the line was not equal to 1, suggesting a basic flaw in one or both of the methods used. This could be either due to a real difference in uptake caused by differences in the experimental protocols or by apparent differences due to errors in the analysis. At least two possible reasons could explain these observed differences: (1) specific activity may be one possible reason as differences were observed in uptake between imaging doses and biodistribution doses in GRP-R expressing and non-expressing tissues (Figure 4.21). (2) Definition of the ROI could also introduce errors. It is important to ensure that the ROI is obtained correctly. The widest part of the tumour is generally selected and the ROI drawn, as shown in Figure 4.32. The analysis programme, then gives a value for the volume of the tumour in cm^3. Errors can arise if the ROI is drawn around a narrower region, eliminating sections of the tumour which fall outside this region and thus will not be recorded. As previously explained, it can be difficult to obtain by this technique the correct volume of the desired tissue/organ, without also acquiring surrounding unwanted tissue. However, since tumours on the flanks of hind legs are surrounded by tissue (muscle) showing these would not be expected to result in a large difference in the total %ID calculated with the ROI.

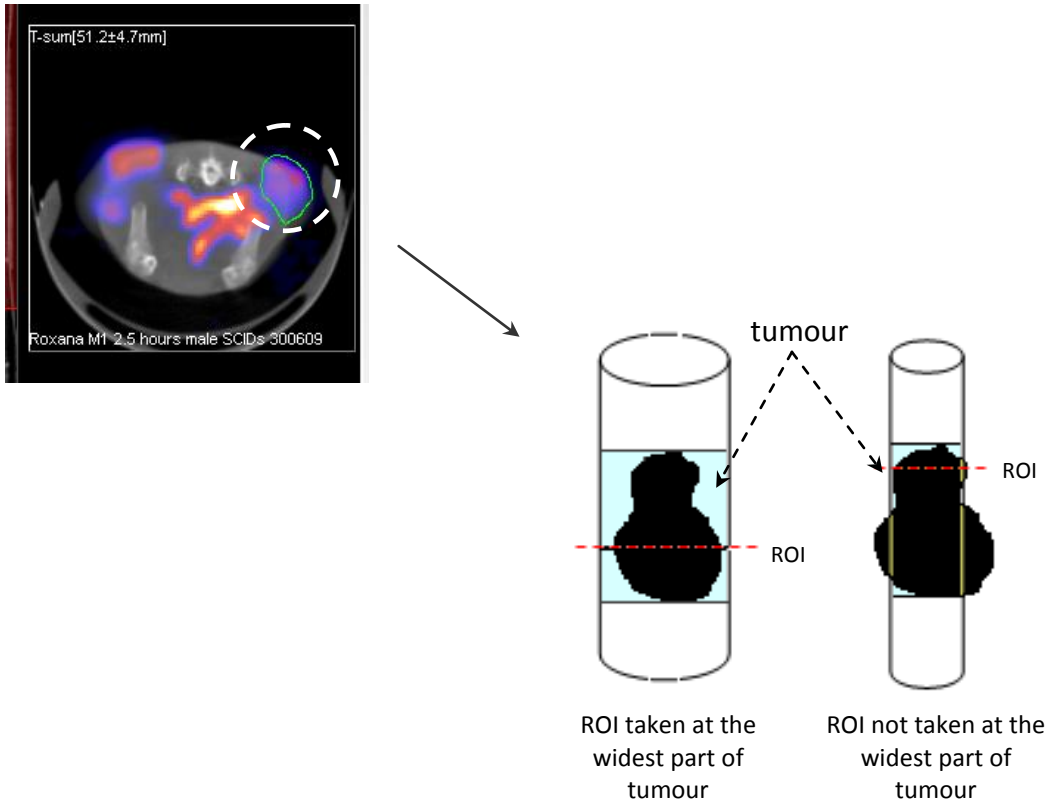

Figure 4.32: Schematic representation of the importance of drawing ROI round the widest part of tissue. Dashed white circle highlights the region from which the ROI is drawn. MBq values from tissue within the cylinder are taken; values for any tissue which falls outside the cylinder are not recorded and are therefore lost. Red dashed line indicates the diameter of the cylinder drawn which contains the ROI. Blue area indicates surrounding tissue which is also included in the reading; therefore if the tissue being measured is in close proximity to other positive tissue, minimal surrounding tissue must be taken, otherwise they affect the MBq readings.

Quantification in the other tested cell lines (Figure 4.30) showed a close similarity between the two procedures in C81, PC3 and LNCaP tumours, but with C42B and C42B androgen-deprived showing greater variability. These differences may be attributed to the causes discussed above.

4.4 SUMMARY & CONCLUSION

4.4.1 GRP-R Expression in Prostate Cancer Cell Lines

Using a range of *in vitro*, *ex vivo* and *in vivo* techniques, GRP-R expression was measured and compared over a range of PC cell lines representing different stages of cancer growth. GRP-R was expressed in all the cell lines tested. The highest values were observed in the androgen-independent cell lines PC3 and DU145, followed by LNCaP androgen-dependent which were much lower; B_{max} values were respectively 8345, 4182 and 104 fmol/mg. K_d values for ^{99m}Tc-DB 4 fell within the range 0.3 – 2.2 nM, indicating a high affinity for the receptors.

RT-PCR further showed a very similar trend in GRP-R expression *in vitro* as seen in the radioligand binding assay, with the PC3 line showing the highest level of expression. Changes were observed in GRP-R expression when cells were deprived of and resupplemented with androgens. Passage number, cell culturing techniques and handling were shown to affect the behaviour and subsequent level of expression of GRP-R. The reason for this remains unclear, but nutrient stress, passage number and handling technique have been shown by others to affect GRP-R expression significantly [217]. Androgen deprivation was seen to decrease the expression level slightly, but after resupplementation with androgens, there were significant increases in expression, exceeding the base-line values obtained. This phenomenon was also observed by Schroeder and co-workers [211], and further investigation is needed elucidate the mechanism responsible.

FACS analysis failed to show any specific and selective binding to any of the GRP-R-positive cell lines in comparison with the negative line MKN45. Failure to observe binding was attributed to the two commercial antibodies used, neither of which proved to be suitable for FACS analysis.

Ex vivo analysis of tumours from the cell lines tested was performed in an attempt to bridge the gap between the jump from *in vitro* to *in vivo*. Technical difficulties were encountered by using [^{99m}Tc]-DB 4 for autoradiography but successful results were obtained with [^{125}I]-Bombesin Analogue [[^{125}I]-D-Tyr^{6}, β-Ala^{11}, Phe^{13}, Nle^{14}-BB. Specific binding was observed in all the PC cell lines tested, at significantly higher levels than the binding observed in the GRP-R-negative cell line, MKN45.

Binding trends seen in radioligand binding assays, and the relative quantification afforded by RT-PCR were also reflected in the data obtained from autoradiography, further strengthening and validating the results and patterns previously observed. Autoradiography also revealed a decrease in receptor expression when cells were androgen-deprived, showing a reduction of 35% in LNCaP C42B, but no significant difference in LNCaP C81. Further investigation using castrated mice is needed to confirm these initial findings.

As with FACS, immunohistochemical studies using the commercially-available anti-GRP-R antibodies failed to reveal any binding. Even pancreatic tissue, the positive control, did not demonstrate strong binding, and only diffuse staining was observed in PC3 sections. As GRP-R expression had been revealed by autoradiography, the lack of demonstrable binding was not thought to be due to the absence of receptor expression, but rather to deficiencies in the antibodies used, or perhaps the processing, embedding and sectioning of the sections.

In vivo analysis of the uptake of ^{99m}Tc-DB 4 in tumour-bearing mice did not mirror *in vitro* findings. The androgen-dependent cell line LNCaP showed the highest uptake (% ID/g = 1.98), greater than PC3 (% ID/g = 1.55) at 1 h post injection, and with improved retention at the tumour site even at 4 h post injection, *in vitro* analysis had shown greater GRP-R expression in PC3.

The interpretation of *in vivo* imaging is made difficult because of its questionable reproducibility. Procedural protocols and the approach to the measurement of tumour vascularisation need to be standardised, experimental error needs to be reduced and the relationships between tumour size, uniformity and uptake, need to be better understood, prior to ascertaining whether imaging can provide the same quantitative information as biodistribution studies.

Dose and specific activity issues could partially explain the differences observed between imaging and biodistribution data and would need to be further investigated. Differences in quantification between biodistribution and imaging data were partly attributed to errors in measurements of volume which arose when obtaining the ROI, and further investigation may be needed.

^{99m}Tc-DB 4 successfully bound to GRP-R expressed in a range of PC cell lines. The level of expression was quantified by a variety of different techniques *in vitro*, which showed high levels of expression in the androgen-independent cell lines PC3 and DU145, as well as in LNCaP androgen-dependent, but lower expression in the androgen independent strains of LNCaP C42B and C81. Androgen appeared to have an effect on GRP-R expression; deprivation reduced the levels expressed and resupplementation appeared to drive over-expression. ^{99m}Tc-DB 4 has proven to be a successful candidate for imaging PC in a range of PC cell lines, and could potentially be used as a targeting radiopharmaceutical.

5 THESIS DISCUSSION AND CONCLUSIONS

The aim of this work was to design, syntheise and test two poteintial targets to develop into new radiopharmaceuticals which could be easily radiolabelled and to specifically target PC. As PC switches from androgen-dependence to independence, new radiopharmaceuticals for imaging and therapy would need to target ligands or receptors ideally expressed on all stages of growth, but not in healthy tissue.

Two appropriate molecular targets were developed as potential imaging radiopharmaceuticals for PC. The first target was PSMA, a ligand which is highly expressed in PC with lower expression in healthy tissue and its expression is upregulated with cancer progression. PSMA is a large surface marker, which is not released into the circulation and is internalised after antibody binding.

A number of groups have developed mAb and scFv against PSMA [62, 63, 71] but few have undergone clinical application. ProstaScint® is commercially available, however a drawback to this radiopharmaceutical is its ability to target only the internal domain of PSMA; and is thus only able to detect its target when cells are dying and is not ideally suited to image the early progression or reoccurrence of the disease [65]. To overcome this problem, recombinant PSMA protein was generated for this project in which the internal domain was deleted and phage display was performed on the protein encoding only for the large, extracelluar portion of the PSMA ligand.

The aims of this study were partially met. Using a semi-synthetic phage display library, a number of potential scFv clones were selected and syntheised and shown to specifically bind to PSMA. This was confirmed by FACS analysis whereby both positive phage clones and purified scFv preferentially bound to PSMA expressing cells (LNCaP) over non-expressing cells (DU145).

In a bid to increase the affinity, production of diabodies was performed, as they are known to have an advantage over scFv's *in vivo*. The manipulation of the linker can drive the formation of diabodies or even triabodies as shown by Hudson *et al* [180] and the successful production of diabodies was achieved by the complete removal of the linker, by exploiting the many restriction sites on the phagemid vector. Binding efficacy by ELISA and FACS was studied to ensure production of diabodies, as removing the linker prevents the natural folding of the scFv and prevents the fragment from forming the paratrope. Binding efficiency was compared between the scFv and diabodies by ELISA and FACS to ensure successful production of diabodies which still retained their binding ability; improved binding was observed with the diabodies for all the clones. FACS histograms showed broad peaks, suggesting heterogeneity of the dimeric samples containing diabodies, triabodies and even tetrabodies. Nonetheless, they were able to selectively bind to LNCaP over DU145, confirming specificity to PSMA. These results together with the ELISA results confirm successful manipulation of the linker to drive the formation of dimeric fragments.

HPLC and FPLC confirmed the heterogeneity of the both the monomeric and dimeric preparations, but also confirmed stability of the fragments reducing the possibility of dissociation.

Radiolabelling of both the monomeric and dimeric R2G10 antibody fragments was achieved using sodium [^{125}I]-iodide in iodogen tubes, with an efficiency of >90%. However no binding of radiolabelled antibody fragments to cells was observed in radioligand binding assays. Studies were undertaken to see if this was due to chemical changes to the antibody during the labelling procedure but it seemed that this was not the case. It was concluded that the differences in binding observed between the FACS and radioligand binding analysis was due to the differences in antibody concentrations employed and that it was likely that the antibodies were binding to PSMA with only low affinity. Binding both *in* vitro and *in vivo* was unsuccessful using the radiolabelled antibody fragments, however this as well as the antibody fragments themselves, other factors such as the choice of

radioisotope and methodology used, could have played a crucial role in this failure to show binding with the PSMA-specific antibody fragments.

The second target GRP-R is highly expressed neuropeptide receptors in PC. GRP-R is known to be expressed in early stages of PC; however recent studies have questioned its expression in advanced, androgen-independent PC. Expression in the androgen independent PC3 cell line has been observed in a number of research groups [116, 136], however in human prostate xenografts of advanced androgen-independent PC, expression was not observed [134, 202].

GRP-R expression was successfully designed, synthesised and evaluated *in vitro* and *ex vivo* by a number of techniques (radioligand binding assay, RT-PCR, autoradiography and immunohistochemistry) and results obtained were comparable showing an level of expression in the order PC3>DU145>LNCaP>LNCaP C42B>LNCaP C81 using these different analytical methods. Expression was then studied *in vivo* by injection of the radiolabelled peptide ^{99m}Tc-DB4 into xenograft bearing mice and results compared with those obtained *in vitro.* Although specific uptake of the radiopharmaceutical by the tumours was observed there was not a good correlation between uptake *in vivo* and expression levels observed *in vitro*; with expression being observed predominately in LNCaP and PC3. Quantification of imaged data was performed and compared to *in vitro* findings, but again were found not to be directly comparable.

Androgen dependence and GRP-R expression was also assessed to determine a possible relationship between the two. It was found that androgen ablation appeared to cause the down-regulation of GRP-R expression in LNCaP cells but when resupplemented with androgens the levels of expression not only recovered but expression were increased considerably. This confirmed findings from Schroeder *et al* who also observed this relationship [134].

The majority of the aims of this project were met. ^{99m}Tc-DB 4 successfully bound to a range of PC cell lines; the level of expression was quantified by a variety of different techniques *in vitro*. Androgen appeared to have an effect of GRP-R expression as deprivation was seen to reduce the levels expressed and resupplementation appeared to drive over-expression. ^{99m}Tc-DB 4 has proven to be a successful candidate for imaging PC in a range of PC cell lines, and could appears to have the potential for clinical application.

The hypothesis for this work is that PC can be imaged by using a suitably designed radioligand directed against an appropriate molecular target such as PSMA or GRP-R. This project to a large extent confirms this hypothesis. ^{99m}Tc-DB 4 was successful designed, synthesised and showed a good level of binding and uptake in *in vivo* analysis and high quality images were produced. Anti-PSMA antibody fragments although were successfully radiolabelled, the radiolabelled product could not be shown to bind PSMA, this could be attributed to the chosen isotope and methodology employed and with further investigation could potentially also be a good imaging radiopharmaceutical.

6 FUTURE WORK

6.1 PSMA PROJECT

6.1.1 Optimisation of Radioimmunoassay and *in vivo* imaging

Further investigation with the positive control antibody D2B, in both the radioimmunoassay and *in vivo* imaging procedure would allow issues with these assays to be addressed, as the D2B binds to PSMA-expressing cells with a higher affinity than any of the positive selected clones from the phage display selection (Figure 3.19). It would also be advantageous to explore an increase in the concentration of the antibody preparation when performing radioimmunoassay, equal to the concentrations used in FACS to enable the results of the two assays to be more directly compared,

If positive data was attained with D2B, this would allow validation of these assay conditions (antibody concentration, incubation time and temperature) with which it would then be beneficial to re-test the four scFv and diabody clones (including analysing R2G10) to see whether improved binding could be observed.

In addition, it may prove advantageous to perform assays on other PSMA-expressing cell lines, such as PSMA transfected PC3 cell line.

6.1.2 Stability Analysis

Analysis of the stability of the antibody preparations would also be important to ensure that the radioisotope and antibody fragments remained intact *in vivo* for long enough to target the expressed PSMA. Analysis in both plasma and PBS at 37°C should be performed.

6.1.3 Radiolabelling with Other Isotopes

Alternative chelate-based radiolabelling chemistry could be investigated such as ^{111}In and ^{99m}Tc to see whether improved binding could be observed using these radioisotopes over ^{125}I.

Proteins cannot be labelled with ^{111}In directly and a multi-stage approach is required, using a bifunctional chelating agent, capable of covalently binding to the protein. The most commonly used is diethylene-triamine-penta-acetic acid (DTPA). Both isotopes have a much shorter half-life and are more appropriate for imaging applications.

One draw-back of substituting ^{125}I with another radioisotope is that radiolabelling requires considerably larger concentrations of protein, requiring an increase of the production in the scale and techniques currently employed.

6.1.4 Binding Affinity Analysis Using Biacore

It would also be of interest to analyse the binding affinity and kinetics of the selected clones using Biacore technology, which is able to provide a range of information regarding the binding interaction of the antibody fragments to the target antigen in real time.

Biacore is a surface plasmon resonance (SPR)-based system for analysing biospecific interactions *viz.* specificity, affinity and kinetics. The protocol requires one interacting molecule to be immobilised to a sensor chip and its counterpart is injected into a continuous buffer flow. The interaction is monitored in real time, thereby offering the possibility of calculating the kinetic rate constant for the interactions [218].

It is possible to use biacore in the selection process of scFv in phage display, allowing for a much quicker high throughput protein interaction analysis, by obtaining high quality kinetic data without the need of antibody purification, facilitating the screening of potential scFv leads.[218, 219].

6.1.5 Repeat Screening

In the event that the above analysis failed to yield any conclusive answers, it may be advantageous to screen the library again, this time alternating between a PSMA transfected cell line and the recombinant PSMA protein to see whether higher affinity scFv would be identified. Perhaps selecting an alternative library could also yield higher affinity scFv, (such as a peptide library).

6.2 BOMBESIN PROJECT

6.2.1 *In Vivo* - Imaging

A critical evaluation of the *in vivo* data obtained raised concerns about its reproducibility and the value of the initial findings, causing difficulties with interpretation. It is therefore crucial to address these shortcomings.

6.2.2 Standardisation of Imaging Studies

Standardisation of the procedure is of upmost importance to reduce as much variation as possible. A study of the effects of Matrigel on [^{99m}Tc]-DB 4 uptake would be beneficial, covering a range of GRP-R-positive cell lines, as well as negative controls. Although Matrigel is commonly used in tumour formation, the uptake observed by Matrigel-assisted tumours was less than those produced without it. It would be important to determine whether this was indeed due to the Matrigel composition, or to over-growth of the tumour, resulting in cell death or senescence.

The pharmacokinetics of radiopharmaceutical uptake by tumours is particularly dependent on vascularity and tumour size. Experience within our laboratories has found that smaller tumours show proportionately greater uptake of radiolabelled peptides than larger ones, possibly due to their greater proportion of proliferating cells and better vascularisation. With increase in tumour size, regions of necrosis become common, and poor vascularisation has been seen within them [220]. An investigation to determine the

tumour size at which necrosis begins and vascularity deteriorates would be advantageous. Angiogenesis is a critical step in tumourigenesis which is necessary to supply the tissue with oxygen, nutrients and growth factors, as well as the delivery of the imaging radiopharmaceuticals used to diagnose such tumours. With this in mind, it would be advantageous to see whether any differences could be observed in the different stages of tumour growth.

A number of techniques can be utilised to measure vascularity, notably histology, Micro CT and ultrasound. Histological measurements of angiogenesis is a possible procedure to measure vascularity using microvessel density (MVD), a widely-employed measure of angiogenesis in pathological specimens and tumour models. Immunohistochemical procedures are used to stain for microvessels, and two methods to count the vessels are currently available; one which counts areas of high vascularity at low magnification, the 'hotspot' method, and another which involves counting randomly selected areas such as tumour edges [221].

Micro CT can visualise the detailed three-dimensional structure of the vascular system in any desired tissue. Although this technique is limited to vessels larger than 10 µm in diameter [222], it could provide a means of measuring vascularity in tumours, and even enable a comparison between Matrigel and non-Matrigel tumours. The contrasting agent Microfil® (Flowtech Inc, Carver, Massachusetts), a CT-dense casting medium which fills and opacifies blood vessels can be injected into perfused animals, which are then scanned for visualisation [223].

A third option would be to look at vascularisation using contrast-enhanced ultrasound (CEUS), which utilises microbubbles, a gas-filled contrast agent administered into the circulation. The high degree of echogenicity (reflection of ultrasound waves) of microbubbles into the surrounding soft tissue enhances the reflection of ultrasound waves, producing a sonogram. CEUS can therefore be used to image blood perfusion in organs, and even to measure blood flow rate [224].

6.2.3 Androgens and GRP-R expression

The preliminary results obtained from RT-PCR have opened up an area of investigation which would be interesting to pursue. Since the vast majority of patients receive hormonal therapy during the course of treatment for prostate cancer, it would be interesting to study the impact of hormonal ablation treatment on GRP-R expression, partly to extend our understanding of the disease, but mainly to reveal whether such patients would still be eligible for GRP-R-targeted imaging modalities. Therefore further investigation into the level of GRP-R expression, both *in vitro* and *in vivo,* after androgen manipulation would be of interest.

6.2.4 Phase I Clinical Trial

[^{99m}Tc]-DB 4 has entered a phase I clinical trial at St. Bartholomew's Hospital this year (2010), and the first PC patient assessment is imminent. The trial is to study the potential side-effects of [^{99m}Tc]-DB 4 and to assess its efficacy at imaging PC patients. The primary objectives are three-fold:

1. To assess the safety of [^{99m}Tc]-DB 4 in patients with PC
2. To assess the biodistribution of [^{99m}Tc]-DB 4 in these patients
3. To assess the pharmacokinetics of [^{99m}Tc]-DB 4 in these patients

As well as these objectives, the ability of [^{99m}Tc]-DB 4 to detect metastatic spread, and a comparison of the binding levels of [^{99m}Tc]-DB 4 with the levels of expression in GRP-R in prostate tumour samples and lymph node specimens will be undertaken.

Trial participants will receive a single injection of [^{99m}Tc]-DB 4 over 1 minute and will undergo imaging by SPECT, CT scan and/or MRI for up to 3 hours after infusion. Urine and blood samples will also be collected to determine how the radiopharmaceutical is processed within the body, and any tissue biopsy will be sent for immunohistochemistry.

7 REFERENCES

1. Litvinov, I.V., De Marzo, A.M., and Isaacs, J.T., Is the achilles' heel for prostate cancer therapy a gain of function in androgen receptor signalling? *Journal of Clinical Endocrinology & Metabolism*, 2003. **88**(7): 2972-2982.
2. Lang, S., Frame, F., and Collins, A., Prostate cancer stem cells. *Journal of Pathology*, 2009. **217**: 299-306.
3. Miki, J. and Rhim, J., Prostate cell cultures as *in vitro* models for the study of normal stem cells and cancer stem cells. *Prostate Cancer and Prostatic Diseases*, 2008. **11**: 32–39.
4. Bonkhoff, H., Neuroendocrine cells in benign and malignant prostate tissue: morphogenesis, proliferation and androgen receptor status. *Prostate*, 1998. **8**: 18-22.
5. Vis, A.N. and Schröder, F.H., Key targets of hormonal treatment of prostate cancer. Part 1: the androgen receptor and steroidogenic pathways. *British Journal of Urology International*, 2010. **104**: 438-448.
6. Grossmann, M.E., Huang, H., and Tindall, D.J., Androgen receptor signalling in androgen-refractory prostate cancer. *Journal of the National Cancer Institute*, 2001. **93**(22): 1687-1697.
7. Aragon-Ching, J.B., Williams, K.M., and Gulley, J.L., Impact of androgen-deprivation therapy on the immune system: implications for combination therapy of prostate cancer. *Frontiers in Bioscience*, 2007. **12**: 4957-4971.
8. Lindzey, J., V, K.M., Grossmann, M.E., Young, C., and Tindall, D.J., Molecular mechanisms of androgen action. *Vitamins and Hormones*, 1994. **49**: 383-432.
9. Feldman, B.J. and Feldman, D., The development of androgen - independent prostate cancer. *Nature Reviews Cancer*, 2001. **1**: 34-45.
10. Debes, J. and Tindall, D.J., Mechanisms of androgen-refractory prostate cancer. *New England Journal of Medicine*, 2004. **351**: 1488-1490.
11. Gao, J., Arnold, J., and Isaacs, J.T., Conversion from a paracrine to an autocrine mechanism of androgen-stimulated growth during malignant transformation of prostatic epithelial cells. *Cancer Research*, 2001. **61**: 5038–5044.
12. Isaacs, J.T. and Isaacs, W.B., Androgen receptor outwits prostate cancer drugs. *Nature Medicine*, 2004. **10**(1): 26-27.
13. Schalken, J.A., Molecular and cellular prostate biology: origin of prostate-specific antigen expression and implications for benign prostatic hyperplasia. *British Journal of Urology International*, 2004. **93**: 5-9.
14. http://vpo.orchid-cancer.org.uk/316/Facts-and-stats, *Facts and stats on prostate cancer*. 2009, Orchid - Fighting Male Cancer
15. http://info.cancerresearchuk.org/cancerstats/types/prostate/, *Cancer Stats - Key Facts - Prostate Cancer*, CRUK, Editor. 2009, CRUK.
16. McNeal, J.E., Zonal anatomy in the prostate. *Prostate*, 1981. **2**: 35-49.
17. Schulz, W.A., Burchardt, M., and Cronauer, M.V., Molecular biology of prostate cancer. *Molecular Human Reproduction*, 2003. **9**(8): 437-448.

18. Brawer, M.K., Prostatic intra-epithelial neoplasia: An overview. *Reviews in Urology*, 2005. **7**: 11-18.
19. Kamoi, K., Tronocoso, P., and Babaian, J., Strategy for the repeat biopsy in patients with high-grade prostatic intraepithelial neoplasia. *Journal of Urology*, 2000. **163**: 819–823.
20. Humphrey, P., Gleason grading and prognostic factors in carcinoma of the prostate. *Modern Pathology*, 2004. **17**: 292-306.
21. Lilja, H., Ulmert, D., and Vickers, A., Prostate-specific antigen and prostate cancer: prediction, detection and monitoring. *Cancer*, 2008. **8**: 268-278.
22. Makarov, D.V., Loeb, S., Getzenberg, R.H., and Partin, A.W., Biomarkers for prostate cancer *Annual Reviews of Medicine*, 2009. **60**: 139-151.
23. Stavridi, F., Karapanagiotou, E.M., and Syrigos, K.N., Targeted therapeutic approaches for hormone-refractory prostate cancer. *Cancer Treatment Reviews*, 2010. **In Press**.
24. Martinez, A.A., Gonzalez, J.A., Chung, A.K., Kestin, L.L., Balasubramaniam, M., Diokno, A., Ziaja, E.L., Brabbins, D.S., and Vicini, F.A., A comparison of external beam radiation therapy versus radical prostatectomy for patients with low risk prostate carcinoma diagnosed, staged and treated at a single institution. *Cancer*, 2000. **88**: 425-432.
25. Merrick, G.S., Butler, W.M., Tollenaar, B.G., Galbreath, R.W., and Lief, J.H., The dosimetry of prostate brachytherapy-induced urethral strictures. *International Journal of Radiation Oncology, Biology and Physics*, 2002. **52**: 461-468.
26. Burri, R., Stone, N., Unger, P., and Stock, R., Long-term outcome and toxicity of salvage brachytherapy for local failure after initial radiotherapy for prostate cancer. *International Journal of Radiation Oncology Biology and Physics*, 2009. **In Press**.
27. Ritch, C. and Katz, A., Prostate cryotherapy: current status. *Current Opinion in Urology*, 2009. **19**: 177–181.
28. Reese, M., Choice of hormonal therapy for prostate cancer. *Lancet*, 2000. **355**: 1474-1475.
29. So, A.I., Hurtado-Coll, A., and Gleave, M.E., Andogens and prostate cancer. *World Journal of Urology*, 2003. **21**: 325–337.
30. Labrie, F., Bélanger, A., Luu-The, V., Labrie, C., Simard, J., Cusan, L., Gomez, J., and Candas, B., Gonadotropin-releasing hormone agonists in the treatment of prostate cancer. *Endocrine reviews*, 2005. **26**: 361–379.
31. Knudsen, K. and Penning, T., Partners in crime: deregulation of AR activity and androgen synthesis in prostate cancer. *TRENDS in Endocrinology and Metabolism*, 2010. **In Press**.
32. Isaacs, J.T., The biology of hormone refractory prostate cancer: why does it develop? *Urologic Clinics of North America*, 1999. **26**: 263-273.
33. Schally, A., Comaru-Schally, A., Nagy, A., Kovacs, M., Szepeshazi, K., Plonowski, A., Varga, J., and Halmos, G., Hypothalamic hormones and cancer. *Neuroendocrinology*, 2001. **22**: 248-291.

34. Bonkhoff, H., Stein, U., and Remberger, K., Androgen receptor status in endocrine-paracrine cell types of the normal hyperplastic and neoplastic human prostate. *European Journal of Pathology*, 1993. **423**: 291-294.
35. Locke, J.A., Guns, E.S., Lubik, A.A., Adomat, H.H., Hendy, S.C., Wood, C.A., Ettinger, S.L., Gleave, M.E., and Nelson, C.C., Androgen levels increase by intra-tumoral *de novo* steroidogenesis during progression of castration-resistant prostate cancer. *Cancer Research*, 2008. **68**: 6407-6416.
36. Tannock, I., Wit, R., Berry, W., Horti, J., Pluzanska, A., Chi, K., Oudard, S., Théodore, C., James, N., Turesson, I., Rosenthal, M., and Eisenberger, M., Docetaxel plus Prednisone or Mitoxantrone plus Prednisone for Advanced Prostate Cancer. *New England Journal of Medicine*, 2004. **351**: 1502-1512.
37. Carter, P., Improving the efficacy of antibody-based cancer therapies. *Nature*, 2001. **1**: 118-129.
38. Tanaka, M., Kano, Y., Akutsu, M., Tsunda, S., Izumi, T., Yazawa, Y., Miyawki, S., Mano, H., and Furukawa, Y., The cytotoxic effects of gemtuzumab ozogamicin (Mylotarg) in combination with conventional antileukemic agents by isobologram analysis in vitro. *Anticancer Research*, 2009. **29**: 4589-4596
39. Zhanga, G., Zhanga, H., Wanga, Q., Lala, P., Carrolla, A.M., Llera-Moyab, M., Xua, X., and Greenea, M.I., Suppression of human prostate tumour growth by a unique prostate-specific monoclonal antibody F77 targeting a glycolipid marker. *Proceedings of the National Academy of Sciences*, 2010. **107**(2): 732–737.
40. Rajasekaran, A.K., Anilkumar, G., and Christiansen, J., Is prostate-specific membrane antigen a multifunctional protein? *American Journal Physiology - Cell Physiology*, 2005. **288**: 975-981.
41. Ghosh, A. and Heston, W.D.W., Tumour target prostate specific membrane antigen (PSMA) and its regulation in prostate cancer. *Journal of Cellular Biochemistry*, 2004. **91**: 528-539.
42. Davis, M.I., Bennett, M.J., Thomas, L.M., and Bjorkman, P.J., Crystal structure of prostate specific membrane antigen, a tumour marker and peptidase. *Proceedings of the National Academy of Sciences*, 2005. **102**: 5981-5986.
43. Fair, W.R., Israeli, R.S., and Heston, W., Prostate-specific membrane antigen. *Prostate*, 1997. **32**: 140-148.
44. Lui, H., Rajasekaran, A., Moy, P., Xia, Y., Kim, S., Navarro, V., Rahmati, R., and Bander, N., Constitutive and antibody-induced internalisation of prostate-specific membrane antigen. *Cancer Research*, 1998. **58**: 4055-4060.
45. Elsässer-Beile, U., Bühler, P., and Wolf, P., Targeted therapies for prostate cancer against the prostate-specific membrane antigen. *Current Drug Targets*, 2009. **8**: 118-125
46. Schulke, N., Varamova, O.A., Donovan, G.P., Ma, D., Gardner, J.P., Morrissey, D.M., Arrigale, R.R., Zhan, C., Chodera, A.J., Surowitz, K., Heston, W.D.W., and Olson, W.C., The homodimer of prostate-specific membrane antigen is a functional target for cancer therapy. *Proceedings of the National Academy of Sciences*, 2003. **100**(22): 12590-12595.
47. Tiffany, C., Lapidus, R., Calvin, D., and Slusher, B., Characterisation of the enzymatic activity of PSM:comparison with brain NAALADase. *Prostate*, 1999. **39**: 28-35.

48. Troyer, J., Beckett, M., and Wright, G., Detection and characterisation of the prostate-specific embrane antigen (PSMA) in tissue extracts and body fluids. *International Journal of Cancer*, 1995. **62**: 552-558.
49. Todorova, K., Ignatova, I., Tchakarov, S., Altankov, I., Zoubak, S., Kyurchiev, S., and Mincheff, M., Humoral immune response in prostate cancer patients after immunisation with gene-based vaccines that encode for a protein that is proteasomally degraded. *Cancer Immunity*, 2005. **5**(1-8).
50. Abdel-Aziz, A., Elgamal, M., Homes, E., Su, S.L., Tinto, W., Simmons, S., Peterson, M., Greene, T., Boynton, A., and Murphy, G., Prostate-specific membrane antigen (PSMA): current benefits and future value. *Seminars in surgical oncology*, 2000. **18**: 10-16.
51. Ross, J., Gray, K., Webb, I., Gray, G., Rolfe, M., Schenkein, D., Nanus, D.M., Millowsky, M., and Bander N, H., Correlation of primary tumour prostate-specific membrane antigen expression with disease recurrence in prostate cancer. *Clinical Cancer Research*, 2003. **9**: 6357-6362.
52. Tasch, J., Gong, M., Sadelain, M., and Heston, W.D., A unique folate hydrolase, prostate-specific membrane antigen (PSMA): a target for immunotherapy? *Critical Reviews in Immunology*, 2001. **21**: 249-261.
53. Sokoloff, R., Norton, K., Gasior, C., Marker, K., and Grauer, L.S., A dual-monoclonal sandwich assay for prostate-specific membrane antigen: levels in tissues, seminal fluid and urine. *Prostate*, 2000. **43**: 150-157.
54. Mannweiler, S., Amersdorfer, P., Trajanoski, S., Terrett, J., King, D., and Mehes, G., Heterogeneity of prostate-specific membrane antigen (PSMA) expression in prostate carcinoma with distant metastasis. *Pathology and Oncology Research*, 2009. **15**: 167–172.
55. Tagawa, S., Beltran, H., Vallabhajosula, S., Goldsmith, S.J., Osborne, J., Matulich, D., Petrillo, K., Parmar, S., Nanus, D.M., and Bander, N.H., Anti–prostate specific membrane antigen based radioimmunotherapy for prostate cancer. *Cancer*, 2010. **116**: 1075-1083.
56. Wolf, P., Alt, K., Bühler, P., Katzenwadel, A., Wetterauer, U., Tacke, M., and Elsässer-Beile, U., Anti-PSMA immunotoxin as novel treatment for prostate cancer? High and specific anti-tumour activity on human prostate xenograft tumours in SCID mice. *Prostate*, 2008. **68**: 129-138.
57. Chang, S., Reuter, V.E., Heston, W.D.W., Bander, N.H., Grauer, L.S., and Gaudin, P.B., Five different anti-prostate-specific membrane antigen (PSMA) antibodies confirm PSMA expression in tumour-associated neovasculature. *Cancer Research*, 1999. **59**: 3192–3198.
58. Wang, S., Diamond, D.L., Hass, M., Sokoloff, R., and Vessella, R.L., Identification of PSMA as the target of monoclonal antibody 107-1A4 by Proteinchip array, surface-enhanced laser desorption/ionization (SELDI) technology. *International Journal of Cancer*, 2001. **92**: 871-876.
59. Grauer, L.S., Lawler, K.D., Marignac, J.L., Kumar, A., Goel, A.S., and Wolfert, R.L., Identification, purification, and subcellular localisation of prostate-specific membrane antigen PSM' protein in the LNCaP prostatic carcinoma cell line. *Cancer Research*, 1998. **58**: 4787-4789.

60. Liu, H., Moy, P., Kim, S., Xia, Y., Rajasekaran, A., Navarro, V., Knudsen, B., and Bander, N.H., Monoclonal antibodies to the extracellular domain of prostate-specific membrane antigen also react with tumour vascular endothelium. *Cancer Research*, 1997. **57**: 3629-3634.
61. Bühler, P., Wolf, P., Gierschner, D., Schaber, I., Katzenwadel, A., Schultze-Seemann, W., Wetterauer, U., Tacke, M., Swamy, M., Schamel, W., and Elsässer-Beile, U., A bispecific diabody directed against prostate-specific membrane antigen and CD3 induces T-cell mediated lysis of prostate cancer cells. *Cancer Immunology and Immunotherapy*, 2008. **57**: 43–52.
62. Elsässer-Beile, U., Wolf, P., Gierschner, D., Bühler, P., Schultze-Seemann, W., and Wetterauer, U., A new generation of monoclonal and recombinant antibodies against cell-adherent prostate-specific membrane antigen for diagnostic and therapeutic targeting of prostate cancer. *Prostate*, 2006. **66**: 1359-1370.
63. Horoszewicz, J., Kawinski, E., and Murphy, G., Monoclonal antibodies to a new antigenic marker in epithelial prostatic cells and serum of prostatic cancer patients. *Anticancer Research*, 1987. **7**: 927-935.
64. Troyer, J., Feng, Q., Beckett, M., and Wright, G., Biochemical characterisation and mapping of the 7 E11-C5.3 epitope of the prostate-specific membrane antigen. *Urologic Oncology*, 1995. **9**: 29-37.
65. Haseman, M., Seth, A., Rosenthal, M., and Polascik, T., Capromab pendetide imaging of prostate cancer. *Cancer Biotherapy & Radiopharmaceuticals*, 2000. **15**: 131-140.
66. Wolf, P., Freudenberg, N., Bühler, P., Alt, K., Schultze-Seemann, W., Wetterauer, U., and Elsässer-Beile, U., Three conformational antibodies specific for different PSMA epitopes are promising diagnostic and therapeutic tools for prostate cancer. *Prostate*, 2009: Ahead of print.
67. Barren, R., Holmes, E., Boynton, A., Misrock, L., and Murphy, G., Monoclonal antibody 7E11.C5 staining of viable LNCaP cells. *Prostate*, 1997. **30**: 65-68.
68. Lui, H., Moy, P., Kim, S., Xia, Y., Rajasekaran, A., Navarro, V., Kundsen, B., and Bander N, H., Monoclonal antibodies to the extracellular domain of prostate-specific membrane antigen also react with tumour vascular endothelium. *Cancer Research*, 1997. **57**: 3629-3634.
69. Scott, A., Radioimmunotherapy of prostate cancer: Does tumour size matter? *Journal of Clinical Oncology*, 2005. **23**: 4567-4570.
70. Smith, P., Radiolabeled J591 antibody delivers lethal hit to advanced prostate cancers in a phase I trial. *Landes Bioscience*, 2004. **3**: 697 - 698.
71. Wolf, P., Gierschner, D., Bühler, P., Wetterauer, U., and Elsässer-Beile, U., A recombinant PSMA-specific single-chain immunotoxin has potent and selective toxicity against prostate cancer cells. *Cancer Immunology and Immunotherapy*, 2006. **55**: 367–1373.
72. Pollack, M., The role of exotoxin A in pseudomonas disease and immunity. *Reviews of Infectious Diseases*, 1983. **5**: 979-984.
73. Garetto, S., Sizzano, F., Brusa, D., Tizzani, A., Malavasi, F., and Matera, L., Binding of prostate-specifi c membrane antigen to dendritic cells: a critical step in vaccine preparation. *Cryotherapy*, 2009. **11**: 1090–1100.

74. Kiessling, A., Füssel, S., Wehner, R., Bachmann, M., Wirth, M., Rieber, P., and Schmitz, M., Advances in specific immunotherapy for prostate cancer. *European Urology*, 2008. **53**: 694–708.
75. Travers, P., Walport, M., and Shlomchik, M., *Janeway's Immuno Biology*. 7th Edition ed. 2007, New York: Garland Publishing.
76. Begent, R., Verhaar, M., Chester, K., Casey, J., Green, A., Napier, M., Hope-Stone, L., Cushen, N., Keep, P., Johnson, C., Hawkins, R., Hilson, A., and Robson, L., Clinical evidence of efficient tumour targeting based on single-chain Fv antibody selected from a combinatorial library. *Nature Medicine*, 1996. **2**: 979–984.
77. Chester, K. and Hawkins, R., Clinical issues of antibody design. *Trends in Biotechnology*, 1995. **13**: 294-301.
78. Clackson, T., hoogenboom, H., and Griffiths, A., Making antibody fragments using phage display libraries. *Nature*, 1991. **352**: 624-628.
79. Leyton, J., Olafsen, T., Lepin, E., Hahm, S., Bauer, K., Reiter, R., and Wu, A., Humanised radioiodinated minibody for imaging of prostate stem cell antigen-expressing tumours. *Clinical Cancer Research*, 2008. **14**: 7488-7496.
80. Smith, G.P., Filamentous fusion phage: novel expression vectors that display cloned antigens on the virion surface. *Science*, 1985. **228**: 1315-1317.
81. McCafferty, J., Griffiths, A.D., Winter, G., and Chiswell, D.J., Phage Antibodies: filamentous phage displaying antibody variable domains. *Nature*, 1990. **348**: 552-554.
82. Lowman, H.B., Bass, S.H., Simpson, N., and Wells, J.A., Selecting high-affinity binding proteins by monovalent phage display. *Biochemistry*, 1991. **30**: 10832-10838.
83. Azzazy, H. and Highsmith, E., Phage Display Technology: clinical applications and recent innovations. *Clinical Biochemistry*, 2002. **35**: 425-445.
84. Chester, K., Bhatia, J., Boxer, G., Cooke, S., Flynn, A., Huhalov, A., Mayer, A., Pedley, R., Robson, L., Sharma, S., Spencer, D., and Begent, R., Clinical applications of phage-derived scFvs and scFv fusion proteins. *Disease Markers*, 2000. **16**: 53–62.
85. Winter, G., Griffiths, A.D., Hawkins, R., and Hoogenboom, H.R., Making antibodies by phage display technology. *Annual Reviews Immunology*, 1994. **12**: 433-455.
86. Haard, H., Hendrikx, P., and Hoogenboom, H.R., Creating and engineering human antibodies for immunotherapy. *Advanced Drug Delivery Reviews*, 1998. **31**: 5-31.
87. Carmen, S. and Jermutus, L., Concepts in antibody phage display. *Briefings in Functional Genomics and Proteomics*, 2002. **1**(2): 189-203.
88. Nilsson, F., Tarli, L., Viti, F., and Neri, D., The use of phage display for the development of tumour targeting agents. *Advanced Drug Delivery Reviews*, 2000. **43**: 165-196.
89. Pini, A. and Bracci, L., Phage Display Antibody Fragments. *Current Protein and Peptide Science*, 2000. **1**: 155-169.
90. De wildt, R.M.T., Mundy, C.R., Gorick, B.D., and Tomlinson, I.M., Antibody arrays for high-throughput screening of antibody-antigen interactions. *Nature Biotechnology*, 2000. **18**: 989-993.
91. Griffiths, A.D. and Duncan, A.R., Strategies for selection of antibodies by phage display. *Current Opinion Biotechnology*, 1998. **9**: 102-108.

92. de-Haard, H., Neer, N., Reurs, A., Hufton, S., Roovers, R., Henderikx, P., de-Bruïne, A., Arends, J.-W., and Hoogenboom, H., A large non-immunised human Fab fragment phage library that permits rapid isolation and kinetic analysis of high affinity antibodies*. Journal of Biological Chemistry*, 1999. **274**: 18218–11823.
93. B, P.-S., Viswanathan, M., and Margolies , M., Selection of high affinity p-azophenyarsonate Fabs from heavy-chain CDR2 insertion libraries*. Immunological Methods*, 2002. **259**: 43-53.
94. Nissim, A., Hoogenboom, H.R., Tomlinson, I.M., Flynn, G., Midgley, C., Lane, D., and Winter, G., Antibody fragments from a 'single pot' phage display library as immunochemical reagents*. EMBO Journal*, 1994. **13**(3): 692-698.
95. Griffiths, A.D., Williams, S., Hartley, O., Alison, T., Tomlinson, I., Waterhouse, P., Crosbyl, W., Kontermann, R., Jones, P., Low, N., Allison, J., Prospero, T., Hoogenboom, H., Nissim, A., Cox, J., Harrison, J., Zaccolo, M., Gherardi, E., and Winter, G., Isolation of high affinity human antibodies directly from large synthetic repertoires*. EMBO Journal*, 1994. **13**: 3245-3260.
96. *Antibody phage display - methods and protocols*. Methods in molecular biology, ed. O'Brien, P. and Aitken, R. Vol. 178. 2008, Totowa, New Jersey: Humana Press.
97. Sanz, I., Multiple mechanisms participate in the generation of diversity of human H chain CDR3 regions*. Journal of Immunology*, 1991. **147**: 1720-1729.
98. Raaphorst, F., Raman, C., Tami, J., Fischbach, M., and Sanz, I., Human Ig heavy chain CDR3 regions in adult bone marrow pre-B cells display an adult phenotype of diversity: evidence for structural selection of DH amino acid sequences*. International Immunology*, 1997. **10**: 1503–1515.
99. Neuberger, M., Sale, J., Cumbers, S., Jolly, C., Bemark, M., Ehrenstein, M., Lanoue, A., Bruggemann, M., Batista, D., Davies, S., and Williams, G., Diversification and selection mechanisms for the production of protein repertoires:lessons for the immune system*. Applied Biochemical Biotechnology*, 2000. **83**: 53-60.
100. Xu, C., Lo, A., Yammanuru, A., Tallarico, A., Brady, K., Murakami, A., Barteneva, N., Zhu, Q., and Marasc, W.A., Unique biological properties of catalytic domain directed human anti-CAIX antibodies discovered through phage-display technology*. Plos One*, 2010. **5**(3): 9625-9638.
101. Conrad, F., Zhu, X., Zhang, X., Chalkley, R.J., Burlingame, A.L., Marks, J.D., and Liu, B., Human antibodies targeting cell surface antigens overexpressed by the hormone refractory metastatic prostate cancer cells: ICAM-1 is a tumor antigen that mediates prostate cancer cell invasion*. Journal of Molecular Medicine*, 2009. **87**: 507–514.
102. Liu, B., Conrad, F., Roth, A., Drummond, D., Simko, J., and Marks, J., Recombinant full-length human IgG1s targeting hormone-refractory prostate cancer*. Journal of Molecular Medicine*, 2007. **85**(10): 1113-1123.
103. Wu, A.M. and Senter, P.D., Arming antibodies: prospects and challenges for immunoconjugates*. Nature Biotechnology*, 2005. **23**(9): 1137-1147.
104. Reubi, J.C., Neuropeptide receptors in health and disease: the molecular basis for *in vivo* imaging*. Journal of Nuclear Medicine*, 1995. **36**: 1825-1835.
105. Kwekkeboom, D., Kam, B., Essen, M., Teunissen, J., Eijck, C., Valkema, R., Jong, M.d., Herder, W., and Krenning, E., Somatostatin receptor-based imaging and

therapy of gastroenteropancreatic neuroendocrine tumours. *Endocrine related Cancer*, 2010. **In Press**.

106. Prasad, V. and Baum, P., Biodistribution of ^{68}Ga labelled somatostatin analogue DOTA-NOC in patients with neuroendocrine tumours: charaterisation of uptake in normal and tumour lesions. *Journal of Nuclear Medicine and Imaging*, 2010. **54**: 61-68.
107. Jong, M., Breeman, W., Kwekkeboom, D., Valkema, R., and Krenning, E., Tumor imaging and therapy using radiolabeled somatostatin analogues. *Accounts of Chemical Research*, 2009. **42**(7): 873-880.
108. Ozker, K., Hellman, R., and Krasnow, A., Preparation of ^{99m}Tc labelled substance P (SP). *Applied Radiation and Isotopes*, 2002. **57**: 729–732.
109. Collado, B., Carmena, M., Sanchez-Chapado, M., Ruiz-Villaespesa, A., Bajo, A., Fernandez-Martinez, A., Varga, J., Schally, A., and Prieto, J., Expression of vasoactive intestinal peptide and functional VIP receptors in human prostate cancer: antagonistic action of a growth-hormone-releasing hormone analogue. *International Journal of Oncology*, (2005) **26**: 1629–1635.
110. Collado, B., Carmena, M., Clemente, C., Prieto, J., and Bajo, A., Vasoactive intestinal peptide enhances growth and angiogenesis of human experimental prostate cancer in a xenograft model. *Peptides*, 2007. **28**: 1 8 96 – 91 90 91.
111. Sastry, K., Smith, A., Karpova, Y., Datta, S., and Kulik, G., Diverse antiapoptotic signaling pathways activated by VIP, EGF and PI3K in prostate cancer cells converge on BAD. *Journal of Biological Chemistry*, 2006. **281**: 20891–20901.
112. Xie, Y., Wolff, D., Lin, M.-F., and Tu, Y., Vasoactive intestinal peptide transactivates the androgen receptor through a protein kinase A-dependent extracellular signal-regulated kinase pathway in prostate cancer LNCaP cells. *Molecular Pharmacology*, 2007. **72**(1): 73–85.
113. Rekasi, Z., Varga, J., Schally, A., Halmos, G., Armatis, P., Groot, K., and Czompoly, T., Antagonists of growth hormone-releasing hormone and vasoactive intestinal peptide inhibit tumour proliferation by different mechanisms: evidence from *in vitro* studies on human prostatic and pancreatic cancers. *Endocrinology*, 1999. **141**(6): 2120-2029.
114. Reubi, J.C., Waser, B., Friess, H., Büchler, M., and Laissue, J., Neurotensin receptors: a new marker for human ductal pancreatic adenocarcinoma. *Gut*, 1998. **42**: 546–550.
115. Reubi, J.C. and Waser, B., Unexpected high incidence of cholecystokinin-B/gastrin receptors in human medullary thyroid carcinomas. *International Journal of Cancer*, 1996. **67**(5): 644-670.
116. Nock, B., Nikolopoulou, A., Galanis, A., Cordopatis, P., Waser, B., Reubi, J.C., and Maina, T., Potent bombesin-like peptides for GRP-receptor targeting of tumours with ^{99m}Tc: a preclinical study. *Journal of Medical Chemistry*, 2005. **48**: 100-110.
117. Wesley, K., Sheffler, D., and Roth, B., G-protein-coupled receptors at a glance. *Journal of Cell Science*, 2003. **116**: 4867-4869.
118. Markwalder, R. and Reubi, J.C., Gastrin-releasing peptide receptors in the human prostate: relation to neoplastic transformation. *Cancer Research*, 1999. **59**: 1152-1159.

119. Flores, D.G., Lenz, G., Roesler, R., and Schwartsmann, G., Gastrin-releasing peptide receptor signalling in cancer. *Cancer Therapy*, 2009. **7**: 332-346.
120. Jensen, R., Moody, T., Pert, C., Rivier, J., and Gardner, J., Interaction of bombesin and litorin with specific membrane receptors on pancreatic acinar cells. *Proceedings of the National Academy of Sciences USA*, 1978. **75**: 6239–6243.
121. Preston, S., Miller, G., and Primrose, J., Bombesin-like peptides and cancer. *Critical Reviews in Oncology and Haematology,*, 1996. **23**: 225-238.
122. Nagakawa, O., Ogasawara, M., Fujii, H., Murakami, K., Murata, J., Fuse, H., and Saiki, I., Effect of prostatic neuropeptides on invasion and migration of PC-3 prostate cancer cells. *Cancer Letters*, 1998. **133**: 27-33.
123. Gugger, M. and Reubi, J.C., Gastrin-releasing peptide receptors in non-neoplastic and neoplastic human breast. *American Society for Investigative Pathology*, 1999. **155**: 2067-2076.
124. Cornelio, D., Roesler, R., and Schwartsmann, G., Gastrin-releasing peptide receptor as a molecular target in experimental anticancer therapy. *Annals of Oncology*, 2007. **18**: 1457-1466.
125. Preston, S., Miller, G., and Primrose, J., Bombesin-like peptides and cancer. *Clinical Reviews in Oncology and Hematology*, 1996. **23**: 255-238.
126. Carney, D., Cuttita, F., Moody, T., and Minna, J., Bombesin-like peptides can function as autocrine growth factors in human small-cell lung cancer. *Nature*, 1985. **316**: 823-826.
127. Plonowski, A., Schally, A., Varga, J., Rekasi, Z., Hebert, F., Halmos, G., and Groot, K., Potentiation of the inhibitory effect of growth hormone-releasing hormone antagonists on PC-3 human prostate cancer by bombesin antagonists indicative of interference with both IGF and EGF pathways. *Prostate*, 2000. **44**: 172–180.
128. Erspamer, V., Discovery, isolation, and characterisation of bombesin-like peptides. *Annais' New York Academy of Sciences*, 1988. **547**: 3-9.
129. Scott, N., Millward, E., Cartwright, E., Preston, S., and Coletta, P., Gastrin releasing peptide and gastrin releasing peptide receptor expression in gastrointestinal carcinoid tumours. *Journal of Clinical Pathology*, 2004. **57**: 189–192.
130. Van de Wiele, C., Dumont, F., Broecke, V., Oosterlinck, W., Cocquyt, V., Serreyn, R., Peers, S., Thornback, J., Slegers, G., and Dierckx, R., ^{99m}Technetium RP527, a GRP analogue for visualisation of GRP receptor-expressing malignancies: a feasibility study. *European Journal of Nuclear Medicine*, 2000. **27**: 1694-1699.
131. Hoffman, T., Gali, H., Smith, J., Sieckman, G., Hayes, D., Owen, N., and Volkert, W., Novel series of ^{111}In-labelled bombesin analogs as potential radiopharmaceuticals for specific targeting of gastrin-releasing peptide receptors expressed on human prostate cancer cells. *Journal of Nuclear Medicine*, 2003. **44**: 823-831.
132. Smith, C., Volkert, W., and Hoffman, T., Gastrin releasing peptide (GRP) receptor targeted radiopharmaceuticals: A concise update. *Nuclear Medicine and Biology*, 2003 **30**: 861–868.
133. Nock, B., Nikolopoulou, A., Chiotellis, E., Loudos, G., Maintas, D., Reubi, J.C., and Maina, T., [^{99m}Tc] Demobesin 1, a novel potent bombesin analogue for GRP receptor-targeted tumour imaging. *European Journal of Nuclear Medicine and Molecular Imaging*, 2003. **30**: 247-259.

134. Schroeder, R., Müller, C., Reneman, S., Melis, M., Breeman, W., Blois, E., Bangma, C., Krenning, E., Weerden, W., and Jong, M.d., A standardised study to compare prostate cancer targeting efficacy of five radiolabelled bombesin analogues. *European Journal of Nuclear Medicine Molecular Imaging*, 2010 **In press**.
135. Maddalena, M., Fox, J., Chen, J., Feng, W., Cagnolini, A., Linder, K., Tweedle, M., Nunn, A., and Lantry, L., ^{177}Lu-AMBA biodistribution, radiotherapeutic efficacy, imaging, and autoradiography in prostate cancer models with low GRP-R expression. *Journal of Nuclear Medicine*, 2009. **50**: 2017–2024.
136. Schroeder, J., Weerden, W., Bangma, C., Krenning, E., and Jong, M., Peptide receptor imaging of prostate cancer with radiolabelled bombesin analogues. *Methods*, 2009. **48**: 200–204.
137. Britton, K., Towards the goal of cancer-specific imaging and therapy. *Nuclear Medicine Communications*, 1997. **18**(11): 992-1007.
138. Hosseinimehr, S., Potential utility of radioprotective agents in the practice of nuclear medicine. *Cancer Biotherapy & Radiopharmaceuticals*, 2009. **24** 723-733.
139. Liu, S. and Edwards, S., [^{99m}Tc]-labeled small peptides as diagnostic radiopharmaceuticals. *Chemical Review*, 1999. **99**(9): 2235-2268.
140. Josephs, D., Spicer, J., and O'Doherty, M., Molecular imaging in clinical trials. *Target Oncology*, 2009. **4**: 151–168.
141. Long-Huaa, Q., Qina, X., Wen-Taob, Y., Fenga, T., Kun-Weic, S., and Wu Bina, G.Y.-J., Diffusion-weighted MRI evaluation of breast cancer extension. *Cancer Imaging*, 2009. **34**: 89–96.
142. Wen, Z., Hu, S., Huang, F., Wang, X., Guo, L., Quan, X., Wang, S., and Zhou, J., MR Imaging of high-grade brain tumors using endogenous protein and peptide-based contrast. *Neuro Image*, 2009. **In Press**.
143. Halpern, E., Contrast-enhanced ultrasound imaging of prostate cancer. *Reviews in Urology*, 2006. **8**: 29-37.
144. Mather, S.J., *Radiolabelled antibodies and peptides*. Third Edition ed. Textbook of Radiopharmacy, ed. Sampson, C.B. 1999: Gordon and Breach Science Publishers.
145. Nair, V., Krupitskaya, Y., and Gould, M., Positron emission tomography ^{18}F-Fluorodeoxyglucose uptake and prognosis in patients with surgically treated, stage I non-small cell lung cancer. *Journal of Thoracic Oncology*, 2009. **4**: 1473-1480.
146. Brassell, S., Rosner, I., and McLeod, D., Update on magnetic resonance imaging, ProstaScint, and novel imaging in prostate cancer. *Current Opinion in Urology*, 2005. **15**: 163–166.
147. Hustinx, R. and Lucignani, G., PET/CT in head and neck cancer: an update. *European Journal of Nuclear Medicine*, 2010. **37**: 645–651.
148. Mariani, G., Bruselli, L., Kuwert, T., Kim, E.E., Flotats, A., Israel, O., Dondi, M., and Watanabe, N., A review on the clinical uses of SPECT/CT. *European Journal of Nuclear Medicine*, 2010. **In press**.
149. Kazumasa, I., Tani, K., Umeda, I., Yamaguchi, M., Mutou, Y., Fukushi, M., and Fujii, H., *Evaluation of SPECT-CT performance for optimal small animal imaging*, in *World Molecular Imaging Congress*. 2008, www.spect-ct.com.

150. Mather, S., Sosabowski, J., Finucane, C., Foster, J., King, R., Vassaux, G., and Garrood, T., *High resolution, small animal SPECT-CT imaging as a tool in preclinical development*. 2009, www.spect-ct.com.
151. Wilbur, D., radiohalogenation of proteins: an overview of radionuclides, Labelling methods, and reagents for conjugate labelling. *Bioconjugate Chemistry*, 1992. **3**(6): 433-470.
152. Bakker, W., Krenning, E., Breeman, W., Koper, J., Kooij, P., Reubi, J.C., Klijn, J., Visser, T., Docter, R., and Lamberts, S., Receptor scintigraphy with a radioiodinated somatostatin analogue: radiolabeling, purification, biological activity, and *in vivo* application in animals. *Journal of Nuclear Medicine*, 1990. **31**(9): 1501-1509.
153. Hunter, W. and Greenwood, F., Preparation of Iodine-131 labelled human growth hormone of high specfic activity. *Nature*, 1962. **194**: 495.
154. Fraker, P. and Speck, J., Protein and cell membrane iodinations with a sparingly soluble chloroamide 1,3,4,6-tetrchloro, 3a, 6a diphenylglycouril. *Biochemical and Biophysical Research Communications*, 1978. **80**: 849.
155. Liu, S., Edwards, S., and Barrett, J.A., ^{99m}Tc labeling of highly potent small peptides. *Bioconjugate Chemistry*, 1997. **8**: 621-636.
156. *Tc-99m Pharmaceuticals: Preparation and quality control in Nuclear Medicine*, ed. Zolle, I. 2007, Berlin: Springer.
157. Vigna, S., Giraud, A., Reeve, J., and J, W., Biological activity of oxidised and reduced iodinated bombesins. *Peptides*, 1988. **9**: 923-926.
158. Novak-Hofer, I., Waibel, R., Zimmermann, K., Schibli, R., Grunberg, J., Chester, K., Murray, A., Lo, B., Perkins, A., and Schubiger, P., *Radiometal labelling of antibodies and antibody fragments for imaging and therapy*. Methods in Molecular Biology, ed. Lo, B. Vol. 248. 2008, Totowa: Humana Press Inc.
159. Waibel, R., Alberto, R., Willuda, J., Finnern, R., Schibli, R., Stichelberger, A., Egli, A., Abram, U., Mach, J., Pluckthun, A., and Schubiger, P., Stable one-step technetium-99m labelling of His-tagged recominant proteins with a novel Tc(I)-carbonyl complex. *Nature Biotechnology*, 1999. **17**: 897-901.
160. Rao, T., Adhikesavalu, D., Cainennan, A., and Fritzberg, A., Technefium (V) and rhenium (V) complexes of 2,3-bis(mercaptoacetamidpor)opanoate chelate ring stereochemistry and influence on chemical and biological properties. *Journal American Chemical Society*, 1990. **112**: 5798-5804.
161. Fritzberg, A., Abrams, P., and Beaumier, P.L., Specific and stable labeling of antibodies with technetium-99m with a diamidedithiolate chelating agent. *Proceedings of the National Academy of Sciences*, 1988. **85**: 4025-4029.
162. Jurisson, S., Pirrot, J., Dircocco, R., Rosenspire, K., Jagoda, E., Nanjappan, P., Eckelmant, W., Nowotnikii, D., and Nunn, A., Boronic acid adducts of technetium dioxime (BATO) complexes derived from quinuclidine benzilate (QNB) boronic acid stereoisomers: syntheses and studies of their binding to the muscarinic acetylcholine receptor. *Nuclear Medicine and Biology*, 1995. **22**(3): 269-281.
163. Liu, S., Edwards, S., Looby, R., Harris, A., Poirier, M., Barrett, J., Heminway, S., and Carroll, T., Labeling a hydrazino nicotinamide-modified cyclic IIb/IIIa receptor antagonist with ^{99m}Tc using aminocarboxylates as coligands. *Bioconjugate Chemistry*, 1996. **7**(1): 63–71.

164. Fischman, A., Babich, J., and Strauss, W., A ticket to ride: peptide radiopharmaceuticals. *Journal of Nuclear Medicine*, 1993. **34**: 2253-2263.
165. Murphy, C., Piwnica-Worms, H., Grunwald, S., Romanow, W., Francis, N., and Hua-Ying, F., Overview of the baculovirus expression system. *Current Protocols in Molecular Biology*, 2004: 169-179.
166. Tomlinson, I.M., Walter, G., Marks, J.D., Llewelyn, M.B., and Winter, G., The repertoire of human germline V_H sequences reveals about fifty groups of V_H segments with different hypervariable loops. *Journal of Molecular Biology*, 1992. **227**: 776-798.
167. Barkhordarian, H., Emadi, S., Schulz, P., and Sierks, M.R., Isolating recombinant antibodies against specific protein morphologies using atomic force microscopy and phage display technologies. *Protein Engineering, Design & Selection*, 2006. **19**: 497–502.
168. Neu, H.C. and Heppel, L.A., The release of enzymes from *E. coli* by osmotic shock and during the formation of spheroplasts. *The Journal of Biological Chemistry*, 1965. **240**: 3685-3692.
169. Roben, P.W., Aram, S.N., and Silverman, G.J., VH_3 family antibodies bind domain D of staphylococcal protein A. *The Journal of Immunology*, 1995. **154**: 6437-6445.
170. Casey, J., Keep, P., Chester, K., Robson, L., Hawkins, R., and Begent, R., Purification of bacterially expressed single chain Fv antibodies for clinical applications using metal chelate chromatography. *Journal of Immunological Methods*, 1995. **179**: 105-116.
171. Givan, A., L, *Flow cytometry: first principles*. 1st ed. 1992, New York: Wiley-Liss.
172. Mather, S.J., *Chapter 6: radiolabelled antibodies and peptides*. 3rd Edition ed. Textbook of Radiopharmacy, Theory and Practice, ed. Sampson, C. 1999, Amsterdam: Gordon and Breach Science Publishers: 63-82.
173. Shaw, G. and Prowse, D., Inhibition of androgen-independent prostate cancer cell growth is enhanced by combination therapy targeting Hedgehog ErbB signalling. *Cancer Cell International*, 2009. **8**: 3-14.
174. Dawson, R.M.C., Elliott, E.C., Elliott, W.H., and Jones, K.M., *Data for Biochemical Research*, ed. 3rd. 1986, Oxford Science Publications: 541 - 542.
175. Kumada, Y., Kawasaki, T., Kikuchi, Y., and Katoh, S., Polypeptide linkers suitable for the efficient production of dimeric scFv *Escherichia coli. Biochemical Engineering Journal*, 2007. **35**: 158-165.
176. Plückthun, A. and Pack, P., New protein engineering approaches to multivalent and bispecific antibody fragments. . *Immunotechnology*, 1997. **2**: 83-105.
177. Kent, U.M., *Purification of antibodies using protein A-sepharose and FPLC* Immunocytochemical Methods and Protocols Methods in Molecular Biology, ed. Javois, L.C. Vol. 34. 2008, London: Humana Press: 37-41.
178. Harrison, J., Williams, S.C., Winter, G., and Nissim, A., Screening of phage antibody libraries. *Methods in Enzymology*, 1996. **267**: 83-109.
179. Bellis, D.D. and Schwartz, I., Regulated expression of foreign genes fused to lac: control by glucose levels in growth mediumNucleic Acids Res. 1990. **18**: 1311.
180. Hudson, P.J. and Kortt, A.A., High avidity scFv multimers; diabodies and triabodies. *Journal of Immunological Methods*, 1999. **231**: 177-189.

181. Schiweck, W., Buxbaum, B., Schaëtzlein, C., Neiss, H.G., and Skerra, A., Sequence analysis and bacterial production of the anti-c-myc antibody 9E10: the VH domain has an extended CDR-H3 and exhibits unusual solubility. *FEBS Letters*, 1997. **414**: 33-38.
182. Kaufmann, M., Lindner, P., Honegger, A., Blank, K., Tschopp, M., Capitani, G., Plückthun, A., and Grütter, M.G., Crystal Structure of the Anti-His Tag Antibody 3D5 Single-chain Fragment Complexed to its Antigen. *J. Mol. Biol*, 2002. **318**: 135-147.
183. Kortt, A., Dolezal, O., Power, B., and Hudson, P., Dimeric and trimeric antibodies: high avidity scFvs for cancer targeting. *Biomolecular Engineering*, 2001. **18**: 95-108.
184. Holliger, P. and Winter, G., Diabodies: small bispecific antibody fragments. *Cancer Immunol Immunother*, 1997. **45**: 128 - 130.
185. Grasshoffa, C., Thiermanna, H., Gillessena, T., Zilkerb, T., and Szinicza, L., Internal standard high-performance liquid chromatography method for the determination of obidoxime in urine of organophosphatepoisoned patients. *Journal of Chromatography B*, 2001. **753**: 203–208.
186. Creighton, T.E., *Protein Function: A Practical Approach*. 2nd ed, ed. Hames, B.D. 1997, Oxford: Oxford University Press.
187. Gooding, K. and Regnier, F., *HPLC of biological macromolecules*. 2nd ed. Chromatographic Science Series ed. Vol. 87. 2002, New York.
188. Bonner, P., *Protein purification, the basics*, ed. Owen, E. 2007, New York: Taylor and Francis Group.
189. Mather, S.J., McKenzie, A., Sosabowski, J., Morris, T., Ellison, D., and Watson, S., Selection of radiolabelled gastrin analogues for peptide receptor–targeted radionuclide therapy. *Journal of Nuclear Medicine*, 2007. **48**: 615-622.
190. Jong, M., Rolleman, E.J., Bernard, B.F., Visser, T.J., Bakker, W.H., Breeman, W.A.P., and Krenning, E.P., Inhibition of renal uptake of [^{111}Indium]-DTPA Octreotide *in vivo. Journal of Nuclear Medicine*, 1996. **37**: 1388-1392.
191. Motulsky, H. and Christopoulos, A., *Fitting models to biological data using linear and nonlinear regression - A practical guide to curve fitting*. Graphpad Prism. 2003, San Diego CA: Graphpad Software Inc.: 351.
192. Singh, P., Draviam, E., Guo, Y., and Kurosky, A., Molecular characterisation of bombesin receptors on rat pancreatic acinar AR42J cells. *AJP - Gastrointestinal and Liver Physiology*, 1990. **258**(5): 803-809.
193. Motta, M., Dondi, D., Moretti, R.M., Marelli, M.M., Pimpinelli, F., Maggi, R., and Limonta, P., Role of growth factors, steroid and peptide hormones in the regulation of human prostatic tumour growth. *The Journal of Steroid Biochemistry and Molecular Biology*, 1996. **56**: 107-111.
194. Esquenet, M., Swinnen, J.V., Heyns, W., and Verhoeven, G., LNCaP prostatic adenocarcinoma cells derived from low and high passage numbers display divergent responses not only to androgens but also to retinoids *The Journal of Steroid Biochemistry and Molecular Biology*, 1997. **62**(5-6): 391-399
195. La Bella, R., Garcia-Garayoa, E., Bähler, M., Bläuenstein, P., Schibli, R., Conrath, P., Tourwé, D., and Schubiger, P., A ^{99m}Tc(I)-postlabeled high affinity bombesin

analogue as a potential tumour imaging agent. *Bioconjugate Chemistry*, 2002. **13**: 599-604.

196. Smith, C., Volkert, W., and Hoffman, T., Radiolabelled peptide conjugates for targeting of the bombesin receptor superfamily subtypes. *Nuclear Medicine and Biology*, 2005. **32**: 733-740.
197. Zhang, J., Xiang, J.-Q., Zhang, Y.-W., Chen, Y.-Y., Zhou, X.-Y., Liu, Y., and Li, S., Cell adhesion regulates expression of the androgen receptor and coregulators in different prostate cancer cells. *International Journal of Molecular Sciences*, 2007. **8**: 156-165.
198. Liu, A., Brubaker, K., Goo, Y., Quinn, J., Kral, S., Sorensen, C., Vessella, R., Belldegrun, A., and Hood, L., Lineage relationship between LNCaP and LNCaP-derived prostate cancer cell lines. *Prostate*, 2004. **60**: 98-108.
199. Tilley, W., Wilson, C., Marcelli, M., and McPhaul, M., Androgen receptor gene expression in human prostate carcinoma cell lines. *Cancer Research*, 1990. **50**: 5382-5386.
200. Tilley, W., Bentel, J., Aspinall, J., Hall, R., and Horsfall, D., Evidence for a novel mechanism of androgen resistance in the human prostate cancer cell line, PC3. *Steroids*, 1995. **60**: 180–186.
201. Alimiraha, F., Chena, J., Basrawalab, Z., Xina, H., and Choubey, D., DU145 and PC-3 human prostate cancer cell lines express androgen receptor: Implications for the androgen receptor functions and regulation. *FEBS Letters*, 2006. **580**: 2294–2300.
202. Visser, M.d., Weerden, W.v., Ridder, C., Reneman, S., Melis, M., Krenning, R., and Jong, M.d., Androgen-dependent expression of the gastrin-releasing peptide receptor in human prostate tumour xenografts. *Journal of Nuclear Medicine*, 2007. **48**: 88-93.
203. Weerden, W. and Romijn, J., Use of nude mouse xenograft models in prostate cancer research. *Prostate*, 2000. **43**: 263-271.
204. Aprikian, A., Han, K., Chevalier, S., Bazinet, M., and Viallet, J., Bombesin specifically induces intracellular calcium mobilisation via gastrin-releasing peptide receptors in human prostate cancer cells. *Journal of Molecular Endocrinology*, 1996. **16**: 297-306.
205. Bologna, M., Festuccia, C., Muzi, P., Biordi, L., and Ciomei, M., Bombesin stimulates growth of human prostatic cancer cells *in vitro. Cancer*, 1989. **63**: 1714–1720.
206. Cescato, R., Maina, T., Nock, B., Nikolopoulou, A., Charalambidis, D., Piccand, V., and Reubi, J.C., Bombesin receptor antagonists may be preferable to agonists for tumour targeting. *Journal of Nuclear Medicine*, 2008. **49**: 318-326.
207. Greiner, M. and Zimmermann, R., *Real-time analysis of LNCaP cell growth in different media*. 2009, www.Bionity.com.
208. Bevan, C., Androgen receptor in prostate cancer: cause or cure? *TRENDS in Endocrinology and Metabolism*, 2005. **16**: 395-397.
209. Bektic, J., Berger, A.P., Pfeil, K., Dobler, G., Bartsch, G., and Klocker, H., Androgen receptor regulation by physiological concentrations of the isoflavonoid genistein in androgen-dependent LNCaP cells is mediated by estrogen receptor β. *European Urology*, 2004. **45**: 245–251.

210. Sotomayor, S., Muñoz-Moreno, L., Carmena, M.J., Schally, A.V., Sánchez-Chapado, M., Prieto, J.C., and Bajo, A.M., Regulation of HER expression and transactivation in human prostate cancer cells by a targeted cytotoxic bombesin analogue (AN-215) and a bombesin antagonist (RC-3095). *International Journal of Cancer*, 2010. **In Press**.
211. Schroeder, R., Visser, M., Weerden, W., Ridder, C., Reneman, S., Melis, M., Breeman, W., Krenning, E.P., and Jong, M., Androgen-regulated gastrin-releasing peptide receptor expression in androgen-dependent human prostate tumour xenografts. *International Journal of Cancer*, 2009. **In press**.
212. Schulz, S., Röcken, C., and Schulz, S., Immunohistochemical detection of bombesin receptor subtypes GRP-R and BRS-3 in human tumors using novel antipeptide antibodies. *Virchows Archive*, 2006. **449**: 421–427.
213. Carroll, R.E., Matkowskyj, K.A., Chakrabarti, S., McDonald, T.J., and Benya, R.V., Aberrant expression of gastrin-releasing peptide and its receptor by well-differentiated colon cancers in humans. *American Journal Physiology*, 1999. **276**: G655–665.
214. Wiele, C.V.d., Phonteyne, P., Pauwels, P., Goethals, I., Broecke, R.V.d., Cocquyt, V., and Dierckx, R.A., Gastrin-releasing peptide receptor imaging in human breast carcinoma versus immunohistochemistry. *Journal of Nuclear Medicine*, 2008. **49**: 260–264.
215. Mather, S., Molecular Imaging with Bioconjugates in Mouse Models of Cancer. *Bioconjugate Chemistry*, 2009. **20**(4): 631-644.
216. Xiaoa, D., Wanga, J., Hamptonb, L., and Weber, C., The human gastrin-releasing peptide receptor gene structure, its tissue expression and promoter. *Gene*, 2001. **264**(1): 95-103
217. Giovannucci, E., Nutritional factors in human cancers. *Advanced Experimental Medicine and Biology*, 1999. **472**: 29-42.
218. Yuan, Q., Wang, Z., Nian, S., Yin, Y., Chen, G., and Xia, Y., Screening of high-affinity scFvs from a ribosome displayed library using BIAcore biosensor. *Applied Biochemical Biotechnology*, 2009 **152**: 224-234.
219. Leonard, P., Säfsten, P., Hearty, S., McDonnell, B., Finlay, W., and O'Kennedy, R., High throughput ranking of recombinant avian scFv antibody fragments from crude lysates using the Biacore A100. *Journal of Immunological Methods*, 2007. **323**: 172-179.
220. Harrington, K., Rowlinson-Busza, G., Syrigos, K., Abra, R., Uster, P., Peters, A., and Stewart, J., Influence of tumour size on uptake of [^{111}In]-DTPA-labelled pegylated liposomes in a human tumour xenograft model. *British Journal of Cancer*, 2000. **83**: 684–688.
221. Goddard, J., Sutton, C., Furness, P., Kockelbergh, R., and O'Byrne, K., A computer image analysis system for microvessel density measurement in solid tumours. *Angiogenesis*, 2002. **5**: 15–20.
222. Marxen, M., Thornton, M.M., Chiarot, C.B., Klement, G., Koprivnikar, J., Sled, J.G., and Henkelman, M., MicroCT scanner performance and considerations for vascular specimen imaging. *Medical Physics*, 2004. **31**: 305-313.

223. Goodale, K.R., *Microfil compounds*, in *Flowtech Incorporated*. 1999, www.flowtech-inc.com.
224. Ellegala, D., Leong-Poi, H., Carpenter, J.E., Klibanov, A.L., Kaul, S., Shaffrey, M.E., Sklenar, J., and Lindner, J.R., Imaging tumour angiogenesis with contrast ultrasound and microbubbles targeted to αvβ3. *Circulation*, 2003. **108**: 336-341.

8 APPENDICIES

VECTOR MAP AND SEQUENCE OF pIT2 VECTOR

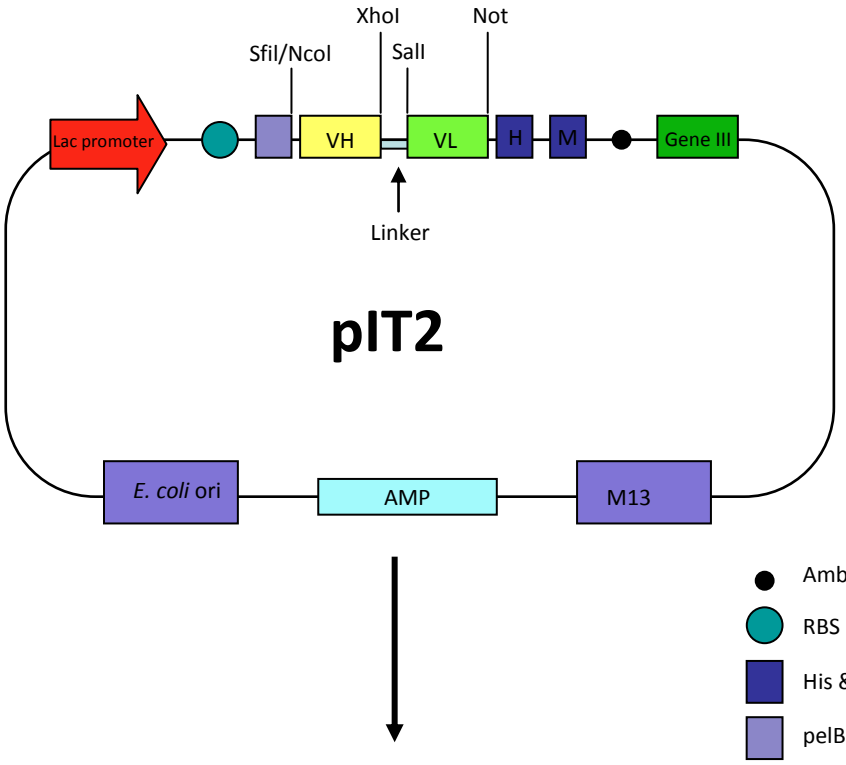

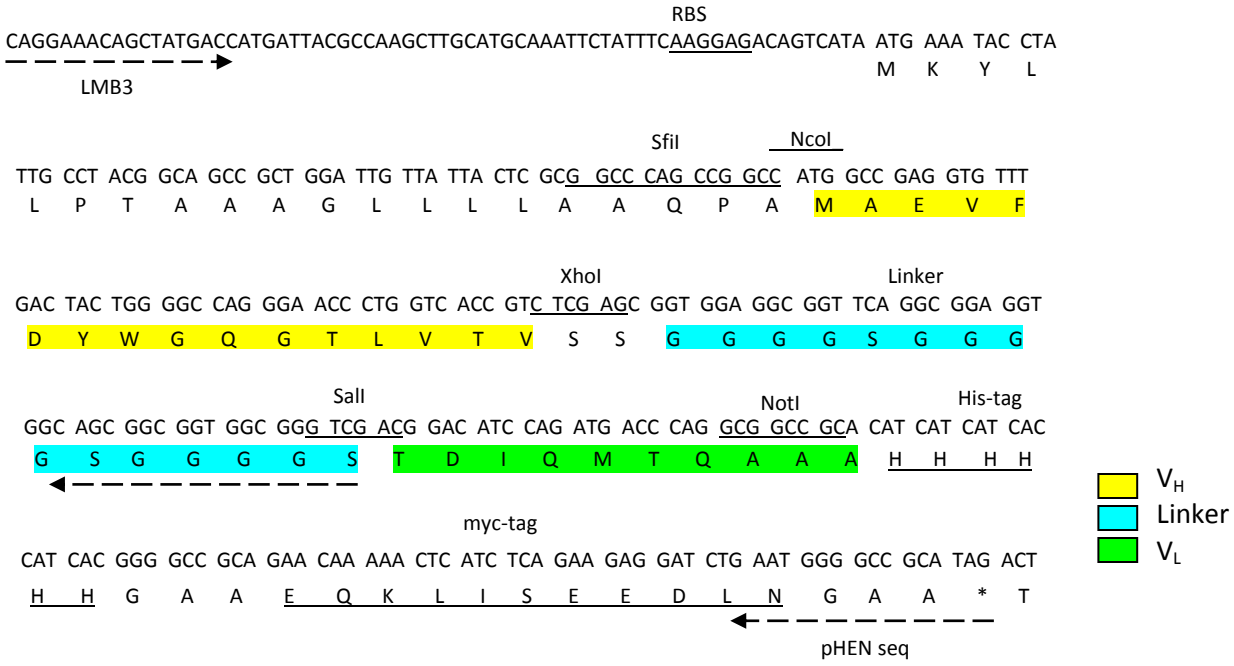

Phagemid vector – pIT2 constructed by Dr. I. M. Tomlinson, Laboratory of Molecular Biology, MRC, Cambridge [90, 94]

The pIT2 vector contains a lac promoter and a pelB leader sequence (an amino-acid sequence that directs the protein to the cytoplasmic membrane of *E. coli*, where the sequence is removed by pelB peptidase) up-stream of the scFv insert, followed by His and Myc tags, an amber stop codon, and the gene encoding the pIII phage coat protein. After infection with helper phage M13K07, scFv up-stream of the amber stop codon is displayed on the phage particle by use of a suppressor strain such as TG1. Alternatively, scFv with both His and Myc tags are secreted into the supernatant using a non-suppressor strain such as HB2151.

Amber Stop Codon

The amber stop codon, UAG, stops protein synthesis and is positioned between antibody gene and phage gene III. In some bacterial suppressor strains (SupE), such as TG1, there is a mutation in the aminoacyl-tRNA of this codon, which prevents it from being read as a stop, and consequently the antibody fragment is produced as a fusion protein together with coat protein pIII of the phage. In non-suppressor strains, this codon is read as a stop, and the antibody fragment is secreted into the periplasm.

SCREENING LOWER-AFFINITY BINDERS FROM ELISA

The initial selection of scFv identified the highest-binding antibody fragments from ELISA results; however, lower-affinity binders were not discarded as these may later have been shown to have improved affinity but lower secretion levels. For that reason, further screening of these lower binders was also performed. To facilitate rapid screening selected antibodies were not purified but instead the periplasmic fractions of the purified clones were evaluated. FACS analysis of these lower binders shows that they were able to differentiate between the two cell lines, but showed decreased levels of affinity to the LNCaP C81 than other previously-screened clones.

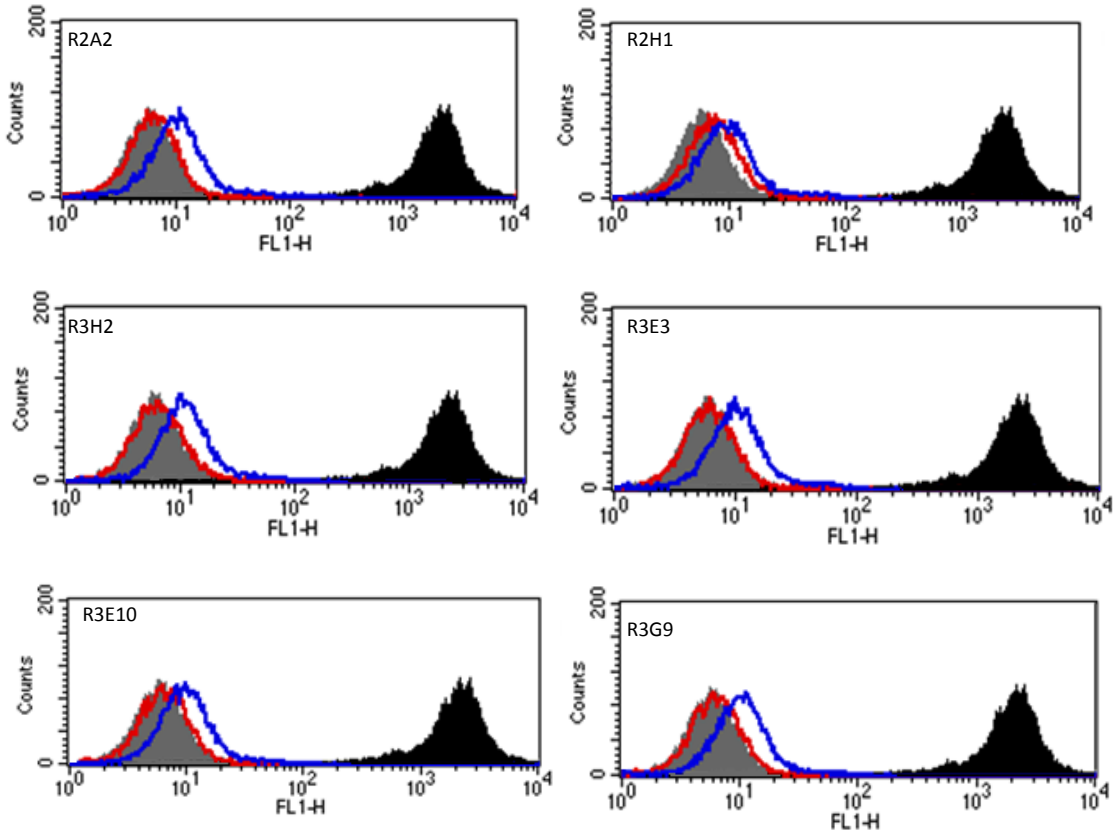

FACS analysis of other lower-affinity binders selected by phage display. Non-purified periplasmic fractions were used on both LNCaP C81 and DU145. Solid grey: DU145 with D2B anti-PSMA antibody; Solid black: LNCaP C81 with D2B anti-PSMA antibody; Red line: DU145 with tested clone; Blue line: LNCaP C81 with tested clone.

Marginally improved binding to the positive cell line LNCaP C81 with the clones tested was observed compared with the PSMA-negative cells, DU145. It was concluded that high affinity antibodies had not been missed in the screening process.

A

pIT2 PHAGEMID VECTOR

Digestion of the plasmid during the formation of diabody

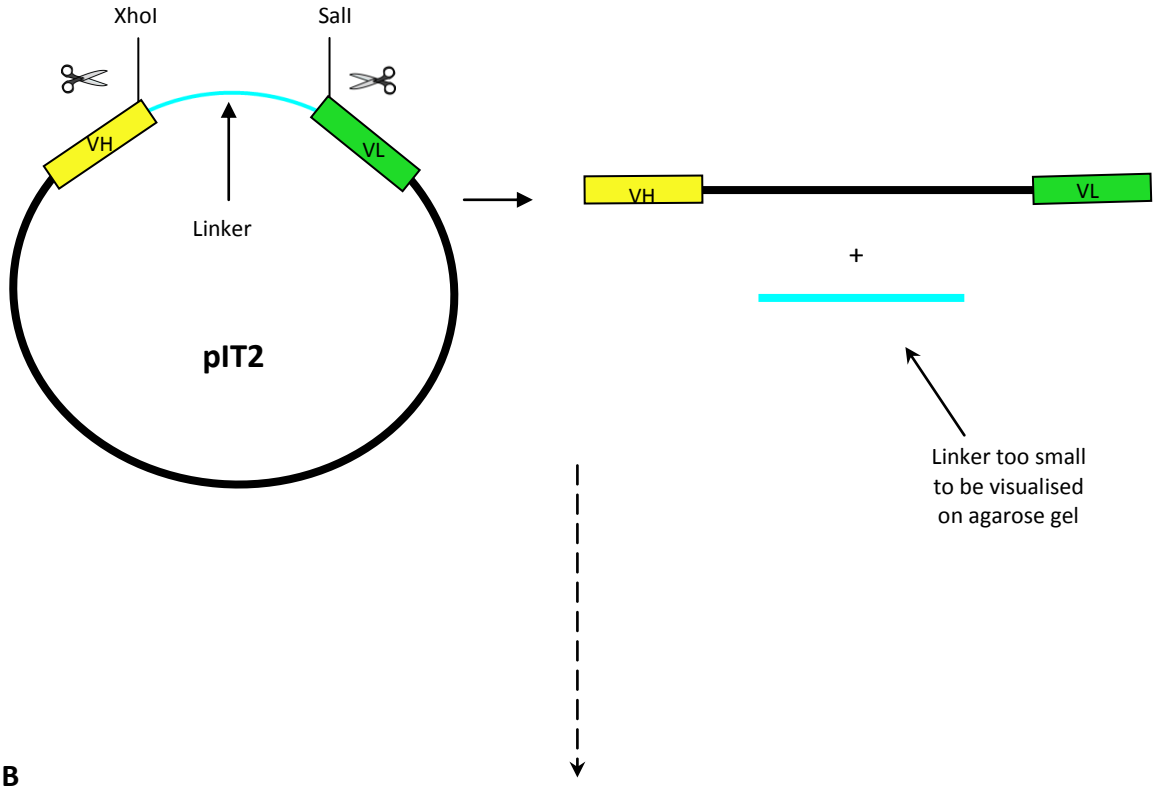

B

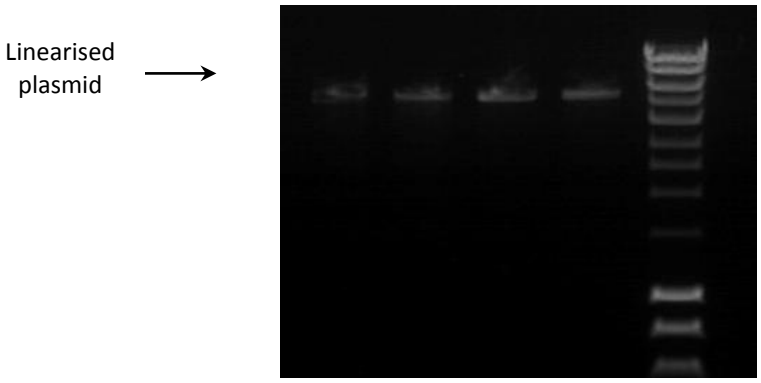

(A) Schematic diagram illustrating the action of the restriction enzymes to linearise the plasmid and remove the glycine-serine linker. (B) Agarose gel revealing one band representing the linearised plasmid from the four selected clones. The linker was too small to be visualised.

HPLC Analysis of scFv and Diabodies

HPLC analysis of the remaining monomeric and dimeric scFv clones, R2F3, R2H2 and R3F5, performed twice, with and without internal standard.

A

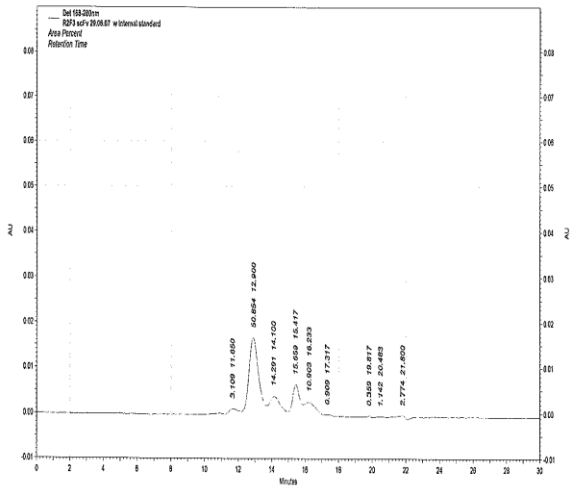

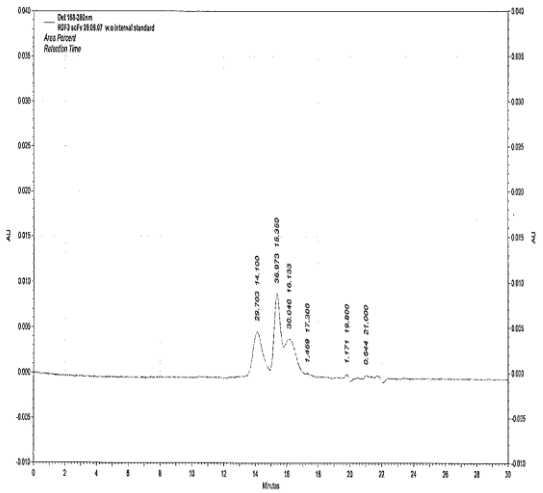

B

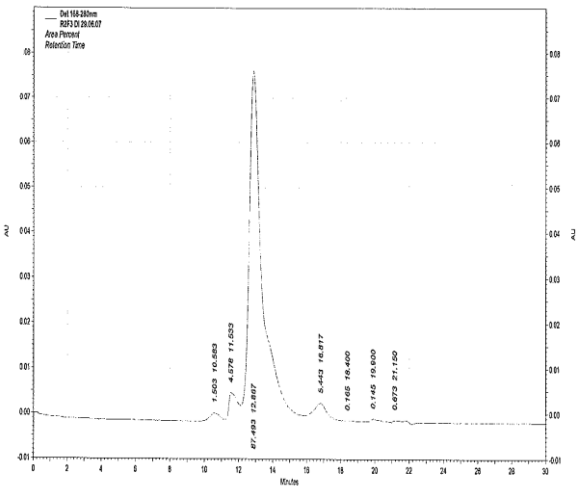

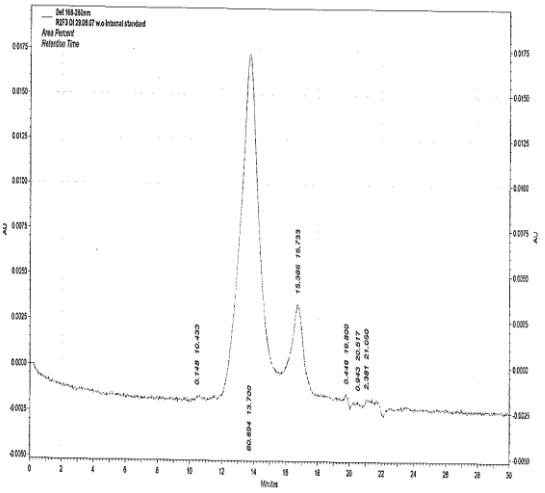

C

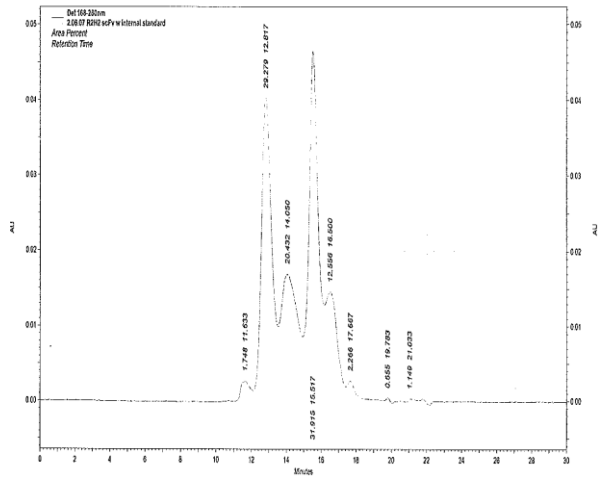
Area Percent
Retention Time
AU
Minutes

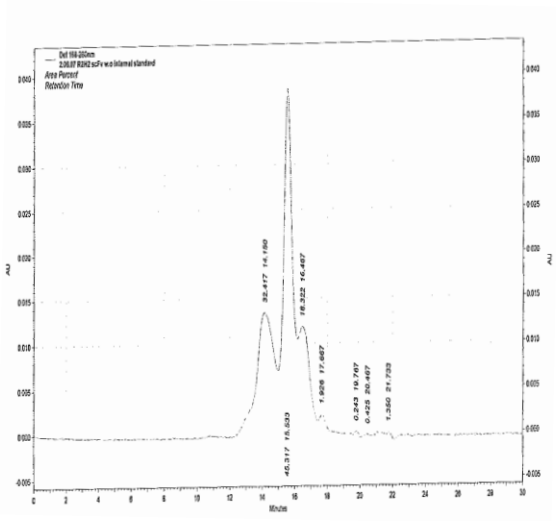
Area Percent
Retention Time
AU
Minutes

D

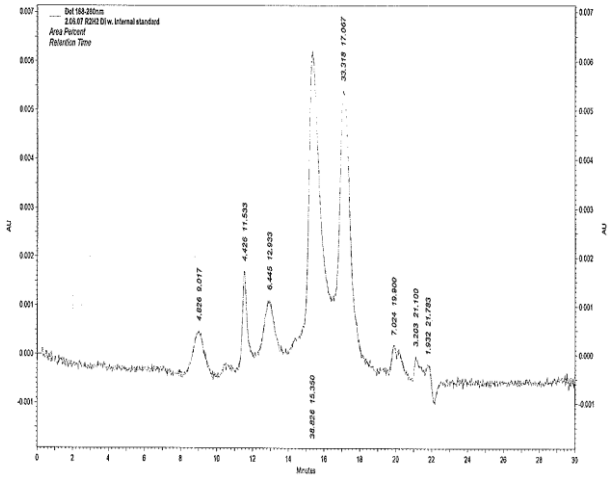
Area Percent
Retention Time
AU
Minutes

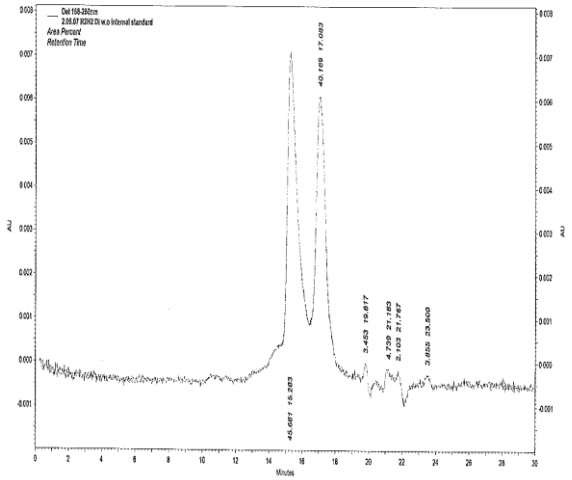
Area Percent
Retention Time
AU
Minutes

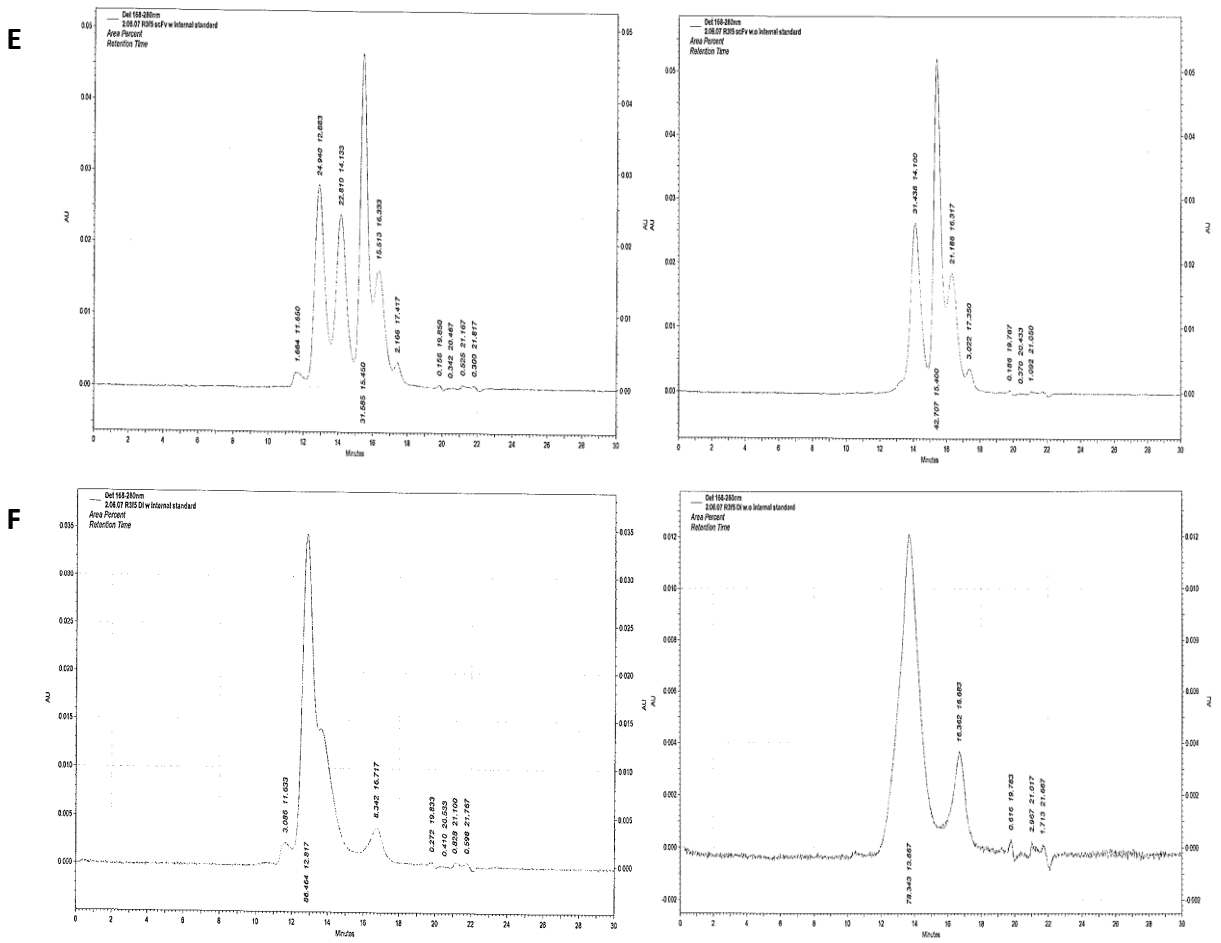

HPLC chromatograms of monomeric and dimeric antibody fragments. A, C & E - Respectively R2F3, R2H2 & R3F5 scFv with and without internal standard. B, D & F - Respectively R2F3, R2H2 & R3F5 diabody with and without internal standard.

RADIOLIGAND BINDING ASSAY

Assays for Specific Binding Performed on All Prostate Cell Lines

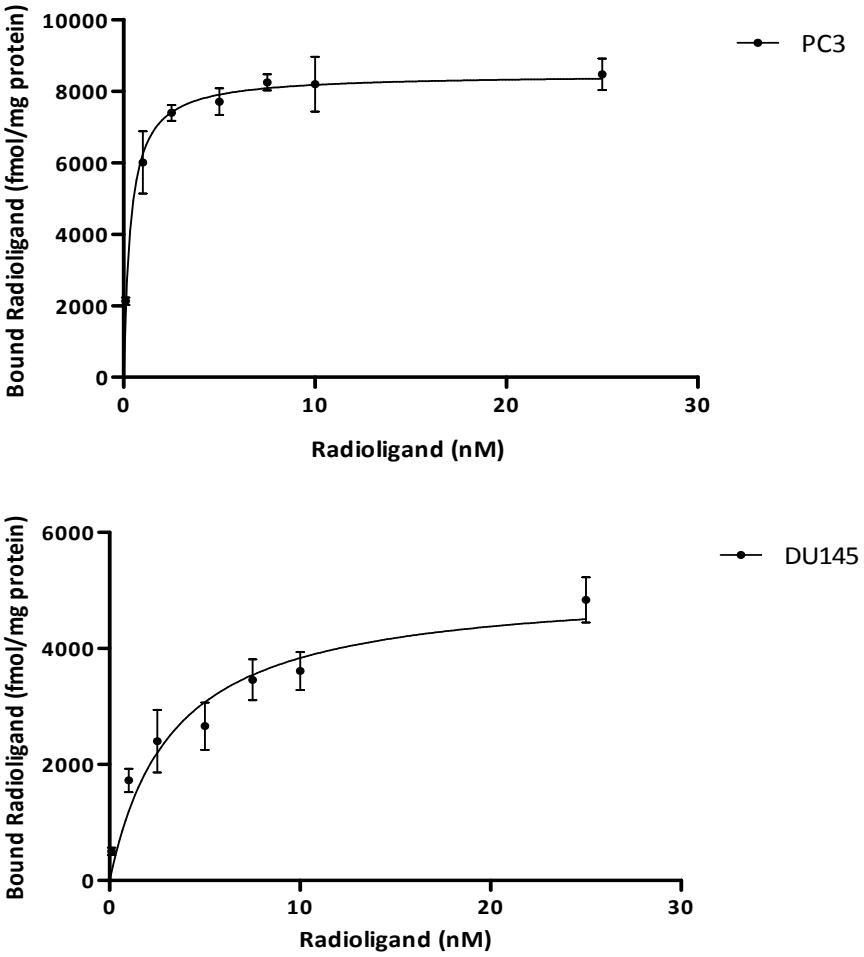

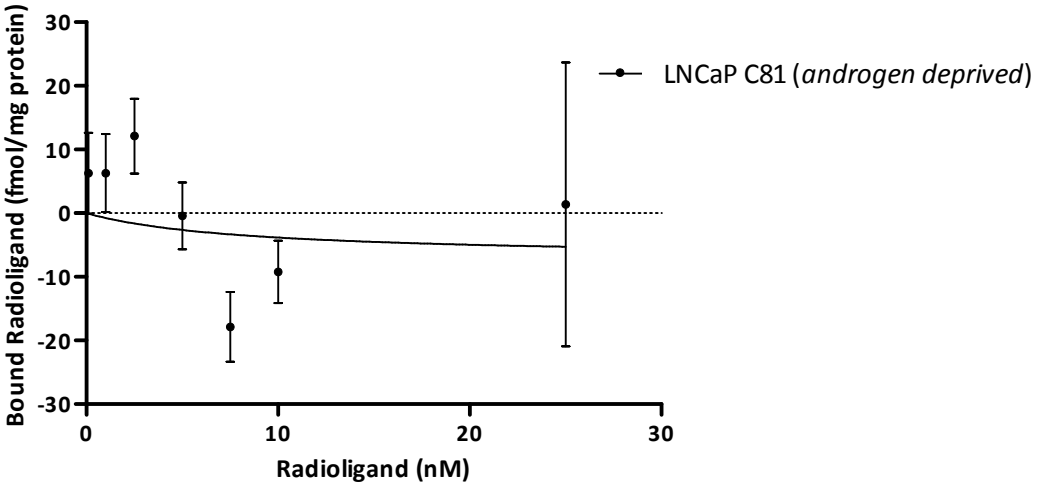

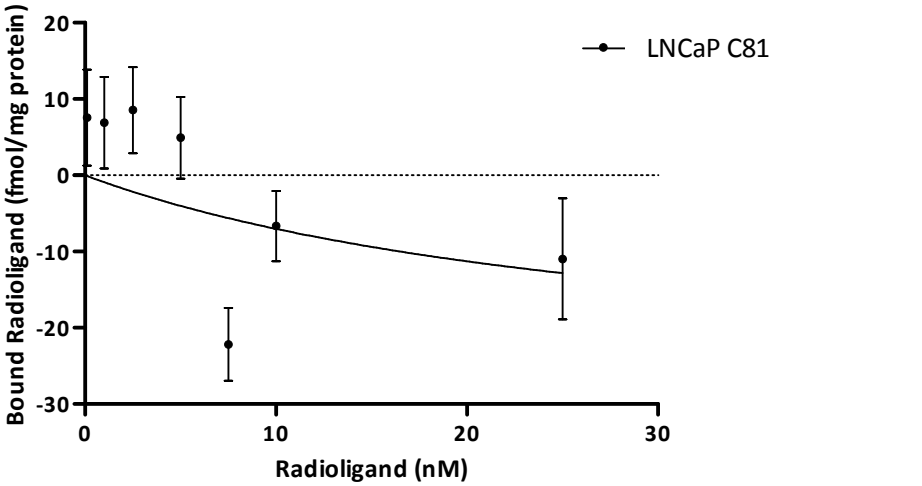

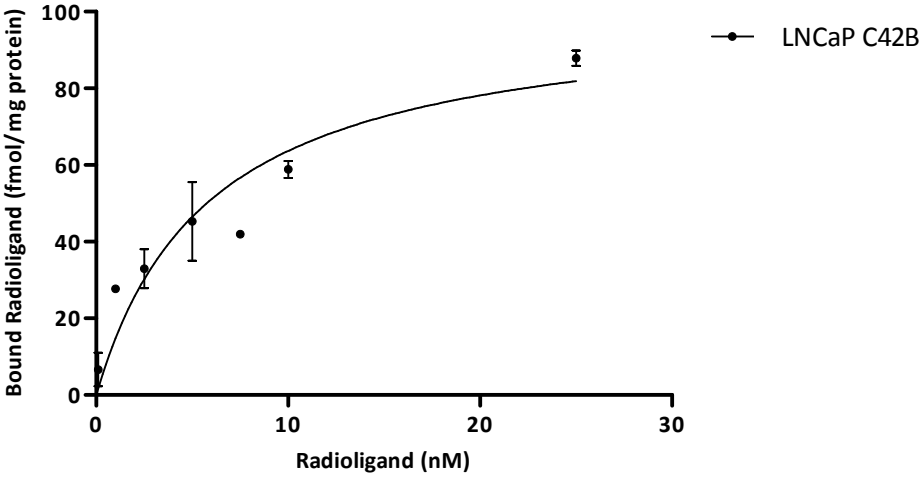

Assays for specific binding performed on all PC cell lines, using radioligand binding assay. Specific binding was not observed with either LNCaP C81 or LNCaP C81 (androgen-deprived).

PCR – Validation Experiment

A validation experiment was performed on two randomly-selected cell lines, LNCaP (androgen-dependent) and LNCaP C42B, to verify that the efficiencies of the target (GRP-R) and the reference (endogenous control) were approximately equal.

A serial dilution series of cDNAs for both the target and endogenous control was performed and C_t values were obtained, from which delta C_t values were calculated. Log input amount was plotted against ΔC_t.

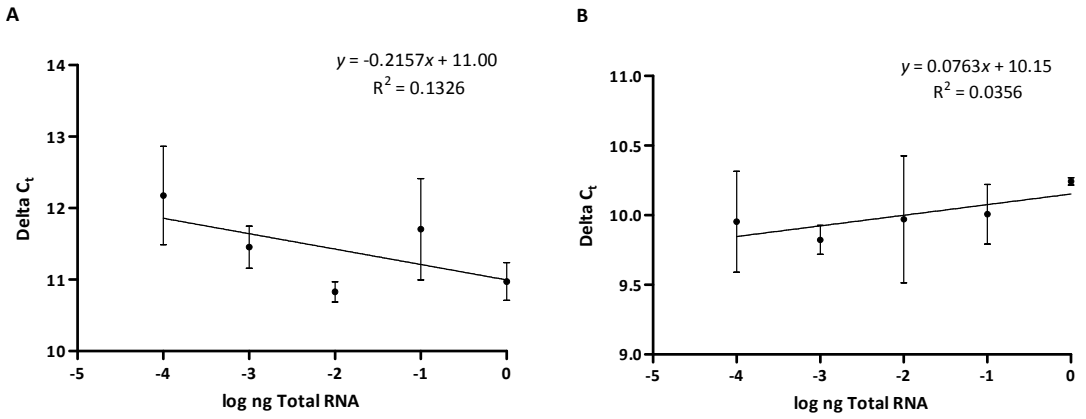

Relative efficiency plot of Log input amount of GRP-R vs. weight of β-actin RNA for (A) LNCaP C42B and (B) LNCaP (androgen-dependent)

The absolute value from the slopes should be <0.1, which represents a low degree of experimental variation. This validates the use of $^{\Delta\Delta}C_t$[79] calculation for the relative quantification of the target, without the need to perform a standard curve on the same reaction plate. Both graphs revealed values <0.1.

[79] ΔC_t Target - ΔC_t Calibrator = $^{\Delta\Delta}C_t$

BIODISTRIBUTION AND IMAGING STUDIES

Neuroendocrine AR42J Rat Pancreatic Cell Line

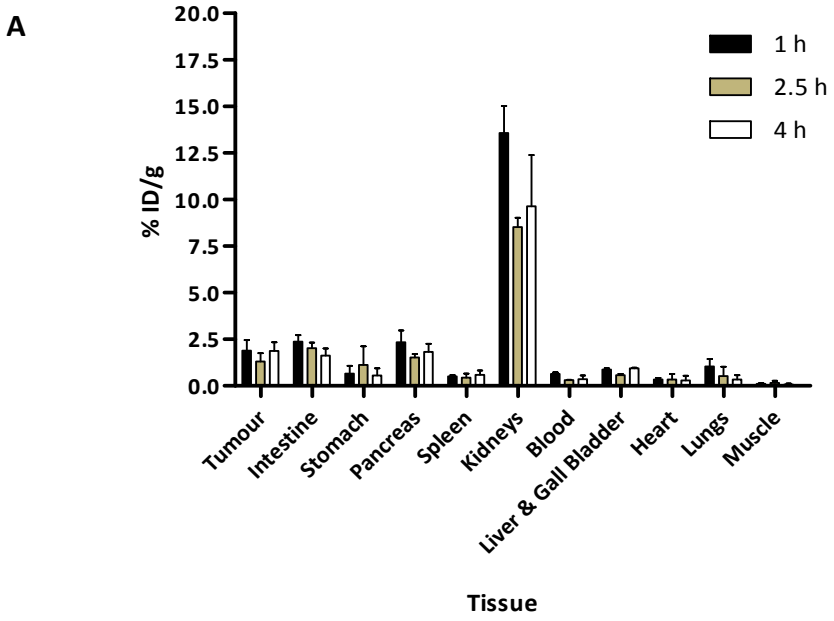

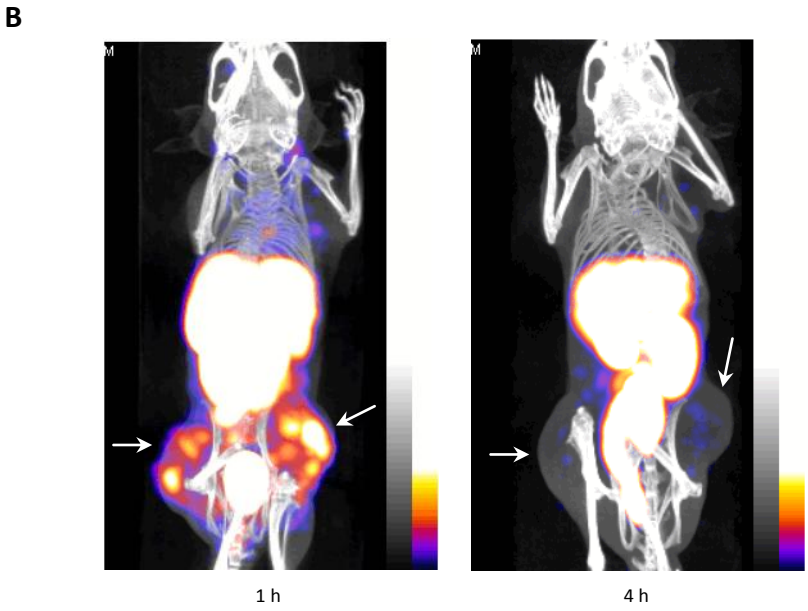

(A) Biodistribution in mice (n= 3) per time group. (B) Coronal pictures of an AR42J tumour-bearing mouse scanned after 1 and 4 h post injection with [^{99m}Tc]-DB 4. Arrows indicate the AR42J tumours on both left and right flanks. Images were scaled to be the same size to enable direct comparison.

LNCaP C81 (androgen-independent) Prostate Cancer Cell Line

A

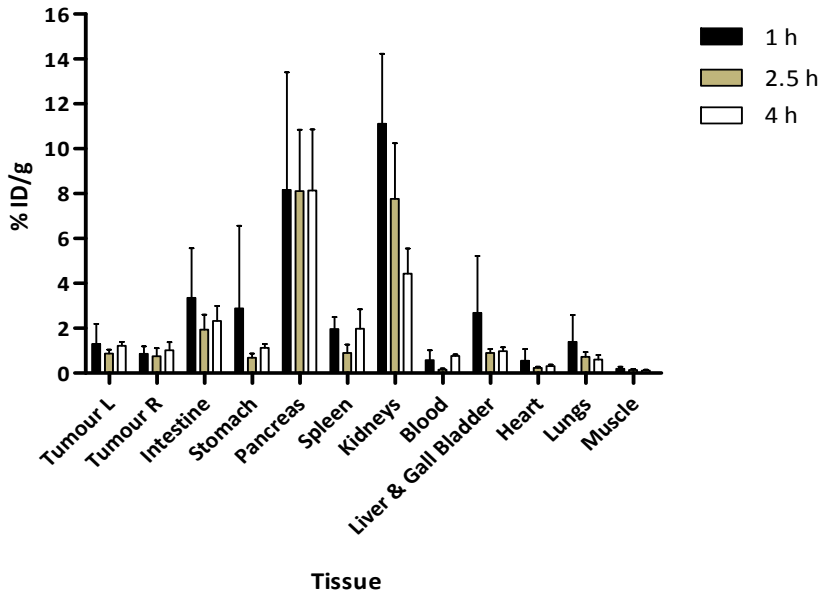

B

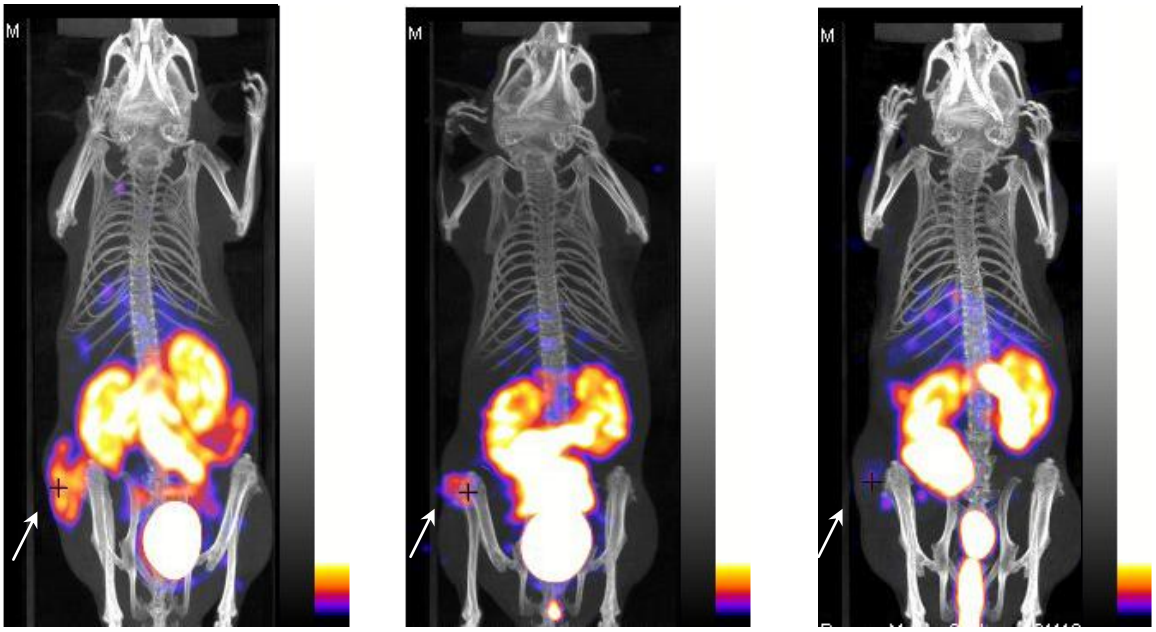

(A) Biodistribution in mice (n = 3) per time group. (B) Coronal pictures of an imaged LNCaP C81 tumour-bearing mouse scanned after 1, 2.5 and 4 h post injection with [^{99m}Tc]-DB 4. Arrows indicate the left tumours. Images were scaled to be the same size to enable direct comparison.

LNCaP Androgen-Dependent Prostate Cancer Cell Line

A

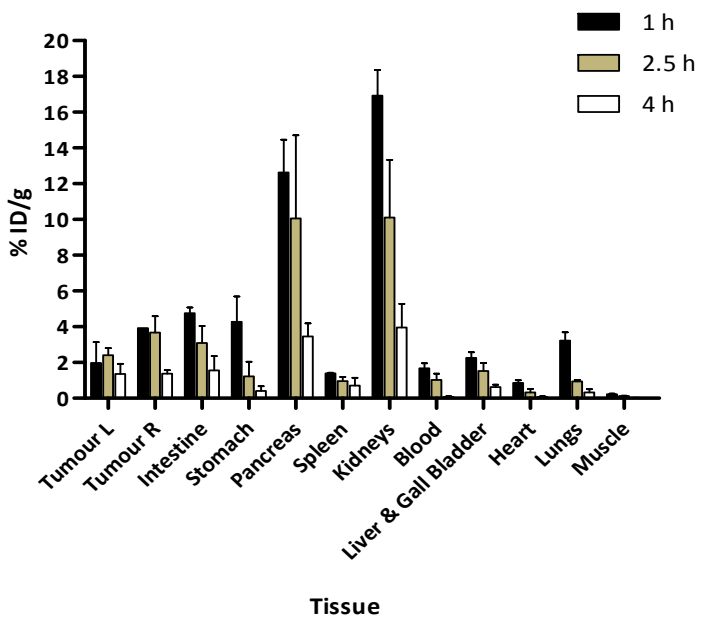

B

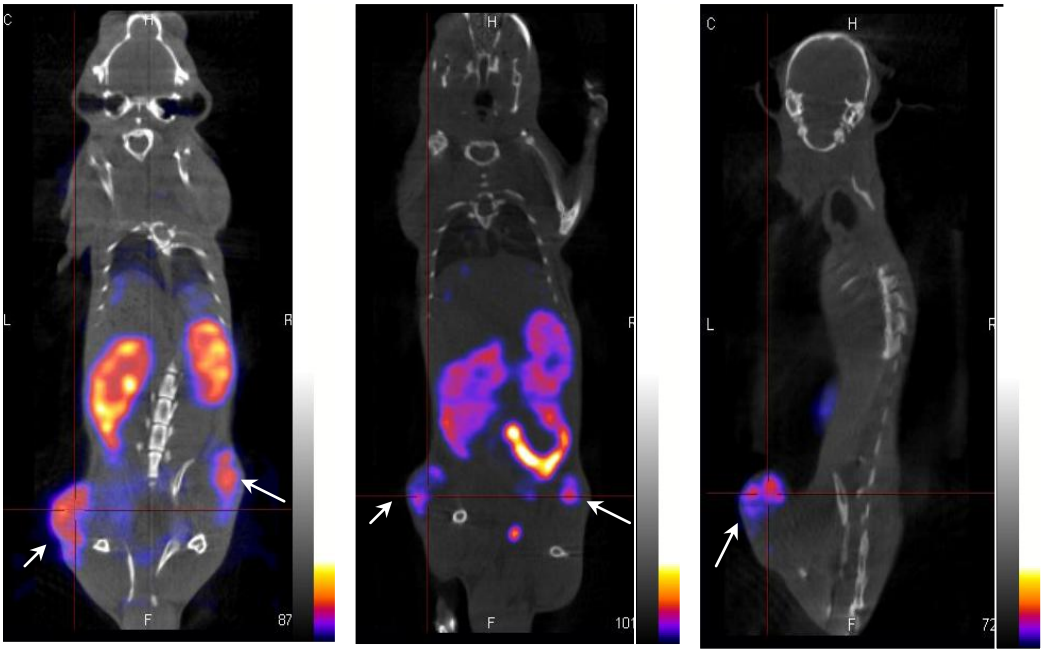

(A) Biodistribution in mice (n = 3) per time group. (B) Coronal pictures of an imaged LNCaP androgen-independent (<15 passage number) tumour-bearing mouse scanned after 1, 2.5 and 4 h post injection with [^{99m}Tc]-DB 4. Arrows indicate tumour growth. Images were scaled to be the same size to enable direct comparison.

LNCaP C42B (Androgen Independent) Prostate Cancer Cell Line

A

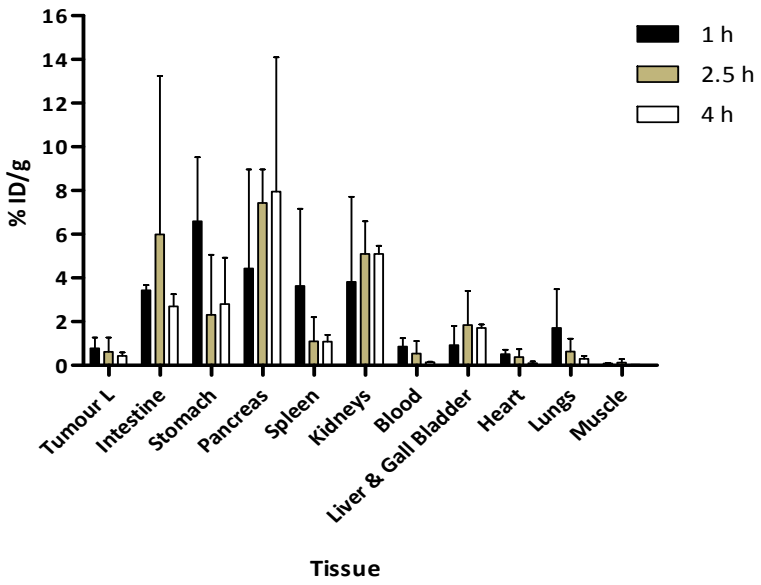

B

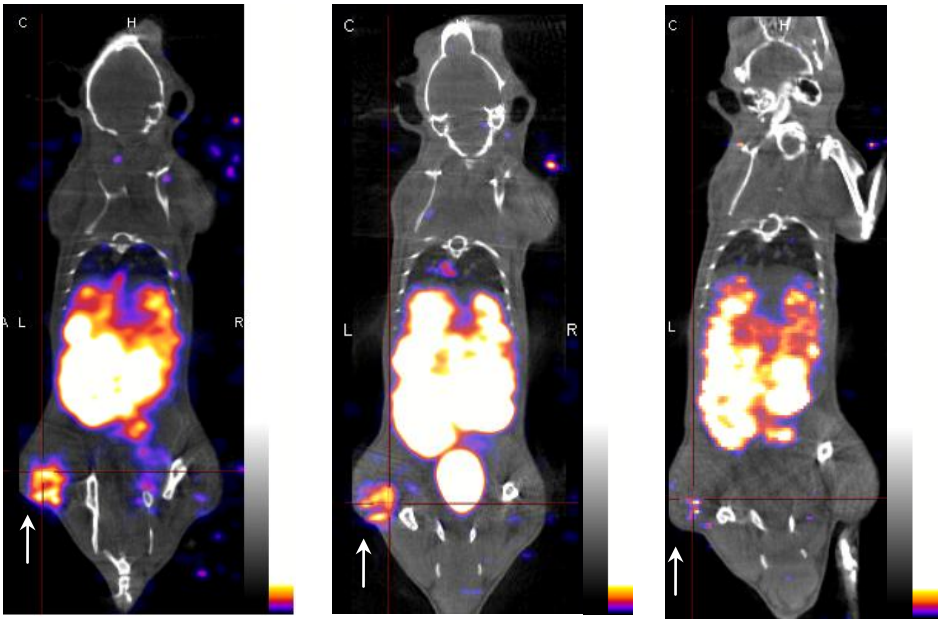

1 h 2.5 h 4 h

(A) Biodistribution analysis on mice (n=3) per time point. (B) Coronal pictures of an imaged LNCaP C42B tumour-bearing mouse scanned after 1, 2.5 and 4 h post injection with [^{99m}Tc]-DB 4. Arrows indicate tumour growth. Images were scaled to be the same size to enable direct comparison.

LNCaP C81 (Androgen-Deprived) Prostate Cancer Cell Line

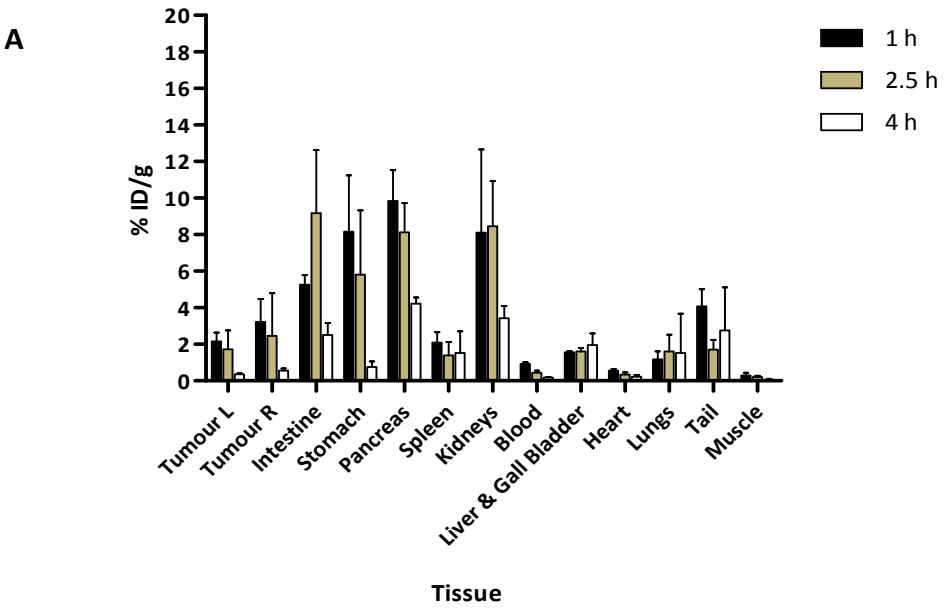

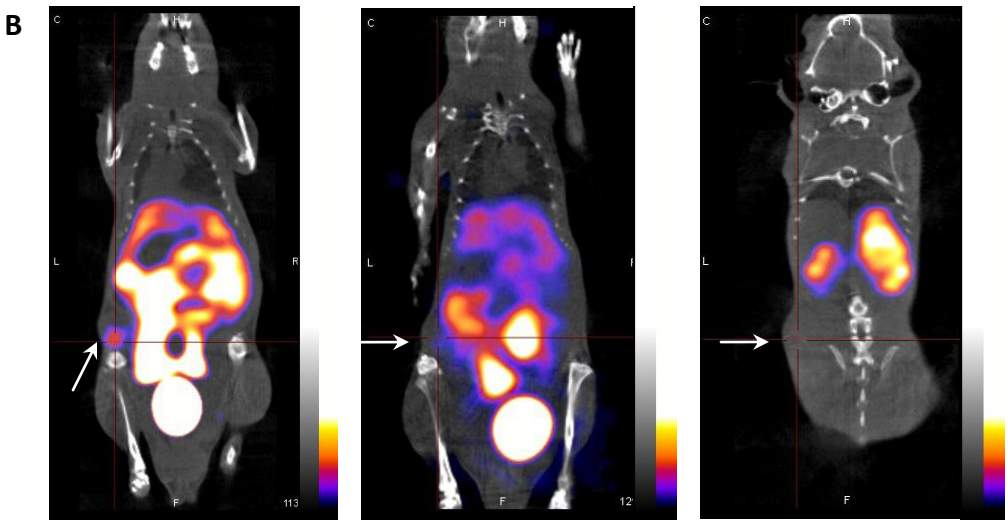

(A) Biodistribution analysis on mice (n=3) per time point. (B) Coronal pictures of an imaged LNCaP C81 androgen-deprived tumour bearing mouse scanned after 1, 2.5 and 4 h post injection with [^{99m}Tc]-DB 4. Arrows indicate tumour growth. Images were scaled to be the same size to enable direct comparison.

LNCaP C42B (Androgen-Deprived) Prostate Cancer Cell Line

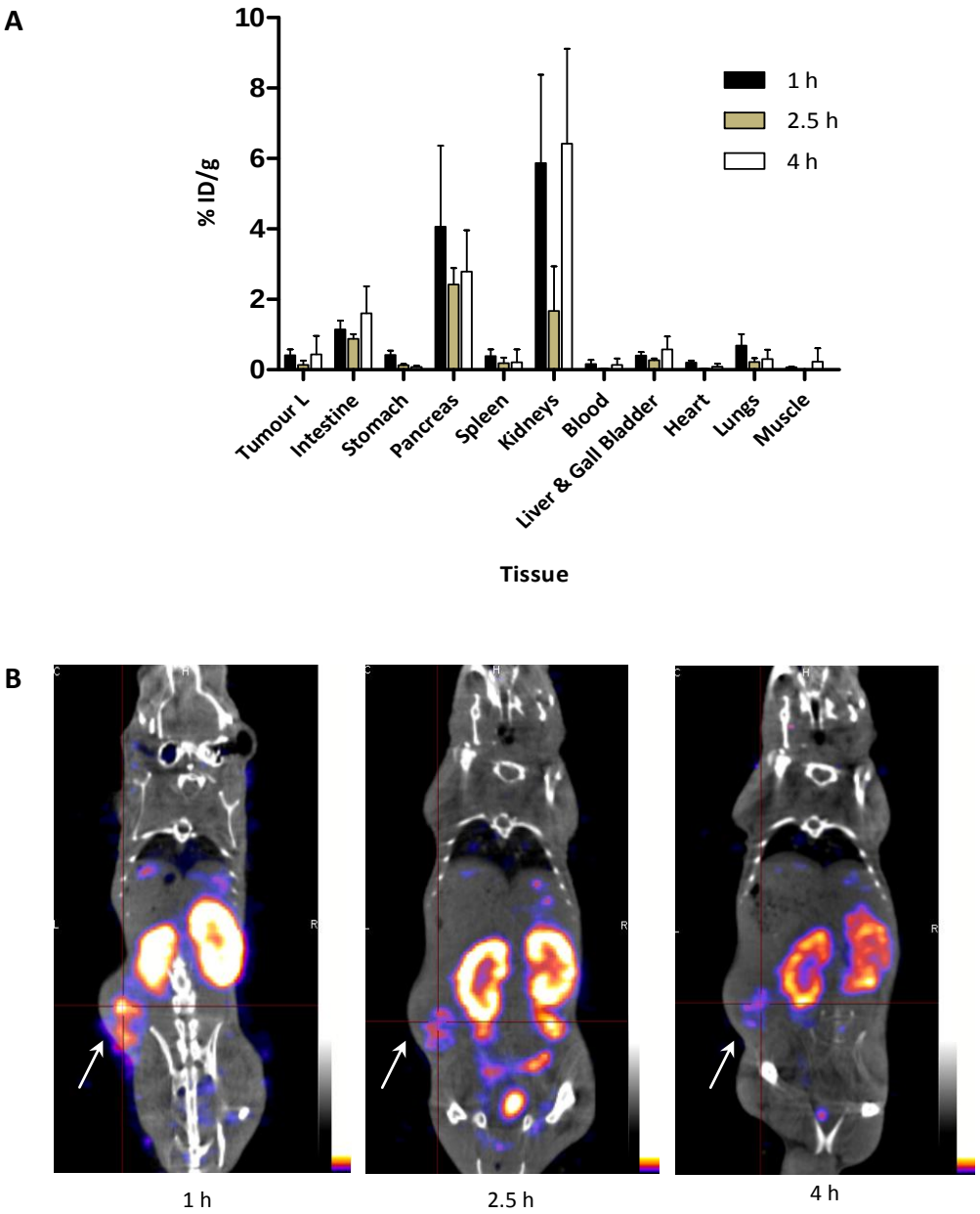

(A) Biodistribution analysis on mice (n=3) per time point. (B) Coronal pictures of an imaged LNCaP C42B androgen-deprived tumour bearing mouse scanned after 1, 2.5 and 4 h post injection with [^{99m}Tc]-DB 4. Arrows indicate tumour growth. Images were scaled to be the same size to enable direct comparison.